Bioengineered Novel MicroRNA-7-5p to Modulate Non-Small Cell Lung Cancer Cell Metabolism and Improve Therapy

By

GAVIN MCALLISTER TRABER

DISSERTATION

Submitted in partial satisfaction of the requirements for the degree of

DOCTOR OF PHILOSOPHY

in

Biochemistry, Molecular, Cellular, and Developmental Biology

in the

OFFICE OF GRADUATE STUDIES

of the

UNVERSITY OF CALIFORNIA

DAVIS

Approved:

_____

Ai-Ming Yu, Chair

_____

Kermit Carraway

_____

Hongwu Chen

Committee in Charge

2024

Acknowledgements

The works presented in this dissertation are supported by the National Cancer Institute [**R01CA225958** and **R01CA253230**] and National Institute of General Medical Sciences [**R35GM140835**] from the National Institutes of Health awarded to Ai-Ming Yu and by a National Institutes of General Medical Sciences-funded Pharmacology Training Program Grant [**T32GM099608 and T32GM144303**] from the National Institutes of Health awarded to Gavin M. Traber (myself).

Dedications

I would like to offer a personal thanks to Drs. Mei-Juan Tu, Neelu Batra, and Su Guan for their efforts in the completion of this dissertation and to my Dissertation Committee members Drs. Kermit Carraway and Hongwu Chen. Further thanks and gratitude to Dr. Ai-Ming Yu for his guidance, mentorship, and support in my training and the completion of this dissertation. Final thanks go to both my family and, in particular, my wife (Brittany Traber) for their consistent support of my aspirations.

Dissertation Abstract

Lung cancer remains the leading cause of cancer-related deaths among both men and women in the United States and worldwide with 80% of cases classified as Non-Small Cell Lung Cancer (NSCLC). While significant advancements have been made in cancer biology and therapies, overall survival of NSCLC patients remains one of the lowest among all cancer types. Therefore, the need for novel therapeutics to combat NSCLC is in high demand. RNA interfering (RNAi) provides researchers with a versatile and powerful tool for basic genetic and biomedical research and advancements in RNAi technologies have also introduced a novel, growing class of RNAi therapeutics into the clinic practice. By examining the six RNAi drugs, namely small interfering RNAs, being approved by the FDA, we revealed their overlapping characteristics with functional microRNAs (miRNAs or miRs) derived from the genome. With improved understanding of roles of miRNAs in NSCLC, replacement therapy may provide a novel route to reintroduce target tumor suppressive miRNAs found depleted in tumors to improve NSCLC therapy. Regrettably, current miRNA studies typically use chemically synthesized and modified miRNA mimics that might not truly represent the physicochemical and biological properties of natural miRNAs. To address this concern, our laboratory has developed an *in vivo* fermentation based platform technology to offer bioengineered RNAi agents (BioRNA). Using our BioRNA technology, we have successfully produced a panel of 48 novel BioRNAs, among them the BioRNA^{Gly} and BioRNA^{Leu} panels showed comparable overall yields, purities, and antiproliferative activities against NSCLC cells. Noticing miR-7-5p (miR-7) one of the most effective miRNAs, we further found that BioRNA^{Gly}/miR-7 (termed BioRNA/miR-7) offered higher levels of mature miR-7-5p to regulate the expression known targets, namely EGFR, MRP1, and VDAC1, with comparable or slightly

greater activities compared with a commercial miR-7-5p mimic.

Indeed, miR-7 is a known tumor suppressive miRNA regulating some target genes important in metabolism, whereas it is commonly found with low levels of expression in NSCLC. Moreover, repression of efflux transporter MRP1 by miR-7 may be implicated in sensitizing NSCLC cells by increasing intracellular drug accumulation. Therefore, we aim to define the impact of miR-7 on NSCLC cell metabolism and anticancer activity of a co-administered small molecule drug. First, we identified the impact of BioRNA/miR-7 on mitochondrial EGFR expression along with two additionally known mitochondrial targets, namely SLC25A37 and TIM50, in NSCLC cells, leading to an abnormal, condensed mitochondria morphology. Second, we validated a new and direct target for miR-7, mitochondrial AGK, and observed a reduction of mitochondrial respiration and glycolytic capacity by BioRNA/miR-7. Further, we revealed a synergism for co-administered pemetrexed (PEM) to inhibit NSCLC growth, accompanied by a sharp increase in intracellular PEM levels. Moreover, we demonstrated the effectiveness of BioRNA/miR-7, alone and combined with PEM, to control tumor growth in a NSCLC patient-derived xenograft mouse model.

Thus, we have identified BioRNA/miR-7 from a set of BioRNAs as a potential anticancer agent that functions through endogenous RNAi mechanisms to disrupt NSCLC cell metabolism and MRP1-mediated drug efflux. Together, our collective works demonstrate a widening role for miR-7 in NSCLC biology and supports the use of miR-7 to improve current therapeutics for NSCLC.

Table of Contents

Chapter 1: RNAi Based Therapeutics and Novel RNA Bioengineering Technology

Abstract

RNA interference (RNAi) provides researchers with a versatile means to modulate target gene expression. The major forms of RNAi molecules, genome-derived microRNAs (miRNAs) and exogenous small interfering RNAs (siRNAs), converge into RNA-induced silencing complexes to achieve post-transcriptional gene regulation. RNAi has proven to be an adaptable and powerful therapeutic strategy where advancements in chemistry and pharmaceutics continue to bring RNAi-based drugs into the clinic. With four siRNA medications already approved by the United States Food and Drug Administration (FDA), several RNAi-based therapeutics continue to advance to clinical trials with functions that closely resemble their endogenous counterparts. Although intended to enhance stability and improve efficacy, chemical modifications may increase risk of off-target effects by altering RNA structure, folding, and biological activity away from their natural equivalents. Novel technologies in development today seek to utilize intact cells to yield true biological RNAi agents that better represent the structures, stabilities, activities, and safety profiles of natural RNA molecules. In this review, we provide an examination of the mechanisms of action of endogenous miRNAs and exogenous siRNAs, the physiological and pharmacokinetic barriers to therapeutic RNA delivery, and a summary of the chemical modifications and delivery platforms in use. We overview the pharmacology of the four FDA approved siRNA medications (patisiran, givosiran, lumasiran, and inclisiran), as well as five siRNAs and several miRNA-based therapeutics currently in clinical trials. Furthermore, we discuss the direct expression and stable carrier-based, in vivo production of novel biological RNAi agents for research and development.

Graphical Abstract

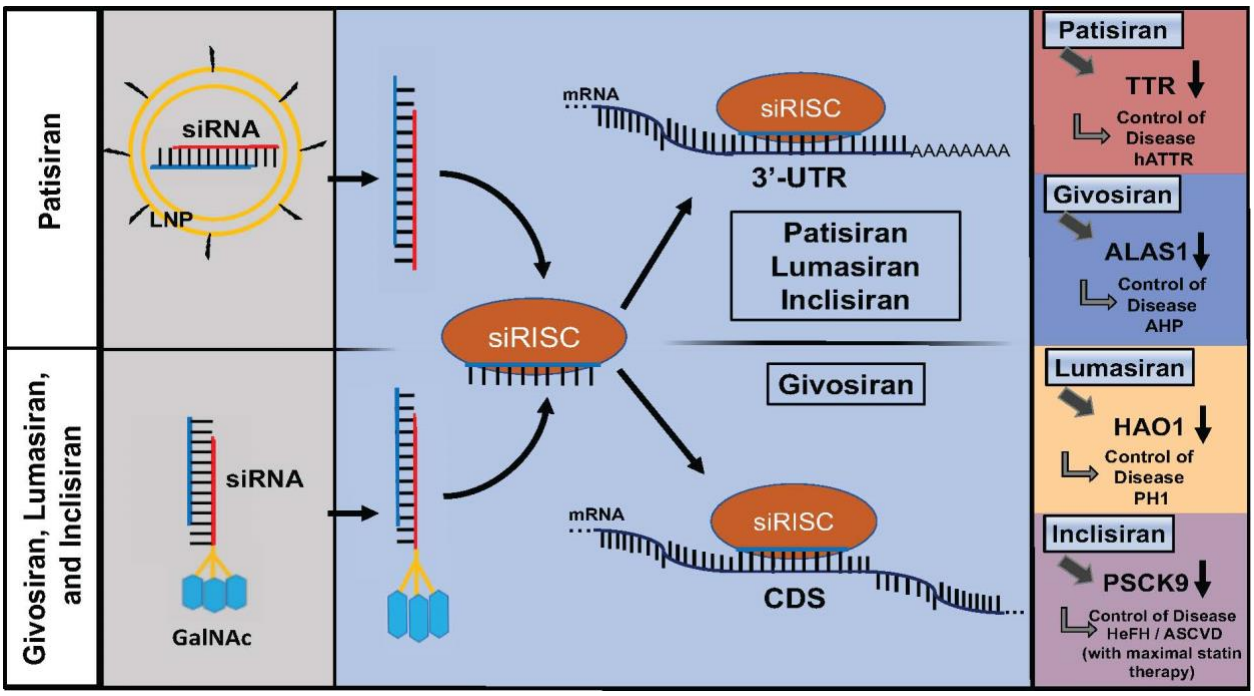

Significance Statement

In our review, we summarize the major concepts of RNA interreference (RNAi), molecular mechanisms, and current state and challenges of RNAi drug development. We focus our discussion on the pharmacology of FDA-approved RNAi medications and those siRNAs and miRNA-based therapeutics entered the clinical investigations. Novel approaches to producing new true biological RNAi molecules for research and development are highlighted.

Introduction

Genome-derived functional microRNA (miRNA) was initially elucidated in *Caenorhabditis elegans* during the characterization of the *lin-4* gene encoding a small RNA (sRNA) with antisense complementarity and the capacity for posttranslational regulation of target gene *lin-14* [1, 2]. Later on, miRNAs were identified as a superfamily of conserved and functional noncoding RNAs (ncRNAs) that are present in a wide range of animal species [3, 4], including humans [5]. Since then, the development of RNA interference (RNAi) technology [6, 7] has offered new routes for the studies of reverse genetics, specific gene expression and regulation, and targeted therapy with the potential to study, manipulate, and achieve control of disease. In particular, RNAi is accomplished through the interactions of sRNA molecules, namely small interfering RNAs (siRNAs) and miRNA, with functions that lie outside the confines of the central dogma of molecular biology [8, 9]. Aside from miRNAs and siRNAs, a third major class of RNAi molecules exist, termed P-Element induced wimpy testis (PIWI)-interaction RNA (piRNA). Although piRNAs typically function in complex with piwi proteins to posttranscriptionally regulate several

pathways important in transposon silencing, genome rearrangement, and germ stem-cell maintenance, the most well-studied RNAi molecules are siRNAs and miRNAs that regulate gene expression at the posttranscriptional level by specific or semi-specific targeting of messenger RNA (mRNA) [10-12]. Altogether, the discovery and application of RNAi technology provides a unique and adaptable tool for basic genetic and biomedical research and opens doors for its exploitation in the development of novel biotechnologies and therapies.

RNAi therapy uses the natural, cellular mechanisms of RNAi to bring gene regulation into clinical practice [13-16]. With four novel RNAi-based therapeutics approval by the United States Food and Drug Administration (FDA), namely patisiran [17], givosiran [18], lumasiran [19], and inclisiran [20], each siRNA drug selectively acts on a target mRNA transcript to combat a disease. In addition, several siRNA agents (e.g., fitusiran, nedosiran, teprasiran, tivanisiran, and vutrisiran) have entered Phase III clinical trials with many other RNAi-based therapeutics progressing through early-stage clinical trials or preclinical development [21]. However, delivery of RNAi therapeutics has long been the root obstacle in the way of clinical success. Once an RNAi drug is administered to the body there are several physical and pharmacokinetic barriers that limit its actions and desired efficacy [16, 22-24]. Chemical modifications and the development of novel delivery methods compatible with RNAi machinery help researchers overcome these barriers [16, 25]. Although these modifications are intended to enhance stability and improve efficacy, growing evidence suggests that chemical modifications of *in vivo* synthesized RNAi molecules can increase the risk of off-target effects by altering their structure, folding, biological activity, and safety away from natural RNAi agents [26, 27]. To address this challenge, novel technologies in development

today seek to utilize intact cells to yield true biological RNA molecules that better recapitulate the structures, stabilities, activities, and safety profiles of endogenous RNAi molecules.

In this review, we provide an examination of the mechanisms of action of endogenous miRNAs and exogenous siRNAs, the pharmacokinetic barriers to therapeutic RNAs, and a summary of the viable chemical modifications and delivery platforms in use. We overview the pharmacology of the four siRNA medications approved by the United States FDA, as well as five therapeutic siRNAs and several RNAi-based therapeutics currently in clinical trials. Furthermore, we discuss novel approaches to *in vivo* production of RNA agents, including direct expression and utilization of stable carriers, which represent a novel class of real biological RNAi molecules for research and development.

RNAi Molecules and Mechanisms

Genome-derived miRNAs and exogenous siRNAs are classes of ncRNA molecules of with functions in posttranslational gene regulation that make up two of the most well-studied RNAi molecules [28]. Functional genome-derived miRNAs rang from eighteen to twenty-five nucleotides in length and are capable of targeting the mRNA transcripts of multiple genes to regulate common or several cellular pathways, while exogenous siRNA are generally introduced into the cells to control the expression of a single target gene [9, 10, 16, 29, 30]. As such, these ncRNA molecules can play critical roles in modulating essentially all cellular functions, including cell signaling, proliferation, metabolism, immunity, and senescence among others [10, 28, 31].

Genome-derived miRNAs

Canonical biogenesis of genome-derived miRNA is categorized into two major phases, nuclear and cytosolic (**Figure 1**). Furthermore, depending on the location of the miRNA gene within the genome, miRNAs can be further classified into intergenic- and intragenic-derived miRNAs. Intergenic-derived miRNA come from regions of the genome located in noncoding regions of the DNA between genes, have unique promoter regions, and are transcribed either by RNA polymerase II or III [32-34]. By contrast, the genes of intragenic-derived miRNA are located within exons or introns of protein-coding genes, are co-expressed with their host gene, and transcribed by RNA polymerase II [32, 34]. Initiating in the nuclear phase, DNA sequences encoding miRNA genes are transcribed by RNA polymerases into long hairpin transcripts called primary-miRNAs (pri-miRNAs) [32]. A pri-miRNA is typically over one thousand nucleotides in length and consists of three major domains important to miRNA processing: a thirty-three to thirty-five nucleotide long stem, terminal loop, and two single-stranded RNA (ssRNA) segments flaking both ends [32]. Pri-miRNA is further processed in the nucleus by the microprocessor which contains a nuclear RNase III enzyme (Drosha) and its cofactor, DiGeorge Syndrome Critical Region 8 (DGCR8) [35], to release a smaller hairpin RNA (approximately 65 nucleotides in length), termed pre-miRNA. Between the major nuclear and cytosolic phases, pre-miRNA form a complex with Exportin 5 transporter and GTP-binding nuclear protein (RAN) to exit the nucleus and release the pre-miRNA into the cytosol upon GTP hydrolysis [36].

In the cytosolic phase, pre-miRNAs are identified and further processed by RNase III endonuclease (Dicer) and the transactivating response RNA-binding protein (TRBP) [32, 35, 36]

at the terminal loops of the hairpins to miRNA duplexes with two 3' overhangs [37]. After a duplex is unwound, the guide (antisense) strand or mature miRNA is loaded into the RNA-Induced Silencing Complex (RISC) to form a miRNA-RISC complex (miRISC) while the passenger (sense) strand is degraded [38]. Determining the guide strand from the miRNA duplex is believed to be a result of Argonaute 2 endonuclease (AGO2) preference for the 3-prime terminus (3') or 5-prime terminus (5') and is typically variable and dependent heavily on both cell type and function [39]. AGO2 tends to preferentially select the guide strand (3' or 5') of the miRNA duplex with a lower stability or instead the presence of an uracil at its 5' terminus [40]. Following the formation of functional miRISC, the mechanism of regulation is then dependent on the interactions between the miRNA and mRNA sequences [32, 39].

In addition to the canonical pathways, previous studies have identified noncanonical biogenesis of miRNAs. The well-studied noncanonical pathways are categorized by the canonical processing steps they circumvent. The first major noncanonical biogenesis pathway pertains to the nuclear processing phase, independent of Drosha/DGCR8 (**Figure 1**). In particular, short hairpin RNA (shRNA)-bearing miRtrons derived from the genome are processed into pre-miRNAs via posttranscriptional splicing to closely resemble Dicer/TRBP recognizable substrates for intracellular translocation and cytoplasmic processing [41]. After the miRtron-derived pre-miRNAs are exported into the cytosol, the second major noncanonical biogenesis pathway pertaining to the cytosolic processing phase independent of the microprocessor [41-43] (**Figure 1**). However, Dicer/TRBP-independent pre-miRNAs require Ago2 to cleave the 3' strand and forming a pseudo-miRISC followed by 5' strand trimming to mature length [44, 45].

Besides canonical and noncanonical biogenesis of miRNAs described above, some miRNAs are directly derived from alternative precursor RNA molecules such as small nucleolar RNAs (snoRNAs) and transfer RNAs (tRNAs) [46-49] [50]. SnoRNAs have a generalized and well-established function of controlling gene expression by modifying ribosomal RNA (rRNA) [51]. Like canonical miRNAs, some snoRNAs are found to repress mRNAs by incorporation into the RISC complex [46, 49]. MiRNAs derived from tRNA precursors constitute a unique source for miRNA maturation where suitable Dicer enzyme substrates are found within the colloquial "clover-leaf" structure of tRNAs [47, 48]. Precursor tRNA substrates are cleaved by Dicer into tRNA-derived RNA fragments (tRFs) with the capacity for RISC incorporation and gene regulation [47, 52]. Further, researchers have also revealed tRFs to guide Ago proteins towards target gene regulation independent of Dicer [53].

Exogenous siRNAs

Since their discovery following miRNA in 1998, siRNAs have become well-established, gene specific regulatory molecules that function within the RNAi pathway [6, 54]. With several endogenous sources of siRNA identified, a major source for RNAi studies use exogenous siRNAs that are chemically synthesized and highly selectively to the mRNA transcripts of proteins previously considered to be "undruggable" by small molecule inhibitors [9, 16]. Exogenous siRNAs are synthesized as shRNA ranging from twenty to twenty-five base pairs with 3' overhangs that can bypassing Dicer cleavage for direct incorporation into the RISC (siRISC) to control target gene expression when introduced to the cells (**Figure 1**) [9, 55].

There are two well established approaches to produce siRNAs, chemical (e.g., solid-phase synthesis) and biochemical (e.g., *in vitro* transcription) syntheses. Solid-phase organic synthesis is a widely used method that can produce large amounts of RNAs and accommodate a wide range of chemical modifications [56]. The principle is boiled down to the addition of individual ribonucleosides performed on a solid support or resin, consisting of nucleoside deprotection, coupling, oxidation, and capping. By repeating the cycle for desired number and sequence of nucleosides, the process is ended with oligonucleotide cleavage from the solid support and nucleoside deprotection [57, 58]. This general design uses 2'-hydroxyl protecting groups that provide ribonucleoside phosphoramidites with characteristics key to their synthetic oligomerization [57]. As such, various protecting group strategies have been developed to allow for site-specific incorporation of chemically modified groups at specific positions within the siRNA [59]. In fact, the ability to synthesize siRNA with modify chemistries while retaining their regulatory function lead to the development of the enhanced stability chemistry (ESC) platform used in three out of the four FDA approved siRNA therapeutics [18-20, 60].

Another way to produce siRNAs follows the principals of enzymatic reactions which commonly starts from *in vitro* transcription (IVT) [61, 62]. Divergent from chemical synthesis, IVT requires a DNA template corresponding to target RNAs as well as proper RNA polymerases such as T7 phage RNA polymerase [62, 63]. Specifically, siRNA can be produced in two general steps. Firstly, IVTs are constructed to offer two complementary ssRNAs separately, which can be annealed to offer target double-stranded RNA (dsRNAs) [62, 64, 65]. Secondly, recombinant RNases such as Dicer are employed to further process the dsRNAs into desired siRNA agents [66,

67]. Of note, chemically synthesized RNA molecules can also be processed enzymatically to produce target siRNAs *in vitro* [62, 65].

Chemical modifications to siRNAs and miRNA mimics can be quite valuable to investigatory and clinical research, such as changes in phosphodiester backbone, ribose, nucleobases, or addition of non-nucleotide molecules [9, 16]. The theoretical goals of these optimizations are three fold. First, structural optimization may improve RNAi potency and target selectivity besides improved metabolic stability [68, 69]. Second, optimization may decrease therapeutic immunogenicity and therefore improve overall safety [25, 70]. Finally, optimization may increase tissue- or organ-targeting specificity by conjugating receptor specific ligands or by changing the physical conformation or chemical properties to increase uptake and endosomal escape into the cytosol [21, 25, 60, 69, 71-73].

Depending on forms of modifications, a synthetic siRNA can have variable advantages that change properties such as biological activity, thermodynamic stability, and nuclease resistance and are categorized based on the components modified [55]. For example, modifications to the 2' region of the ribose with 2′-O-methyl, 2′-fluoro, or 2′-O-(2-methoxyethyl) can reduce immunogenicity and improve stability and resistance to degradation by nucleases [25, 74]. SiRNA with a partially phosphorothioated (PS) backbone may increase non-specific, gymnotical uptake [75]. It was also reported that replacing the negatively charged phosphodiester backbone with a charge-neutralizing phosphotriester led to an alternative form of siRNAs termed short interfering ribonucleic neutrals that could aid in drug delivery [76].

MiRNA and siRNA functions in posttranscriptional gene regulation

Despite the differences in canonical and noncanonical biogenesis of miRNA as well as the introduction of exogenous RNAi agents, the mechanisms of actions of miRNAs and siRNAs once incorporated within the RISC are largely the same (**Figure 1**). However, the type of regulation imposed on the mRNA is dependent on the RNAi agent. SiRISC typically targets and cleaves a single, specific mRNA transcript leading to mRNA cleavage and degradation while miRISC typically targets several specific mRNA transcripts leading to translational repression, mRNA cleavage and degradation, or occasionally translational activation [32].

Furthermore, both siRNAs and miRNAs are typically selective to specific regions of the mRNAs to regulate gene expression. In general, miRISC act through imperfect or partial complementarity to the 3' untranslated region (3'UTR) of its target mRNA transcripts providing a wider range of target mRNA [32, 46, 47, 49, 53, 77]. Instead, the typical siRISC will create a perfect complimentary match to the protein coding region or coding DNA sequence (CDS) of a single target mRNA [12]. While this is true for most endogenous and synthetic siRNA, three of the FDA approved siRNA therapeutics actually follow the same mechanism of action as miRISC by binding to the 3'UTR, although they bind with perfect complementarity and designed to result in transcript cleavage (**Figure 2**) [78-80].

3. Therapeutic SiRNAs

Four siRNA medications (Patisiran, approved in 2018; Givosiran, 2019; Lumasiran, 2020; Inclisiran, 2021) have been approved by the United States FDA, adding to the growing list of oligoribonucleotide drugs [15, 16, 26]. The designs of these novel siRNA medications are founded on the basic functions and the adaptability of RNAi-based target gene regulation [17-20] (**Table 1**). To gain FDA approval, each siRNA-based medication underwent its own series of rigorous clinical trials to determine both the efficacy and safety.

FDA approved siRNA medications

Patisiran

The development and initial FDA approval of Patisiran (brand name: Onpattro®) in 2018 for the treatment of hereditary transthyretin-mediated amyloidosis (hATTR) (**Table 1**) ushered in a first-of-its kind RNAi therapeutic [17]. Amyloidosis is a rare buildup of amyloid plaques that are not directly produced within the body formed through the aggregation of several different protein types including transthyretin, a protein encoded by the transthyretin (TTR) mRNA transcript primarily produced in the liver [81, 82]. Amyloid formed in hATTR is molecularly characterized as an accumulation of misfolded TTR protein forming amyloid fibrils and clinically manifests as sensorimotor and autonomic neuropathy, cardiomyopathy, arrhythmia, dyspnea, shortness of breath, edema, carpal tunnel syndrome, renal impairment, vitreous opacities, glaucoma and/or pupillary disorders [82-85].

Patisiran is to exhibit effectiveness in specifically reducing the abundance of both the wild-type and mutant, misfolded forms of TTR by RNAi regulation [17]. Patisiran consists of two twenty-one-nucleotide long strands with eleven 2′-OMe modifications on all pyrimidines present in the sense strand and two uridines in the antisense strand, encapsulated within a lipid nanoparticle (LNP) [17, 78] (**Table 1**). This LNP (**Figure 2**) includes cholesterol and distearoylphosphatidylcholine (DSPC) [1,2-distearoyl-sn-glycero-3-phosphocholine] with the addition of polyethylene glycol (PEG)-lipids and ionizable amino DLin-MC3-DMA lipids to transport siRNA for circulation stability [86, 87]. The LNP assists in hepatocyte uptake of patisiran; upon endosomal release, the siRNAs are loaded into the RISC to specifically target and cleave TTR transcripts [82, 86, 87]. Interestingly, the actions of patisiran follows that of miRNAs by specifically target the 3'UTR (**Figure 2**) of TTR instead of the CDS region commonly targeted by a siRNA [82].

Prior to FDA approval, patisiran underwent a series of rigorous clinical trials. Initially, patisiran went through two Phase I, placebo-controlled clinical trials (NCT01559077 and NCT02053454), in particular, dose-escalation studies ranging from 0.01 to 0.5 mg/kg [88]. Phase II placebo-controlled clinical trials were broken into two arms, the first arm (NCT01617967) used a multiple ascending-dose study in patients afflicted by hATTR where patients receive multiple doses in ascending concentration of 0.01, 0.05, 0.15, or 0.3 mg/kg every four weeks or 0.3 mg/kg every three weeks [82, 89, 90]. The second arm was a long-term, placebo-controlled, and open-label extension (OLE) study (NCT01961921) for individuals who successfully completed the initial Phase II study to further characterize the safety and tolerability of long-term patisiran administration [82]. Finally, in the pivotal Phase III, placebo-controlled clinical trials (APOLLO;

NCT1960348), patients received an administration of patisiran (0.3 mg/kg) once every three weeks for 18 months [82, 91, 92]. Conclusion based on the completed Phase III study saw a significant improvement in hATTR clinical manifestations as well as in improvement of patient quality of life in patisiran-treated patients [92, 93]. In addition, the APOLLO clinical trials assessed the effects of patisiran treatment on the cardiac structure and function on hATTR patients and resulted in a reduction of cardiac wall thickness, global longitudinal strain as well as increased end-diastolic volume increased cardiac output suggesting that treatment may also reverse the effects of cardiac associated hATTR [94].

Evidence from clinical trials suggests patisiran to be well tolerated with a consistent and agreeable safety profile in afflicted patients, minimal dispersant of intravenous (iv) administered patisiran to off-target organs, and minimal drug accumulation following additional doses suggesting patisiran siRNA to be cleared via nuclease activity [78, 89, 93]. To further evaluate the safety and efficacy of long-term patisiran administration, patients who completed both the Phase II OLE and Phase III were enrolled into an ongoing global OLE study (NCT02510261) to [95]. Patisiran, is seeing a second ongoing Phase III clinical trial (NCT03997383) for hATTR in patients that suffer with a cardiomyopathy comorbidity. Today, patisiran is commercially available with a recommended dose of 0.3 mg/kg every 3 weeks administered through iv infusion over 80 minutes [17].

Overall, the impact of patisiran provided three major contributions to the areas of RNAi therapy. First, patisiran served as the first RNAi-based therapeutic approved by the FDA that is designed to use endogenous RNAi machinery to control the outcome of disease-causing proteins. This work carved a path of success that other RNAi therapeutics would soon follow. Second, the method of

action of patisiran closely mirrors that of endogenous miRNA by targeting the 3'UTR of TTR and supports the potential of future successful miRNA therapeutic development to combat disease. Finally, the development of patisiran is a foundation upon which ongoing research has improved and innovated RNAi technology to be widely applicable and appropriately manipulated to target and remedy molecular disease components.

Givosiran

Givosiran (brand name: Givlaari®) was the second siRNA drug to receive its first FDA approval in 2019 for the treatment of acute hepatic porphyria (AHP) [18] (**Table 1**). AHP is a rare genetic disorder derived from the liver and caused by a dysfunction within the heme synthesis pathway that causes an upregulation of aminolevulinate synthase 1 (ALAS1) and an increase ALAS1 protein expression [96-100]. Dysregulated ALAS1 expression is known to increase downstream production of neurotoxic metabolites, aminolevulinic acid and porphobilinogen, causing AHP [96, 97]. AHP is clinical characterized by severe and debilitating abdominal pain, hypertension, tachycardia, vomiting, seizures, paralysis, and often associated with neuropathy, chronic kidney disease, and liver disease [96, 100-102].

Givosiran is designed as an effective treatment against AHP by reducing the abundance of ALAS1 by RNAi regulation [18]. Givosiran consists of a double-stranded, chemically synthesized and fully modified twenty-three-nucleotide long antisense strand and twenty-one-nucleotide long sense strand with tri-N-acetylgalactosamine (GalNAc)-conjugation to enhance liver selective delivery [18, 100, 103]. Further, givosiran also uses sixteen 2′-F substitutions with the remaining

as 2′-OMe substitutions as well as six terminal PS chemical modifications [18] (**Table 1**). Unlike patisiran, givosiran is administered via subcutaneous (sc) injection to target and inhibit the translation of ALAS1 mRNA [18]. The tri-GalNAc delivery platform exploits the biological interaction between the GalNAc molecules found on damaged glycoproteins and the asialoglycoprotein receptor 1 (ASGR1) found at high levels on hepatocytes to target givosiran to the liver [100, 103] (**Figure 2**). The givosiran siRNA payload is designed to target a specific sequence on the CDS (**Figure 2**) of ALAS1, decrease ALAS1 protein abundance and the production of the neurotoxic metabolites, and treat AHP [100, 104].

Givosiran also underwent a series of rigorous clinical trials prior to regulatory approval. In Phase I, placebo-controlled clinical trials (NCT02452372) were separated into three dosing regiments based on patient AHP frequency: A (infrequent AHP; single-ascending dose sc injections of 0.035, 0.10, 0.35, 1.0, or 2.5 mg/kg), B (moderate frequency; once monthly dose sc injections of 0.35 or 1.0 mg/kg), and C (frequent; once monthly or quarterly dose sc injections of 2.5 or 5.0 mg/kg) [100, 105]. Patients who successfully completed Phase IC were enrolled in Phase I/II, placebo-controlled OLE with the goal to rapidly and sustainably lower hepatic ALAS1 mRNA and urinary neurotoxic metabolite levels as well as reduce the rate of AHP attacks in patients with ongoing attacks through extended givosiran treatment [100, 106]. In the pivotal Phase III, placebo-controlled clinical trials (ENVISION; NCT03338816) were performed on symptomatic patients who received once monthly sc injections of givosiran (2.5 mg/kg) for six months [100, 107].

Clinical evidence shows that givosiran-treated patients saw a significant reduction in AHP attacks (74%) and sustained reduction in urinary aminolevulinic acid and porphobilinogen neurotoxic

metabolite levels as well as decreased daily pain and an improved quality of life patients [100, 107]. However, success was accompanied by an increase in adverse hepatic and renal events seen in few givosiran-treated patients [100, 107]. In a later study designed to define further assess the safety and efficacy of givosiran showed evidence that regular givosiran treatments did indeed reduce the rate of AHP attacks, benefited patients with recurrent AHP attacks, improved quality of life, and supported the safety of givosiran [100, 108]. Today, givosiran is commercially available with a recommended dose of 2.5 mg/kg once a month via sc injection [18].

The success of givosiran provides three major impacts to the fields of molecular biology and therapeutics. First, as a chemically modified siRNA therapeutic givosiran serves as evidence that chemical alterations to RNAi technology can be implemented and manipulated to optimize molecular interactions to target and remedy disease. Second, the successful delivery of givosiran demonstrates a major advancement in RNAi therapeutics with a drug delivery platform capable of selective delivery to hepatocytes by the GalNAc delivery platform used in future siRNA therapeutics. Finally, givosiran further supports the use of RNAi-based therapeutics to combat diseases that can be largely at the mercy of ineffective treatment options or deemed undruggable targets by small molecules.

Lumasiran

Lumasiran (brand name: Oxlumo®), was the third siRNA medication to receive its first FDA approval in 2020 for the treatment of primary hyperoxaluria type 1 (PH1) [19] (**Table 1**). PH1 is a rare, autosomal recessive disorder originating in the liver that is caused by a decrease in

peroxisomal enzyme alanine-glycolate aminotransferase (AGT), an enzyme responsible for glyoxylate metabolism inhibition, and results in the deposition of calcium oxalate crystals in the kidneys and urinary tract [109, 110]. PH1 is clinically characterized by nephrolithiasis and nephrocalcinosis of the kidney leading to kidney disease or failure and systemic oxalosis, the systemic deposition of calcium oxalate crystals [109].

Lumasiran is designed as an effective treatment for PH1 by reducing the abondance of oxalate deposition by RNAi regulation alternative to dialysis, kidney transplant, or vitamin B6 supplementation [19, 109]. Lumasiran consists of a fully modified siRNA with a twenty-three-nucleotide long antisense strand, twenty-one long sense strand with tri-GalNAc-conjugation, and ten 2′-F, thirty-four 2′-OMe, and six terminal PS chemical modifications (**Table 1**) [19]. Lumasiran is also administered sc to patients with specific delivery to the liver and targets the 3'UTR (**Figure 2**) of the hydroxyacid oxidase 1 (HAO1) mRNA transcript that encodes glycolate oxidase (GO); an upstream enzyme in the oxalate overproduction pathway [19, 80, 103].

Like that of its predecessors, lumasiran underwent a series of rigorous trials to attain FDA approval. Initial Phase I/II, placebo-based clinical trials (NCT02706886) consisted of three different dosing regimens to determine appropriate dosing of either three monthly doses of 1 mg/kg, three monthly doses of 3 mg/kg, or two single doses of 3 mg/kg every three months, followed by an OLE [111]. The pivotal Phase III, placebo-controlled clinical trials were broken into three unique arms termed ILLUMINATE-A (NCT03681184), ILLUMINATE-B (NCT03905694), and ILLUMINATE-C (NCT03681184). ILLUMINATE-A studied the effects of lumasiran in children and adults over the age of six and received three months of lumasiran

followed by quarterly maintenance doses of 3 mg/kg that extended into a 54-month dose evaluation OLE period to assess safety and efficacy [110]. In ILLUMINATE-B, patients under the age of six received similar lumasiran treatments [112]. ILLUMINATE-C (NCT03681184) is currently ongoing and designed to evaluate the efficacy and safety of lumasiran for patients with advanced PH1 and estimated completion date of July 2025 [113]. Following the success of ILLUMINATE-A and ILLUMINATE-B, patients who successfully completed these studies were enrolled into an ongoing OLE period to evaluate the long-term efficacy and safety of lumasiran in adults and children with PH1 (NCT03350451) [113].

Based on evidence from clinical trials, lumasiran was well tolerated in both children and adult cohorts, demonstrated an acceptable safety, and was shown to beneficially reduce oxalate levels independent of age, sex, race, abnormal kidney function, vitamin B6 use, or history of symptomatic kidney stone events [110, 112]. Today, lumasiran is commercially available with a recommended sc administration dose dependent on body weight [19]. For patients less than 10 kg the recommended administration has a loading dose of lumasiran is 6 mg/kg once monthly for 3 doses followed by a once monthly maintenance dose of 3 mg/kg. For patients between 10 kg and 20 kg, the recommended administration has a loading dose of lumasiran is 6 mg/kg once monthly for 3 doses followed by a once quarterly maintenance dose of 6 mg/kg. For patients 20 kg and above, the recommended administration has a loading dose of lumasiran is 3 mg/kg once monthly for 3 doses followed by a once quarterly maintenance dose of 3 mg/kg.

The success and approval of lumasiran provides two major impacts to the fields of molecular medicine. First, lumasiran serves as additional RNAi-based therapeutics that further supports the

use of RNAi as a means to combat disease and the method of action of lumasiran once again closely mirrors that of endogenous miRNA and therefore further support the development of miRNA drugs. Second, successful administration and action of lumasiran further serves as evidence that RNAi technology can be implemented and manipulated to optimize molecular interactions to target and remedy disease.

Inclisiran

The most recent siRNA therapeutics approved by the FDA in 2021, inclisiran (brand name: Leqvio®), is a first-in-class siRNA medication designed to treat heterozygous familial hypercholesterolemia (HeFH) and clinical atherosclerotic cardiovascular disease (ASCVD) in combination with maximally tolerated statin therapy [20] (**Table 1**). Both HeFH and ASCVD are similarly characterized by an increase in low-density lipoprotein cholesterol (LDL-C) in circulation [114, 115]. HeFH is a familial, autosomal codominant genetic disorder caused by a protein mutation within lipoprotein metabolism that leads to a high accumulation of LDL-C in the blood plasma. Mutations in the LDL receptor (LDL-R) are identified in 85%-90% of cases and a gain-of-function (GoF) mutation in the proprotein convertase subtilisin/kexin type 9 (PCSK9) gene identified in roughly 1% of confirmed HeFH cases [115, 116]. PCSK9 is a low abundant circulating protein with a critical function in the low-density lipoprotein cholesterol metabolic pathway were a GoF mutation within the PCSK9 gene further enhances its function to decrease natural LDL recycling untimely resulting in hypercholesterolemia [116]. Chronic elevated LCL-C levels seen in hypercholesterolemia often results in a comorbidity with ASCVD, a thickening and loss of elasticity in the arterial wall [114, 115]. Prior to inclisiran, the PCSK9 inhibition was

facilitated through the use of two monoclonal antibodies, evolocumab and alirocumab, that function by blocking the LDL-R, however their safety and efficacy continue to be under investigation in based on data reported by Clinicaltrials.gov [117, 118].

Unique among siRNA therapeutics, inclisiran is designed as a supplemental, non-statin therapeutic to improve the effects of current treatments for cholesterol management by reducing the abondance of PCSK9 by RNAi regulation [20, 21, 114]. Inclisiran consists of a fully modified siRNA with a twenty-three-nucleotide long antisense strand, twenty-one-nucleotide long sense strand with tri-GalNAc-conjugation, and one 2′-MOE, eleven 2′-F, thirty-two 2′-OMe, and six terminal PS chemical modifications designed to target PCSK9 mRNA [20] (**Table 1**). Inclisiran is administered sc to patients to inhibit PCSK9 protein synthesis, decrease the influence if PCSK9 on natural LDL recycling by binding to the 3'UTR of PCSK9 mRNA and interfering with its translation [20, 79, 119, 120] (**Figure 2**).

As all approved siRNA therapeutics before it, inclisiran underwent a series of rigorous trials to prior to FDA approval. Initial Phase I, placebo-controlled clinical trials (NCT02314442) were broken into two arms to study the effects of inclisiran treatment. Arm one was a single-ascending dose study dosed at either 25, 100, 300, 500, or 800 mg and arm two was a multiple-ascending dose study with dose regimens of either four weekly doses at 125 mg, two doses every other week at 250 mg, or two monthly doses of either 300 or 500 mg done with or without combination statin therapy [121]. Phase II, placebo-controlled clinical trials (NCT02597127) in patients with elevated LDL-C serum levels and high cardiovascular disease risk had two multiple-ascending-dose trials, receiving either a single dose of either 200, 300, or 500 mg or patients received two doses at days

1 and 90 of either 100, 200, or 300 mg [122]. The pivotal Phase III, placebo-controlled clinical trials were broken into three unique arms termed ORION-9 (NCT03397121), ORION-10 (NCT03399370), and ORION-11 (NCT03400800). ORION-9 was performed on adults with heterozygous familial hypercholesterolemia receiving 300 mg administered on days 1, 90, 270, and 450 [123]. ORION-10 and ORION-11 were performed on patients on statin therapy with ASCVD or ASCVD and equivalent ASCVD risk, respectively, receiving 284 mg at day one and day ninety followed by a dose every six months thereafter for 540 days [124].

Clinical results indicate that inclisiran-treated patients saw a reduction of approximately 50% in LDL cholesterol levels of patients treated every six months [123, 124]. As a newly approved therapeutic, inclisiran is currently under several Phase III studies to assess the efficacy, safety, and tolerability of long-term dosing including ORION-8 (NCT03814187), ORION-13 (NCT04659863) and ORION-16 (NCT04652726) [125, 126]. With a recommended initial dose of 284 mg followed by a supplemental dose at three months and maintenance doses every six months administered via sc injection, inclisiran is commercially available and prescribed for combination therapy with the maximally tolerated statins [20].

The success following FDA approval of inclisiran in late December 2021 has three major impacts in the fields of molecular biology and therapeutics. First, the approval of inclisiran is further validation that canonical RNAi machinery is adaptable and that modification to RNAi technology can optimize molecular interactions to specifically target and remedy disease. Second, inclisiran is the third siRNA therapeutic to closely mirrors the function of endogenous miRNA and supports the use of miRNA drug development to combat disease. Finally, with the high incidence of

hypercholesterolemia, inclisiran offers a unique, first-in-class, non-statin treatment to help combat hypercholesterolemia; where a 1.0 mmol/L reduction in LDL is suggested to reduce adverse cardiovascular events by roughly 21% [117].

Continued studies into inclisiran explore the pharmacokinetics and safety as well as investigat emerging pharmacodynamic roles for inclisiran on biological function. In a 2022 study focused on the pharmacokinetics and pharmacodynamics of inclisiran in hepatic impaired patients, researchers found that patients with impaired hepatic function had approximately a two-fold increase in systematic exposure to inclisiran with little change in LDL-C compared to patients with no or mild hepatic impairment [127]. This suggested that hepatic impairment had little effect on treatment efficacy and showed no issues in the safety or tolerability of inclisiran which further suggested no need for dose adjustment for patients with mild or moderate hepatic impairment [127]. An additional study published recently looks into the effects of inclisiran on the formation of oxidized-LDL-induced (ox-LDL), macrophage-derived foam cells [128]. In this study, the authors found inclisiran to reduce lipid accumulation and inhibited macrophage-derived foam cell formation through the activation of the PPARγ pathway [128]. Since activation of the PPARγ pathway is important in fatty acid uptake and lipogenesis the results of this study suggest a possible off-target effect of inclisiran by increasing the expression of increased both the gene and protein expression of PPARγ [128, 129]. Investigations into the pharmacodynamic roles of therapeutics on biological function are critical not only for understanding how medications interact with the body but also to better understand what pathways or unknown interactions are inadvertently activated that may contribute to the success or potential adverse effects of a therapeutic.

Therapeutic siRNAs in clinical trials

In addition to the four FDA approved siRNA therapeutics, several other novel siRNA have entered clinical trials with several in preclinical development (**Table 2**). Of these, five have reached the pivotal Phase III clinical trials, namely fitusiran [130], nedosiran [131], teprasiran [132], tivanisiran [133], and vutrisiran [134].

Fitusiran

Fitusiran (ALN-AT3SC) is a therapeutic siRNA designed for the treatment of both Hemophilia A and B, and fitusiran is currently undergoing Phase II and Phase III clinical trials [130] (**Table 2**). Hemophilia A and B are X-linked bleeding disorders that are the result of mutations within the genes encoding coagulation factor VIII and IX, respectively, and interfere with normal blood clotting mechanisms of the body [135]. Fitusiran consists of a fully modified double-stranded siRNA of twenty-one- and twenty-three-nucleotides long with a tri-GalNAc-conjugate and contains twenty-one 2′-F substitutions, twenty-three 2′-OMe substitutions, and six PS modifications at the strand ends [136]. Fitusiran functions by inhibiting the production of the antithrombin proteins to increase the generation of pro-coagulation enzyme, thrombin, and improve the blood clotting mechanism [130, 137].

Nedosiran

Nedosiran (DCR-PHXC) is another therapeutic siRNA currently in Phase III clinical trials that is designed for the treatment of primary hyperoxaluria [131] (**Table 2**). Nedosiran consists of a nearly fully modified siRNA duplex that forms a tetraloop configuration through interactions between its twenty-two-nucleotide long antisense strand and thirty-six-nucleotide long sense strand with tri-GalNAc conjugation as well as nineteen 2′-F substitution, thirty-five 2′-OMe substitution, and six PS modifications [131, 138]. Nedosiran is an up-and-coming competitor of lumasiran that is being clinically assessed for the treatment of both PH1 and primary hyperoxaluria type 2 (PH2) subtypes of primary hyperoxaluria. However, instead of targeting the upstream GO protein mRNA, nedosiran is designed to target the mRNA of the hepatic enzyme lactate dehydrogenase (LDH), an enzyme that controls the final step in glyoxylate metabolism to oxalate [109, 131].

Teprasiran

Teprasiran (QPI-1002) is a therapeutic siRNA currently in Phase III clinical trials that is designed to treat acute kidney injury (AKI), specifically after kidney transplant or cardiovascular surgery [132, 139] (**Table 2**). AKI is not inherently classified as a disease, but instead is classified as a clinical syndrome that afflicts many hospitalized patients and is defined as an abrupt decrease in kidney function because of structural damage or impairment [140]. Teprasiran is unique among current siRNAs in that it only consists of 2′-OMe modifications. Specifically, half of ribonucleosides within the nineteen-nucleotide long siRNA duplex are comprised of 2′-OMe substitutions, and teprasiran is delivered as naked siRNA without other delivery system [132]. Teprasiran functions by targeting the mRNA of the well-known tumor suppressor protein, p53, which is involved in apoptotic induction during physiological stress [132, 141, 142].

Tivanisiran

Tivanisiran (SYL-1001) is a therapeutic siRNA designed for the treatment of ocular pain and dry eye disease (DED), and it is currently in Phase III clinical trials [133] (**Table 2**). DED is a multifactorial disease of the eye that results in several ocular abnormalities including pain, discomfort, dryness, itching, burning, and photophobia due to a disruption in the healthy tear film, ocular inflammation, or neurosensory abnormalities [143]. Tivanisiran stands alone as the only completely unmodified therapeutic siRNA composed of a nineteen-nucleotide long duplex in Phase III that is also delivered naked and without a delivery platform [133]. Tivanisiran functions by targeting the mRNA of transient receptor potential cation channel subfamily V member 1 (TRPV1) that plays an important role in several pathways including pain signal transduction, fibrogenesis modulation, the stress response, and the innate inflammatory response [133].

Vutrisiran

Vutrisiran (ALN-TTRSC02) is a therapeutic siRNA in Phase III clinical trials that is also designed for the treatment of hATTR [134] (**Table 2**). Vutrisiran is an up-and-coming competitor of patisiran since both are designed to treat hATTR. Vutrisiran consists of two fully modified strands of twenty-one- and twenty-three-nucleotides long with the latest version of the tri-GalNAc conjugate delivery platform, and it also contains thirty-five 2′-OMe, nine 2′-F, and contains six PS modifications at the strand ends [60, 144]. With improved delivery to the liver by tri-GalNAc conjugation, vutrisiran is believed to be a more potent than patisiran yet functions similarly in the

hepatocyte by targeting a conserved sequence on all TTR variants with similar actions as patisiran to treat hATTR [60, 134, 144].

MicroRNA-Based Therapies under Development

Strategies of miRNA-based therapies

Alongside the extensive list of siRNAs in clinical trials, several miRNA detection technologies are FDA approved and available today to determine miRNA profiles as potential biomarkers for clinical diagnostic or prognostic purposes [16, 145, 146]. In terms of miRNA-based interventions, there are two major approaches [14, 15, 147, 148]. One strategy, namely miRNA antagonism (anti-miR), is to inhibit or repress the expression or function of a target miRNA; and the other approach, namely miRNA replacement therapy, is to restore the expression or function of target miRNA.

Anti-miR therapy relies on sequence complementarity between the single stranded antagomir (or ASO) and target miRNA [149]. In particular, antagomirs inhibit miRNA function by complimentary hybridization and/or steric hindrance of miRNA with its target mRNA or for DNA/RNA hybridization degradation by RNase H [150-152]. There is also growing interest in developing small molecule compounds to interfere with miRNA biogenesis or function [15, 153-155]. Therapeutic antagomirs are typically deployed to target disease causing and overabundant miRNAs in the diseased cells, such as oncogenic miRNAs overexpressed in carcinoma cells [14, 156]. While miRNA replacement therapy restores miRNAs downregulated or completely lost in the diseased cells which actually function to suppress the disease, such as tumor suppressor

miRNAs [14]. Chemo-engineered miRNA mimics or viral or nonviral vectors expressing systems are typically deployed with the goal of reintroducing target miRNAs to combat disease [14, 15, 157].

While anti-miR therapy is the prominent miRNA-based intervention currently under clinical trials, the application of miRNA replacement therapy is exemplified in previous study focused on miR-29 mimicry to block pulmonary fibrosis [158]. MiR-29 was selected for this study based on its ability to regulate extracellular matrix proteins important in tissue fibrosis and is downregulated in fibrotic diseases [158, 159]. In this study, after confirming its functionality *in vitro*, the chemically modified, synthetic RNA duplex of miR-29 was injected iv into a mouse model of pulmonary fibrosis resulting in a sustained increase miR-29 levels and restored endogenous miR-29 function by decreasing collagen expression and treating the disease [158].

One major area of study is miRNA-based anticancer treatments to combat various types of cancer [16, 160]. This is because some miRNAs, such as let-7 and miR-34, are master regulators of gene expression with the capability to modulate several critical, homeostatic cellular pathways and functions that are often found dysregulated in cancer [10, 31, 160]. Specific miRNAs have emerging roles in particular cancer types including human papillomavirus (HPV)-related cancers [161], colorectal cancers [162], lung cancers [163], and acute myeloid leukemias [164] among others. As more and more oncogenic miRNAs are being examined, there has been a large influx of strategies aimed at miRNA inhibition such as: miRNA-masks, miRNA-sponges, and miRNA-zippers among others [160]. MiRNA-masks are ASOs designed to bind the 3'UTR of target mRNA and shield or protect the mRNA from endogenous miRNA regulation in an inhibitory manner [165,

166]. MiRNA-sponges are often circular RNA (circRNA) molecules that function as a decoy to sequester or “sponge” multiple miRNAs from their target mRNA transcripts and can more easily evade nuclease degradation compared to linearized ASOs [166, 167]. MiRNA-zippers are designed to connect miRNA molecules end-to-end forming a highly specific, highly stable DNA–RNA duplex to inhibit miRNAs from performing their functions [168].

Further, miRNA-based therapies are also used in combination with other well-established therapies towards optimal outcomes. In fact, combination therapy can come in many flavors and includes either miRNA antagonism in combination miRNA replacement therapy or a miRNA-based therapy in combination with existing or new treatment for a given disease. Combination therapies are most prevalent in anticancer therapy to play supportive roles in oncogenic miRNA inhibition or tumor-suppressive miRNA reintroduction. Some common forms of miRNA-based combination therapy include chemotherapy [169, 170], immunotherapy [171-173], radiotherapy [174-177], and photodynamic therapy [178] [179]. Of interest, one form of combination therapy uses multiple tumor-suppressor miRNA reintroduction or anti-miR miRNA inhibition to synergize and bolster the antitumor effects of treatment [180, 181]. In a 2016 article, the expression of miR-621 was demonstrated to be a predictive marker for chemosensitivity to paclitaxel plus carboplatin (PTX/CBP) treatment of breast cancer patients where elevated levels of miR-621 predicted a better response to PTX/CBP treatment [182]. Researchers further established this correlation in a combination therapy study demonstrating that increased ectopic expression of miR-621 increased chemosensitivity to PTX/CBP in vitro and in vivo [182]. This study demonstrates the promise of miRNA therapeutics and supports a potential role in combination thearpy.

MiRNA-based therapies in clinical trials

Several miRNAs have been and continue to be tested for remedies of several disease types (**Table 3**), including anticancer treatment. For example, MRX34, a mimic of miR-34a, was tested as an anticancer therapeutic in two Phase II clinical trials (NCT01829971; NCT02862145) for primary liver cancer (PLC), small cell lung cancer (SCLC), lymphoma, melanoma, multiple myeloma (MM), renal cell carcinoma (RCC), and non-small cell lung cancer (NSCLC). MiR-34a is a key regulator of tumor suppression controlling the expression of several targets involved in cell cycle (e.g., c-MYC, E2F, CDK4 and CDK6) and apoptosis (e.g., BCL2 and SIRT1), and tumor-associated processes such as invasion (e.g., c-MET) [183, 184]. MiR-34a has also shown antagonistic characteristics to cancer cell viability, stemness, metastasis and resistance to chemotherapy [184]. Decreased expression of miR-34a is often associated with several types of cancer, including MM [185] and melanoma [184, 186]. The molecular structure of MRX34 consists of a twenty-three-nucleotide long, double-stranded miRNA resembling the endogenous miR-34a duplex that is encapsulated in LNP for iv administered delivery to tumors located in the liver, bone marrow, spleen, lung, and a variety of other tissues [187]. Once delivered, MRX34 would interfere with target gene translation by binding to its complementary sequence in the 3′UTR of mRNAs. Although both Phase II trials were terminated due to immune related serious adverse events, MRX34 demonstrated a successful regulation of relevant target genes that provided the necessary proof-of-concept for the efficacy of miRNA-based anticancer therapy [188].

Alongside a promising future in miRNA-based anti-cancer therapy, miRNA also show potential in the treatment of cardiovascular disease. In particular, several miRNA are under investigation for their roles in cardiomyocyte necrosis, apoptosis, and autophagy as all as cardiac fibroblast proliferation, inflammation, and angiogenesis [189, 190]. One miRNA-based cardiovascular therapeutic, termed CDR132L, is currently starting Phase II clinical trials for the treatment of myocardial infarctions and acute heart failure of the left sided and functions as an antagomir of miR-132; a miRNA important in maladaptive cardiac remodeling, transformation, and hypertrophy (NCT05350969) (**Table 3**). A second miRNA-based cardiovascular therapeutic, MRG-110, is an antagomir of miR-92a, that has currently completed phase I clinical trials and is intended to promote angiogenesis by inhibiting the regulatory function of miR-92a (NCT03603431) (**Table 3**). Together these miRNA demonstrate the critical importance of miRNA regulation to cardiovascular health and further supports the potential for miRNA as a therapeutic strategy.

Miraviren (SPC3649), an antagomir of miR-122 (**Table 3**), is an example of miRNA antagonism therapy which was evaluated in Phase II clinical trials for the treatment of hepatitis C (NCT01727934; NCT01872936; NCT01200420). MiR-122 plays a central role in several aspects of liver function and is shown to stimulate hepatitis C virus (HCV) progression by binding the 5'UTR of the HCV genome [191]. As an anti-miR, miraviren has sequence complementarity to endogenous mature miR-122 and is composed of several locked nucleic acid (LNAs) ribonucleotides along a DNA PS sequence [192]. In its Phase 2a clinical trial (NCT01200420), miraviren-treated patients saw prolonged dose-dependent in HCV RNA levels following sc injection [193]. This early success of antagomirs demonstrated the functionality of anti-miR

therapy as the world's first miRNA-targeted drug and provided a revolutionary drug to treat HCV [194].

Following the footsteps of the CDR132L, MRG-110, and miraviren clinical trials, most current miRNA-based therapies in the clinic investigations are designed as anti-miR therapy discussed previously while restoring miRNAs that are lost or downregulated in diseased cells represents a less tapped means meriting greater attention. As highly potent regulators of gene expression, miRNAs make widely applicable therapeutic candidates since their biological function is to target several mRNA transcripts to potentially alter several cellular pathways [10]. This proves an opportunity for one therapeutic to target and alter the effects of several critical pathways found dysregulated in disease. However, it is this same natural property that limits the specificity of an miRNA as treatment to one disease causing pathway and increases the risk of off-target effects, therefore, complicating its pharmacology and candidacy as a therapeutics, such as seen with MRX34 [188, 195, 196]. This characteristic of miRNA has recently been termed "too many targets for miRNA effect" (TMTME), or in other words the complication that one miRNA therapeutic candidate does indeed have the ability to target many mRNA transcripts and therefore adds another major obstacle unique to miRNA in the path of succuss in clinical trials [158, 196]. While the probability for a single miRNA therapeutic to achieve its targeted effect is likely, the potency of miRNA towards effecting additional targets that are on-target for the miRNA itself but are off-target for the therapeutics, and can have unprecedented or unpreventable consequences depending on its pharmacological properties [195, 196]. Therefore, much work remains to be done to address toxic off-target effects and enhancing specific or targeted delivery platforms to develop and improve miRNA therapeutics with increased odds of clinical success.

However, in a recently published article researchers sought to tackle the challenge of TMTME by integrating data from multi-omic studies with a developed algorithm to identify candidate miRNAs with the potential for miRNA-based therapy for Ewing Sarcoma with minimal effect on essential housekeeping genes [197]. Their approach estimates the "network potential" of a tumor based on collective transcriptomic and protein-protein interactions within the tumor and ranks relevant target mRNAs and identifies prime miRNAs or miRNA combinations to repress those targets [197]. This work is a real time example of current research being done to improve the odds of clinical success and personalize miRNA therapeutics for the greatest effect on cancer progression.

Approaches and Challenges in Delivering RNAi Therapeutics

One obstacle faced by all forms of medications, including RNAi therapeutics discussed in this review, is to ensure an effective and safe level of therapeutic agents to overcome systemic barriers and access the target in specific cells, tissues or organs [16, 87, 198]. Without a viable strategy for protection or tissue-selective delivery, therapeutic RNAs face metabolism by circulating and liver enzymes, such as hydrolases and RNases, and rapid clearance from the body by the kidneys after administration, which both would limit target tissue distribution or delivery. Nevertheless, hepatic and nonhepatic metabolism as well as renal and biliary clearance are critical components for the body to eliminate xenobiotic agents, including medications and toxins.

Furthermore, since RNAi agents typically interact with intercellular components and on intracellular targets, they need to cross the cellular membrane which poses another major challenge

to delivery due to the large molecular structure and strong, negatively charged nature of RNA and oligonucleotide molecules. Therefore, tailoring "delivery" strategies toward favorable pharmacokinetic properties, including biodistribution of the right levels of therapeutic RNAs to the target tissues and into the target cells to selectively access molecular targets, is critical to achieve the desired efficacy and safety among patients. The introduction of chemical modifications [9, 16, 199], as discussed previously, is a proven approach that provides an advantage by increasing RNA metabolic stability, ensuring efficacious pharmacological actions, and avoiding non-selective or adverse effects. As such, delivery strategies using chemically modified siRNA such as patisiran, givosiran, lumasiran, and inclisiran discussed previously have attained FDA approval. However, chemical modifications introduce a disadvantage by compromising the initial chemical and physical characteristics and activities of naturally synthesized, modified, and folded RNA [15, 26, 27, 62]. In fact, recent studies on inclisiran discussed previously suggest possible off-target effects of the therapeutic away from its FDA designated biological activity providing the possibility for off-target effects even in RNAi designed with chemically modifications for target specificity [20, 128, 129].

Delivery platforms can also be tailored to the unique characteristics of a diseased cell. For example, some delivery tactics connect RNAi agents to tissue- or receptor-specific ligands, such as an antibody fragment, an entire antibody, or the FDA approved tri- GalNAc conjugate to target specific receptors or membrane proteins for internalization [18-20, 24, 25, 87]. While conjugating unique ligands or antibodies my improve tissue specificity or disease targeting, available natural ligands and target receptor density can be limiting factors to an effective delivery and by changing the chemical or physical makeup can add additional cost and complexity to both formulation and

delivery [87, 200]. RNA delivery with nanoparticle (NP) such as FDA approved LNPs for RNAi delivery discussed previously and polymer-based systems are also commonly used to improve blood pharmacokinetics [16, 17, 86, 87, 201-205]. For example, in a recently published article researchers implemented a liposome nanoparticle fitted with polymers consisting of six repeats of aspartate, serine and serine ($(DSS)_6$) that is shown to target bone formation surfaces to enhance the delivery of a casein kinase-2 interacting protein-1 (Ckip-1) mRNA targeting siRNA to osteogenic lineage cells involved in the progression of osteoporosis [206]. Both *in vitro* and *in vivo* findings supported this novel liposome-based osteoanabolic therapy to treat osteoporosis by targeting and deliver an siRNA payload [206].

By using NP formulation, an RNAi-based drug like patisiran can remain chemically unmodified or to a less degree but protected from degradation by serum RNases [17] (**Table 4**). However, NP-based formulations can be compromised by non-selective tissue distribution barring them from FDA approval for RNAi delivery (**Table 4**). Therefore, tissue- or receptor-specific ligands are under investigation and may be incorporated into NPs towards an optimal formulation to enhance target tissue delivery and drug internalization [16, 23, 87, 207, 208].

While an adaptable means of delivery, there is the concern about risk of inducing immunogenic effects by non-natural NPs themselves, beyond the RNAi macromolecules, and the barrier for endosomal escape once endocytosed [209-211]. To address these concerns, employing exosome-based delivery offer an alternative to NPs as endogenous vehicles under investigation that can load, protect, and deliver therapeutic RNAs [209, 211-213]. Exosomes are endogenous extracellular vesicles that play important roles in cell-cell communications and can transfer genetic

and biochemical information and fuse with cell membranes to directly deliver cargo into the cytoplasm [209]. Using exosomes over traditional NPs provides a more advantageous natural means of drug delivery that are hoped to increase delivery, membrane permeation efficiency, and biocompatibility to overcome both immunogenicity and endosomal escape [16, 209, 213-217]. One example is the exosome-GE11 peptide, a modified exosome with a surface GE11 peptide designed to target the epidermal growth factor receptor (EGFR) to deliver RNAi agents to EGFR-expressing cancer tissues [218]. However, the use of exosomes comes with some disadvantages including inefficient or low extraction, and isolation yield as well as exosome encapsulation and loading of hydrophilic molecules and the delivery of unwanted, off-target components inherent in exosome composition providing an opportunity for researchers to investigate and improve exosome extraction methodology, isolation yield, and loading prior to FDA approval for RNAi delivery [219].

Other methods of RNA delivery under investigation include viral systems to express genes holding their RNAi into desired tissues, inorganic material-based NPs such as gold-, mesoporous silicon-, graphene oxide-, or iron(III) oxide (Fe_3O_4)-mediated NPs, and polymeric vectors among others [87, 198, 220]. Each class of RNA delivery come with both advantages and disadvantages increasing the difficulty of choosing the most appropriate delivery vehicle. Viral systems including adenoviral, adeno-associated viral, retroviral, lentiviral vectors are useful for long-term gene expression by can transfer genes into different target tissues [220]. However, viral delivery is complicated by the induction of immunogenicity and toxicity as well as a low loading capacity impeding FDA approval for RNAi delivery [220, 221] (**Table 4**). Gold-mediated NPs can interact with thiol and amino functional groups that can be conjugated to RNAi agents to enhance loading

and delivery [220, 222, 223]. Mesoporous silica-mediated NPs provide more biocompatible a large, easily modified, and thermodynamically stable surface area [220, 224]. Graphene oxide-mediated NPs are contain a unique honeycomb-like network that can absorb a wide array of nucleic acids [220, 225]. Fe_3O_4-mediated NPs can form nanocomplexes with mesoporous magnetic clusters and link with polymeric vectors such as polyethylenimine (PEI) or polyacrylic acid (PAA) to load RNAi agents and increase uptake *in vivo* [220, 226]. However, much like viral based vectors, most non-viral vectors are limited in current clinical research and lack FDA approved use for RNAi delivery because of their toxicity and potential for off-target delivery [220] (**Table 4**).

In a recent publication, researchers had developed a novel delivery system for miRNA based on *in situ* self-assembly between gold (Au) salts and tumor suppressor miRNA mimics to form Au-miRNA nanocomplexes [223]. In this study, *in situ* self-assembled Au-miRNA nanocomplexes were found not only to be present in cancer cells and to inhibit proliferation *in vitro*, but also demonstrated tumor suppression and enhanced antitumor effects in sc tumor models *in vivo* [223]. Their novel and current work provides supportive evidence for NP delivery strategies to effectively transport large and negatively charged RNA and oligonucleotide molecules cargo. However, the most important aspect in the pursuit of "targeted delivery" is to develop and formulate a drug to improve its pharmacokinetics, pharmacodynamics, and safety profile all while simultaneously maintaining the drugs functionality and, in the case of RNAi, its interactions with endogenous RNAi machinery and intracellular target transcripts at the right level and right time to achieve the right outcomes [26, 196].

Novel Biotechnologies to Produce RNAi Agents

While chemical and biochemical synthesis remains a consistent means of RNA molecule production, there is a growing concern that these methods introduce changes to the physical and chemical properties of RNAi agents that likely exhibit distinct efficacy and safety profiles from those of naturally synthesized and modified RNA equivalents [15, 26, 27, 62]. To address these concerns, alternative methods have emerged to steer RNA production back into live cells for natural products. Two genres of *in vivo* RNA production are through direct expression using specific host bacteria strains and RNA production using stable carriers (**Figure 3**).

Direct expression

In vivo RNA production by direct expression was initiated by the identification of two bacterial strains, *Rhodovulum sulfidophilum* and an RNase III deficient-*Corynebacterium glutamicum* [227, 228] (**Figure 3**). *R. sulfidophilum,* is a marine phototrophic bacterium with the capability to efflux nucleic acids but not RNases [227, 229, 230] (**Figure 3**). Such characteristics allow *R. sulfidophilum* to accumulate RNA products in culture medium without fear of nuclease degradation and has shown success in producing a variety of RNA molecules such as tRNAs, rRNAs, aptamers [83, 231, 232] and human pre-miRNAs [233]. RNA accumulated in culture media can be isolated and purified to attain the target RNA molecule [62, 229] (**Figure 3**). However, direct expression by *R. sulfidophilum* demonstrated a low yield of recombinant RNA production that is likely due to an ineffective diffusion or efflux of RNA into the medium or the presence of intracellular RNases that can readily degrade recombinant RNAs before they can exit the cells and accumulate in medium [62, 227, 229].

Recent exploration into a novel strain of *C. glutamicum* is being studied to produce RNA molecules *in vivo* through direct expression [228, 234] (**Figure 3**). This particular strain of *C. glutamicum* lacks the RNAse III ribonuclease because of a disruption in its encoding gene (2256LΔrnc) [228, 234]. Therefore, in combination with a strong promoter driving the overexpression of recombinant RNA, target RNA can be accumulated in RNase III deficient-*C. glutamicum* towards mass production [228, 234] (**Figure 3**). This novel strain is expected to have direct application to *in vivo* production of biologic RNAs [62].

Another form of direct expression is co-expression of target RNA molecules with protective RNA-binding proteins. Plant RNA virus tombusvirus encoded 19 kD protein (p19) is an RNA-binding protein known to selectively bind and suppress the RNAi function of double-stranded siRNAs with high affinity and it is being implemented today for the isolation, detection, and stabilization of both siRNA and miRNA [235, 236]. Through co-expression, siRNA-embedded within an shRNA is designed to be processed by bacterial RNases to target siRNAs and form stable complexes with p19 to avoid degradation [235, 237]. Following co-expression, total protein containing siRNA-p19 complexes can be extracted from bacteria, purified, and the complexes can be dissociated with denaturing agents (e.g., SDS) for the fully processed and protected RNAi agents to be purified [62].

Using stable carriers

The use of stable carriers offers an alternative to direct expression. There are several stable carriers available to produce recombinant RNA molecules including viroid-derived circRNA carriers, tRNA or rRNA scaffolds, and chimeric tRNA/pre-miRNA carriers. The viroid-derived circRNA carrier is a relatively new form of stable carrier capable of producing large amounts of stable recombinant RNAs in *Escherichia coli* [238]. Viroids are a special class of infectious agents that contain short, single-stranded circRNAs found in higher plant species [239, 240]. The viroid-derived circRNA carrier uses the co-expression of two plasmids to produce and circularize recombinant RNA molecules into viroids [238]. The first plasmid offers the recombinant RNA-viroid molecule from the eggplant latent viroid (ELVd) to form the pLELVd-BZB plasmid [238], and the second plasmid produces the tRNA ligase used for viroid circularization into chimeric circRNA [238]. The viroid-carrying target RNA can be isolated from bacterial cell lysate and purified by gel electrophoresis or fast protein liquid chromatography (FPLC) methods [238].

Another form of stable carriers uses rRNA as a scaffold to produce recombinant RNA molecules in bacteria [241] (**Figure 3**). As the most abundant species of RNA found in living cells by mass, rRNA-based carriers resembling rRNA exploit endogenous recognition and are capable of accommodating and protecting target RNAs [241]. The 5S rRNA is used as a scaffold because of its stability to carry and protect a variety of sRNA molecules with DNAzyme-specific sequences within its stem II and stem III site structures [205, 241-243] (**Figure 3**). By using this stable carrier, a plasmid containing the 5S rRNA-scaffold with an embed target RNA can be overexpressed in bacteria by rRNA gene promoters, rrnB P1 and P2 and rRNA transcription terminators, rrnB T1 and T2, prior to recombinant RNA isolation and purification from cell lysate [241, 243]. Target

RNAs can then be selectively released from their rRNA-scaffold by DNAzyme-mediated recovery [241, 243].

Compared to rRNA, the tRNA offers a simple scaffold to produce recombinant RNA molecules in bacteria [244-246] (**Figure 3**). TRNA are an endogenous molecule found with high abundance in living cells, the tRNA scaffold uses intracellular recognition of the tRNA structure to carry recombinant RNA for overexpression and accumulation in bacteria [247, 248]. In this design, the tRNA anticodon sequence is replaced with an RNA sequence of interest all while leaving the remainder of the tRNA sequence intact to conserve the recognizable cloverleaf structure and overall stability of the tRNA *in vivo* [246] (**Figure 3**). To implement this stable carrier *in vivo*, a plasmid containing the recombinant RNA within a tRNA scaffold is overexpressed in *E. coli*, driven by a murein lipoprotein (lpp) promoter [245] or T7 promoter [244], and the overexpressed recombinant RNA is then isolated and purified from cell lysate. The tRNA scaffold has been successfully employed for the design and production of various RNA molecules including viral RNAs and aptamers [246], pre-miRNAs [249-251], and snoRNAs [252].

Recently, a novel hybrid tRNA/pre-miRNA carrier platform has been established for large-scale production of bioengineer RNA agents (BioRNA, previously termed BERA) by *in vivo* fermentation with high yield and purity [253-256] (**Figure 3**). The BioRNA consists of a ssRNA molecule with three major components, a tRNA scaffold linked to a pre-miR-34a sequence with an embedded, interchangeable miRNA duplex. As a result, BioRNA can accommodate a wide verity of target RNAi molecules including RNA aptamers and shRNA as well as miRNA, siRNA, or sRNA along with their complimentary sequence [26, 62, 148, 257]. After introduced into human

cells, it is likely that BioRNA enters into endogenous miRNA processing at the pre-miRNA step in the cytoplasm [62, 258] (**Figure 1**). However, both canonical processing and selective RNAi agent release [254-256, 259, 260] and Dicer-independent, non-canonical processing [255] of BioRNAs have been demonstrated, dependent on the RNAi sequence incorporated into the BioRNA.

In its initial design, BioRNA used a chimeric bacterial methionyl tRNA ($btRNA^{Met}$) fused with human hsa-pre-miR-34a ($btRNA^{Met}$/hsa-pre-miR-34a) to determine its capability of overexpression in bacteria [254]. What separates hybrid BioRNA from tRNA stable carriers is the inclusion of a pre-miR-34a as a critical component designed for effective and natural cleavage, guidance, and incorporation into the RISC complex by endogenous machinery [253]. To improve compatibility in human cells, the BioRNA design was adapted by substituting the bacterial tRNA with human versions [253]. Several human tRNA (htRNA) were screened and identified to effetely couple with hsa-pre-miR-34a, among them seryl ($htRNA^{Ser}$) and leucyl ($htRNA^{Leu}$) htRNAs led to an improved overexpressed in *E. coli*, making up over 40% of the total bacterial RNA [253].

The BioRNA carrier enables recombinant RNA production in live culture to yield more natural RNA molecules [253-255]. To do so, the protein coding sequence the BioRNA construct is cloned into a pBSTNAV vector with a lpp promoter and transformed into *E. coli* for fermentation and overexpression of the recombinant RNA [253]. Total RNA is then extracted from cell lysate and purified by anion exchange FPLC chromatography to yield an BioRNA product with preserved structure, stability, activity, and safety like that of endogenous RNAi molecules [251, 253, 255]. The resulting products are high-quality, biologically active RNA molecules that are well tolerated

in animal models and resemble the functions of endogenous cellular RNAi mechanisms [249, 253-255, 259-270].

Conclusions and Perspectives

Since its discovery, evidence suggests that RNAi is an adaptable and versatile tool that can be modified by researchers to study reverse genetics, specific gene repression, and develop targeted therapies. More importantly, the components that make up the RNAi pathway are not a static set of sequential steps but instead an expanding pool of adaptable components that function to deliver gene specific regulation (RNAi Molecules and Mechanisms) (**Figure 1**). This is evident in new and developing technologies that use the foundations of RNAi to develop novel synthesis, improve functionality, potency, stability, and pharmacology (**Figure 3**) as well as establish new methods of delivery (**Table 4**), and form groundbreaking therapeutic strategies against diseases by acting on previously considered un- or non-druggable targets. This notion is supported in the wake of the fourth therapeutic siRNA to gain approval by the FDA (inclisiran) and are further supported by the numerous RNAi-based therapeutics advancing through clinical trials (**Tables 1, 2, and 3**). However, with most RNAi therapeutics functioning as siRNA (**Tables 1 and 2**) or anti-miRs there are few miRNA mimics to made into clinical trials (**Table 3**). This leaves a vastly untapped market for miRNA replacement therapy. MiRNA has the unique property of targeting several mRNA transcripts and creates an opportunity for a single drug to regulate multiple targets or biological pathways that are often dysregulated in a disease. To achieve this, factors such as dosing, cross-reactivity, on-target efficacy, and unwanted effects need to be addressed through comprehensive basic and clinical research before they can attain regulatory approval.

Efforts continue to be made to bring the production of various RNAi molecules back into the cells and away from chemical modifications by using direct expression in bacteria and the use of stable carriers to preserve these natural properties while continuing to maintain stability, biological activity, and safety, discussed in the (Novel Biotechnologies to Produce RNAi Agents). Among them, the tRNA/pre-miRNA carrier-based platform technology has proven to be a robust and versatile means of harnessing *in vivo* RNA production of biologically active miRNAs, siRNAs, aptamers, and sRNAs that are designed to recapitulate several of the physical and chemical properties of natural RNA molecules needed for RNAi-based therapy. Future research exploring the use of bioengineered or recombinant RNAi molecules against chemo-engineered RNA analogs will provide insight and define their efficacy as biochemical candidates for both biological research and as clinical treatments for disease.

Table 1. FDA approved siRNA medications. Abbreviations: A, adenosine; Af, adenine 2'-F ribonucleoside; AHP, acute hepatic porphyria; ALAS1, aminolevulinate synthase 1; Am, adenine 2'-OMe ribonucleoside; ASCVD, atherosclerotic cardiovascular disease; C, cytidine; Cf, cytosine 2'-F ribonucleoside; Cm, cytosine 2'-OMe ribonucleoside; dT, thymidine; G, guanosine; Gf, guanine 2'-F ribonucleoside; Gm, guanine 2'-OMe ribonucleoside; HAO1, hydroxyacid oxidase 1; hATTR, hereditary transthyretin-mediated amyloidosis; HeFH, heterozygous familial hypercholesterolemia; L96, tri-N-acetylgalactosamine; PCSK9, proprotein convertase subtilisin/kexin type 9; PH1, primary hyperoxaluria type 1; s, phosphorothioate; TTR, transthyretin; U, uracil; Uf, uracil 2'-F ribonucleoside; Um, uracil 2'-OMe ribonucleoside.

Medication	Chemistry	Target	Disease	FDA Approval	Reference
Patisiran (Onpattro®)	Sense: 5’-GUmAACmCmAAGAGUmAUmUmCmCmAUmdTdT-3’ Antisense: 3’-dTdTCAUmUGGUUCUCAUmAAGGUA-5’	TTR	hATTR	2018	[17]
Givosiran (Givlaari®)	Sense: 5’-CmsAmsGmAmAmAmGfAmGfUmGfUmCfUmCfAmUmCmUmUmAm-L96-3’ Antisense: 3’-UmsGmsGmUfCmUfUmUfCmUfCmAfCmAfGmAfGmUfAmGfAfsAfsUm-5’	ALAS1	AHP	2019	[18]
Lumasiran (Oxlumo®)	Sense: 5’-GmsAmsCmUmUmCfAmUfCfCfUmGmGmAmAmAmUmAmUmAm-L96-3’ Antisense: 3’-AmsCmsCmUmGmAmAmAfGmUfAmGmGmAmCfCfUmUfUmAmUmsAfsUm-5’	HAO1	PH1	2020	[19]
Inclisiran (Leqvio®)	Sense: 5’-CmsUmsAmGmAmCmCfUmGfUmdTUmUmGmCmUmUmUmUmGmUm-L96-3’ Antisense: 3’-AmsAmsGmAmUmCfUmGfGmAfCmAfAmAfAmCfGmAfAfAfAmsCfsAm-5’	PCSK9	HeFH and ASCVD	2021	[20]

Table 2. Therapeutic siRNAs in clinical trials. Abbreviations: ACC, adrenocortical carcinoma; AKI, acute kidney injury; DED, dry eye disease; AMD, age-related macular degeneration; ARF, acute renal failure; CNV, choroidal neovascularization; DGF, delayed graft function; DME, diabetic macular edema; DR, diabetic retinopathy; hATTR, hereditary transthyretin-mediated amyloidosis; HCC, hepatocellular carcinoma; NAION, non-arteritic anterior ischemic optic neuropathy; PDAC, pancreatic ductal adenocarcinoma; PDC, pancreatic ductal carcinoma.

Product	Sponsor Company	Target	Disease	Current Development
Fitusiran (ALN-AT3SC)	Sanofi Genzyme	Antithrombin	Hemophilia A & B	Phase III – NCT03417245 (ATLAS-A/B) Phase III – NCT03417102 (ATLAS-INH) Phase III – NCT03549871 (ATLAS-PPX) Phase II/III – NCT03974113 (ATLAS-PEDS) Phase III – NCT03754790 (ATLAS-OLE)
Nedosiran (DCR-PHXC)	Dicerna Pharmaceuticals	Hepatic LDH	Primary Hyperoxaluria	Phase III – NCT04042402 (PHYOX3) Phase II – NCT05001269 (PHYOX8)
Teprasiran (QPI-1002)	Quark Pharmaceuticals	p53	AKI	Phase III – NCT02610296 (ReGIFT)
Tivanisiran (SYL-1001)	Sylentis S.A.	Transient Receptor Potential Cation Channel Subfamily V member 1	Ocular Pain and DED	Phase III – NCT03108664 (HELIX)
Vutrisiran (ALN-TTRSC02)	Alnylam Pharmaceuticals	Transthyretin	hATTR	Phase III – NCT03759379 (HELIOS-A) Phase III – NCT04153149 (HELIOS-B)
Cosdosiran (QPI-1002)	Quark Pharmaceuticals	Caspase-2	NAION	Phase II/III (Terminated) - NCT02341560

AGN211745 (Sirna-027)	Allergan	VEGFR1	CNV and AMD	Phase I/II - NCT00363714
PF-04523655	Quark Pharmaceuticals	VEGFR1	AMD	Phases I - NCT00725686
			AMD	Phase II - NCT00713518
			CNV, RN, and DME	Phase II - NCT01445899
siG12D LODER	Silenseed Ltd	KRASG12D	PDAC Pancreatic Cancer	Phase I - NCT01188785 Phase II - NCT01676259
TKM-080301	Arbutus Biopharma Corporation	PLK1	HCC	Phases I/II - NCT02191878
			Neuroendocrine Tumors and ACC	Phase I/II - NCT01262235
Atu027	Silence Therapeutics GmbH	Protein Kinase N3	Advanced Solid Tumors	Phase I - NCT00938574
			PCD	Phases I/II - NCT01808638
TD101	Pachyonychia Congenita Project	KRT6A	Pachyonychia congenita	Phase I - NCT00716014
ARC-520	Arrowhead Pharmaceuticals	cccDNA-derived viral mRNA	Safety/Tolerability in Healthy Volunteers	Phase I - NCT01872065
QPI-1002	Quark Pharmaceuticals	p53	ARF and AKI	Phase I - NCT00554359
			DGF and Complications of Kidney Transplant	Phases I/II - NCT00802347

Table 3. MiRNA-based therapies in clinical and preclinical investigations. Abbreviations: AHF, acute heart failure; ARBCP, abnormal red blood cell production; CHF, chronic heart failure; CMD, cardiometabolic disease; MPM, malignant pleural mesothelioma; MI, Myocardial Infarction; NAFLD, nonalcoholic fatty liver disease; NASH, non-alcoholic steatohepatitis; NSCLC, non-small cell lung cancer; PAD, peripheral arterial disease; PKD, polycystic kidney disease; PLC, primary liver cancer; RCC, renal cell carcinoma; SCLC, small cell lung cancer.

Product	Sponsor company	miRNA	Disease	Current Development
Miravirsen (SPC3649)	Roche/Santaris	Anti-miR-122	Hepatitis C	Phase II - NCT01727934, NCT01872936, NCT01200420
CDR132L	Cardior Pharmaceuticals GmbH	Anti-miR-132	MI and AHF (Left Sided)	Phase II - NCT05350969
Lademirsen (SAR339375, RG-012)	Sanofi Genzyme	Anti-miR-21	Alport syndrome	Phase I - NCT03373786
AZD4076 (RG-125)	AstraZeneca	Anti-miR-103/107	NAFLD	Phase I - NCT02826525
			NASH	Phase I - NCT02612662
RGLS4326	Regulus Therapeutics	Anti-miR-17	PKD	Phase I - NCT04536688
TargomiRs	Asbestos Diseases Research Foundation	miR-16 mimic	MPM and NSCLC	Phase I - NCT02369198
MRX34	Mirna Therapeutics	miR-34 mimic	Melanoma	Phase I/II (Withdrawn) - NCT02862145
			PLC, SCLC, Lymphoma, Melanoma, Multiple Myeloma, RCC, and NSCLC	Phase I (Terminated) - NCT01829971
Remlarsen (MRG-201)	MiRagen Therapeutics/Viridian	miR-29 mimic	Keloid	Phase II - NCT02603224 NCT03601052
MRG-110		Anti-miR-92a	Angiogenesis/ Ischemia	Phase I - NCT03603431
MRG-107		Anti-miR-155	Atherosclerosis	Preclinical
MGN-1374		Anti-miR-15 and Anti-miR-195	Post-Myocardial Infarction	Preclinical

MGN-2677	Anti-miR-143/145	Vascular Disease	Preclinical
MGN-4220	Anti-miR-29	Cardiac Fibrosis	Preclinical
MGN-4893	Anti-miR-451	ARBCP – like disorders	Preclinical
MGN-5804	Anti-miR-378	CMD	Preclinical
MGN-6114	Anti-miR-92	PAD	Preclinical
MGN-9103	Anti-miR-208	CHF	Preclinical

Table 4. Non-viral systems and vehicles for the delivery of RNAi therapeutics. Abbreviations: ELV, exosome-like vesicle; DSPC, [1,2-distearoyl-sn-glycero-3-phosphocholine]; Fe_3O_4, Iron(III) oxide; LNP, lipid nanoparticle; NP, nanoparticle; PACE, poly(amine-co-ester); PEG, polyethylene glycol; PEI, polyethylenimine; tri-GalNAc, tri-N-acetylgalactosamine.

RNAi Delivery Means	System Composition	FDA Approved RNAi Medications
Ribonucleoside modifications	Adenine 2'-F ribonucleoside	Yes – Givosiran; Lumasiran; Inclisiran
	Adenine 2'-OMe ribonucleoside	Yes – Givosiran; Lumasiran; Inclisiran
	Cytosine 2'-F ribonucleoside	Yes – Givosiran; Lumasiran; Inclisiran
	Cytosine 2'-OMe ribonucleoside	Yes – Patisiran; Givosiran; Lumasiran; Inclisiran
	Guanine 2'-F ribonucleoside	Yes – Givosiran; Inclisiran
	Guanine 2'-OMe ribonucleoside	Yes – Givosiran; Lumasiran; Inclisiran
	Thymidine	Yes – Patisiran; Inclisiran
	Uracil 2'-F ribonucleoside	Yes – Givosiran; Lumasiran
	Uracil 2'-OMe ribonucleoside	Yes – Patisiran; Givosiran; Lumasiran; Inclisiran
Phosphate linkage modifications	Phosphorothioate	Yes – Givosiran; Lumasiran; Inclisiran
	Charge-neutralizing phosphotriester	No
Receptor ligand conjugates	Tri-GalNAc	Yes – Givosiran; Lumasiran; Inclisiran
Antibody conjugates	Entire Antibody	No
	Antibody fragment	No
LNP	DSPC	Yes – Patisiran
	PEG-lipids	Yes – Patisiran
	Ionizable	Yes – Patisiran
Polymer-based NP	PEI	No
	PEI-PEG	No
	Polyurethane	No
	PACE	No
	Micelle	No
Inorganic material-based NP	Gold-mediated	No
	Mesoporous silicon	No
	Graphene oxide-mediated	No

	Fe_3O_4-mediated	No
Liposome	Neutral	No
	Cationic	No
	pH-sensitive cationic	No
	Ionizable	No
	Chemotherapeutic coated	No
Exosome	Exosome	No
	Exosome-GE11 peptide	No
	ELV	No

Figure legends

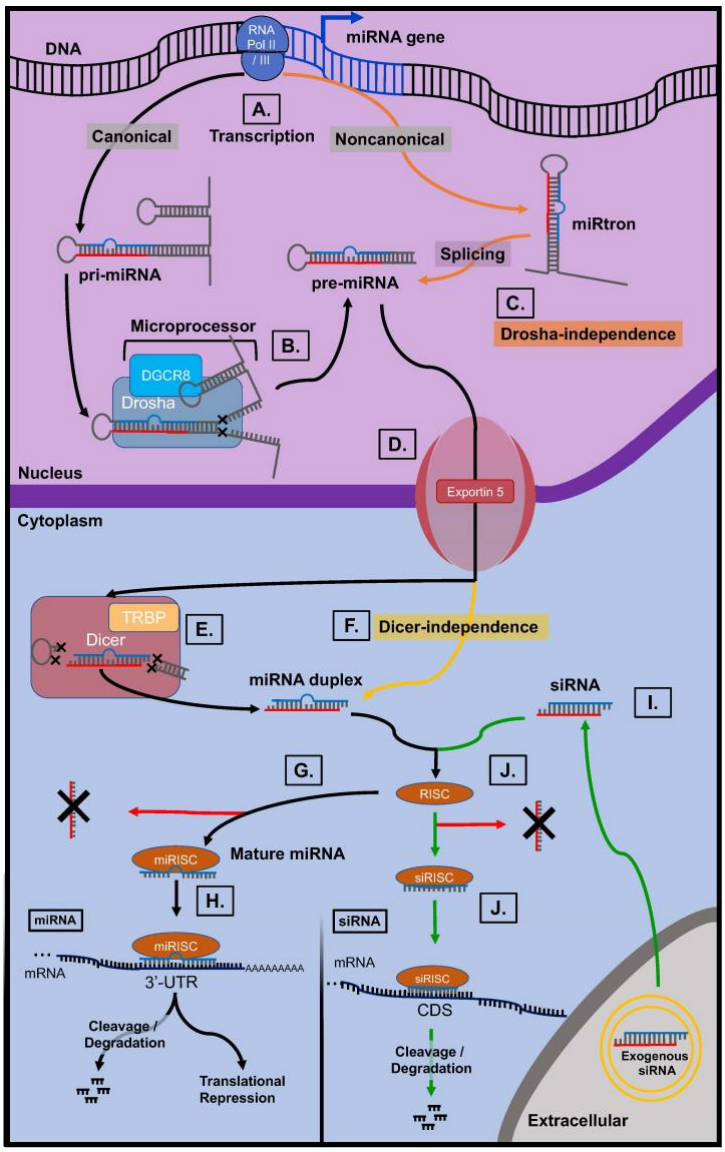

Figure 1. Overview of miRNA biogenesis and functions and siRNA mechanisms of action. (**A**) Intragenic or intergenic miRNA genes are transcribed by RNA polymerases II or III into primary miRNA (pri-miRNA; > 1,000 nt) transcripts in canonical pathway (black lines). (**B**) Pri-miRNAs are subjected to nuclear processing by the microprocessor, Drosha-DGCR8 complex, to release shorter precursor miRNAs (pre-miRNAs) (e.g., ~65 nt). (**C**) Noncanonical miRNA transcripts (e.g., miRtrons) are derived from the genome and subjected to RNA splicing to form pre-miRNAs independent on the microprocessor (orange lines). (**D**) Pre-miRNAs are exported into the cytoplasm via Exportin 5 transport complex. (**E**) In the cytoplasm, pre-miRNAs are processed by Dicer/TRBP complex to form miRNA duplexes (18-25 nt). (**F**) Dicer-independent production of miRNA duplexes (yellow). (**G**) The guide strand (blue) of the miRNA duplex is selected and loaded into the RNA-induced silencing complex (RISC) to form the miRNA-RISC complex (miRISC) while the passenger strand (red) is degraded. (**H**) Functional miRNA binds to the 3'-untranslated region (3'UTR) of targeted mRNA to perform posttranscriptional gene regulation, either to accelerate mRNA cleavage or degradation or repress translation. (**I**) Exogenous siRNAs can be introduced into cytoplasm through endocytosis or receptor-mediated uptake (green). (**J**) The antisense strand (blue) is selectively loaded into the RISC to form the siRNA-RISC complex (siRISC) while the sense strand (red) is degraded. (**K**) Functional siRNA typically acts on the protein coding sequence (CDS) of target transcript to cleave or initiate transcript degradation.

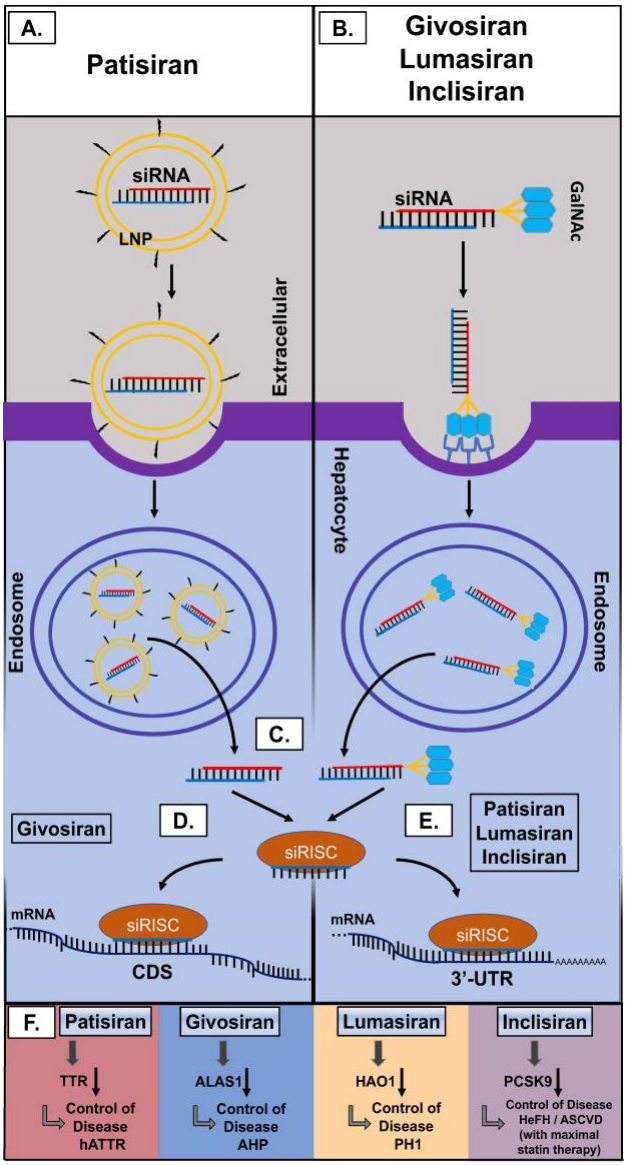

Figure 2. Common actions of four FDA approved siRNA medications in hepatocytes. (**A**) Patisiran is a double stranded siRNA drug (sense in red, and antisense in blue) formulated in a lipid nanoparticle (LNP) decorated with polyethylene glycol (pegylation) and it is administered intravenously for the treatment of hereditary transthyretin-mediated amyloidosis. The LNP induces an opsonization-based immune response and is endocytosed by the hepatocyte prior to endosomal escape. (**B**) Givosiran, lumasiran, and inclisiran, in which the sense strand (red) is conjugated with three *N*-acetylgalactosamine (GalNAc) moieties, are administered sc for the treatments of acute hepatic porphyria, primary hyperoxaluria type 1, and heterozygous familial hypercholesterolemia, respectively. The GalNAc moieties are recognized by asialoglycoprotein receptor 1 (ASGR1), which is highly expressed on the surface of hepatocytes, to facilitate the uptake of siRNAs. (**C**) The antisense strand (blue) is preferably loaded into the RNA-induced silencing complex (RISC) to form the siRNA-RISC complex (siRISC) while the passenger strand (red) is degraded. (**D**) Givosiran-derived siRISC binds to the protein coding sequence (CDS) of target mRNA towards cleavage or degradation. (**E**) Patisiran-, lumasiran-, and inclisiran-derived siRISC interact with the 3'-untranslated regions (3'UTRs) of target mRNAs to achieve gene silencing. (**F**) SiRNA drugs (givosiran, patisiran, lumasiran, and inclisiran) target specific mRNAs to achieve control of their respective diseases. Abbreviations: AHP, acute hepatic porphyria; ALAS1, aminolevulinate synthase 1; HAO1, hydroxyacid oxidase 1; hATTR, hereditary transthyretin-mediated amyloidosis; HeFH, heterozygous familial hypercholesterolemia; PCSK9, proprotein convertase subtilisin/kexin type 9; PH1, primary hyperoxaluria type 1; TTR, transthyretin.

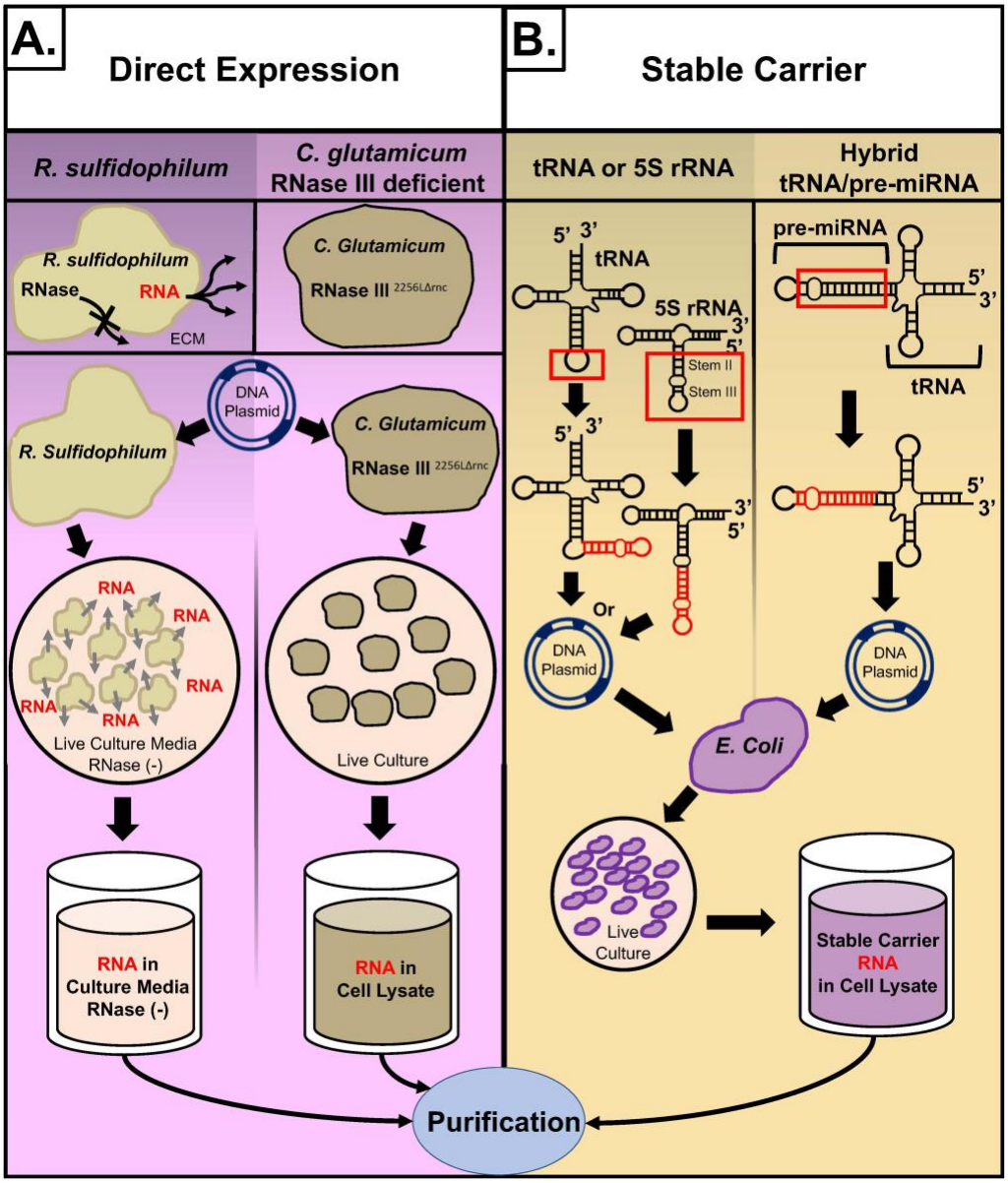

Figure 3. Novel biotechnologies to produce RNAi agents. (**A**) Direct expression is one class of novel RNAi agent production. Two forms of direct expression make use of two bacterial strains, *Rhodovulum sulfidophilum* and an RNase III deficient-*Corynebacterium glutamicum.* The marine phototropic bacterium *R. sulfidophilum* has the capability to efflux oligonucleotides such as RNA but not RNases. These characteristics allow researchers to transform *R. sulfidophilum* with an RNA-expressing plasmid to directly express the target RNA followed by efflux and accumulate in RNase-free culture media and can be isolated and purified to attain the target RNA molecule. A novel strain of *C. glutamicum* containing a mutation in the RNase III gene (2256LΔrnc) and provides an RNAse III ribonuclease-free bacterium for RNA accumulation. Target RNA may be directly expressed and accumulated in *C. glutamicum* free from RNase degradation for later isolation from cell lysate and purification. (**B**) The use of stable carriers constitutes a second class of novel RNAi agent production. Transfer RNA (tRNA) and ribosomal RNA (rRNA) can each function as stable RNA scaffolds. By retaining structures and sequences of these highly abundant RNA classes, target RNA is expected to exploit endogenous recognition and accumulate within bacteria. As many recombinant RNAs cannot be overexpressed with tRNA or rRNA scaffold, specific hybrid tRNA/pre-miRNA molecules showing high-level expression in *E. coli* has been identified, developed, and proven as unique carriers to effectively accommodate a wide verity of target RNAi molecules including RNA aptamers, miRNAs, siRNAs, or sRNA along with their complimentary sequences for high-yield and large-scale production of biologic RNAi agents.

Chapter 2: The Growing Class of Novel RNAi Therapeutics

Abstract

The clinical use of RNA interference (RNAi) molecular mechanisms has introduced a novel, growing class of RNA therapeutics capable of treating diseases by controlling target gene expression at the posttranscriptional level. With the newly approved nedosiran (Rivfloza™), there are now six RNAi-based therapeutics approved by the United States Food and Drug Administration (FDA). Interestingly, five of the six FDA-approved small interfering RNA (siRNA) therapeutics [patisiran (Onpattro™), lumasiran (Oxlumo™), inclisiran (Leqvio™), vutrisiran (Amvuttra™), and nedosiran (Rivfloza™)] were revealed to act on the 3'-untranslated regions of target mRNAs, instead of coding sequences, thereby following the common mechanistic action of genome-derived microRNAs (miRNA). Furthermore, three of the FDA-approved siRNA therapeutics [patisiran, givosiran (Givlaari™), and nedosiran] induce target mRNA degradation or cleavage via near-complete rather than complete base-pair complementarity. These features along with previous findings confound the currently held characteristics to distinguish siRNAs and miRNAs or biosimilars, of which all converge in the RNAi regulatory pathway action. Herein, we discuss the RNAi mechanism of action and current criteria for distinguishing between miRNAs and siRNAs while summarizing the common and unique chemistry and molecular pharmacology of the six FDA-approved siRNA therapeutics. The term "RNAi" therapeutics, as used previously, provides a coherently unified nomenclature for broader RNAi forms as well as the growing number of therapeutic siRNAs and miRNAs or biosimilars that best aligns with current pharmacological nomenclature by mechanism of action.

Graphical Abstract

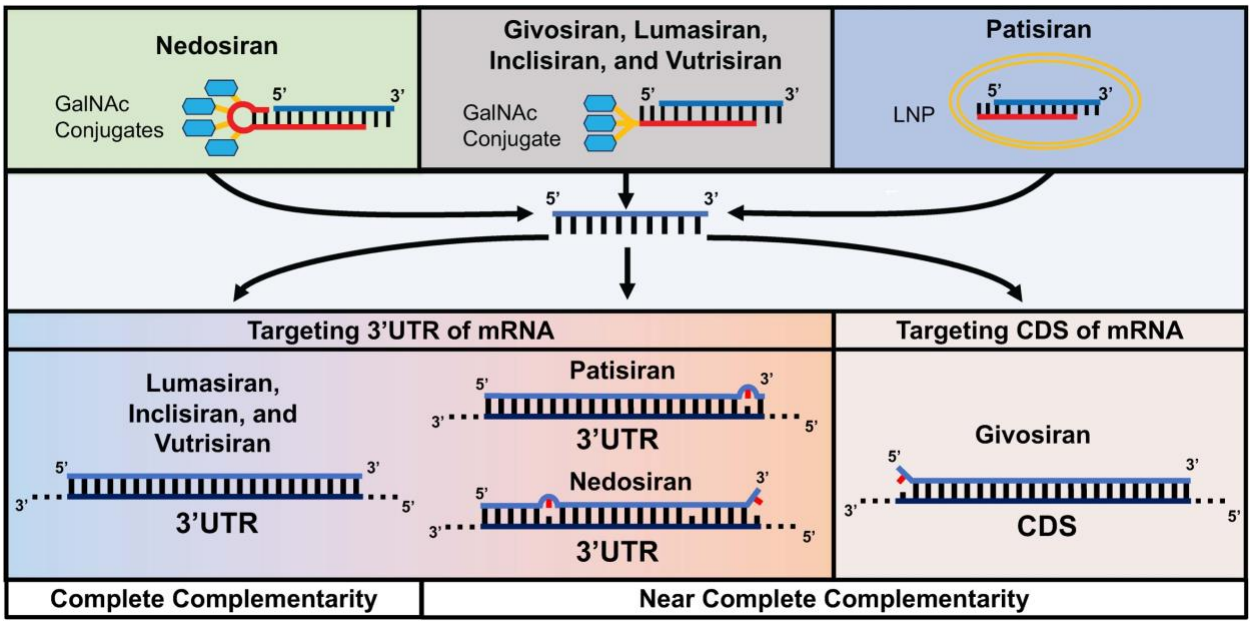

Significance Statement

The common and unique chemistry and molecular pharmacology of six FDA-approved siRNA therapeutics are summarized, in which nedosiran is newly approved. We point out rather a surprisingly mechanistic action as miRNAs for five siRNA therapeutics and discuss the differences and similarities between siRNAs and miRNAs that supports using a general and unified term "RNAi" therapeutics to align with current drug nomenclature criteria in pharmacology based on mechanism of action and embraces broader forms and growing number of novel RNAi therapeutics.

Introduction - RNAi tools and therapeutics

Since the discovery of functional, small noncoding RNAs, RNA interference (RNAi) has been revealed as a critical mechanism in cells to govern posttranscriptional gene regulation [1, 2, 6, 54] that has provided researchers with the foundational means to selectively manipulate target gene expression and develop novel therapies [15, 148, 271-275]. The major forms of RNAi molecules, genome-derived microRNAs (miRNA) or exogenous miRNA mimics or biosimilars and exogenously introduced small interfering RNAs (siRNAs), converge into the RNA-induced silencing complexes to achieve posttranscriptional gene regulation (**Fig. 1A**) [273, 276, 277]. Endogenous miRNAs have been revealed to control target gene expression through the cleavage, degradation, and/or translational repression of the targeted mRNA that may be dependent on the extent of miRNA-mRNA sequence complementarity ranging from partial (e.g., only requiring 7-9 nt from the 5' end of a 22-nt miRNA) to near complete base pairing [278-282]. By contrast,

exogenous siRNAs are often designed to target a singular, specific mRNA sequence through complete base-pair complementarity to exert mRNA cleavage and degradation [116, 283-289]. Besides double-stranded miRNAs and siRNAs, their respective precursors, namely single-strand pre-miRNAs and short hairpin RNAs (shRNA), are also employed to achieve target gene regulation upon entering the RNAi machineries [21, 274, 290-293].

Furthermore, while it is well established that canonical miRNA-controlled gene regulation is enhanced when acting on the 3'-untranslated region (3'UTR) of target mRNAs [276, 294], some miRNAs exhibit non-canonical binding at the protein coding sequence (CDS) in the vicinity of rare codons or within CDS repeats [276, 277]. Even so, it should be noted that binding to the 3'UTR of target mRNA remains the main criterion for the prediction of miRNA target sites [277] and tend to be both more selective and effective around 15 nt downstream of the stop codon [294]. Controversially, there has yet to be a clear definition regarding the primary target binding sites for siRNAs, although siRNAs are traditionally and usually designed to target the CDS segments of their respective mRNAs [15, 273, 284, 287, 295]. Designing siRNA in this way is typically favored to take advantage of CDS harboring fewer polymorphisms and more conserved sequences compared to the UTRs [283-285, 295]. Rather, given their effectiveness in controlling target gene expression, RNAi molecules continue to be developed as novel therapeutics whose chemistry and clinical pharmacology are different from conventional small molecule and protein therapeutics [148, 272, 273, 296].

Since 2018, a total of six siRNA therapeutics have been approved by the United States Food and Drug Administration (FDA) for the treatment of various diseases through the RNAi regulatory

mechanism [148, 272, 273, 297], in which nedosiran was approved most recently for the control of hyperoxaluria (**Fig. 1B**; **Table 1**) [297]. The growing number and expanding disease indications of approved siRNA therapeutics provide incentives to develop more RNAi therapies. Interestingly, in-house sequence alignment analyses of vutrisiran and nedosiran antisense sequences with their mRNA targets, transthyretin (TTR) [298, 299] and lactate dehydrogenase enzyme A (LDHA) [297], respectively, have revealed that both act on the 3'UTRs of their respective targets, following the canonical miRNA mechanistic action. Thus, vutrisiran and nedosiran follow similar mechanistic actions of patisiran, lumasiran, and inclisiran disclosed very recently [148, 273]. By contrast, only one (givosiran) of the six FDA-approved siRNA therapeutics is directed to interfere with the CDS of its target mRNA (**Fig. 1B**). In addition, the antisense strands of patisiran, givosiran, and nedosiran [17, 18, 297, 300, 301] contain one or two mismatched nucleotides to their corresponding target mRNA sequences. Indeed, previous works have showed that both miRNAs and siRNAs share overlapping characteristics in base-pairing complementarity as well as regulatory mechanisms [282, 289, 302, 303], yet they still retain their respective nomenclatures. While the current drug labels are informative regarding the chemistries of individual siRNA therapeutics and their RNAi mechanisms of action, specifically naming each as an "siRNA" therapeutic might not fully recapitulate the pharmacology of this novel class of therapeutics nor embrace the growing number and forms of double- or single-stranded therapeutic RNAs such as miRNA mimics, pre-miRNAs, and shRNAs, as the term "RNAi therapeutics" having been used in the fields [15, 93, 107, 110, 148, 272-274].

In this minireview, we summarize the common and unique chemistry and molecular pharmacology of all six FDA-approved siRNA therapeutics and discuss the current and perplexing naming

systems to support the use of a general and unified nomenclature of “RNAi” therapeutic to align with the current therapeutic nomenclature criteria in pharmacology based on mechanism of action.

Common and unique chemistry and delivery of the FDA-approved RNAi therapeutics

As the primary ribonucleotide sequence of the siRNA antisense strand is designed for complete complementary base pairing with a target transcript, application of chemical modifications is expected to increase the metabolic stability and optimize target selectivity, potency, and safety of the RNAi molecules [15, 148, 273, 274, 281, 283, 287, 292, 295]. The six FDA-approved siRNA therapeutics all contain extensive chemical modifications on the ribose subunit of individual ribonucleotides, including methylation of the 2’-hydroxyl group (2'-*O*-methyl) (2'-*O*-methyladenosine; Am) and substitution of the 2’-hydroxyl group with fluorine (2'-fluoro) (2'-fluoroadenosine; Af) [272, 273, 297] (**Table 1**). Interestingly, the antisense strand of the newly approved nedosiran consists of a uniquely modified uridine at the 5’-end with conventional 2'-*O*-methyl and novel 4’-*O*-((methoxy)phosphoryl)methyl modifications of the ribose subunit [297]. Moreover, the 3’-ends of both antisense and sense strands of the first siRNA medication (patisiran) include two thymidine nucleosides (dT) while maintaining internucleotide phosphonate linkages [273]. By contrast, two phosphorothioate linkages are applied to the 3’-ends of antisense strands as well as 5’-ends of sense strands for all other FDA-approved siRNA therapeutics to improve their metabolic stability [272, 273, 297].

In addition to extensive chemical modification, two other main techniques are employed to achieve optimal pharmacokinetic properties or delivery of current siRNA therapeutics, namely siRNA

encapsulation within a lipid nanoparticle (LNP) or conjugation to a ligand to enhance targeted tissue or organ distribution or selectivity (**Fig. 1B**; **Table 1**) [15, 272, 273, 297]. Patisiran remains the only siRNA medication to employ LNP formulation, while all five remaining siRNA therapeutics incorporate *N*-acetylgalactosamine (GalNAc; L96) ligands to enhance hepatocyte uptake [273, 297]. Differing from all previous siRNA therapeutics, the newly approved nedosiran is comprised of a novel hairpin sense strand [297], which is likely important for its overall metabolic stability. Likewise, the four ribonucleotides that form this loop structure within nedosiran are all conjugated to similar GalNAc aminosugar ligands for hepatocyte targeted delivery and subsequent pharmacological action (**Fig. 1B; Table 1**) [297]. Interestingly, while information regarding sequences, chemistries, and target mRNA binding locations of siRNA therapeutics currently in clinical trials may not yet be as transparent as those FDA-approved, it is of interest to note that currently two siRNA therapeutic candidates use a nanoparticle system like that of patisiran while the remaining majority employ GalNAc conjugation for siRNA-payload delivery [304].

Common and unique molecular pharmacology of the FDA-approved RNAi therapeutics

All FDA-approved siRNA therapeutics utilize endogenous RNAi machinery to achieve posttranscriptional gene regulation by mRNA cleavage and degradation for the treatment of respective diseases with differing therapeutic targets, as described in their FDA-approved prescribing information (**Fig. 1B**). Patisiran and vutrisiran are both indicated for the treatment of hereditary transthyretin-mediated amyloidosis (hATTR) [17, 93, 273, 298, 299], a disease characterized by the buildup of amyloid fibrils in the liver caused by the unregulated aggregation

of TTR [81, 82]. The patisiran and vutrisiran antisense strands target for cleavage and degradation the TTR mRNA at the 3'UTR (**Table 2**) that encodes the TTR protein important in amyloid fibril formation in several tissue types [17, 82, 89, 93, 298, 299]. Of particular note, the antisense stand of patisiran contains a two-nucleotide overhang at the 3' end (**Table 1**) of which the second is mismatched to the target mRNA sequence (**Table 2**). The RNAi of TTR mRNA by patisiran and vutrisiran function to specifically reduce TTR protein production in liver and thus the abundance of both wild-type and mutant TTR in blood circulation and TTR deposits in tissues [17, 299]. More specifically, analyses from Phase 3 clinical trials showed that patients exhibited mean maximum reductions of 84.3% (sustained over 18 months) and 96% (sustained over 90 days) in serum TTR levels after treatment with patisiran and vutrisiran, respectively [134, 305]. Between the two, the more recently approved vutrisiran exhibits improved liver-specific delivery and may contribute to increased potency compared to its predecessor, patisiran [60, 134, 144, 273]. Both patisiran and vutrisiran are available for prescription and administered either intravenously at a dose of 0.3 mg/kg every 3 weeks or by subcutaneous injection (s.c.) of 25 mg administered once every 3 months, respectively [17, 299].

Similarly, lumasiran and nedosiran are indicated to treat primary hyperoxaluria type 1 (PH1), an autosomal recessive disorder of the liver characterized by increased deposition of calcium oxalate crystals in the kidneys and urinary tract [19, 109, 110, 273, 297]. Instead of targeting the same mRNA to treat PH1, the antisense strands of lumasiran and nedosiran instead target the 3'UTRs of hydroxyacid oxidase 1 (HAO1) and LDHA transcripts (**Table 2**), respectively, to achieve mRNA cleavage and degradation to decrease the production of their respective proteins in the liver and downstream calcium oxalate crystal formation and subsequent oxalate accumulation in the

kidneys and urinary tract [19, 110, 112, 113, 273, 297]. The HAO1 mRNA, targeted by lumasiran, encodes the glycolate oxidase enzyme that is upstream in the oxalate production pathway, while the LDHA mRNA, targeted by nedosiran, encodes the hepatic enzyme LDHA enzyme responsible for the final step in oxalate production by metabolizing glyoxylate to oxalate [110, 112, 113, 297, 306]. Specifically, analyses from pivotal clinical trials demonstrated mean maximum reduction in unitary oxalate excretion of 76% and 68% when treated with lumasiran and nedosiran, respectively [110, 307]. With the recent approval of nedosiran, both siRNA therapeutics are available for prescription and are administered through s.c. injection. Lumasiran has a dosing regimen of either 6 mg/kg or 3 mg/kg once monthly for 3 doses for patients with body weights between 10 - 20 kg or 20 kg and above, respectively, with variable maintenance doses dependent on patient body weight [19]. Alternatively, nedosiran has a dosing regimen for adults of either 160 mg or 128 mg monthly for patients with body wright greater or equal to 50 kg or less than 50 kg, respectively, while dosing for children follow the same weigh distinctions wither either 160 mg or 3.3 mg/kg monthly [297]. Interestingly, the antisense strand of nedosiran is comprised of two mismatched nucleotides to the target LDHA mRNA sequence, one within the 5' end "seed sequence" and another at the 3' end (**Table 2**) [297, 300]. It should be noted that an alternative source [301] to the FDA insert opposes the 5' end "seed sequence" mismatch and instead place a modified cytosine in place of the modified guanosine (**Table 2**).

Moreover, inclisiran is the first non-statin, siRNA medication indicated to treat both heterozygous familial hypercholesterolemia (HeFH) as well as clinical atherosclerotic cardiovascular disease (ASCVD) [20, 117, 273], characterized by elevated blood circulation of low-density lipoprotein cholesterol (LDL-C) [114, 115, 273]. The antisense stand of inclisiran targets the 3'UTR of the

proprotein convertase subtilisin/kexin type 9 (PCSK9) mRNA encoding the PCSK9 protein (**Table 2**). PCKS9 is a low abundant circulating protein responsible for decreasing the natural LDL-C receptor endocytosis and lysosomal degradation cycle leading to increased circulating LDL-C and downstream incidence of HeFH and ASCVD [20, 119, 123, 128, 273]. By reducing PCSK9 protein levels, inclisiran enhances low-density lipoprotein cholesterol (LDL-C) receptor recycling and decreases LDL-C levels in blood circulation [119, 123, 128, 273]. More specially, analyses of a phase 3 clinical trial resulted in a 52.6% reduction in circulating LDL-C levels after two injections of inclisiran over 180 days [124]. Inclisiran is available and prescribed in combination with the maximally tolerated statins with an initial s.c. dose of 284 mg with subsequent maintenance doses every six months [20].

Finally, givosiran is indicated for the treatment of acute hepatic porphyria (AHP) [18, 100, 273]. AHP is characterized by a dysfunction within the heme synthesis pathway that results in an increase in aminolevulinate synthase 1 (ALAS1) and downstream production of aminolaevulinic acid and porphobilinogen neurotoxic metabolites [96-100, 273]. However, compared to the all FDA-approved siRNA therapeutics, the antisense strand of givosiran instead targets for cleavage and degradation the CDS of the ALAS1 mRNA (**Table 2**). Thus, givosiran functions to decrease the protein levels of ALAS1 responsible for the downstream production of neurotoxic metabolites leading to the reduction of circulating neurotoxins [18, 98, 104, 107, 273]. Specifically, analysis of a Phase 3 clinical trial demonstrated that treatment with givosiran resulted in an 86% and 91% reduction in urinary aminolaevulinic acid and porphobilinogen neurotoxic metabolites, respectively, as a proxy for measuring siRNA induced ALAS1 reduction [107]. Givosiran is available for prescription and administered though s.c at a dose of 2.5 mg/kg once a month [18].

Of note, the antisense strand of givosiran contains a 5' end mismatch to the targeted sequence on the ALAS1 mRNA (**Table 2**), a well-known characteristic of miRNA [18, 300, 308].

Interestingly, while all FDA-approved siRNA therapeutics cleave and degrade target mRNAs, givosiran remains the only FDA-approved siRNA medication that follows the generally accepted siRNA mechanistic action by binding to the CDS segment, although with incomplete complementarity (**Fig. 1B; Table 2**). By contrast, the five remaining siRNA therapeutics all bind to the 3'UTRs of their respective mRNA targets with three (lumasiran, inclisiran, and vutrisiran) exhibiting complete base-pair complementarity [17-20, 299] and two (patisiran and nedosiran) exhibiting miRNA-like, incomplete base-pair complementarity (**Fig. 1; Table 2**) [297, 301] to incite their mRNA cleavage and degrative activities. Therefore, these five "siRNA" therapeutics, especially the newly approved nedosiran, instead follow canonical miRNA mechanistic action, indicating that these "siRNA" therapeutics behave as "miRNAs" or at least "miRNA biosimilars" designed with complete or near complete complementarity to their target transcripts [15, 148, 273]. In addition, this further suggests that targeting the 3'UTR might be more efficacious than the CDS as the 3'UTR is closely related to mRNA stability and miRNA function [276, 277, 309]. Thus, this finding may also offer an insight into the strategy employed by these RNAi therapeutics to increase the effectiveness by more closely mimicking the functional and conserved miRNAs derived from the genomes within eukaryotes (**Fig. 1A**) [273, 276, 277, 309], in support of the use of miRNA or RNAi molecules targeting the 3'UTRs in basic research and clinical therapy. Together, this inherent difference newly discovered within a common RNAi molecule class further supports the return to a more transparent, precise, and comprehensive nomenclature embrace the growing number and forms of therapeutic RNAi molecules.

Today, there are around tens of therapeutic RNAi molecules making their way through clinical trial pipeline [272, 273, 304, 310]. In fact, there are eight RNAi therapeutics candidates named as "siRNAs" (fitusiran, tivanisiran, fazirsiran, olpasiran, belcesiran, cemdisiran, revusiran, and ARO-APOC3) that have recently completed or are currently in Phase 3 clinical trials with several others in Phase 2 and earlier preclinical trials to treat infectious, hematological, hereditary, fibrotic, and metabolic diseases as well as diseases of the eye, skin, lung, kidney, and brain [272, 273, 304]. In comparison, there are three RNAi therapeutics candidates named as "miRNAs" or "miRNA mimics" (MRX34, TargomiRs, and Remlarsen) that entered clinical investigations, with several others that act as anti-miRNAs or antagomirs [273, 310, 311]. Further, an additional therapeutic candidate termed "miRNA" (AMT-130) is currently in a Phase 1/2 clinical trial for Huntington's disease and uses a modified viral vector to express its therapeutic miRNA in cells as compared to other synthetic miRNA mimic or siRNA candidates and approved RNAi therapeutics [273, 310, 311]. However, it should be noted that, while most clinical emphases remains on "siRNA"-termed therapeutics, the use of miRNA therapy remains in its infancy with several candidates under preclinical investigation in several disease types including malignant, neurological, and cardiovascular diseases for known and putative roles in inflammation, proliferation, necrosis, apoptosis, and autophagy [273, 310, 311].

Unifying and pharmacological nomenclature of RNAi therapeutics

While complete sequence complementarity between siRNA and target mRNA, and not mRNA target site, have been inherently used to classify siRNA and miRNA molecules or biosimilars,

previous studies have revealed that “siRNAs” engineered with miRNA characteristics [i.e., imperfect (40-80%) complementarity or "bulge” binding] are able to effectively regulate target gene expression through mRNA cleavage and degradation [282, 297, 302, 303]. Consequently, effective “siRNA” molecules can now be designed with sequences that exhibit incomplete complementary to their target mRNAs, as miRNAs are defined [278-282, 289], yet regulate target gene expression though mRNA cleavage, as both siRNAs and miRNAs are defined [116, 283-288], all while retaining the nomenclature of “siRNA”. Further, it has been well documented that siRNAs may induce cleavage of target mRNAs with complete [116, 283-288] or partial complementarity [289, 303, 312-314], in direct contrast with the problematic distinguishment of miRNAs from siRNAs simply by partial or complete, respectively, sequence complementarity-dependent mRNA cleavage or translational repression [273, 281]. In fact, the antisense strands of patisiran, givosiran, and nedosiran exhibit this near complete complementarity with mismatched nucleotides (**Table 2**), yet called as “siRNA” therapeutics [17, 18, 297, 300, 301, 308].

These findings, together with the implications that five siRNA therapeutics follow canonical miRNA mechanistic action by binding the 3’UTR, disrupt the traditional “siRNA” molecule nomenclature paradigm as the term “siRNA” therapeutic might not fully describe their complete pharmacology. Moreover, any attempt to alternatively distinguish therapeutic siRNAs and miRNAs based on the targeted mRNA sites would then require both siRNA and miRNA molecules to have a defined canonical binding location on target mRNAs [15, 148, 273]. As a result, it is then conceivable that therapeutic “siRNAs” and siRNA molecules alike, might be seen as exogenous “miRNAs” designed to bind their target mRNA sequences with complete complementarity.

Instead, an alternative means of naming therapeutic siRNAs, miRNAs, and other forms of RNAi molecules being approved by the FDA and under clinical and preclinical development [15, 272, 273] is to return to a nomenclature that embraces the growing number and various forms of therapeutic RNAi molecules and aligns with current pharmacological criteria, i.e., nomenclature by mechanism of action. Typically, therapeutics on the market are classified either by their disease indication (e.g., antidepressant therapeutics) or pharmacological action (e.g., selective serotonin reuptake inhibitors) while some are classified by their chemistry (e.g., sulfonamides). Hence, it would be advantageous for basic and translational scientists, clinicians, and educators to follow a known and more cohesive nomenclature with fewer confounding exceptions. In this way, all FDA-approved siRNA therapeutics and the growing number and forms of therapeutic RNAi molecule candidates are appropriately named according to their complete pharmacology, and not their chemistry or extent of sequence complementary.

Thus, the most clear, informative, transparent, and complete means of naming therapeutic siRNAs and miRNAs is under the simple and pharmacologically unified nomenclature of "RNAi" therapeutics having been previously used in the field [15, 93, 107, 110, 148, 272-274]. Accordingly, while, for example, givosiran and inclisiran target two different mRNAs at different binding locations, with variable degrees of binding complementarities, and for different disease indications, both would be recapitulated pharmacologically as RNAi therapeutics. Following this unified nomenclature leaves no room for error in naming current and future RNAi therapeutics and provides a clear and fully defined pharmacological action that is independent of unique chemistry, therapeutic targets, binding locations, sequence complementarity, and disease indications. Therefore, a return to the term "RNAi" therapeutics [15, 93, 107, 110, 315] is in

concordance with recognized criteria for therapeutic nomenclature in the fields of pharmacology and pharmacological sciences based on the common mechanism of action of all siRNA therapeutics being approved and the growing number and variable forms of therapeutic RNAi molecules under development.

Concluding remarks

With the recent addition of nedosiran, there are now six FDA-approved siRNA therapeutics which share a common RNAi mechanism by acting on their specific therapeutic targets for the control of respective diseases. Notably, all siRNA therapeutics share characteristics of both siRNA and miRNA molecules by either exhibiting complete (lumasiran, inclisiran, and vutrisiran) or near complete (patisiran, givosiran, and nedosiran) base-pair complementarity with targeted mRNAs to incite cleavage and degradation via the RNAi pathway, in which five (patisiran, lumasiran, inclisiran, vutrisiran, and nedosiran) interfere with the 3'UTRs and only one (givosiran) act on the CDS. Therefore, the term "RNAi" therapeutics coherently aligns the growing number and various forms of novel RNAi therapeutics based on common pharmacological action and is more informative for professionals and the general public.

Table 1. Chemistries of individual FDA-approved RNAi therapeutics. Abbreviations: A, adenosine; AdemA, GalNAc aminosugar conjugated adenosine; AdemG, GalNAc aminosugar conjugated guanosine; Af, 2'-fluoroadenosine; Am, 2'-*O*-methyladenosine; C, cytidine; Cf, 2'-fluorocytidine; Cm, 2'-*O*-methylcytidine; dT, thymidine; G, guanosine; Gf, 2'-fluoroguanosine; Gm, 2'-*O*-methylguanosine; L96, tri-*N*-acetylgalactosamine (GalNAc); s, phosphorothioate; U, uridine; Uf, 2'-fluorouridine; Um, 2'-*O*-methyluridine; Um*, 2'-*O*-methyl-4′ -*O*-((methoxy)phosphoryl)methyluridine. Sense sequences and antisense sequences were obtained from the FDA inserts. Interestingly, the sense strand of newly approved nedosiran is designed to form a hairpin or stem-loop structure in which the loop is comprised of four GalNAc aminosugar conjugated ribonucleosides. As another note, the guanosine at position 6 from the 5′ end of the nedosiran antisense strand is instead called a modified cytosine in an alternative source [301] to the FDA label.

RNA Therapeutic	Chemistry	Year approved
Patisiran (Onpattro™)	Sense: 5'-GUmAACmCmAAGAGUmAUmUmCmCmAUmdTdT-3' Antisense: 3'-dTdTCAUmUGGUUCUCAUmAAGGUA-5'	2018
Givosiran (Givlaari™)	Sense: 5'-CmsAmsGmAmAmAmGfAmGfUmGfUmCfUmCfAmUmCmUmUmAm-L96-3' Antisense: 3'-UmsGmsGmUfCmUfUmUfCmUfCmAfCmAfGmAfGmUfAmGfAfsAfsUm-5'	2019
Lumasiran (Oxlumo™)	Sense: 5'-GmsAmsCmUmUmUmCfAmUfCfCfUmGmGmAmAmAmUmAmUmAm-L96-3' Antisense: 3'-AmsCmsCmUmGmAmAmAfGmUfAmGmGmAmCfCfUmUfUmAmUmsAfsUm-5'	2020
Inclisiran (Leqvio™)	Sense: 5'-CmsUmsAmGmAmCmCfUmGfUmdTUmUmGmCmUmUmUmUmGmUm-L96-3' Antisense: 3'-AmsAmsGmAmUmCfUmGfGmAfCmAfAmAfAmCfGmAfAfAfAmsCfsAm-5'	2021
Vutrisiran (Amvuttra™)	Sense: 5'-UmsGmsGmGmAmUmUfUmCfAfUfGmUmAmAmCmCmAmAmGmAm-L96-3' Antisense: 3'-CmsUmsAmCmCmCmUmAfAmAfGmUmAmCmAfUmUmGfGmUmUmsCfsUm-5'	2022
Nedosiran (Rivfloza™)	Sense: 5'-AmsUmGfUmUfGmUmCfCfUfUfUmUfUmAfUmCfUmGmAmGmCmAmGmCm-Cm-AdemG-AdemA-AdemA-AdemA-GmGmCmUmGmCm-3' Antisense: 3'-GmsGmsUmAmCfAmAfCmAfGmGmAmAfAfAmAf**Gm**AfGfsAfsCfsUm*-5'	**2023**

Table 2. Base pairings between individual antisense strands of FDA-approved RNAi therapeutics and respective mRNA targets. Abbreviations: 3′ UTR, 3′ untranslated region; ALAS1, 5′ -aminolevulinate synthase 1; CDS, protein coding region; HAO1, hydroxyacid oxidase 1; LDHA, lactate dehydrogenase A; PCSK9, proprotein convertase subtilisin/kexin type 9; TTR, transthyretin. Antisense sequences were obtained from the FDA inserts, and mRNA sequences were obtained from the National Center for Biotechnology Information. Nedosiran is the most recently approved siRNA therapeutics and harbors unique binding complementarity. Antisense nucleotides mismatched to their target mRNA sequences are lacking a connecting line, among them the guanosine at position 6 from the 5′ end of the nedosiran antisense strand is instead called a modified cytosine in an alternative source [301] to the FDA drug label.

RNA Therapeutic	mRNA target	NCBI mRNA sequence ID	Start nucleotide	Base pairing	End nucleotide
Patisiran	TTR	NM_000371.4	3'UTR 46-	5'-AUGUAACCAAGAGUAUUCCAU-3' 3'-U**U**CAUUGGUUCUCAUAAGGUA-5'	-66
Givosiran	ALAS1	NM_000688.6	CDS 534-	5'-ACCAGAAAGAGUGUCUCAUCUUC-3 3'-UGGUCUUUCUCACAGAGUAGAA**U**-5'	-556
Lumasiran	HAO1	NM_017545.3	3'UTR 204-	5'-UGGACUUUCAUCCUGGAAAUAUA-3' 3'-ACCUGAAAGUAGGACCUUUAUAU-5'	-226
Inclisiran	PCSK9	NM_174936.4	3'UTR 1160-	5'-UUCUAGACCUGUUUUGCUUUUGU-3' 3'-AAGAUCUGGACAAAACGAAAACA-5'	-1182
Vutrisiran	TTR	NM_000371.4	3'UTR 35-	5'-GAUGGGAUUUCAUGUAACCAAGA-3' 3'-CUACCCUAAAGUACAUUGGUUCU-5'	-57
Nedosiran	LDHA	NM_005566.4	3'UTR 63-	5'-GCAUGUUGUCCUUUUUAUCUGA-3' 3'-**G**GUACAACAGGAAAAA**G**AGACU-5'	-84

Figure legends

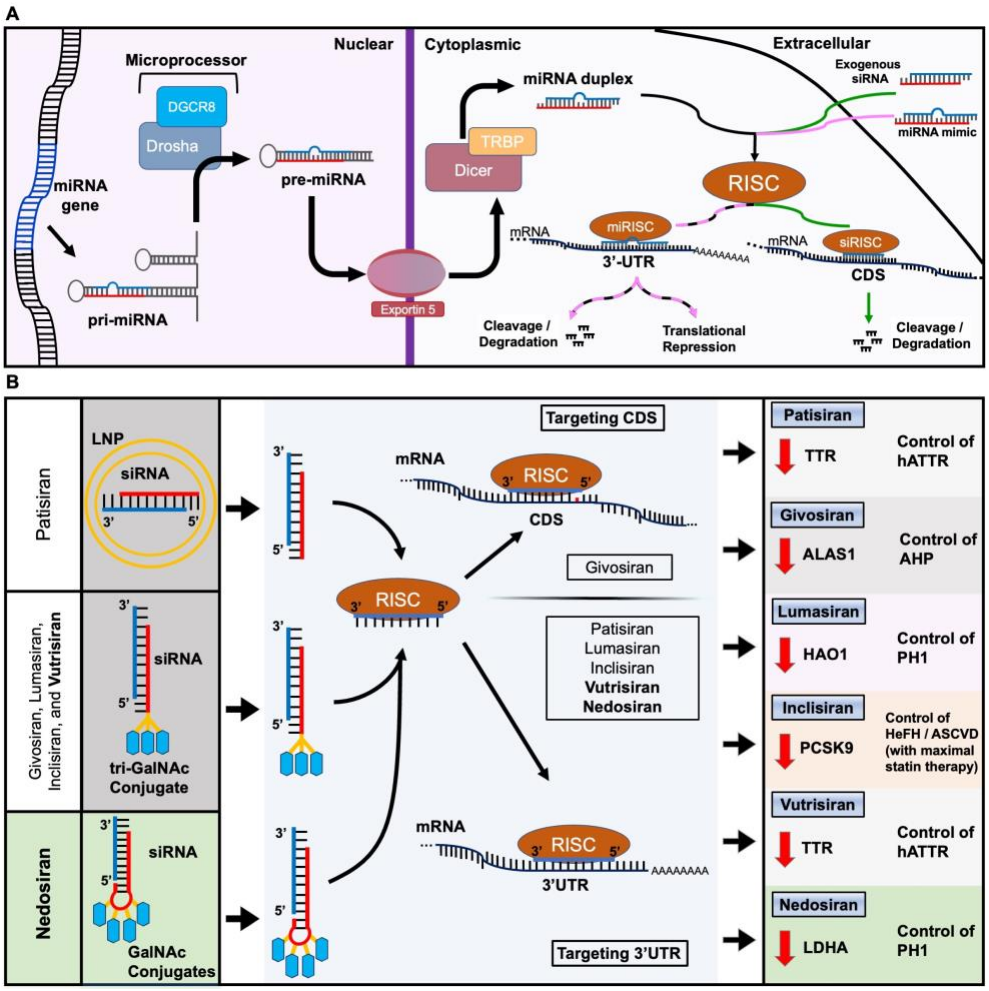

Figure 1. RNAi mechanisms and clinical pharmacology of six FDA-approved RNAi therapeutics. (**A**) Mechanistic actions of the genome-derived miRNAs and exogenous RNAi agents. MiRNA genes are transcribed into primary miRNA transcripts (pri-miRNAs) and processed by the nuclear microprocessor, Drosha-DGCR8 complex, to release shorter precursor miRNAs (pre-miRNAs) and further by cytoplasmic Dicer/TRBP complex to offer miRNA duplexes. The guide or antisense strand (blue) of endogenous miRNA or exogenous siRNA and miRNA mimics is loaded into the RNA-induced silencing complex (RISC) where canonical miRNAs partially bind to the 3'UTR of target transcripts while siRNAs are typically designed to act on the CDS of target transcript via complete base pairing to induce posttranscriptional gene regulation. (**B**) Molecular pharmacology of six FDA-approved siRNA therapeutics (antisense in blue, and sense in red). Patisiran is formulated as LNP for the treatment of hereditary transthyretin-mediated amyloidosis (hATTR) by downregulating transthyretin (TTR). Givosiran, lumasiran, inclisiran, vutrisiran, and nedosiran are all conjugated with GalNAc moieties to improve hepatocyte targeting for the treatments of acute hepatic porphyria (AHP) by downregulating 5'-aminolevulinate synthase 1 (ALAS1), primary hyperoxaluria type 1 (PH1) by reducing hydroxyacid oxidase 1 (HAO1), heterozygous familial hypercholesterolemia (HeFH) and atherosclerotic cardiovascular disease (ASCVD) by suppressing proprotein convertase subtilisin/kexin type 9 (PCSK9), hATTR by downregulating TTR, and PH1 by silencing lactate dehydrogenase enzyme A (LDHA), respectively. Note that, while givosiran targets the CDS of ALAS1 mRNA with near-complete binding, patisiran, lumasiran, inclisiran, vutrisiran, and nedosiran are all designed to act on the 3'UTRs of target mRNAs via complete or near-complete binding to achieve gene silencing as endogenous miRNAs.

Chapter 3: Novel RNA molecular bioengineering technology efficiently produces functional miRNA agents

Abstract

Genome-derived microRNAs (miRNAs or miRs) govern posttranscriptional gene regulation and play important roles in various cellular processes and disease progression. While chemo-engineered miRNA mimics or biosimilars made *in vitro* are widely available and used, miRNA agents produced *in vivo* are emerging to closely recapitulate natural miRNA species for research. Our recent works have demonstrated the success of high-yield, *in vivo* production of recombinant miRNAs by using human tRNA (htRNA) fused precursor miRNA (pre-miR) carriers. In this study, we aim to compare the production of bioengineered RNA (BioRNA) molecules with glycyl *versus* leucyl htRNA fused hsa-pre-miR-34a carriers, namely BioRNA^{Gly} and BioRNA^{Leu}, respectively, and perform initial functional assessment. We designed, cloned, overexpressed, and purified a total of 48 new BioRNA/miRNAs, and overall expression levels, final yields, and purities were revealed to be comparable between BioRNA^{Gly} and BioRNA^{Leu} molecules. Meanwhile, the two versions of BioRNA/miRNAs showed similar activities to inhibit non-small cell lung cancer cell viability. Interestingly, functional analyses using model BioRNA/miR-7-5p demonstrated that BioRNA^{Gly}/miR-7-5p exhibited greater efficiency to regulate a known target gene expression (*EGFR*) than BioRNA^{Leu}/miR-7-5p, consistent with miR-7-5p levels released in cells. Moreover, BioRNA^{Gly}/miR-7-5p showed comparable or slightly greater activities to modulate MRP1 and VDAC1 expression, compared with miRCURY LNA miR-7-5p mimic. Computational modeling illustrated overall comparable 3D structures for exemplary BioRNA/miRNAs with noticeable differences in htRNA species and payload miRNAs. These findings support the utility of hybrid htRNA/hsa-pre-miR-34a as reliable carriers for RNA molecular bioengineering, and the resultant BioRNAs serve as functional biologic RNAs for research and development.

Introduction

MicroRNAs (miRNAs or miRs) are a superfamily of functional noncoding RNAs (ncRNAs) that are present in almost all species [316, 317]. Upon entering the RNA induced silencing complex (RISC) and binding with target transcripts, miRNAs exert RNA interference (RNAi) mechanism to achieve posttranscriptional gene regulation to modulate many critical cellular processes. The potency and versatility of miRNA to target multiple transcripts provides an opportunity for a single molecule to modulate common pathways that may be dysregulated in diseases [15, 273]. Beyond initial discovery, researchers have developed novel, adaptable RNAi-based tools and biotechnologies for basic genetic and biomedical research as well as RNAi-based therapeutics [15, 273]. In fact, there are a number of RNAi-based therapies being approved by the US Food and Drug Administration and many others in clinical or preclinical development for the treatment of various human diseases, including lung cancer [14, 15, 148, 272, 273].

Lung cancer remains the leading cause of cancer-related deaths in the United States and worldwide with 85% of cases classified as non-small cell lung cancer (NSCLC) [318, 319]. The low survival rate of NSCLC patients warrants the development of more effective pharmacotherapies [319, 320]. However, growing interest in RNAi-based interventions and lung cancer associated miRNAs positions NSCLC as a prime candidate for miRNA replacement therapy [163, 320, 321]. In particular, miRNA replacement therapy reintroduces tumor suppressive miRNAs depleted in disease cells to harness endogenous RNAi machinery for the treatment of human disease, representing a new viable strategy [14, 147, 273]. However, most conventional miRNA interventions make use of *in vitro* synthesized miRNA mimics or biosimilars bearing extensive

chemical modifications whose physiochemical and biological properties may not truly recapitulate their endogenous counterparts [15, 26, 257, 273]. While chemical modifications may improve metabolic stability and binding affinity, such as the modifications on the ribose subunit of individual ribonucleotides as demonstrated in the approved RNAi medications and the latest locked nucleic acids (LNA) under active development, the inclusion and introduction of non-natural chemical modifications might increase the risk of severe immune responses [15, 26, 273].

To address these concerns, our lab has developed a novel *in vivo* fermentation based, RNA molecular bioengineering platform technology by using a human transfer RNA (htRNA) fused hsa-pre-miR-34a carrier, which offers true, biologic RNAi agents (termed BioRNA, previously BERA; **Fig. 1A**) with high yield and purity that might more closely represent the structural and chemical properties of endogenous miRNAs [253-255]. Furthermore, our BioRNAs exhibit biocompatibility and efficacy to suppress tumor growth *in vivo* and regulate target gene expression *in vitro* [253-256, 259, 260, 322]. Through our previous works, the hybrid htRNA/hsa-pre-miR-34a carriers are imperative for *in vivo* microbial fermentation production and efficient release of payload RNAi molecules to exert their biologic functions in mammalian cells [253-255, 265, 323].

From an initial screening, leucyl htRNA/hsa-pre-miR-34a-based BioRNAs ($BioRNA^{Leu}$) consistently showed a high level of heterogenous overexpression in bacteria and were selectively processed to target miRNAs in human cancer cells [253]. A more comprehensive screening suggested that glycyl htRNA/hsa-pre-miR-34a-based BioRNA ($BioRNA^{Gly}$) exhibited a low cytotoxicity while showing higher yield than other htRNAs (unpublished data). Therefore, in the present study, we aim to compare the utility of $htRNA^{Gly}$- versus $htRNA^{Leu}$-fused hsa-pre-miR-

34a carriers in producing corresponding BioRNA^{Gly} and BioRNA^{Leu} molecules with the same panel of payload miRNAs and in regulating target gene expression with a model miRNA, miR-7-5p (BioRNA^{Gly}/miR-7-5p versus BioRNA^{Leu}/miR-7-5p). Our data demonstrated that all 48 new BioRNA^{Gly}/miRNAs and BioRNA^{Leu}/miRNAs were successfully produced, and overall yields, purities, and antiproliferative activities were comparable between BioRNA^{Gly}- and BioRNA^{Leu}-based miRNAs. Furthermore, we validated the release of payload miR-7-5p and its efficiency to regulate the expression of several well-known target genes in two human NSCLC cell lines. Through computational modeling we found the overall 3D structures of BioRNA/miRNAs and their subcomponents to be comparable amid notable differences in htRNAs and payload miRNAs. These findings support the robustness and reliability of hybrid tRNA/pre-miRNA carriers for molecular bioengineering of functional RNAi molecules that represent a novel class of true, biological RNAs for research and development.

Results

In vivo fermentation production of novel biologic RNA agents and purification to a high degree of homogeneity

To compare the utilities of htRNA^{Gly}- and htRNA^{Leu}-fused hsa-pre-miR-34a carriers (**Fig. 1A**), we first identified a panel of recombinant miRNAs (**Table 1**) for *in vivo* fermentation production. Our BioRNA panel consisted of 22 novel BioRNA^{Leu}/miRNAs and 26 BioRNA^{Gly}/miRNAs, the latter including 4 counterparts to previously published BioRNA^{Leu}/miRNAs, specifically BioRNA^{Leu}/miR126b-3p, /miR133a-3p, /miR-200b-3p, and /miR-7-5p [253].

BioRNA^{Gly}/miRNAs and BioRNA^{Leu}/miRNAs (**Fig. 1B; Supplementary Fig. S1; Tables S1-S2**) were cloned into pBSKrna vector to offer target pBSK/BioRNA plasmids subsequently verified by DNA sequencing. Individual plasmids were transformed into HST08 *E. coli* competent cells, and overexpression of target BioRNA/miRNAs were confirmed through urea-PAGE analyses of total RNAs isolated from *E. coli* (**Fig 1C-D**). We confirmed the heterogeneous overexpression of all 26 BioRNA^{Gly}/miRNAs (**Fig. 1C**) and 22 BioRNA^{Leu}/miRNAs (**Fig. 1D**) through the appearance of strong new bands at expected size, offering a 100% success rate and each accounting for >40% of total RNA based on the density of RNA band (Fig. 1C-D).

Each BioRNA was thus subjected to anion exchange FPLC purification. Fractions of eluted BioRNA monitored by UV detection (**Fig. 2A**) were collected and verified through urea-PAGE analysis as a single RNA band (**Fig. 2B**). The fractions were pooled, desalted, and concentrated to generate BioRNA product whose homogeneity was semi-quantitatively and quantitatively determined by urea-PAGE analysis (**Fig. 2D-E**) and HPLC-UV analysis (**Fig. 2C**), respectively. Their endotoxin levels (**Table 1**) were further measured with an LAL assay kit. All FPLC-purified BioRNAs were highly homogenous (> 97%) and most exhibited low endotoxin activity (≤ 5 EU/μg RNA) (**Table 1**). The majority of pure BioRNA products accounted for more than 30% of the total RNA, yielding 5–10 mg of pure BioRNA from 250 mL bacterial culture. Overall, the production yields, purity, and endotoxin levels of recombinant miRNAs using BioRNA^{Gly} and BioRNA^{Leu} carriers were not statistically significant (**Table 1**), supporting their applications to molecular bioengineering of target RNAs.

Antiproliferative activities of novel BioRNAs against human NSCLC cells

To examine possible functional differences between BioRNA^{Gly}- and BioRNA^{Leu}-based miRNAs, we first employed the CellTiter-Glo biochemical assay to determine their activities to inhibit NSCLC A549 and H1975 cell viability. Several recently published [253] BioRNAs (**Table 1**) were included for comparison. A549 (**Fig. 3A**) and H1975 (**Fig. 3B**) cell viabilities were reduced to various degrees by 15 nM BioRNA^{Gly}/ and BioRNA^{Leu}/miRNAs. Overall, the antiproliferative effects were comparable between the paired BioRNA^{Gly}/miRNAs and BioRNA^{Leu}/miRNAs (e.g., miR-206-3p, miR-125b-5p, and miR-7-5p) and demonstrated putative cell line-specific differences. Similar results were obtained in pancreatic cancer AsPC-1 cells (**Supplementary Fig. S2**). Interestingly, A549 cells seemed more sensitive to a few BioRNA^{Leu}/miRNAs (e.g., miR-370-3p and -146a-5p) than corresponding BioRNA^{Gly}/miRNAs (**Fig. 3A**), while H1975 cells seemed slightly more sensitive to particular BioRNA^{Gly}/miRNAs (e.g., miR-495-3p and -146b-5p) than corresponding BioRNA^{Leu}/miRNAs with some exceptions (e.g., miR-133a-3p and -100-5p; **Fig. 3B**). BioRNA^{Leu}/miR-22-3p exhibited a strong antiproliferation activity with putative cell line-specific differences, similar as those reported recently [322]. Notably, miR-7-5p demonstrated comparable antiproliferative activities between BioRNA^{Gly}- and BioRNA^{Leu}-based carriers as well as against both NSCLC A549 and H1975 cells (**Fig. 3A-B**). These results support the activities of both BioRNA^{Gly}- and BioRNA^{Leu}-based miRNAs to inhibit NSCLC cell viability with putative dependence on cell line and the embedded payload miRNAs.

BioRNA^{Gly}/miR-7-5p is selectively processed to target miR-7-5p in human NSCLC cells

We thus selected miR-7-5p as a model to assess the release of payload miRNA from BioRNA based on the comparable effectiveness of BioRNA^{Gly}/ and BioRNA^{Leu}/miR-7-5p to inhibit cell viability as well as the well-established anticancer function of miR-7-5p in NSCLC cells [324-326]. We employed selective stem-loop RT-qPCR method to determine the levels of mature miR-7-5p in NSCLC cells following transfection with 15 nM of BioRNA^{Gly}/ and BioRNA^{Leu}/miR-7-5p and controls for 48 h. The data showed that BioRNA/miR-7-5p led to higher levels of miR-7-5p in NSCLC cells (**Fig. 4A-B**). Surprisingly, BioRNA^{Gly}/miR-7-5p resulted in a significant higher mature miR-7-5p level than BioRNA^{Leu}/miR-7-5p. In addition, BioRNA^{Gly}/miR-7-5p led to about 10-fold higher change in miR-7-5p levels in H1975 cells (**Fig. 4A**) than A549 cells (**Fig. 4B**). By contrast, the levels of miR-7-5p were similar between A549 and H1975 cells transfected with BioRNA^{Leu}/miR-7-5p or chemo-engineered mimic, and levels of miR-7-5p increased in BioRNA^{Leu}/miR-7-5p-transfected cells did not reach statistical significance when compared to each control. These results demonstrate the selective release of payload miRNA from BioRNA/miRNA in human NSCLC cells.

BioRNA^{Gly}/miR-7-5p effectively regulates target gene expression in human NSCLC cells

We next performed Western blot analyses to investigate the effectiveness of BioRNA/miR-7-5p to regulate the expression of a well-known target, namely *EGFR*, in NSCLC cells after a 72-h transfection. Our data showed that BioRNA^{Gly}/miR-7-5p suppressed EGFR protein levels by 76% and 68% in A549 and H1975 cells, respectively (**Fig. 4B**), while the same dose of BioRNA^{Leu}/miR-7-5p did not alter EGFR protein outcomes. Additionally, the extent of EGFR downregulation by

the same dose of BioRNA^{Gly}/miR-7-5p and commercial miRCURY LNA miR-7-5p mimic was comparable in both A549 and H1975 cells.

Based on these results, coupled with the findings on the increases in miR-7-5p levels, we elected to further evaluate the function of BioRNA^{Gly}/miR-7-5p to control the expression of two other targets, multidrug resistance protein 1 (MRP1) and voltage dependent anion channel 1 (VDAC1). Western blot analyses revealed that BioRNA^{Gly}/miR-7-5p effectively reduced the protein levels of both MRP1 (73% and 75%; **Fig. 4C**) and VDAC1 (82% and 72%; **Fig. 4D**) in NSCLC cells (A549 and H1975, respectively). Additionally, the extents of MRP1 and VDAC1 downregulation were comparable or slightly less in cells transfected with miR-7-5p mimics, as compared with BioRNA^{Gly}/miR-7-5p. These results confirm the effectiveness of BioRNA/miRNA to control target gene expression. Taken together, while both BioRNA^{Gly}/ and BioRNA^{Leu}/miR-7-5p were processed to mature miR-7-5p in NSCLC cells, much higher levels of miR-7-5p were noted in cells transfected with BioRNA^{Gly}/miR-7-5p than BioRNA^{Leu}/miR-7-5p, and thus BioRNA^{Gly}/miR-7-5p demonstrated a consistent efficacy in the control of target gene expression that was comparable as or slightly greater than the same dose of chemo-engineered LNA miR-7-5p mimics.

Computational modeling of BioRNA 3D structures

To explore possible effects of htRNA^{Gly} and htRNA^{Leu} on hsa-pre-miR-34a and overt BioRNA structures, we employed the RNAComposer to determine the 3D structures of several BioRNAs that were further visualized and analyzed with ChimeraX (**Fig. 5**). Computational modeling revealed that htRNA^{Gly} and htRNA^{Leu} maintained their canonical L-shaped 3D structures [327]

(**Fig. 5A**) when their anticodon sequences were replaced with hsa-pre-miR-34a (**Fig. 5A**). Similarly, the 3D structure of hsa-pre-miR-34a remained unchanged within the recombinant BioRNA (**Fig. 5A**).

As we were curious if functional difference observed between BioRNA^{Gly}/ and BioRNA^{Leu}/miR-7-5p (**Fig. 4A-B**) were reflected by any structural elements, no meaningful steric differences were noted in the hsa-pre-miR-34a/miR-7-5p (**Fig. 5B**) besides changes in overall length of BioRNA and noticeable differences in respective htRNA subcomponents. Similar results were seen in paired BioRNA^{Gly}/, BioRNA^{Leu}/miR-124-3p, and their subcomponent derivatives (**Fig. 5C**). Overall, computational modeling indicated that structures of hsa-pre-miR-34a carrier and miRNA duplexes were unaltered in the paired BioRNA^{Gly}/miRNAs and BioRNA^{Leu}/miRNAs while noticeable differences depend on their respective htRNA species. In addition, exchanging the hsa-miR-34a duplex induced little change in chimeric hsa-pre-miR-34a/miR-7-5p and hsa-pre-miR-34a/miR-124-3p structures, as well as the whole BioRNAs.

Discussion

The discovery and application of RNAi has ushered in a new era of adaptable biological and biomedical research with the development of novel routes for therapeutic intervention of human diseases [14, 147, 163, 273]. With the understanding of loss or downregulation of tumor suppressive miRNAs in lung and other types of cancers, novel tools may be developed to restore or reintroduce such miRNAs to achieve the control of disease progression, namely miRNA replacement therapy. Nevertheless, RNAi research and therapy are dominated by using chemically

or enzymatically synthesized RNA analogs [15, 257, 273]. Alternatively, our present study, built upon our recent efforts in bioengineering recombinant RNA agents, demonstrates the reliability of both htRNA^{Gly}- and htRNA^{Leu}-fused hsa-pre-miR-34a carriers to achieve consistent, high-yield, *in vivo* fermentation production of recombinant RNAs, BioRNA^{Gly}/miRNAs and BioRNA^{Leu}/miRNAs, respectively, which are effective to inhibit human NSCLC cell viability with both putative cell line- [328-330] and embedded payload miRNA-dependence [321].

Through functional analyses using model BioRNA/miR-7-5p, our results indicate that BioRNA/miRNAs are intracellularly processed to release the miRNA payload and effectively regulate the expression of well-known targets, namely EGFR [331], MRP1 [332], and VDAC1 [333]. As BioRNA^{Gly}/miR-7-5p exhibits a greater degree of efficacy to regulate EGFR expression than the same dose of BioRNA^{Leu}/miR-7-5p, further assessment demonstrates that BioRNA^{Gly}/miR-7-5p is equally or slightly more efficacious to regulate target gene expression when compared to the miR-7-5p mimic with popular LNA structures [334, 335], associated with higher levels of mature miR-7-5p in BioRNA^{Gly}/miR-7-5p-transfected cells. These results suggest possible impact of htRNA on the release of payload miRNA that may subsequently affect the efficacy to modulate target gene expression. Furthermore, the antiproliferative activities of individual BioRNA/miRNAs may be cell line-dependent in concert with the results from our unbiased viability screen. Therefore, it should be noted that possible differences in processing and target gene regulation between BioRNA^{Gly} and BioRNA^{Leu} may be sequence dependent and requires further examination of additional targeted genes as well as paired BioRNA/miRNAs.

Although the limiting factor of BioRNA^{Leu}/miR-7-5p processing is not fully known, one may suspect that the structural or steric interactions induced by the htRNA^{Leu} sequence on the chimeric structure may affect identification and/or cytoplasmic processing by the microprocessor complex of the miRNA biogenesis pathway [336]. The inclusion of the hsa-pre-miR-34a sequence is intended to guide BioRNA into the miRNA biogenesis pathway to interact with the microprocessor and release the mature and functional miRNAs, which may or may not be Dicer-dependent [255, 273]. However, a lower extent of miRNA payload release from BioRNA^{Leu}/miR-7-5p than BioRNA^{Gly}/miR-7-5p, together with their antiproliferation and target gene regulation activities, suggest possible effects of the tRNA scaffold, which warrants further validation prior extrapolating the observed effects to the full BioRNA/miRNA panel discussed in this study. Furthermore, although efforts were made to optimize the experimental conditions with multiple cell lines showing high transfection efficiency, caution should be noted that transfection efficiencies might vary among different BioRNA/miRNAs and mimics, as well as various cell lines, which, if any, would also contribute to the observed differences in particular effects.

While exploration of RNA structure is currently limited by the lack of available and confirmed RNA 3D structures [337-339], the integration of computational 3D predictive modeling allows for initial assessments of RNA structures. Through predictive modeling, our results demonstrate little change between both hsa-pre-miR-34a/miRNA chimeras and overall BioRNA structures with putative dependence on payload RNAs and respective htRNA species. Still, previous works have demonstrated both the effective processing and target gene regulation of BioRNA^{Leu}/miR-34a-5p and /miR-124-3p [253, 261] and BioRNA^{Gly}/miR-124-3p (unpublished data), though to a lesser degree than BioRNA^{Gly}/miR-7-5p found in this study. Yet, all predicted 3D structures assessed in

this study remain highly comparable to BioRNA^{Gly}/ and BioRNA^{Leu}/miR-7-5p. Together, these results suggest the sequence-and cell line-dependence in the structural and functional analyses of our BioRNA/miRNAs warrants a more comprehensive study to compare between heterogeneous BioRNA/miRNA panels. Nevertheless, provided that computational modeling remains only the initial work into determining the 3D structure of BioRNA/miRNA, it should be noted that experimental, structural studies may provide further insight into true differences in BioRNA/miRNA structure and functional efficiency.

In addition, to the best of our knowledge these results demonstrate the first evidence of hsa-miR-7-5p to regulate both MRP1 and VDAC1 in human NSCLC cells, alongside EGFR [340]. Regulation by hsa-miR-7-5p in NSCLC compliments similar findings in previous reports of MRP1 regulation in breast cancer [341, 342], hepatocellular carcinoma (HCC) [343], and small cell lung cancer [332, 344] cells. Similar regulation compliments previous cancer study findings of VDAC1 regulation by hsa-miR-7-5p in cervical cancer [345], HCC [346], neuroblastoma [333], and rhabdomyosarcoma [347] cells. The regulation of both MRP1 and VDAC1 in NSCLC alongside EGFR introduces new therapeutic routes by using biologic miR-7-5p to sensitize drug resistant NSCLC cells which awaits future exploration.

Conclusions

In conclusion, this study demonstrates the reliability of our novel RNA molecular bioengineering platform technology to allow *in vivo* fermentation production of target BioRNA/miRNA agents by using glycyl and leucyl htRNA/hsa-pre-miR-34a stable carriers. BioRNAs are produced with high-

yield, high degree of homogeneity, and 100% success rate to closely represent the properties of natural miRNA molecules. Overall antiproliferative activities between paired BioRNA^{Leu}/ and BioRNA^{Gly}/miRNA are comparable with putative cell line-specific differences. Functional studies with model BioRNA/miR-7-5p validate the intracellular release of miRNA payload and confirm the effectiveness of BioRNA/miRNA to regulate the expression of targeted genes in NSCLC cells. Further, computational modeling suggests a highly similar structure for the BioRNAs with noticeable differences in htRNA scaffolds. Lastly, our study also confirms the regulation of MRP1 and VDAC1 in NSCLC cells by hsa-miR-7-5p. Overall, these findings support the robustness of tRNA/pre-miRNA carrier-based RNA biotechnology and the applications of novel BioRNA molecules to basic research as well as development of therapeutic RNAs for NSCLC.

Materials and Methods

Chemicals and materials

Lipofectamine 3000 (Cat# L3000001), RPMI medium 1640 (Cat# 11875119), DMEM medium (Cat# 11965092), 0.05% trypsin-EDTA (Cat# 25300054), phosphate-buffered saline (PBS; Cat# 10010023), fetal bovine serum (Cat# 26140079), opti-MEM (Cat# 31985070), RIPA buffer (Cat# 89900), and bicinchoninic acid (BCA) Protein Assay Kit (Cat# 23227) were purchased from Thermo Fisher Scientific (Waltham, MA). Saturated phenol (pH 4.5; Cat# 97064-716) was purchased from VWR (Radnor, PA). Pure ethanol (Cat# E7023), and protease inhibitor cocktail (Cat# P8340) were purchased from Sigma-Aldrich (St. Louis, MO). CellTiter-Glo® 2.0 Cell Viability Assay kit (Cat# G9241) was purchased from Promega **(**Madison, WI). miRCURY LNA

hsa-miR-7-5p mimic (Cat# 339174 YM00472714-AGA) and negative control (Cat# 339174 YM00479902-AGA) were purchased from QIAGEN (Germantown, MD). Directzol RNA miniPrep kit (Cat# R2061) was bought from Zymo Research (Irvine, CA). All primers (**Table S3**) were synthesized and purchased from Integrated DNA Technologies (Coralville, IA). iTaq™ Universal SYBR® Green Supermix (Cat# 1725121), TGX Stain-Free FastCast Acrylamide Kit (7.5%; Cat# 1610181, and 10%; Cat# 1610183), Clarity Western Enhanced Chemiluminescence Substrates (Cat# 1705061), blotting-grade blocker (Cat# 1706404), and polyvinylidene difluoride (PVDF) membranes (Cat# 1620177) were purchased from Bio-Rad (Hercules, CA). All other chemicals and organic solvents of analytical grade were purchased from Thermo Fisher Scientific, VWR, or Sigma-Aldrich. All lab supplies and reagents used in our protocols are DNase and RNase free.

Cloning of BioRNA expression plasmids

Novel BioRNAs with payload miRNAs (**Table S1**) as well as control BioRNAs, htRNA^{Gly}/sephadex-aptamer (BioRNA^{Gly} Control RNA) and htRNA^{Leu}/sephadex-aptamer (BioRNA^{Leu} Control RNA), were designed as reported [253]. In short, human tRNA (Genomic tRNA Database GtRNAdb; [348]) and miRNA (miRbase; [349, 350] sequences were obtained to clone BioRNA expression plasmids (**Fig. 1B**) by following two basic strategies to amplify target inserts (**Supplementary Fig. S1**). Inserts for BioRNA^{Leu} were obtained directly through PCR amplification using primers with 16-nt complementary base pair overlaps (IDT; San Diego, CA) (**Table S2**). The inserts were cloned into the pBSKrna vector, linearized by endonucleases EcoRI-HF® (Cat# R3101) and PstI-HF® (Cat# R3140; New England Biolabs, Ipswitch, MA) with an In-

Fusion cloning kit (Cat# 638949; Takara Bio, Mountain View, CA), following manufacturer's instructions. Inserts for BioRNA^{Gly} were produced through PCR amplification using the respective BioRNA^{Leu}/miRNA plasmids as a template and htRNA^{Gly} specific primers (**Table S2**) and similarly cloned into a linearized pBSKrna vector. The ligation products (5 μL) were individually transformed into HST08 *E. coli* Stellar™ Competent Cells (Cat# 636766; 30 μL) (Takara Bio; Mountain View, CA) and inoculated in Luria-Bertani (LB) media (400 μL) without selection on a shaker for 60 min (37°C, 225 rpm). Inoculated LB media (Cat# DF0446-17-3; Fisher Scientific) was plated on LB-ampicillin [100 μg/mL] agar plate and incubated overnight at 37°C. Three positive colonies were chosen and transferred separately to 15 mL of LB-ampicillin [100 μg/mL] medium and incubated overnight on a shaker (37°C, 225 rpm). Plasmids were individually extracted from 2 mL of the media via QIAprep Spin Miniprep Kit (QIAGEN) and subject to DNA sequencing (Genewiz from Azenta Life Sciences; South San Francisco, CA). Sequence verified BioRNA expression plasmids, namely pBSK/BioRNA, were preserved at -80°C for future use.

Small- and large-scale overexpression of target BioRNAs in *E. coli*

Small- and large-scale BioRNA production was conducted as previously detailed [253], to confirm target BioRNA overexpression and further purification, respectively. In brief, *E. coli* transformed with pBSKrna/BioRNA plasmids were cultured in 2×YT media (Cat# BP9743-500; Fisher Scientific) for small- (15 mL) or large-scale (250 mL) production and incubated on a shaker (225 rpm and 37 °C for 16 h). Total RNAs were isolated from centrifuged (10,000 × *g* and 4 °C for 2 min) bacteria pellets though Tris-HCL (magnesium acetate [10 mM]–Tris–HCl)-saturated phenol (pH 4.7) extraction. The aqueous phase supernatant of the extraction was mixed with NaCl [5 M]

(10% of supernatant volume), centrifuged (10,000 × *g* and 4°C for 10 min), and RNA contained supernatant was precipitated with ethanol (ethanol/sample solution = 2/1, v/v; -80°C for 60 min). Precipitated RNA was centrifuged (10,000 × *g* and 4°C for 10 min), RNA pellets were dried, resuspended in autoclaved diethylpyrocarbonate (DEPC)-treated H_2O for small- (500 µL) and large-scale (3 mL) production. For large-scale, resuspended RNAs were centrifuged (16,000 × *g* and 4°C for 15 min) and filtered through a 0.22 µm sterile syringe filter. Total RNAs were quantified with a Tecan SPARK (Männedorf, Switzerland) running SPARKCONTROL, Nucleic Acid Quantification software (v2.3; Männedorf, Switzerland). Urea-PAGE analyses were performed to verify individual BioRNA levels in total RNAs (300 ng in 10 µL) (**Fig. 1C-D**) using an 8% polyacrylamide-urea [8 M] denaturing gel (urea-PAGE) in fresh 0.5× tris–acetate–ethylenediamine tetraacetic acid (TAE) buffer (50 min at 120 V). Urea-PAGE gels were incubated with ethidium bromide [0.5 µg/mL] for 5 min on a rocker and visualized under UV detector using the ChemiDoc MP Imaging System (BioRad).

Purification and quality control of target BioRNAs

BioRNAs were purified by anion exchange fast protein liquid chromatography (FPLC) as previously detailed [253]. In brief, total RNAs (5 mg/injection) were separated on an ENrichTM Q 10×100 column (Cat# 7800003) by using an NGC Quest 10 Plus Chromatography FPLC system (BioRad). PVDF durapore membrane (0.22 µm) filtered and sonicated (20 min) mobile phases consisting of Buffer A [10 mM NaH_2PO_4] and Buffer B [10 mM NaH_2PO_4, 1 M NaCl] were used for elution, each adjusted pH to 7.0 with NaOH. The FPLC gradient schematic (flow rate 2 mL/min) was as follows: 100% Buffer A 0–5 min; 55% Buffer B 5–10 min; 55–75% Buffer B 10–

40 min followed by washing with 100% Buffer B and re-equilibrating with 100% Buffer A before a subsequent injection. FPLC injection loop was washed with autoclaved DEPC treated H_2O (6 mL) in-between purification of individual BioRNAs. FPLC traces were monitored using a UV/Vis detector (260 nm) (**Fig. 2A**), and peak areas were used to evaluate the relative levels of BioRNA within the total RNA, which were consistent with the relative levels of BioRNA estimated from the initial urea-PAGE analyses. Fractions of target BioRNA peak were collected, verified by urea-PAGE analysis (**Fig. 2B**). Pure fractions were pooled, precipitated (ethanol/sample solution = 2/1, v/v), resolubilized with sterile DEPC treated H_2O, and desalted and concentrated (2 mL sterile autoclaved DEPC treated H_2O, 3×) using Amicon ultra-0.5 mL centrifugal filters (30 kDa; Cat# UFC203024; Sigma-Aldrich) following manufactures instructions. Purified BioRNAs were quantified using a Spark plate reader. Urea-PAGE was carried out to further verify individual final BioRNAs (50 ng in 10 μL) (**Fig. 2D-E**).

Quality of each BioRNA (**Table 1**) was determined by quantification of purity with high-performance liquid chromatography (HPLC) and measurement of endotoxin level, as previously detailed [253]. In brief, individual BioRNA purities were quantitated using an XBridge OST C18 column (2.1 × 50 mm, 2.5 μm particle size, maintained at 60°C; Cat# 186003953; Waters; Milford, MA) on a Shimadzu LC-20AD HPLC system (Columbia, MD). Individual BioRNAs were diluted in 100 μL of DEPC [10 ng/μL]. BioRNA (5 μL) were injected and eluted (flow rate 0.2 mL/min) with Buffer C [8.6 mM TEA, 100 mM Hexafluoro-2-propanol (HFIP) in HPLC grade H_2O] and Buffer D [8.6 mM TEA, 100 mM Hexafluoro-2-propanol (HFIP) in HPLC grade methanol] as follows: 16% Buffer D 0–1 min, and 16–22% Buffer D at 1–21 min followed by system washing with 22% Buffer D at 21–22 min and re-equilibration with 16% Buffer D. RNAs were detected

using a photodiode array detector (260 nm) (**Fig. 2C**), and purity was determined by dividing the area under the BioRNA peak by all peaks displayed on the HPLC chromatogram. Endotoxin levels were measured with the Pyrogent-5000 kinetic LAL assay (Cat# N383; Lonza; Walkersville, MD) by following manufacturer's instructions. BioRNA [100 ng/μL] and quantification standards were solubilized and diluted in endotoxin free H_2O instructed. The assay was performed over 40 min to assess turbidity (340 nm) as a readout of endotoxin levels using a SpectraMax iD5 plate reader (Molecular Devices; San Jose, CA). Provided endotoxin standards were used to generate a standard curve to determine endotoxin activity. BioRNAs with highly purity (>98% by HPLC) and low endotoxin activity (<10 EU/μg RNA) were used for this study.

Cell culture

Human NSCLC lung carcinoma A549 (Cat# CRM-CCL-185) and H1975 (Cat# CRL-5908), and pancreatic carcinoma AsPC-1 (Cat# CRL-1682) cell lines were purchased from American Type Culture Collection (Manassas, VA). Cells were maintained in RPMI medium 1640 supplemented with 10% fetal bovine serum (Thermo Fisher Scientific; Waltham, MA) at 37°C in a humidified atmosphere with 5% CO_2 and tested for mycoplasma contamination on a bi-monthly basis.

CellTiter-Glo cell viability assay

A549, H1975, and AsPC-1 cells were individually seeded in flatbottom 96-well plates at 5,000, 8,000, and 6,000 cells/well, respectively, as calculated with the Countless II FL system (Life Technologies; Carlsbad, CA). After RNA [15 nM] transfection using Lipofectamine 3000

(Vehicle) for 72 h with 4 biological replicates (N = 4/group), cell viability values were determined in proxy by luminescence using the CellTiter-Glo® 2.0 Cell Viability Assay kit per manufacturer's instructions (Promega; Madison, WI). Luminescence per well was determine by a SpectraMax® iD5 plate reader. Viability of cells transfected with respective control RNAs were defined as 100%. Each experiment/study was repeated at least twice, and similar results were obtained.

RNA isolation and reverse transcription (RT), quantitative real-time PCR (qPCR) analysis

NSCLC cells were seeded in 6-well plates (500,000 cells/well), incubated overnight, and transfected with 15 nM of BioRNA^{Gly}/miR-7-5p, BioRNA^{Leu}/miR-7-5p, BioRNA Control RNA, mimic has-miR-7-5p, mimic negative control, or Vehicle for 48 h with 3 biological replicates (N = 3/group). Total RNA was extracted using Direct-zol RNA isolation kit (Zymo Research; Irvine, CA), quantified with a Spark microplate reader, and total RNA (500 ng) was used for cDNA synthesis with random hexamers or miR-7-5p stem-loop primer (**Table S3**) by reverse transcription (RT) using NxGen M-MuLV reverse transcriptase (Cat# 30222-1; Lucigen; Middleton, WI). Quantitative PCR (qPCR) analyses were carried out on a CFX96 Touch real-time PCR system (BioRad; Hercules, CA) using gene specific primers (**Table S3**) and iTaq ™ Universal SYBR® Green Supermix (BioRad; Hercules, CA) according to the manufacturer's protocols. Each individual biological replicate was assessed with 2 technical replicates. Levels of mature miR-7-5p were normalized to U6 snRNA in corresponding samples and determined using the formula $2^{-\Delta\Delta CT}$. Each experiment/study was repeated at least twice, and similar results were obtained.

Protein isolation and Western blot analysis

Cells were seeded into 6-well plates (500,000 cell/well) and transfected with 30 nM BioRNA^{Gly}/miR-7-5p, BioRNA^{Leu}/miR-7-5p, BioRNA Control RNA, mimic hsa-miR-7-5p, mimic negative control (**Table S3**), or Vehicle for 72 h with 3 biological replicates (N = 3/group). Cells were lysed by using Pierce™ RIPA buffer supplemented with complete protease inhibitors for 30 minutes on ice. Centrifuged supernatant (12,000 × *g* and 4°C for 10 min) was transferred to a 1.7 mL microcentrifuge tube and protein concentrations were determined with a BCA Protein Assay Kit. Whole cell proteins (20 μg/lane) were separated via gel electrophoresis on a 7.5% (MRP1 and VDAC1) or 10% (EGFR) TGX StainFree SDS-PAGE gel. Protein gels were electrophoretically transferred onto methanol activated polyvinylidene fluoride (PVDF) membranes using the Trans-Blot Turbo Transfer System (BioRad; Hercules, CA). Membranes were imaged for total protein with a ChemiDoc MP Imaging System, blocked with 5% blotting-grade blocker, and incubated overnight at 4°C with primary antibodies against target proteins EGFR (1:1,000; Cat# 4267S; Cell Signaling Technology; Danvers, MA), MRP1/ABCC1 (1:1,000; Cat# 14685S; Cell Signaling Technology), VDAC1 (1:1,000; Cat# ab15895; Abcam; Boston, MA), or β-actin (1:1,000; Cat# A5441; Sigma-Aldrich). Membranes were incubated (2 h, 25°C) with anti-rabbit (1:10,000; Cat# 111-035-003; Jackson ImmunoResearch Inc.; West Grove, PA) or anti-mouse IgG HRP-linked (1:3,000; Cat# 7076S; Cell Signaling Technology) secondary antibody. Clarity Western Enhanced Chemiluminescence Substrates were mixed (1:1) and applied to develop and image the membrane using a ChemiDoc MP Imaging System. The intensity values of the protein bands were determined by the Image Lab software (BioRad; Hercules, CA) and

normalized to corresponding β-actin and total protein for comparison. Each experiment/study was repeated at least twice, and similar results were obtained.

Computation modeling of BioRNA 3D structures

Predictive modeling of novel BioRNA and BioRNA derivatives was performed using sequences (**Table S4**) attained from the GtRNAdb, our previous publication [257], and *miRbase.org* [349, 350]. Tertiary structure was prediction using RNAComposer: Automated RNA Structure 3D Modeling Server [351, 352] with incorporated secondary structure prediction method using RNAFold WebServer (Institute for Theoretical Chemistry, University of Vienna). The resulting prediction was manipulated using ChimeraX Next-Generation Molecular Visualization software (Resource for Biocomputing, Visualization, and Informatics, University of California, San Francisco). The sequence selection application was used to color code each BioRNA derivative. BioRNA and BioRNA derivatives include: htRNA (Black), hsa-premiR-34a (Blue), miRNA guide sequence (antisense; Red), passenger sequences (Light Blue or Light Grey), five-prime (5'; Magenta); three-prime (3'; White). Nucleotide code includes adenine (Red), thymine (Blue), guanine (Green), and cytosine (Yellow).

Statistics

Values are mean ± standard deviation (SD) and all data were analyzed with one-way ANOVA with Bonferroni post-tests (Prism, GraphPad Software; San Diego, CA). Difference between

analyzed groups was considered as statistically significant when the probability value (P value) was less than an alpha level of 0.05 ($P < 0.05$).

Table 1. Yields, purities, and endotoxin activity levels of individual BioRNA/miRNAs using human leucyl or glycyl tRNA fused hsa-pre-miR-34a carrier, and isolated by anion exchange FPLC methods. The shaded BioRNAs were reported recently and included for comparison. [NS]Not statistically significant, compared with BioRNA[Leu] (one-way ANOVA with Bonferroni *post hoc* tests).

microRNA	BioRNA[Leu]					BioRNA[Gly]				
	Total RNA (mg/250mL fermentation)	Yield of Pure BioRNA		Purity (%, by HPLC)	Pure BioRNA Endotoxin activity (EU/µg RNA)	Total RNA (mg/250 mL fermentation)	Yield of Pure BioRNA		Purity (%, by HPLC)	Pure BioRNA Endotoxin activity (EU/µg RNA)
		mg/250 mL fermentation	% of Total RNA				mg/250mL fermentation	% of Total RNA		
miR-126b-3p	11.3	6.01	53.2	99.7	1.51	23.2	10.1	43.5	99.1	4.20
miR-133a-3p	13.8	6.65	48.2	98.2	3.00	18.2	8.16	44.8	99.4	3.90
miR-200b-3p	19.0	7.80	41.1	98.7	0.18	24.1	9.20	38.2	99.6	3.86
miR-7-5p	9.00	2.63	29.2	99.5	5.88	16.0	5.00	31.3	98.7	0.68
miR-143-3p	14.2	6.70	47.2	98.8	4.70	30.9	14.3	46.3	98.9	0.28
miR-206-3p	10.5	4.77	45.4	97.7	2.30	17.8	4.65	26.1	97.8	2.26
miR-375-3p	14.3	11.2	78.3	98.3	4.30	26.5	11.9	44.9	99.1	0.46
miR-497-5p	18.0	5.10	28.3	97.6	2.80	22.3	7.75	34.8	99.0	1.00
miR-125b-5p	37.8	14.1	37.3	97.5	0.75	20.2	9.29	46.0	98.6	0.80
let-7a-5p	19.3	10.9	56.5	99.5	0.60	28.4	14.7	51.8	99.1	1.20
let-7b-5p	17.2	10.5	61.0	98.5	0.98	31.4	12.6	40.1	99.2	0.70
let-7c-5p	16.2	4.13	25.5	99.1	1.20	13.8	6.78	49.1	98.8	0.70
let-7d-5p	18.1	9.66	53.4	98.6	3.00	15.6	8.68	55.6	99.1	0.58
let-7e-5p	14.7	6.99	47.6	98.4	2.50	17.3	6.63	38.3	99.0	1.00
let-7f-5p	22.8	11.4	50.0	98.8	1.25	14.4	6.86	47.6	99.1	0.30
let-7g-5p	18.1	8.91	49.2	99.5	0.68	19.1	9.13	47.8	99.0	0.54
miR-101-3p	19.8	11.6	58.6	99.1	2.90	16.5	5.87	35.6	99.0	2.45
miR-195-5p	20.4	9.70	47.5	99.8	5.00	17.4	6.64	38.2	99.2	2.10
miR-370-3p	16.4	10.4	63.4	99.4	1.90	26.1	9.00	34.5	99.0	4.90
miR-495-3p	20.7	7.54	36.4	97.8	1.08	12.9	1.68	13.0	97.1	5.00
miR-519a-5p	21.8	8.92	40.9	97.6	2.29	16.5	4.75	28.8	99.0	4.49
miR-29a-3p	18.2	10.0	54.9	97.6	1.97	21.9	7.97	36.4	97.5	1.22
miR-99-5p	16.7	6.76	40.5	99.8	6.80	23.9	11.8	49.4	99.1	3.18
miR-100-5p	18.8	7.85	41.8	99.5	8.64	18.9	8.14	43.1	98.9	3.34
miR-146a-5p	16.2	8.20	50.6	99.5	5.29	19.3	7.96	41.2	99.0	4.25
miR-146b-5p	17.8	7.78	43.7	99.1	4.82	16.2	5.72	35.3	99.2	5.00
Mean ± SD	17.7 ± 5.3	8.32 ± 2.6	47.3 ± 11.5	98.8 ± 0.8	2.94 ± 2.2	20.3 ± 5.2[NS]	8.28 ± 3.0[NS]	40.1 ± 9.1[NS]	98.9 ± 0.6[NS]	2.25 ± 1.7[NS]

Supplemental Table S1. Sequences of novel BioRNAs bearing target RNAi warheads produced in this study. Underlined, htRNA; Black, hsa-pre-miR-34a; Red and Green, miRNA guide and passenger strand, respectively.

BioRNA	Length (nt)	Sequence (5' to 3')	MW (Da)
BioRNA^{Leu}			
miR-143b-3p	192	ACCAGGAUGGCCGAGUGGUUAAGGCGUUGGACU GGCCAGCUGUGAGUGUUUCUUUGAGAUGAAGCA CUGUAGCUCUUGUGAGCAAUAGUAAGGAAGGA GCUGCAUGCAUUCAUCUCUCAGAAGUGCUGCAC GUUGUUGGCCCGAUCCAAUGGACAUAUGUCCGC GUGGGUUCGAACCCCACUCCUGGUACCA	62,093
miR-206-3p	192	ACCAGGAUGGCCGAGUGGUUAAGGCGUUGGAC UGGCCAGCUGUGAGUGUUUCUUUGGAAUGUAA GGAAGUGUGUGGUGUGAGCAAUAGUAAGGAAU CACACACUCCUGUACAUUCCCUAGAAGUGCUGC ACGUUGUUGGCCCGAUCCAAUGGACAUAUGUCC GCGUGGGUUCGAACCCCACUCCUGGUACCA	62,117
miR-375-3p	192	ACCAGGAUGGCCGAGUGGUUAAGGCGUUGGAC UGGCCAGCUGUGAGUGUUUCUUUUUGUUCGUU CGGCUCGCGUGAUGUGAGCAAUAGUAAGGAAU CGCGCGAGCGACACGAACAACUAGAAGUGCUGC ACGUUGUUGGCCCGAUCCAAUGGACAUAUGUCC GCGUGGGUUCGAACCCCACUCCUGGUACCA	62,123
miR-497-5p	192	ACCAGGAUGGCCGAGUGGUUAAGGCGUUGGAC UGGCCAGCUGUGAGUGUUUCUUCAGCAGCACAC UGUGGUUUGUUUGUGAGCAAUAGUAAGGAAGG CAAACCAAGUAGUGCUGUUAUAGAAGUGCUGC ACGUUGUUGGCCCGAUCCAAUGGACAUAUGUCC GCGUGGGUUCGAACCCCACUCCUGGUACCA	62,157
miR-125b-5p	192	ACCAGGAUGGCCGAGUGGUUAAGGCGUUGGAC UGGCCAGCUGUGAGUGUUUCUUUCCCUGAGACC CUAACUUGUGAUGUGAGCAAUAGUAAGGAAUC ACGGGUUGGGCUCUUGGGGCUAGAAGUGCUGC ACGUUGUUGGCCCGAUCCAAUGGACAUAUGUCC GCGUGGGUUCGAACCCCACUCCUGGUACCA	62,117
let-7a-5p	192	ACCAGGAUGGCCGAGUGGUUAAGGCGUUGGACU GGCCAGCUGUGAGUGUUUCUUUGAGGUAGUAG GUUGUAUAGUUUGUGAGCAAUAGUAAGGAAAA CUGUACACCUGACUACCUUUCAGAAGUGCUGCA CGUUGUUGGCCCGAUCCAAUGGACAUAUGUCCG CGUGGGUUCGAACCCCACUCCUGGUACCA	62,080

let-7b-5p	192	ACCAGGAUGGCCGAGUGGUUAAGGCGUUGGACU GGCCAGCUGUGAGUGUUUCUUUGAGGUAGUAG GUUGUGUGGUUUGUGAGCAAUAGUAAGGAAAA CUGUACACCUGACUACCUUUCAGAAGUGCUGCA CGUUGUUGGCCCGAUCCAAUGGACAUAUGUCCG CGUGGGUUCGAACCCCACUCCUGGUACCA	62,112
let-7c-5p	192	ACCAGGAUGGCCGAGUGGUUAAGGCGUUGGAC UGGCCAGCUGUGAGUGUUUCUUUGAGGUAGUA GGUUGUAUGGUUUGUGAGCAAUAGUAAGGAAA ACUGUACACCUGACUACCUUUCAGAAGUGCUGC ACGUUGUUGGCCCGAUCCAAUGGACAUAUGUCC GCGUGGGUUCGAACCCCACUCCUGGUACCA	62,096
let-7d-5p	192	ACCAGGAUGGCCGAGUGGUUAAGGCGUUGGAC UGGCCAGCUGUGAGUGUUUCUUAGAGGUAGUA GGUUGCAUAGUUUGUGAGCAAUAGUAAGGAAA ACUGUGCACCUGACUACCUUCCAGAAGUGCUGC ACGUUGUUGGCCCGAUCCAAUGGACAUAUGUCC GCGUGGGUUCGAACCCCACUCCUGGUACCA	62,117
let-7e-5p	192	ACCAGGAUGGCCGAGUGGUUAAGGCGUUGGAC UGGCCAGCUGUGAGUGUUUCUUUGAGGUAGGA GGUUGUAUAGUUUGUGAGCAAUAGUAAGGAAA ACUGUACACCUGCCUACCUUUCAGAAGUGCUGC ACGUUGUUGGCCCGAUCCAAUGGACAUAUGUCC GCGUGGGUUCGAACCCCACUCCUGGUACCA	62,095
let-7f-5p	192	ACCAGGAUGGCCGAGUGGUUAAGGCGUUGGAC UGGCCAGCUGUGAGUGUUUCUUUGAGGUAGUA GAUUGUAUAGUUUGUGAGCAAUAGUAAGGAAA ACUGUACAUCUGACUACCUUUCAGAAGUGCUGC ACGUUGUUGGCCCGAUCCAAUGGACAUAUGUCC GCGUGGGUUCGAACCCCACUCCUGGUACCA	62,065
let-7g-5p	192	ACCAGGAUGGCCGAGUGGUUAAGGCGUUGGAC UGGCCAGCUGUGAGUGUUUCUUUGAGGUAGUA GUUUGUACAGUUUGUGAGCAAUAGUAAGGAAA ACUGUACAACUGACUACCUUUCAGAAGUGCUGC ACGUUGUUGGCCCGAUCCAAUGGACAUAUGUCC GCGUGGGUUCGAACCCCACUCCUGGUACCA	62,064
miR-101-3p	192	ACCAGGAUGGCCGAGUGGUUAAGGCGUUGGAC UGGCCAGCUGUGAGUGUUUCUUUACAGUACUG UGAUAACUGAAUUGUGAGCAAUAGUAAGGAAG UUCAGUUACACUAGUGCUGUCUAGAAGUGCUGC ACGUUGUUGGCCCGAUCCAAUGGACAUAUGUCC GCGUGGGUUCGAACCCCACUCCUGGUACCA	62,064
miR-195-5p	192	ACCAGGAUGGCCGAGUGGUUAAGGCGUUGGAC UGGCCAGCUGUGAGUGUUUCUUUAGCAGCACAG AAAUAUUGGCUUGUGAGCAAUAGUAAGGAAGG CCAAUAUUCUAGUGCUGCUCCAGAAGUGCUGCA	62,100

		CGUUGUUGGCCCGAUCCAAUGGACAUAUGUCCG CGUGGGUUCGAACCCCACUCCUGGUACCA	
miR-370-3p	192	ACCAGGAUGGCCGAGUGGUUAAGGCGUUGGAC UGGCCAGCUGUGAGUGUUUCUUGCCUGCUGGGG UGGAACCUGGUUGUGAGCAAUAGUAAGGAAGC CAGGUUCGCCAUCAGCAGGAUAGAAGUGCUGCA CGUUGUUGGCCCGAUCCAAUGGACAUAUGUCCG CGUGGGUUCGAACCCCACUCCUGGUACCA	62,257
miR-495-3p	192	ACCAGGAUGGCCGAGUGGUUAAGGCGUUGGAC UGGCCAGCUGUGAGUGUUUCUUAAACAAACAU GGUGCACUUCUUUGUGAGCAAUAGUAAGGAAG AGAAGUGCCCACUGUUUGUUCUAGAAGUGCUGC ACGUUGUUGGCCCGAUCCAAUGGACAUAUGUCC GCGUGGGUUCGAACCCCACUCCUGGUACCA	62,062
miR-519a-5p	192	ACCAGGAUGGCCGAGUGGUUAAGGCGUUGGAC UGGCCAGCUGUGAGUGUUUCUUCUCUAGAGGG AAGCGCUUUCUGUGUGAGCAAUAGUAAGGAAU GGAAAGUGUUCGCUUUUAGACUAGAAGUGCUG CACGUUGUUGGCCCGAUCCAAUGGACAUAUGUC CGCGUGGGUUCGAACCCCACUCCUGGUACCA	62,151
miR-29a-3p	192	ACCAGGAUGGCCGAGUGGUUAAGGCGUUGGAC UGGCCAGCUGUGAGUGUUUCUUUAGCACCAUCU GAAAUCGGUUAUGUGAGCAAUAGUAAGGAAUG ACUGAUUCAGCAUGGUGUUCUAGAAGUGCUGC ACGUUGUUGGCCCGAUCCAAUGGACAUAUGUCC GCGUGGGUUCGAACCCCACUCCUGGUACCA	62,079
miR-99a-5p	192	ACCAGGAUGGCCGAGUGGUUAAGGCGUUGGAC UGGCCAGCUGUGAGUGUUUCUUAACCCGUAGAU CCGAUCUUGUGUGUGAGCAAUAGUAAGGAAUA CAAGGUCGAUACUAUGGGUCUAGAAGUGCUGC ACGUUGUUGGCCCGAUCCAAUGGACAUAUGUCC GCGUGGGUUCGAACCCCACUCCUGGUACCA	62,117
miR-100-5p	192	ACCAGGAUGGCCGAGUGGUUAAGGCGUUGGAC UGGCCAGCUGUGAGUGUUUCUUAACCCGUAGAU CCGAACUUGUGUGUGAGCAAUAGUAAGGAAUA CAAGUUCGAUACUAUGGGUCUAGAAGUGCUGC ACGUUGUUGGCCCGAUCCAAUGGACAUAUGUCC GCGUGGGUUCGAACCCCACUCCUGGUACCA	62,101
miR-146a-5p	194	ACCAGGAUGGCCGAGUGGUUAAGGCGUUGGAC UGGCCAGCUGUGAGUGUUUCUUUGAGAACUGA AUUCCAUGGGUUUGUGAGCAAUAGUAAGGAAG ACCUGUGGAUUACAGUUCUUCUAGAAGUGCUGC ACGUUGUUGGCCCGAUCCAAUGGACAUAUGUCC GCGUGGGUUCGAACCCCACUCCUGGUACCA	62,096

miR-146b-5p	192	ACCAGGAUGGCCGAGUGGUUAAGGCGUUGGAC UGGCCAGCUGUGAGUGUUUCUUUGAGAACUGA AUUCCAUAGGCUGGUGAGCAAUAGUAAGGA**U**G GCCUGUGGAUUACAGUUCUCCUAGAAGUGCUGC ACGUUGUUGGCCCGAUCCAAUGGACAUAUGUCC GCGUGGGUUCGAACCCCACUCCUGGUACCA	62,110
BioRNA^{Gly}			
miR-7-5p	180	GCAUGGGUGGUUCAGUGGUAGAAUUCUCGCCU GGCCAGCUGUGAGUGUUUCUUUGGAAGACUAG UGAUUUUGUUGUGUGAGCAAUAGUAAGGAACA ACAAAAUACUCAGUCUUCCCUAGAAGUGCUGCA CGUUGUUGGCCCACGCGGGAGGCCCGGGUUCGA UUCCCGGCCCAUGCACCA	58,174
miR-126b-3p	180	GCAUGGGUGGUUCAGUGGUAGAAUUCUCGCCU GGCCAGCUGUGAGUGUUUCUUUCGUACCGUGAG UAAUAAUGCGUGUGAGCAAUAGUAAGGAAUGC AUUAUUCUCUAUGGUACGCUAGAAGUGCUGCAC GUUGUUGGCCCACGCGGGAGGCCCGGGUUCGAU UCCCGGCCCAUGCACCA	58,183
miR-133a-3p	180	GCAUGGGUGGUUCAGUGGUAGAAUUCUCGCCU GGCCAGCUGUGAGUGUUUCUUUUUGGUCCCCUU CAACCAGCUGUGUGAGCAAUAGUAAGGAAGCA GCUGGUUAAGUGGGACCAACUAGAAGUGCUGC ACGUUGUUGGCCCACGCGGGAGGCCCGGGUUCG AUUCCCGGCCCAUGCACCA	58,540
miR-200b-3p	180	GCAUGGGUGGUUCAGUGGUAGAAUUCUCGCCU GGCCAGCUGUGAGUGUUUCUUUAAUACUGCCUG GUAAUGAUGAUGUGAGCAAUAGUAAGGAAUCA UCAUUAUAGUGCAGUAUUCUAGAAGUGCUGCA CGUUGUUGGCCCACGCGGGAGGCCCGGGUUCGA UUCCCGGCCCAUGCACCA	58,176
miR-143b-3p	180	GCAUGGGUGGUUCAGUGGUAGAAUUCUCGCCU GGCCAGCUGUGAGUGUUUCUUUGAGAUGAAGC ACUGUAGCUCUUGUGAGCAAUAGUAAGGAAGG AGCUGCAUGCAUUCAUCUCUCAGAAGUGCUGCA CGUUGUUGGCCCACGCGGGAGGCCCGGGUUCGA UUCCCGGCCCAUGCACCA	58,220
miR-206-3p	180	GCAUGGGUGGUUCAGUGGUAGAAUUCUCGCCU GGCCAGCUGUGAGUGUUUCUUUGGAAUGUAAG GAAGUGUGUGGUGUGAGCAAUAGUAAGGAAUC ACACACUCCUGUACAUUCCCUAGAAGUGCUGCA CGUUGUUGGCCCACGCGGGAGGCCCGGGUUCGA UUCCCGGCCCAUGCACCA	58,244

miR-375-3p	180	GCAUGGGUGGUUCAGUGGUAGAAUUCUCGCCU GGCCAGCUGUGAGUGUUUCUUUUUGUUCGUUC GGCUCGCGUGAUGUGAGCAAUAGUAAGGAAUC GCGCGAGCGACACGAACAACUAGAAGUGCUGCA CGUUGUUGGCCCACGCGGGAGGCCCGGGUUCGA UUCCCGGCCCAUGCACCA	58,250
miR-497-5p	180	GCAUGGGUGGUUCAGUGGUAGAAUUCUCGCCU GGCCAGCUGUGAGUGUUUCUUCAGCAGCACACU GUGGUUUGUUUGUGAGCAAUAGUAAGGAAGGC AAACCAAGUAGUGCUGUUAUAGAAGUGCUGCA CGUUGUUGGCCCACGCGGGAGGCCCGGGUUCGA UUCCCGGCCCAUGCACCA	58,284
miR-125b-5p	180	GCAUGGGUGGUUCAGUGGUAGAAUUCUCGCCU GGCCAGCUGUGAGUGUUUCUUUCCCUGAGACCC UAACUUGUGAUGUGAGCAAUAGUAAGGAAUCA CGGGUUGGGCUCUUGGGGCUAGAAGUGCUGCAC GUUGUUGGCCCACGCGGGAGGCCCGGGUUCGAU UCCCGGCCCAUGCACCA	58,244
let-7a-5p	180	GCAUGGGUGGUUCAGUGGUAGAAUUCUCGCCU GGCCAGCUGUGAGUGUUUCUUUGAGGUAGUAG GUUGUAUAGUUUGUGAGCAAUAGUAAGGAAAA CUGUACACCUGACUACCUUUCAGAAGUGCUGCA CGUUGUUGGCCCACGCGGGAGGCCCGGGUUCGA UUCCCGGCCCAUGCACCA	58,207
let-7b-5p	180	GCAUGGGUGGUUCAGUGGUAGAAUUCUCGCCU GGCCAGCUGUGAGUGUUUCUUUGAGGUAGUAG GUUGUGUGGUUUGUGAGCAAUAGUAAGGAAAA CUGUACACCUGACUACCUUUCAGAAGUGCUGCA CGUUGUUGGCCCACGCGGGAGGCCCGGGUUCGA UUCCCGGCCCAUGCACCA	58,239
let-7c-5p	180	GCAUGGGUGGUUCAGUGGUAGAAUUCUCGCCU GGCCAGCUGUGAGUGUUUCUUUGAGGUAGUAG GUUGUGUGGUUUGUGAGCAAUAGUAAGGAAAA CUGUACACCUGACUACCUUUCAGAAGUGCUGCA CGUUGUUGGCCCACGCGGGAGGCCCGGGUUCGA UUCCCGGCCCAUGCACCA	58,239
let-7d-5p	180	GCAUGGGUGGUUCAGUGGUAGAAUUCUCGCCU GGCCAGCUGUGAGUGUUUCUUAGAGGUAGUAG GUUGCAUAGUUUGUGAGCAAUAGUAAGGAAAA CUGUGCACCUGACUACCUUCCAGAAGUGCUGCA CGUUGUUGGCCCACGCGGGAGGCCCGGGUUCGA UUCCCGGCCCAUGCACCA	58,244
let-7e-5p	180	GCAUGGGUGGUUCAGUGGUAGAAUUCUCGCCU GGCCAGCUGUGAGUGUUUCUUUGAGGUAGGAG GUUGUAUAGUUUGUGAGCAAUAGUAAGGAAAA CUGUACACCUGCCUACCUUUCAGAAGUGCUGCA	58,222

		CGUUGUUGGCCCACGCGGGAGGCCCGGGUUCGA UUCCCGGCCCAUGCACCA	
let-7f-5p	180	GCAUGGGUGGUUCAGUGGUAGAAUUCUCGCCU GGCCAGCUGUGAGUGUUUCUUUGAGGUAGUAG AUUGUAUAGUUUGUGAGCAAUAGUAAGGAAAA CUGUACAUCUGACUACCUUUCAGAAGUGCUGCA CGUUGUUGGCCCACGCGGGAGGCCCGGGUUCGA UUCCCGGCCCAUGCACCA	58,19
let-7g-5p	180	GCAUGGGUGGUUCAGUGGUAGAAUUCUCGCCU GGCCAGCUGUGAGUGUUUCUUUGAGGUAGUAG UUUGUACAGUUUGUGAGCAAUAGUAAGGAAAA CUGUACAACUGACUACCUUUCAGAAGUGCUGCA CGUUGUUGGCCCACGCGGGAGGCCCGGGUUCGA UUCCCGGCCCAUGCACCA	58,191
miR-370-3p	180	GCAUGGGUGGUUCAGUGGUAGAAUUCUCGCCU GGCCAGCUGUGAGUGUUUCUUGCCUGCUGGGGU GGAACCUGGUUGUGAGCAAUAGUAAGGAAGCC AGGUUCGCCAUCAGCAGGAUAGAAGUGCUGCAC GUUGUUGGCCCACGCGGGAGGCCCGGGUUCGAU UCCCGGCCCAUGCACCA	58,384
miR-495-3p	180	GCAUGGGUGGUUCAGUGGUAGAAUUCUCGCCU GGCCAGCUGUGAGUGUUUCUUAAACAAACAUG GUGCACUUCUUUGUGAGCAAUAGUAAGGAAGA GAAGUGCCCACUGUUUGUUCUAGAAGUGCUGCA CGUUGUUGGCCCACGCGGGAGGCCCGGGUUCGA UUCCCGGCCCAUGCACCA	58,189
miR-519a-5p	180	GCAUGGGUGGUUCAGUGGUAGAAUUCUCGCCU GGCCAGCUGUGAGUGUUUCUUCUCUAGAGGGA AGCGCUUUCUGUGUGAGCAAUAGUAAGGAAUG GAAAGUGUUCGCUUUUAGACUAGAAGUGCUGC ACGUUGUUGGCCCACGCGGGAGGCCCGGGUUCG AUUCCCGGCCCAUGCACCA	58,278
miR-29a-3p	180	GCAUGGGUGGUUCAGUGGUAGAAUUCUCGCCU GGCCAGCUGUGAGUGUUUCUUUAGCACCAUCUG AAAUCGGUUAUGUGAGCAAUAGUAAGGAAUGA CUGAUUCAGCAUGGUGUUCUAGAAGUGCUGCAC GUUGUUGGCCCACGCGGGAGGCCCGGGUUCGAU UCCCGGCCCAUGCACCA	58,206
miR-101-3p	180	GCAUGGGUGGUUCAGUGGUAGAAUUCUCGCCU GGCCAGCUGUGAGUGUUUCUUUACAGUACUGU GAUAACUGAAUUGUGAGCAAUAGUAAGGAAGU UCAGUUACACUAGUGCUGUCUAGAAGUGCUGCA CGUUGUUGGCCCACGCGGGAGGCCCGGGUUCGA UUCCCGGCCCAUGCACCA	58,191

miR-195-5p	180	GCAUGGGUGGUUCAGUGGUAGAAUUCUCGCCU GGCCAGCUGUGAGUGUUUCUUUAGCAGCACAGA AAUAUUGGCUUGUGAGCAAUAGUAAGGAAGGC CAAUAUUCUAGUGCUGCUCCAGAAGUGCUGCAC GUUGUUGGCCCACGCGGGAGGCCCGGGUUCGAU UCCCGGCCCAUGCACCA	58,227
miR-99-5p	180	GCAUGGGUGGUUCAGUGGUAGAAUUCUCGCCU GGCCAGCUGUGAGUGUUUCUUAACCCGUAGAUC CGAUCUUGUGUGUGAGCAAUAGUAAGGAAUAC AAGGUCGAUACUAUGGGUCUAGAAGUGCUGCA CGUUGUUGGCCCACGCGGGAGGCCCGGGUUCGA UUCCCGGCCCAUGCACCA	58,244
miR-100-5p	180	GCAUGGGUGGUUCAGUGGUAGAAUUCUCGCCU GGCCAGCUGUGAGUGUUUCUUAACCCGUAGAUC CGAACUUGUGUGUGAGCAAUAGUAAGGAAUAC AAGUUCGAUACUAUGGGUCUAGAAGUGCUGCA CGUUGUUGGCCCACGCGGGAGGCCCGGGUUCGA UUCCCGGCCCAUGCACCA	58,228
miR-146a-5p	180	GCAUGGGUGGUUCAGUGGUAGAAUUCUCGCCU GGCCAGCUGUGAGUGUUUCUUUGAGAACUGAA UUCCAUGGGUUUGUGAGCAAUAGUAAGGAAGA CCUGUGGAUUACAGUUCUUCUAGAAGUGCUGCA CGUUGUUGGCCCACGCGGGAGGCCCGGGUUCGA UUCCCGGCCCAUGCACCA	58,223
miR-146b-5p	180	GCAUGGGUGGUUCAGUGGUAGAAUUCUCGCCU GGCCAGCUGUGAGUGUUUCUUUGAGAACUGAA UUCCAUAGGCUGGUGAGCAAUAGUAAGGA**U**GG CCUGUGGAUUACAGUUCUCCUAGAAGUGCUGCA CGUUGUUGGCCCACGCGGGAGGCCCGGGUUCGA UUCCCGGCCCAUGCACCA	58,237

Supplemental Table S2. Primers used for the construction of RNA expression plasmids in this study. Black, BioRNA; Orange, *EcoRI* restriction site overhang; Blue, *PstI* restriction site overhang; F, forward primer; R, reverse primer.

BioRNA		**Cloning Primers (5' to 3')**
BioRNA^{Leu}		
miR-143b-3p	F	TTGTAACGCTGAATTCACCAGGATGGCCGAGTGGTTAAGGCGTTGGACTGGCCAGCTGTGAGTGTTTCTTTGAGATGAAGCACTGTAGCTCTTGTGAGCAATAGTAAGGAAGGAGCTGCATGC
	R	CTTTCGCTAAGGATCTGCAGTGGTACCAGGAGTGGGGTTCGAACCCACGCGGACATATGTCCATTGGATCGGGCCAACAACGTGCAGCACTTCTGAGAGATGAATGCATGCAGCTCCTTCC
miR-206-3p	F	TTGTAACGCTGAATTCACCAGGATGGCCGAGTGGTTAAGGCGTTGGACTGGCCAGCTGTGAGTGTTTCTTTGGAATGTAAGGAAGTGTGTGGTGTGAGCAATAGTAAGGAATCACACACTCC
	R	CTTTCGCTAAGGATCTGCAGTGGTACCAGGAGTGGGGTTCGAACCCACGCGGACATATGTCCATTGGATCGGGCCAACAACGTGCAGCACTTCTAGGGAATGTACAGGAGTGTGTGATTC
miR-375-3p	F	TTGTAACGCTGAATTCACCAGGATGGCCGAGTGGTTAAGGCGTTGGACTGGCCAGCTGTGAGTGTTTCTTTTTGTTCGTTCGGCTCGCGTGATGTGAGCAATAGTAAGGAATCGCGCGAGCG
	R	CTTTCGCTAAGGATCTGCAGTGGTACCAGGAGTGGGGTTCGAACCCACGCGGACATATGTCCATTGGATCGGGCCAACAACGTGCAGCACTTCTAGTTGTTCGTGTCGCTCGCGCGATTCC
miR-497-5p	F	TTGTAACGCTGAATTCACCAGGATGGCCGAGTGGTTAAGGCGTTGGACTGGCCAGCTGTGAGTGTTTCTTCAGCAGCACACTGTGGTTTGTTTGTGAGCAATAGTAAGGAAGGCAAACCAAG
	R	CTTTCGCTAAGGATCTGCAGTGGTACCAGGAGTGGGGTTCGAACCCACGCGGACATATGTCCATTGGATCGGGCCAACAACGTGCAGCACTTCTATAACAGCACTACTTGGTTTGCCTTC
miR-125b-5p	F	TTGTAACGCTGAATTCACCAGGATGGCCGAGTGGTTAAGGCGTTGGACTGGCCAGCTGTGAGTGTTTCTTTCCCTGAGACCCTAACTTGTGATGTGAGCAATAGTAAGGAATCACGGGTTGG
	R	CTTTCGCTAAGGATCTGCAGTGGTACCAGGAGTGGGGTTCGAACCCACGCGGACATATGTCCATTGGATCGGGCCAACAACGTGCAGCACTTCTAGCCCCAAGAGCCCAACCCGTGATTC
let-7a-5p	F	TTGTAACGCTGAATTCACCAGGATGGCCGAGTGGTTAAGGCGTTGGACTGGCCAGCTGTGAGTGTTTCTTTGAGGTAGTAGGTTGTATAGTTTGTGAGCAATAGTAAGGAAAACTGTACAC
	R	CTTTCGCTAAGGATCTGCAGGTGGTACCAGGAGTGGGGTTCGAACCCACGCGGACATATGTCCATTGGATCGGGCCAACAACGTGCAGCACTTCTGAAAGGTAGTCAGGTGTACAGTTTTCCT
let-7b-5p	F	TTGTAACGCTGAATTCACCAGGATGGCCGAGTGGTTAAGGCGTTGGACTGGCCAGCTGTGAGTGTTTCTTTGAGGTAGTAGGTTGTGTGGTTTGTGAGCAATAGTAAGGAAAACTGTACAC

	R	CTTTCGCTAAGGATCTGCAGGTGGTACCAGGAGTGGGGTTCGAA CCCACGCGGACATATGTCCATTGGATCGGGCCAACAACGTGCAG CACTTCTGAAAGGTAGTCAGGTGTACAGTTTTCCT
let-7c-5p	F	TTGTAACGCTGAATTCACCAGGATGGCCGAGTGGTtAAGGCGTTG GACTGGCCAGCTGTGAGTGTTTCTTTGAGGTAGTAGGTTGTATGG TTTGTGAGCAATAGTAAGGAAAACTGTACA
	R	CTTTCGCTAAGGATCTGCAGTGGTACCAGGAGTGGGGTTCGAAC CCACGCGGACATATGTCCATTGGATCGGGCCAACAACGTGCAGC ACTTCTGAAAGGTAGTcAGGTGTACAGTTTTCCTTA
let-7d-5p	F	TTGTAACGCTGAATTCACCAGGATGGCCGAGTGGTTAAGGCGTT GGACTGGCCAGCTGTGAGTGTTTCTTAGAGGTAGTAGGTTGCAT AGTTTGTGAGCAATAGTAAGGAAAACTGTGCAC
	R	CTTTCGCTAAGGATCTGCAGGTGGTACCAGGAGTGGGGTTCGAA CCCACGCGGACATATGTCCATTGGATCGGGCCAACAACGTGCAG CACTTCTGGAAGGTAGTCAGGTGCACAGTTTTCCT
let-7e-5p	F	TTGTAACGCTGAATTCACCAGGATGGCCGAGTGGTTAAGGCGTT GGACTGGCCAGCTGTGAGTGTTTCTTTGAGGTAGGAGGTTGTATA GTTTGTGAGCAATAGTAAGGAAAACTGTACAC
	R	CTTTCGCTAAGGATCTGCAGGTGGTACCAGGAGTGGGGTTCGAA CCCACGCGGACATATGTCCATTGGATCGGGCCAACAACGTGCAG CACTTCTGAAAGGTAGGCAGGTGTACAGTTTTCCT
let-7f-5p	F	TTGTAACGCTGAATTCACCAGGATGGCCGAGTGGTTAAGGCGTT GGACTGGCCAGCTGTGAGTGTTTCTTTGAGGTAGTAGATTGTATA GTTTGTGAGCAATAGTAAGGAAAACTGTACAT
	R	CTTTCGCTAAGGATCTGCAGGTGGTACCAGGAGTGGGGTTCGAA CCCACGCGGACATATGTCCATTGGATCGGGCCAACAACGTGCAG CACTTCTGAAAGGTAGTCAGATGTACAGTTTTCCT
let-7g-5p	F	TTGTAACGCTGAATTCACCAGGATGGCCGAGTGGTTAAGGCGTT GGACTGGCCAGCTGTGAGTGTTTCTTTGAGGTAGTAGTTTGTACA GTTTGTGAGCAATAGTAAGGAAAACTGTACA
	R	CTTTCGCTAAGGATCTGCAGTGGTACCAGGAGTGGGGTTCGAAC CCACGCGGACATATGTCCATTGGATCGGGCCAACAACGTGCAGC ACTTCTGAAAGGTAGTCAGTTGTACAGTTTTCCTT
miR-370-3p	F	TTGTAACGCTGAATTCACCAGGATGGCCGAGTGGTTAAGGCGTT GGACTGGCCAGCTGTGAGTGTTTCTTTACAGTACTGTGATAACTG AATTGTGAGCAATAGTAAGGAAGTTCAGTTACAC
	R	CTTTCGCTAAGGATCTGCAGTGGTACCAGGAGTGGGGTTCGAAC CCACGCGGACATATGTCCATTGGATCGGGCCAACAACGTGCAGC ACTTCTAGACAGCACTAGTGTAACTGAACTTC
miR-495-3p	F	TTGTAACGCTGAATTCACCAGGATGGCCGAGTGGTTAAGGCGTT GGACTGGCCAGCTGTGAGTGTTTCTTTAGCAGCACAGAAATATT GGCTTGTGAGCAATAGTAAGGAAGGCCAATATTCT
	R	CTTTCGCTAAGGATCTGCAGTGGTACCAGGAGTGGGGTTCGAAC CCACGCGGACATATGTCCATTGGATCGGGCCAACAACGTGCAGC ACTTCTGGAGCAGCACTAGAATATTGGCCTTC

miR-519a-5p	F	TTGTAACGCTGAATTCACCAGGATGGCCGAGTGGTTAAGGCGTTGGACTGGCCAGCTGTGAGTGTTTCTTGCCTGCTGGGGTGGAACCTGGTTGTGAGCAATAGTAAGGAAGCCAGGTTCGC
	R	CTTTCGCTAAGGATCTGCAGTGGTACCAGGAGTGGGGTTCGAACCCACGCGGACATATGTCCATTGGATCGGGCCAACAACGTGCAGCACTTCTATCCTGCTGATGGCGAACCTGGCTTCC
miR-29a-3p	F	TTGTAACGCTGAATTCACCAGGATGGCCGAGTGGTTAAGGCGTTGGACTGGCCAGCTGTGAGTGTTTCTTAAACAAACATGGTGCACTTCTTTGTGAGCAATAGTAAGGAAGAGAAGTGCCC
	R	CTTTCGCTAAGGATCTGCAGTGGTACCAGGAGTGGGGTTCGAACCCACGCGGACATATGTCCATTGGATCGGGCCAACAACGTGCAGCACTTCTAGAACAAACAGTGGGCACTTCTCTTCC
miR-101-3p	F	TTGTAACGCTGAATTCACCAGGATGGCCGAGTGGTTAAGGCGTTGGACTGGCCAGCTGTGAGTGTTTCTTCTCTAGAGGGAAGCGCTTTCTGTGTGAGCAATAGTAAGGAATGGAAAGTGTT
	R	CTTTCGCTAAGGATCTGCAGTGGTACCAGGAGTGGGGTTCGAACCCACGCGGACATATGTCCATTGGATCGGGCCAACAACGTGCAGCACTTCTAGTCTAAAAGCGAACACTTTCCATTCC
miR-195-5p	F	TTGTAACGCTGAATTCACCAGGATGGCCGAGTGGTTAAGGCGTTGGACTGGCCAGCTGTGAGTGTTTCTTTAGCACCATCTGAAATCGGTTATGTGAGCAATAGTAAGGAATGACTGATTC
	R	CTTTCGCTAAGGATCTGCAGTGGTACCAGGAGTGGGGTTCGAACCCACGCGGACATATGTCCATTGGATCGGGCCAACAACGTGCAGCACTTCTAGAACACCATGCTGAATCAGTCATTCCT
miR-99-5p	F	TTGTAACGCTGAATTCACCAGGATGGCCGAGTGGTTAAGGCGTTGGACTGGCCAGCTGTGAGTGTTTCTTAACCCGTAGATCCGATCTTGTGTGTGAGCAATAGTAAGGAATACAAGGTCG
	R	CTTTCGCTAAGGATCTGCAGTGGTACCAGGAGTGGGGTTCGAACCCACGCGGACATATGTCCATTGGATCGGGCCAACAACGTGCAGCACTTCTAGACCCATAGTATCGACCTTGTATTCCT
miR-100-5p	F	TTGTAACGCTGAATTCACCAGGATGGCCGAGTGGTTAAGGCGTTGGACTGGCCAGCTGTGAGTGTTTCTTAACCCGTAGATCCGAACTTGTGTGTGAGCAATAGTAAGGAATACAAGTTCG
	R	CTTTCGCTAAGGATCTGCAGTGGTACCAGGAGTGGGGTTCGAACCCACGCGGACATATGTCCATTGGATCGGGCCAACAACGTGCAGCACTTCTAGACCCATAGTATCGAACTTGTATTCCT
miR-146a-5p	F	TTGTAACGCTGAATTCACCAGGATGGCCGAGTGGTTAAGGCGTTGGACTGGCCAGCTGTGAGTGTTTCTTTGAGAACTGAATTCCATGGGTTTGTGAGCAATAGTAAGGAAGACCTGTGGA
	R	CTTTCGCTAAGGATCTGCAGTGGTACCAGGAGTGGGGTTCGAACCCACGCGGACATATGTCCATTGGATCGGGCCAACAACGTGCAGCACTTCTAGAAGAACTGTAATCCACAGGTCTTCCT
miR-146b-5p	F	TTGTAACGCTGAATTCACCAGGATGGCCGAGTGGTTAAGGCGTTGGACTGGCCAGCTGTGAGTGTTTCTTTGAGAACTGAATTCCATAGGCTGGTGAGCAATAGTAAGGA**T**GGCCTGTGGA

	R	CTTTCGCTAAGGATCTGCAGTGGTACCAGGAGTGGGGTTCGAACCCACGCGGACATATGTCCATTGGATCGGGCCAACAACGTGCAGCACTTCTAGGAGAACTGTAATCCACAGGCCATCCT
BioRNA^{Gly}		
miR-126b-3p	F	TTGTAACGCTGAATTCGCATGGGTGGTTCAGTGGTAGAATTCTCGCCTGGCCAGCTGTGAGTG
	R	CTTTCGCTAAGGATCTGCAGTGGTGCATGGGCCGGGAATCGAACCCGGGGCCTCCCGCGTGGGCCAACAACGTGC
miR-133a-3p	F	TTGTAACGCTGAATTCGCATGGGTGGTTCAGTGGTAGAATTCTCGCCTGGCCAGCTGTGAGTG
	R	CTTTCGCTAAGGATCTGCAGTGGTGCATGGGCCGGGAATCGAACCCGGGGCCTCCCGCGTGGGCCAACAACGTGC
miR-200b-3p	F	TTGTAACGCTGAATTCGCATGGGTGGTTCAGTGGTAGAATTCTCGCCTGGCCAGCTGTGAGTG
	R	CTTTCGCTAAGGATCTGCAGTGGTGCATGGGCCGGGAATCGAACCCGGGGCCTCCCGCGTGGGCCAACAACGTGC
miR-7-5p	F	TTGTAACGCTGAATTCGCATGGGTGGTTCAGTGGTAGAATTCTCGCCTGGCCAGCTGTGAGTG
	R	CTTTCGCTAAGGATCTGCAGTGGTGCATGGGCCGGGAATCGAACCCGGGGCCTCCCGCGTGGGCCAACAACGTGC
miR-143b-3p	F	TTGTAACGCTGAATTCGCATGGGTGGTTCAGTGGTAGAATTCTCGCCTGGCCAGCTGTGAGTG
	R	CTTTCGCTAAGGATCTGCAGTGGTGCATGGGCCGGGAATCGAACCCGGGGCCTCCCGCGTGGGCCAACAACGTGC
miR-206-3p	F	TTGTAACGCTGAATTCGCATGGGTGGTTCAGTGGTAGAATTCTCGCCTGGCCAGCTGTGAGTG
	R	CTTTCGCTAAGGATCTGCAGTGGTGCATGGGCCGGGAATCGAACCCGGGGCCTCCCGCGTGGGCCAACAACGTGC
miR-375-3p	F	TTGTAACGCTGAATTCGCATGGGTGGTTCAGTGGTAGAATTCTCGCCTGGCCAGCTGTGAGTG
	R	CTTTCGCTAAGGATCTGCAGTGGTGCATGGGCCGGGAATCGAACCCGGGGCCTCCCGCGTGGGCCAACAACGTGC
miR-497-5p	F	TTGTAACGCTGAATTCGCATGGGTGGTTCAGTGGTAGAATTCTCGCCTGGCCAGCTGTGAGTG
	R	CTTTCGCTAAGGATCTGCAGTGGTGCATGGGCCGGGAATCGAACCCGGGGCCTCCCGCGTGGGCCAACAACGTGC
miR-125b-5p	F	TTGTAACGCTGAATTCGCATGGGTGGTTCAGTGGTAGAATTCTCGCCTGGCCAGCTGTGAGTG
	R	CTTTCGCTAAGGATCTGCAGTGGTGCATGGGCCGGGAATCGAACCCGGGGCCTCCCGCGTGGGCCAACAACGTGC
let-7a-5p	F	TTGTAACGCTGAATTCGCATGGGTGGTTCAGTGGTAGAATTCTCGCCTGGCCAGCTGTGAGTG
	R	CTTTCGCTAAGGATCTGCAGTGGTGCATGGGCCGGGAATCGAACCCGGGGCCTCCCGCGTGGGCCAACAACGTGC

let-7b-5p	F	TTGTAACGCTGAATTCGCATGGGTGGTTCAGTGGTAGAATTCTCG CCTGGCCAGCTGTGAGTG
	R	CTTTCGCTAAGGATCTGCAGTGGTGCATGGGCCGGGAATCGAAC CCGGGCCTCCCGCGTGGGCCAACAACGTGC
let-7c-5p	F	TTGTAACGCTGAATTCGCATGGGTGGTTCAGTGGTAGAATTCTCG CCTGGCCAGCTGTGAGTGTTTCTTTGAGGTAGTAGGTTGTATGGT TTGTGAGCAATAGTAAGGAAAACTGTA
	R	CTTTCGCTAAGGATCTGCAGTGGTGCATGGGCCGGGAATCGAAC CCGGGCCTCCCGCGTGGGCCAACAACGTGCAGCACTTCTGAAAG GTAGTCAGGTGTACAGTTTTCCTTA
let-7d-5p	F	TTGTAACGCTGAATTCGCATGGGTGGTTCAGTGGTAGAATTCTCG CCTGGCCAGCTGTGAGTG
	R	CTTTCGCTAAGGATCTGCAGTGGTGCATGGGCCGGGAATCGAAC CCGGGCCTCCCGCGTGGGCCAACAACGTGC
let-7e-5p	F	TTGTAACGCTGAATTCGCATGGGTGGTTCAGTGGTAGAATTCTCG CCTGGCCAGCTGTGAGTG
	R	CTTTCGCTAAGGATCTGCAGTGGTGCATGGGCCGGGAATCGAAC CCGGGCCTCCCGCGTGGGCCAACAACGTGC
let-7f-5p	F	TTGTAACGCTGAATTCGCATGGGTGGTTCAGTGGTAGAATTCTCG CCTGGCCAGCTGTGAGTG
	R	CTTTCGCTAAGGATCTGCAGTGGTGCATGGGCCGGGAATCGAAC CCGGGCCTCCCGCGTGGGCCAACAACGTGC
let-7g-5p	F	TTGTAACGCTGAATTCGCATGGGTGGTTCAGTGGTAGAATTCTCG CCTGGCCAGCTGTGAGTG
	R	CTTTCGCTAAGGATCTGCAGTGGTGCATGGGCCGGGAATCGAAC CCGGGCCTCCCGCGTGGGCCAACAACGTGC
miR-370-3p	F	TTGTAACGCTGAATTCGCATGGGTGGTTCAGTGGTAGAATTCTCG CCTGGCCAGCTGTGAGTG
	R	CTTTCGCTAAGGATCTGCAGTGGTGCATGGGCCGGGAATCGAAC CCGGGCCTCCCGCGTGGGCCAACAACGTGC
miR-495-3p	F	TTGTAACGCTGAATTCGCATGGGTGGTTCAGTGGTAGAATTCTCG CCTGGCCAGCTGTGAGTG
	R	CTTTCGCTAAGGATCTGCAGTGGTGCATGGGCCGGGAATCGAAC CCGGGCCTCCCGCGTGGGCCAACAACGTGC
miR-519a-5p	F	TTGTAACGCTGAATTCGCATGGGTGGTTCAGTGGTAGAATTCTCG CCTGGCCAGCTGTGAGTG
	R	CTTTCGCTAAGGATCTGCAGTGGTGCATGGGCCGGGAATCGAAC CCGGGCCTCCCGCGTGGGCCAACAACGTGC
miR-29a-3p	F	TTGTAACGCTGAATTCGCATGGGTGGTTCAGTGGTAGAATTCTCG CCTGGCCAGCTGTGAGTG
	R	CTTTCGCTAAGGATCTGCAGTGGTGCATGGGCCGGGAATCGAAC CCGGGCCTCCCGCGTGGGCCAACAACGTGC
miR-101-3p	F	TTGTAACGCTGAATTCGCATGGGTGGTTCAGTGGTAGAATTCTCG CCTGGCCAGCTGTGAGTG
	R	CTTTCGCTAAGGATCTGCAGTGGTGCATGGGCCGGGAATCGAAC CCGGGCCTCCCGCGTGGGCCAACAACGTGC

miR-195-5p	F	TTGTAACGCTGAATTCGCATGGGTGGTTCAGTGGTAGAATTCTCG CCTGGCCAGCTGTGAGTG
	R	CTTTCGCTAAGGATCTGCAGTGGTGCATGGGCCGGGAATCGAAC CCGGGCCTCCCGCGTGGGCCAACAACGTGC
miR-99-5p	F	TTGTAACGCTGAATTCGCATGGGTGGTTCAGTGGTAGAATTCTCG CCTGGCCAGCTGTGAGTG
	R	CTTTCGCTAAGGATCTGCAGTGGTGCATGGGCCGGGAATCGAAC CCGGGCCTCCCGCGTGGGCCAACAACGTGC
miR-100-5p	F	TTGTAACGCTGAATTCGCATGGGTGGTTCAGTGGTAGAATTCTCG CCTGGCCAGCTGTGAGTG
	R	CTTTCGCTAAGGATCTGCAGTGGTGCATGGGCCGGGAATCGAAC CCGGGCCTCCCGCGTGGGCCAACAACGTGC
miR-146a-5p	F	TTGTAACGCTGAATTCGCATGGGTGGTTCAGTGGTAGAATTCTCG CCTGGCCAGCTGTGAGTG
	R	CTTTCGCTAAGGATCTGCAGTGGTGCATGGGCCGGGAATCGAAC CCGGGCCTCCCGCGTGGGCCAACAACGTGC
miR-146b-5p	F	TTGTAACGCTGAATTCGCATGGGTGGTTCAGTGGTAGAATTCTCG CCTGGCCAGCTGTGAGTG
	R	CTTTCGCTAAGGATCTGCAGTGGTGCATGGGCCGGGAATCGAAC CCGGGCCTCCCGCGTGGGCCAACAACGTGC

Supplemental Table S3. Sequences of commercial mimics and primers used for real-time qPCR analyses. F, forward primer; R, reverse primer.

Mimic miRNA		**Sequence (5' to 3')**
miRCURY LNA miR-7-5p (Mimic miR-7-5p)		UGGAAGACUAGUGAUUUUGUUGU (guide sequence)
miRCURY LNA negative control (Mimic Control)		UCACCGGGUGUAAAUCAGCUUG (guide sequence)
Primer		**Primer Sequence (5' to 3')**
hsa-miR-7-5p		
stem-loop RT		GTCGTATCCAGTGCAGGGTCCGAGGTATTCGCACTGGATACGACCAACAA
qPCR	F	CGCGCTGGAAGACTAGTGATT
	R	GTGCAGGGTCCGAGGT
U6 qPCR	F	CTCGCTTCGGCAGCACA
	R	AACGCTTCACGAATTTGCGT

Supplemental Table S4. RNA sequences used for computational modeling. Underlined, htRNA; Black, respective hsa-pre-miRNA sequence; Red and Green, miRNA guide and passenger strand, respectively; Orange, anticodon; Bold, "CCA" tail. Sequences attained from the Genomic tRNA Database (GtRNAdb), *miRBase.org*, or our recent publications.

Target ncRNA	Length (nt)	Sequence (5' to 3')	MW (Da)
htRNA^{Gly} (anticodon GCC)	74	GCAUGGGUGGUUCAGUGGUAGAA UUCUCGCCUGCCACGCGGGAGGCC CGGGUUCGAUUCCCGGCCCAUGCA **CCA**	24,022
htRNA^{Leu} (anticodon UAA)	86	ACCAGGAUGGCCGAGUGGUUAAG GCGUUGGACUUAAGAUCCAAUGG ACAUAUGUCCGCGUGGGUUCGAAC CCCACUCCUGGUA**CCA**	27,905
hsa-pre-miR-34a-5p	114	GGCCGGGCCAGCUGUGAGUGUUUC UUUGGCAGUGUCUUAGCUGGUUG UUGUGAGCAAUAGUAAGGAAGCA AUCAGCAAGUAUACUGCCCUAGAA GUGCUGCACGUUGUUGGCCC	36,975
hsa-pre-miR-124-3p	85	AGGCCUCUCUCUCCGUGUUCACAG CGGACCUUGAUUUAAAUGUCCAUA CAAUUAAGGCACGCGGUGAAUGCC AAGAAUGGGGCUG	27,505
hsa-pre-miR-7-5p	110	UUGGAUGUUGGCCUAGUUCUGUG UGGAAGACUAGUGAUUUUGUUGU UUUUAGAUAACUAAAUCGACAAC AAAUCACAGUCUGCCAUAUGGCAC AGGCCAUGCCUCUACAG	35,461
hsa-pre-miR-34a/miR-124-3p	109	GGCCAGCUGUGAGUGUUUCUUUA AGGCACGCGGUGAAUGCCGUUGUG AGCAAUAGUAAGGAAGCGGUGUU CCCGUCGUGCCUUCUAGAAGUGCU GCACGUUGUUGGCCC	35,351
hsa-pre-miR-34a/miR-7-5p	109	GGCCAGCUGUGAGUGUUUCUUUG GAAGACUAGUGAUUUUGUUGUGU GAGCAAUAGUAAGGAACAACAAA AUACUCAGUCUUCCCUAGAAGUGC UGCACGUUGUUGGCCC	35,266
BioRNA^{Gly}/miR-34a-5p	180	GCAUGGGUGGUUCAGUGGUAGAA UUCUCGCCUGGCCAGCUGUGAGUG UUUCUUUGGCAGUGUCUUAGCUG GUUGUUGUGAGCAAUAGUAAGGA AGCAAUCAGCAAGUAUACUGCCCU AGAAGUGCUGCACGUUGUUGGCCC	58,237

		ACGCGGGAGGCCCGGGUUCGAUUC CCGGCCCAUGCACCA	
BioRNA^{Leu}/miR-34a-5p	192	ACCAGGAUGGCCGAGUGGUUAAG GCGUUGGACUGGCCAGCUGUGAGU GUUUCUUUGGCAGUGUCUUAGCU GGUUGUUGUGAGCAAUAGUAAGG AAGCAAUCAGCAAGUAUACUGCCC UAGAAGUGCUGCACGUUGUUGGCC CGAUCCAAUGGACAUAUGUCCGCG UGGGUUCGAACCCCACUCCUGGUA CCA	62,110
BioRNA^{Gly}/miR-124-3p	180	GCAUGGGUGGUUCAGUGGUAGAA UUCUCGCCUGGCCAGCUGUGAGUG UUUCUUUAAGGCACGCGGUGAAU GCCGUUGUGAGCAAUAGUAAGGA AGCGGUGUUCCCGUCGUGCCUUCU AGAAGUGCUGCACGUUGUUGGCCC ACGCGGGAGGCCCGGGUUCGAUUC CCGGCCCAUGCACCA	58,259
BioRNA^{Leu}/miR-124-3p	192	ACCAGGAUGGCCGAGUGGUUAAG GCGUUGGACUGGCCAGCUGUGAGU GUUUCUUUAAGGCACGCGGUGAA UGCCGUUGUGAGCAAUAGUAAGG AAGCGGUGUUCCCGUCGUGCCUUC UAGAAGUGCUGCACGUUGUUGGCC CGAUCCAAUGGACAUAUGUCCGCG UGGGUUCGAACCCCACUCCUGGUA CCA	62,132
BioRNA^{Gly}/miR-7-5p	180	GCAUGGGUGGUUCAGUGGUAGAA UUCUCGCCUGGCCAGCUGUGAGUG UUUCUUUGGAAGACUAGUGAUUU UGUUGUGUGAGCAAUAGUAAGGA ACAACAAAAUACUCAGUCUUCCCU AGAAGUGCUGCACGUUGUUGGCCC ACGCGGGAGGCCCGGGUUCGAUUC CCGGCCCAUGCACCA	58,174
BioRNA^{Leu}/miR-7-5p	192	ACCAGGAUGGCCGAGUGGUUAAG GCGUUGGACUGGCCAGCUGUGAGU GUUUCUUUGGAAGACUAGUGAUU UUGUUGUGUGAGCAAUAGUAAGG AACAACAAAAUACUCAGUCUUCCC UAGAAGUGCUGCACGUUGUUGGCC CGAUCCAAUGGACAUAUGUCCGCG UGGGUUCGAACCCCACUCCUGGUA CCA	62,093

Figure legends

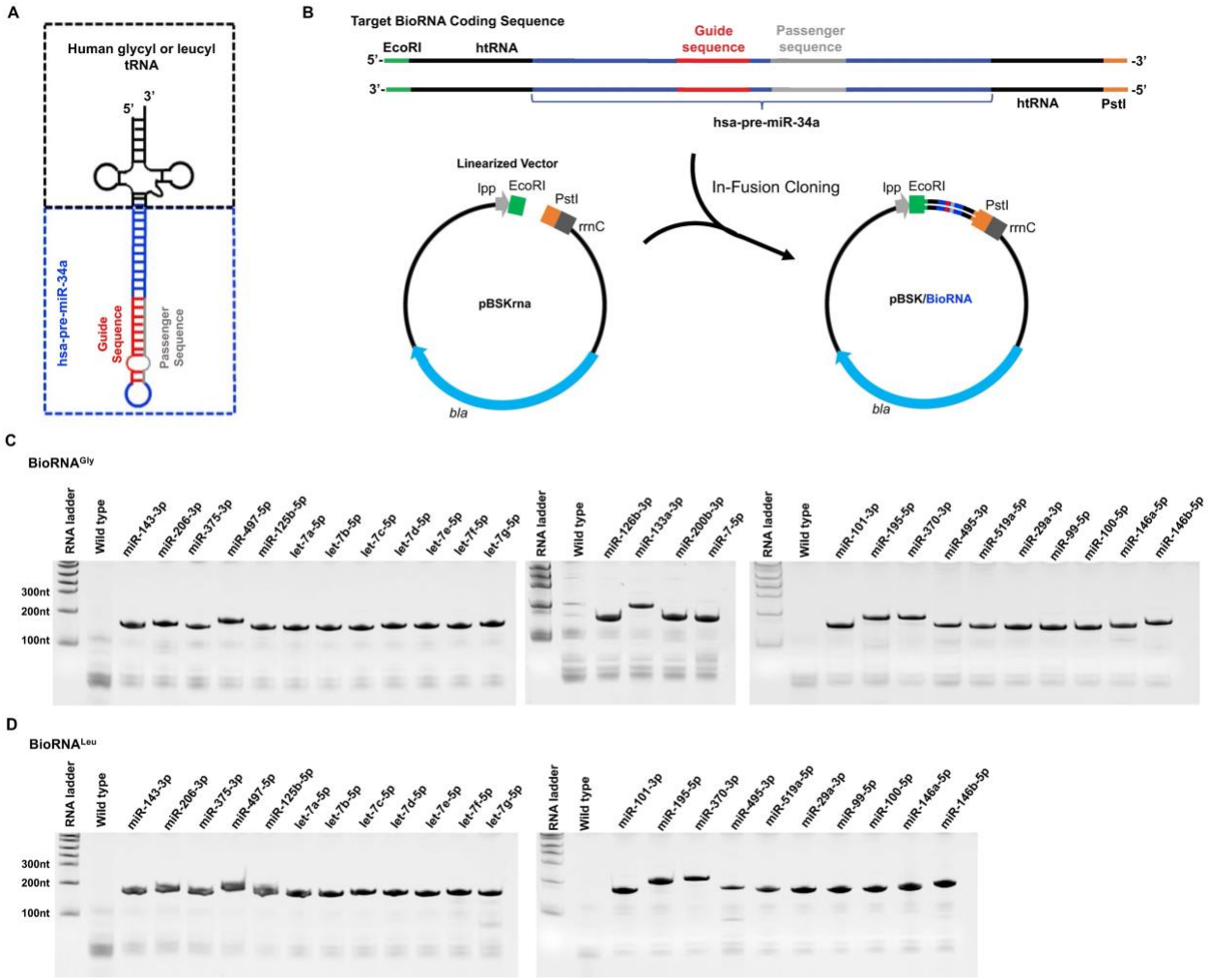

Figure 1. Heterogenous overexpression of a total of 48 new BioRNAs with human glycyl or leucyl tRNA fused hsa-pre-miR-34a carrier (BioRNA^{Gly} or BioRNA^{Leu}). (**A**) The 2D graphic of BioRNA^{Gly} or BioRNA^{Leu} with a payload miRNA whose guide and passenger sequences are highlighted. (**B**) Sequence design of target BioRNA insert for cloning into a pBSKrna vector linearized by EcoRI and PstI restriction enzymes to offer the BioRNA expression plasmid (pBSK/BioRNA), which is comprised of a lipoprotein (lpp) promoter, terminator from the *E. coli* ribosomal RNA rrnC operon (rrnC), and the gene encoding beta-lactamase (*bla*) for antibiotic resistance and selection. (C and D) Urea-PAGE analyses depicting the successful overexpression of 26 BioRNA^{Gly} (**C**) and 22 BioRNA^{Leu} (**D**) versions of recombinant miRNAs, as manifested by the appearance of a strong new band at expected size when compared to total RNA from the wild type HST08 *E. coli*. 300 ng RNA per lane. Urea-PAGE analyses depicting the successful overexpression of BioRNA^{Leu}/miR-126b-3p, -133a-3p, -200b-3p, and -7-5p have been reported recently [253].

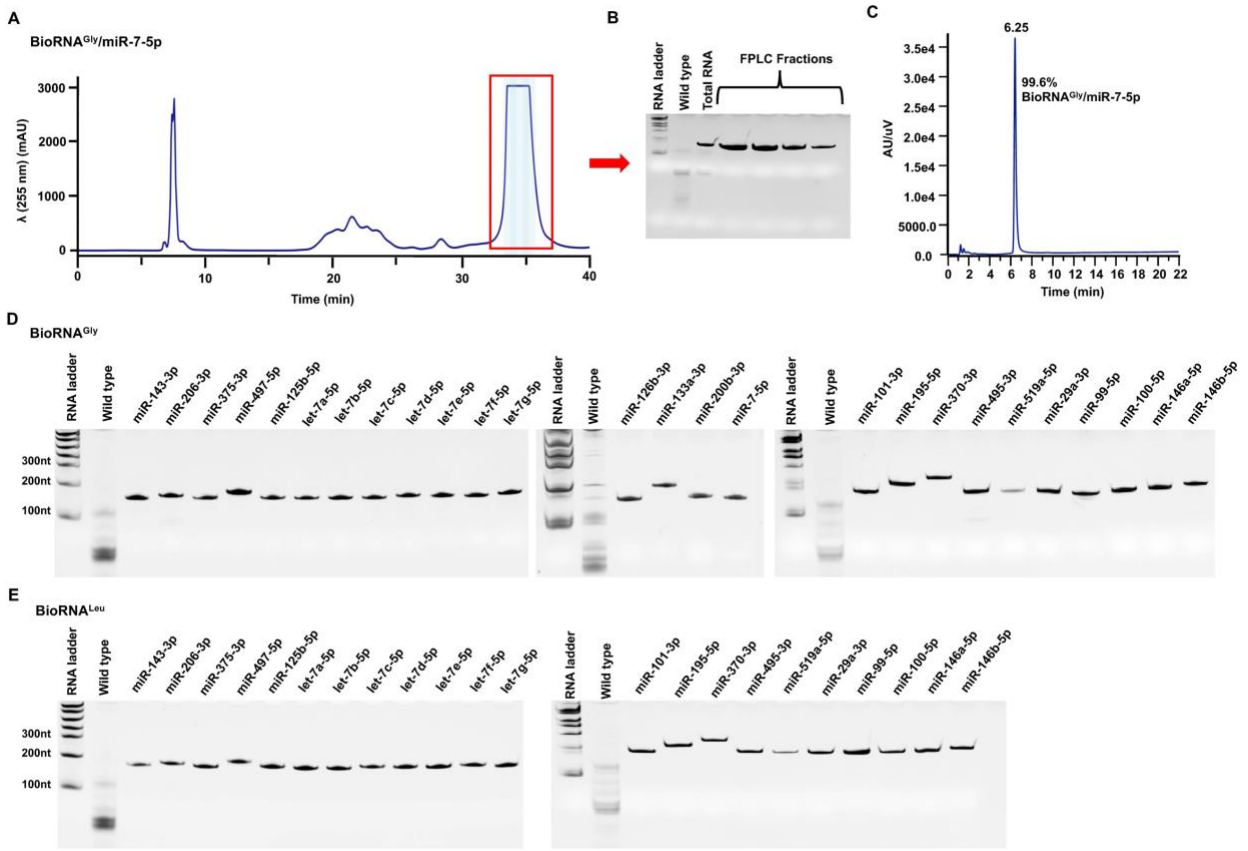

Figure 2. Purification of recombinant miRNA molecules. (**A**) Representative FPLC-UV trace during the purification of the model BioRNA^{Gly}/miR-7-5p with a highlighted peak for target fraction collection. (**B**) Urea-PAGE analysis of BioRNA^{Gly}/miR-7-5p fractions. (**C**) HPLC determination of the purity (99.6%) of final BioRNA^{Gly}/miR-7-5p product. (**D**) and (**E**) Urea-PAGE analyses depicting FPLC-purified BioRNA^{Gly}/miRNAs and BioRNA^{Leu}/miRNAs, respectively (50 ng RNA/lane). Purification of BioRNA^{Leu}/miR-7-5p, -126b-3p, -133a-3p, and -200b-3p has been published recently [253].

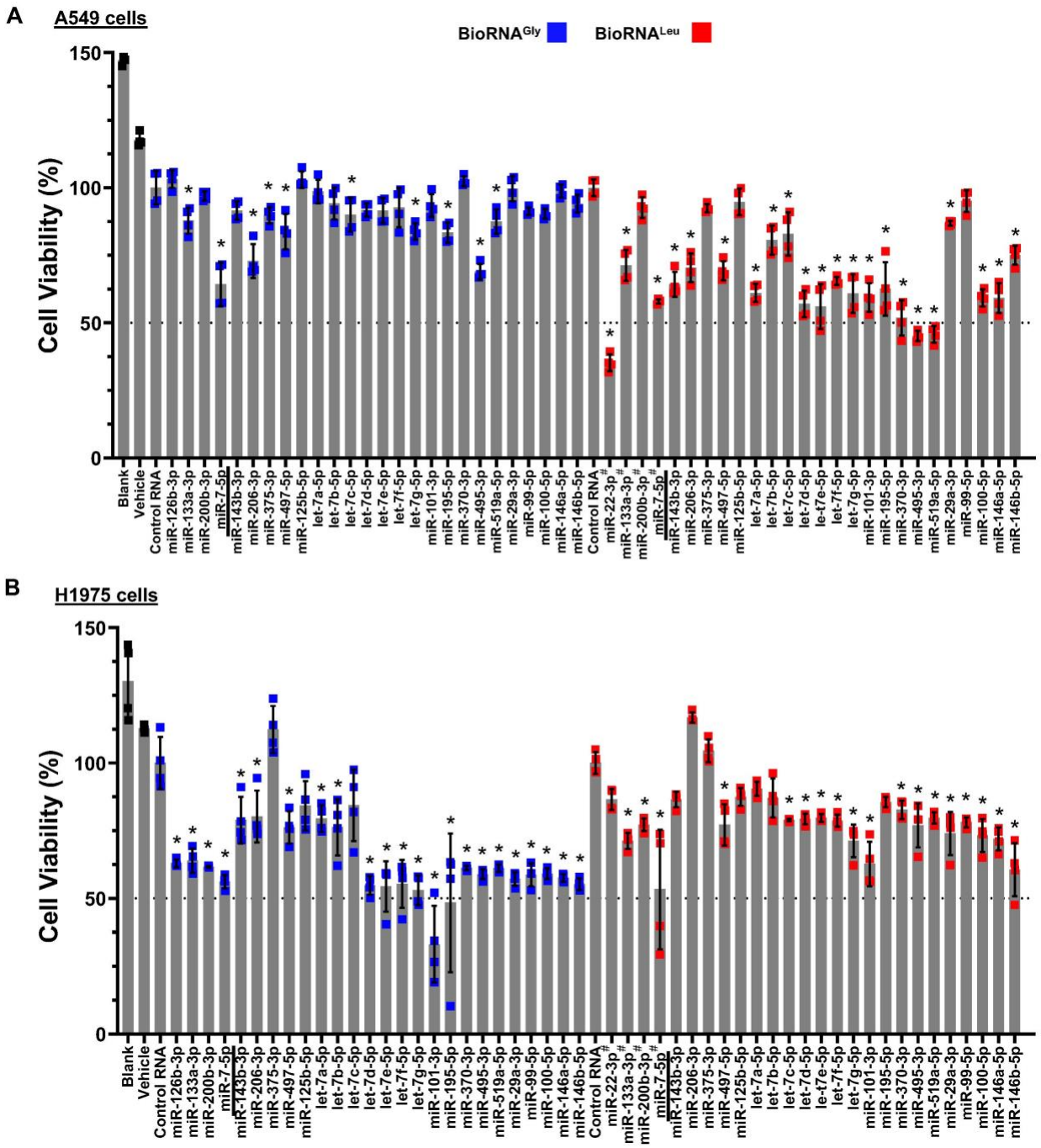

Figure 3. Screen for antiproliferative effects of 48 novel, highly purified BioRNAs against human NSCLC cells. Cell viability of A549 (**A**) and H1975 (**B**) cells were reduced to various degrees by BioRNA^{Gly} (Blue) and BioRNA^{Leu} (Red) based miRNAs (15 nM) as compared with control BioRNA or vehicle as well as untreated cells. Cell viability values were determined by CellTiter-Glo assay at 72 h post-transfection and normalized to respective control RNAs (100%). Values are mean ± SD (N = 4 biological replicates per group). #Several BioRNAs published recently were included for comparison. Overall, the effects on NSCLC cell viability were comparable between the paired BioRNA^{Gly}- and BioRNA^{Leu}-based miRNAs with putative cell line-specific differences. BioRNA/miR-7-5p used for further studies are underlined. *$P < 0.05$, as compared to respective control RNA (one-way ANOVA with Bonferroni *post hoc* tests).

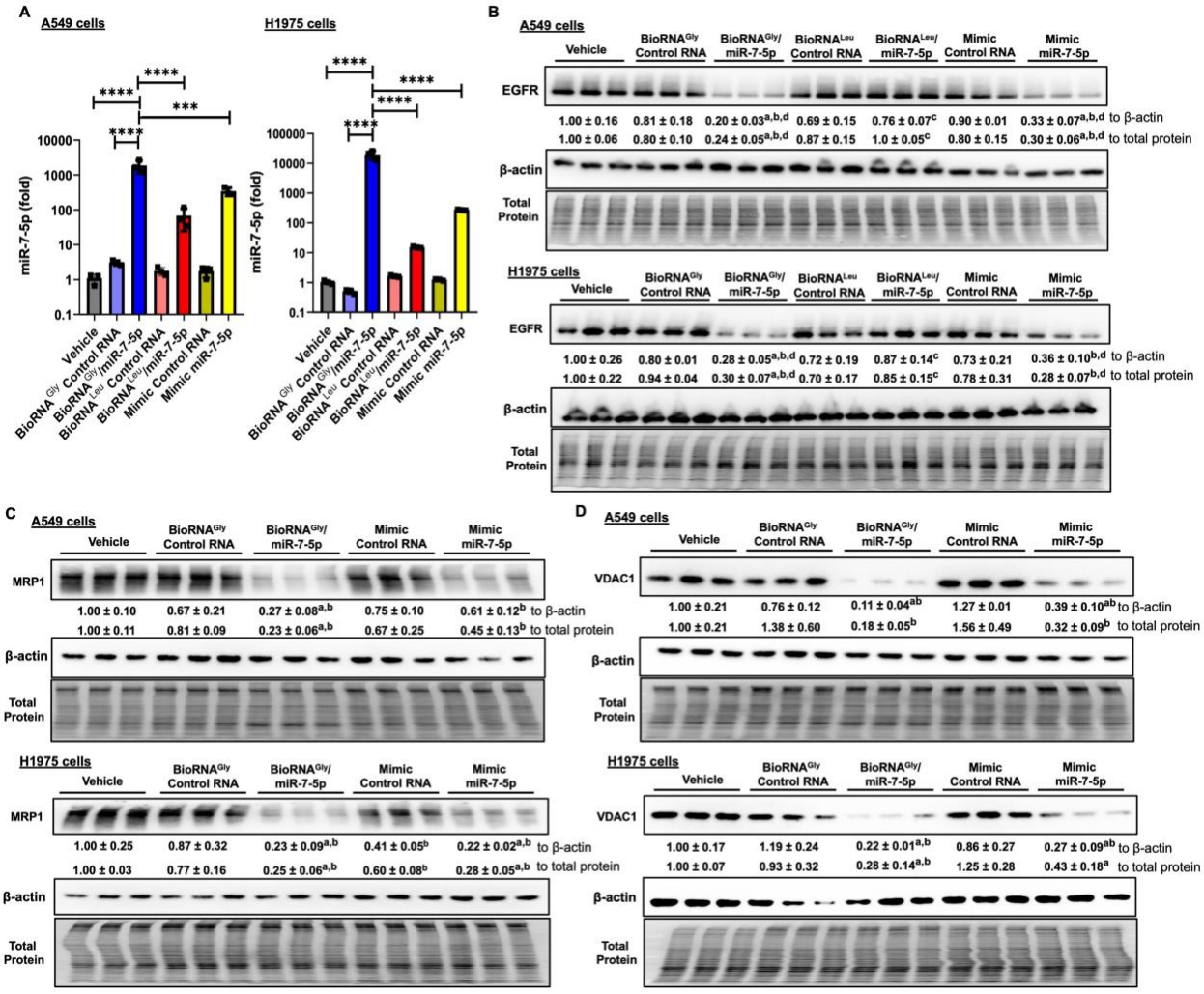

Figure 4. Efficacy of model recombinant miR-7-5p to regulate target gene expression in human NSCLC cells. (**A**) BioRNA^{Gly}- and BioRNA^{Leu}-carried miR-7-5p are processed to target miR-7-5p in A549 and H1975 cells. Cells were transfected with 15 nM BioRNA/miR-7-5p, control BioRNA, or Lipofectamine 3000 (vehicle) for 48 h, and miR-7-5p levels were determined by selective stem loop RT qPCR assay. Commercial miRCURY LNA miR-7-5p mimic (Mimic miR-7-5p) and control RNA (Mimic Control) from Qiagen were used for comparison. (**B**) Impact of BioRNA/miR-7-5p on a well-known miR-7-5p target, epidermal growth factor receptor (EGFR) in A549 and H1975 cells after 72-h transfection, as determined by Western blot analyses. Surprisingly, BioRNA^{Gly}/miR-7-5p more effectively reduced EGFR protein levels than BioRNA^{Leu}/miR-7-5p besides control RNA. Therefore, effects of BioRNA^{Gly}/miR-7-5p versus the mimic on (**C**) multidrug resistance-associated protein 1 (MPR1) and (**D**) voltage-dependent anion channel protein 1 (VDAC1) protein levels were further defined. miR-7-5p and targeted protein levels were normalized to corresponding U6 and β-actin or total protein, respectively, and vehicle control groups were set as 1.0. All values are mean ± SD (N = 3 biological replicates per group). ****P < 0.0001; ***P < 0.001; ^{a}P < 0.05, as compared to respective control RNA; ^{b}P < 0.05, compared to vehicle control; ^{c}P < 0.05, compared to Mimic miR-7-5p; ^{d}P < 0.05, compared to BioRNA^{Leu}/miR-7-5p (one-way ANOVA with Bonferroni *post hoc* tests).

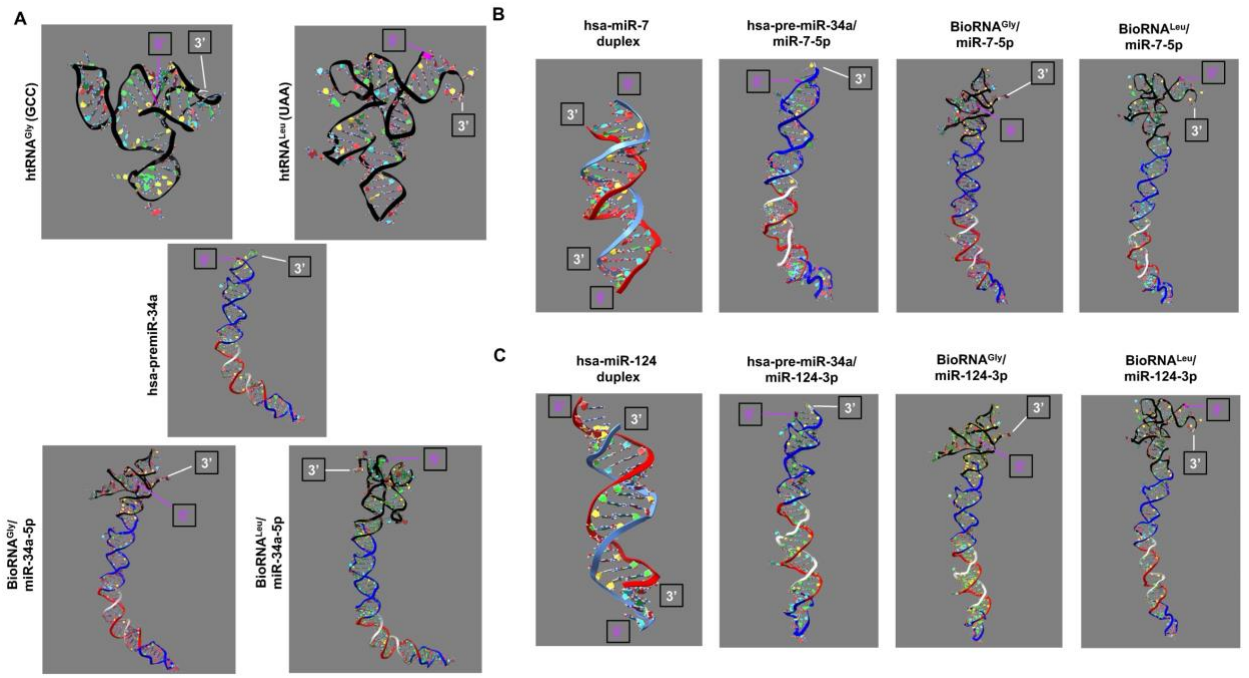

Figure 5. Comparison of computationally predicted 3D structures of BioRNAs. (**A**) Predicted 3D structures of human leucyl (UAA) and glycyl (GCC) tRNAs, hsa-pre-miR-34a, and the hybrid carrier RNAs (BioRNA^{Gly}/miR-34a-5p and BioRNA^{Leu}/miR-34a-5p). (**B**) Predicted structures of the hsa-miR-7 duplex, hsa-pre-miR-34a carrier with payload miR-7 (hsa-pre-miR-34a/miR-7-5p), BioRNA^{Gly}/miR-7-5p, and BioRNA^{Leu}/miR-7-5p. (**C**) 3D structures of the hsa-miR-124 duplex, hsa-pre-miR-34a carrier substituted by miR-124 duplex (hsa-pre-miR-34a/miR-124-3p), BioRNA^{Gly}/miR-124-3p, and BioRNA^{Leu}/miR-124-3p. Colored subcomponents of BioRNAs consist of ribbon structures: htRNA (Black), hsa-pre-miR-34a (Blue), miRNA guide (antisense; Red) and passenger (sense; Light Blue or Light Grey) sequence, five-prime (5'; Magenta), and three-prime (3'; White). Nucleotides consists of color filled nucleobases: adenine (Red), thymine (Blue), guanine (Green), and cytosine (Yellow). Modeling results demonstrate a retained overall structure of BioRNAs when substituted with target miRNAs. All RNA 3D structures were generated by using RNAComposer after inputting the secondary structures predicted by RNAFold, based on the primary sequences showed in Tables S1 and S4. Resulting structures were adapted using UCSF ChimeraX next-generation molecular visualization program.

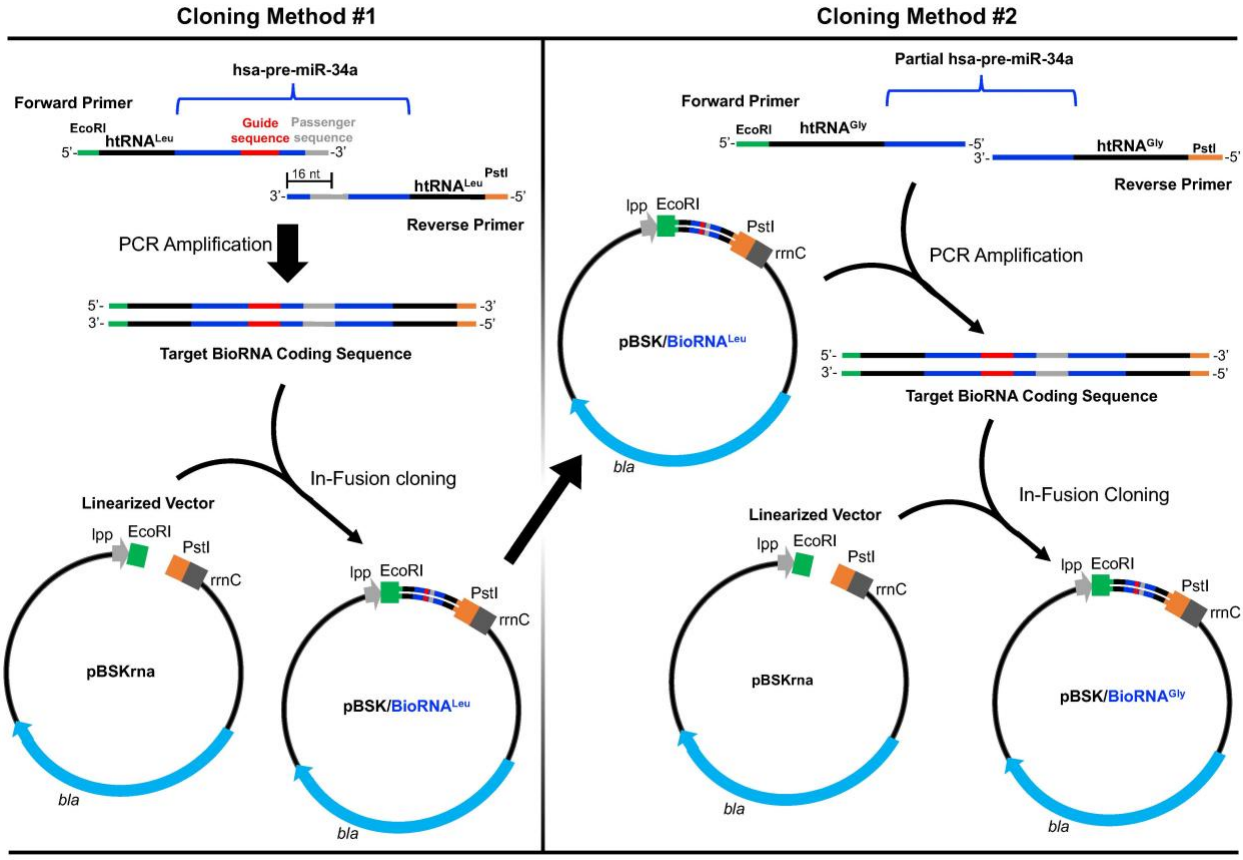

Supplemental Figure S1. Methods for constructing the pBSK/BioRNA plasmids. The BioRNA^{Leu} and BioRNA^{Gly} plasmids were cloned using an In-Fusion cloning kit where the target inserts were amplified by two methods. In Method #1 (BioRNA^{Leu} in this study), the inserts were obtained directly through PCR amplification using primers with 16-nt complementary base pair overlaps (Table S2) and then cloned into the pBSKrna vector. In Method #2 (BioRNAs^{Gly}), the inserts were obtained through PCR amplification using respective pBSK/BioRNA^{Leu} plasmids as templates and htRNA specific primers (Table S2). The resultant pBSK/BioRNA plasmids were transformed into Stellar™ Competent Cells (*E. coli* HST08 stain) for plasmid propagation and target BioRNA overexpression.

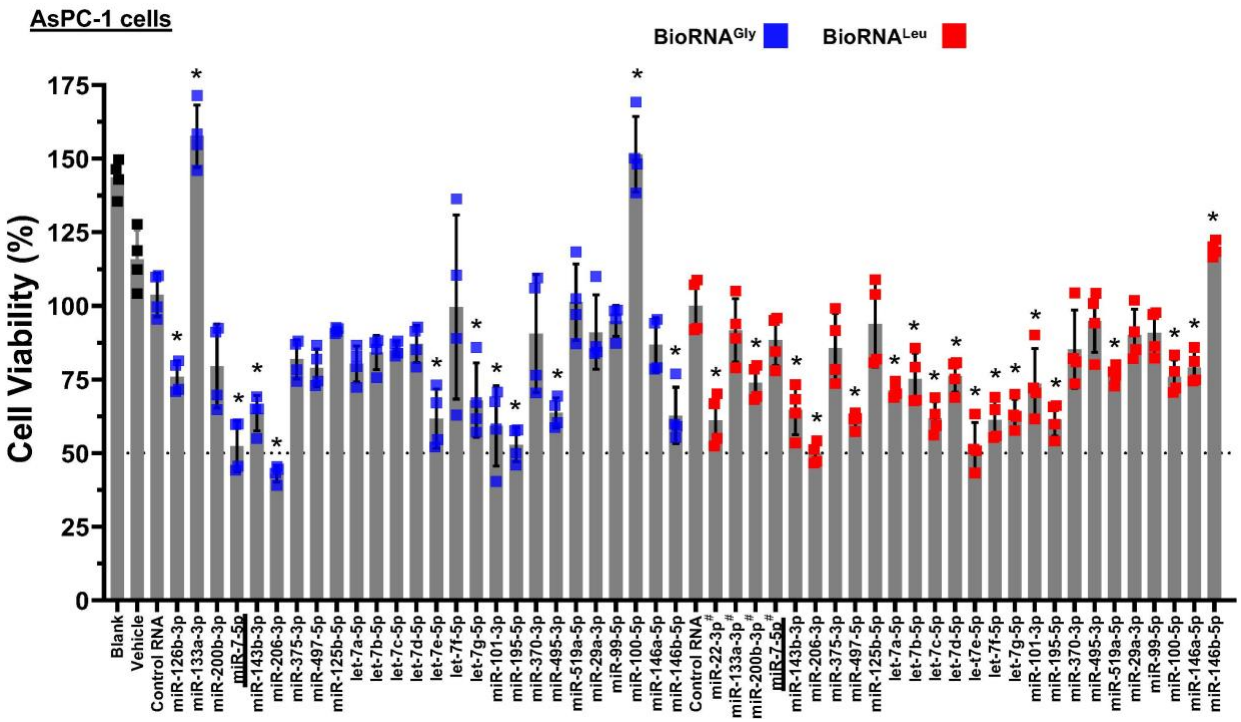

Supplemental Figure S2. Screen for antiproliferative effects of 48 novel BioRNAs against human pancreatic cancer AsPC-1 cells. Cell viability values were determined by CellTiter-Glo assay at 72 h post-transfection with 15 nM recombinant miRNAs, control RNAs or vehicle. Control RNA groups were set as 100%. Values are mean ± SD (N = 4 biological replicates per group). #Several BioRNAs published recently were included for comparison. The data demonstrate an overall similar impact of the BioRNA^{Gly}- and BioRNA^{Leu}-based miRNA on AsPC-1 cell viability.

Chapter 4: Bioengineered miR-7-5p modulates non-small cell lung cancer cell metabolism to improve therapy

Abstract

Background and Purpose:

Reintroduction of tumor-suppressive microR-7-5p (miR-7) found depleted in NSCLC represents a new therapeutic approach, whereas previous studies mainly use chemically synthesized miR-7 mimics. This study aims to establish the pharmacological actions and therapeutic potential of novel bioengineered RNA bearing a payload miR-7 (BioRNA/miR-7) molecule *in vitro* and *in vivo*.

Experimental Approach:

Confocal imaging and immunoblot studies were conducted to define the impact of BioRNA/miR-7 on target gene expression in human NSCLC cells. Mitochondrial functions and cell growth were determined through real-time Live Cell analyses, and drug accumulation was quantified by LC-MS/MS method. Antitumor activities were investigated by using NSCLC patient-derived xenograft (PDX) mouse models.

Key Results:

Firstly, we report BioRNA/miR-7 alters mitochondrial morphology in NSCLC cells accompanied by significant downregulation of and known target genes, *EGFR* and mitochondrial *TIM50* and *SLC25A37*. Secondly, mitochondrial *AGK* is validated as a new direct target for miR-7. Thirdly, BioRNA/miR-7 is revealed to modulate mitochondrial respiration and glycolytic capacity. Fourthly, co-administration of BioRNA/miR-7 with pemetrexed (PEM) elicits a strong synergism to inhibit NSCLC cell growth, associated with sharp increase in intracellular PEM accumulation. Finally, through an *in vivo* therapy study using a NSCLC PDX mouse model we

demonstrate the efficacy and tolerability of BioRNA/miR-7 mono- and combination therapy with PEM to control tumor progression.

Conclusion and Implications:

Our collective works support the use of novel, *in vivo* produced BioRNA/miR-7-5p for basic biochemical and pharmacological research and establishes a role for miR-7 in NSCLC cell metabolism and PEM disposition. Our findings illustrate the potential of BioRNA/miR-7 plus PEM combination as a novel treatment to combat NSCLC tumor progression.

Graphical Abstract

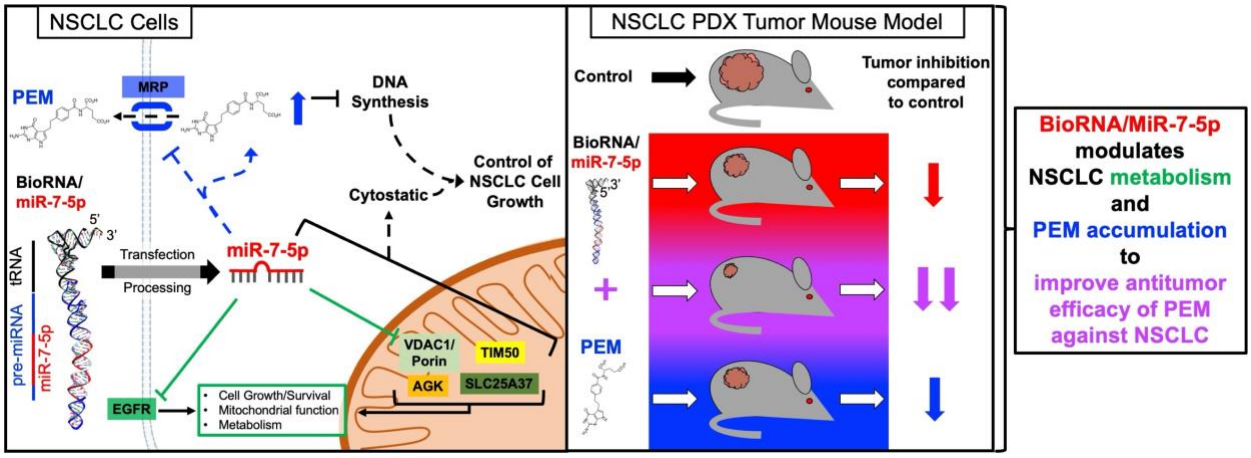

Introduction

Lung cancer accounts for almost 20% of all cancer-related deaths worldwide [353, 354] with 85% of lung cancer cases classified as non-small cell lung cancer (NSCLC) [355-357]. Today, pharmacotherapeutics are the most common treatment for NSCLC, comprised of DNA-intercalating (e.g., doxorubicin), platinum-based (e.g., cisplatin and carboplatin) and anti-folate (e.g., pemetrexed) chemotherapies alongside several forms of targeted therapies (e.g., gefitinib, erlotinib, and mobocertinib) and immunotherapies (e.g., pembrolizumab, atezolizumab, and ipilimumab) [321, 357, 358]. However, their therapeutic indications are to act on single targets thereby limiting efficacy and may lead to developed resistance in highly heterogenous NSCLC [359, 360]. Therefore, due to the lack of effective and sustainable interventions, NSCLC patents are met with a low survival rate thus warranting the development of more effective forms and combinations of pharmacotherapies [320, 356].

Growing interest in lung cancer-associated microRNAs (miRNAs or miRs) and RNA interference (RNAi)-based medications provides a novel route for miRNA replacement therapy to treat NSCLC [321, 361-363]. MiRNAs are a highly conserved family of genome derived, noncoding RNAs that function in posttranscriptional gene regulation [273, 276]. By nature, miRNAs are known to regulate several target mRNA transcripts thus providing an avenue for a single therapeutic agent to influence several biological targets or pathways often dysregulated in cancer and deemed undruggable [273, 276]. Consequently, by reintroducing select, depleted miRNAs with important roles in the control of cellular processes underlying NSCLC progression [320, 321, 361] we may more effectively treat NSCLC.

In recent studies, our lab has expanded on putative NSCLC therapeutic miRNAs using novel, bioengineered RNAs (BioRNAs) produced through *in vivo* fermentation [363]. As opposed to the chemically synthesized and artificially modified mimics used in previous studies [324, 326, 364-366], BioRNAs are true, biologic RNAi agents synthesized *in vivo* to better represent the properties of endogenous miRNAs [363]. By using a human transfer RNA (tRNA) fused hsa-pre-miR-34a carrier, various BioRNAs of interest can be produced heterologously at a high yield and in large scale and are subsequently utilized to introduce select RNAi molecule payloads in to mammalian cells *in vitro* and animals *in vivo* to exert their biological or pharmacological functions [253-256, 260, 265, 322, 363].

Very recently, we have identified miR-7-5p (miR-7) as one of the most effective miRNAs among a panel of newly produced BioRNAs to inhibit human NSCLC cell viability [363]. Further, we have demonstrated the function of BioRNA/miR-7 to regulate the expression of epidermal growth factor receptor (EGFR), a known miR-7 target and oncogenic apex growth signaling protein in NSCLC [331, 340], as well as voltage dependent anion channel 1 (VDAC1) and multidrug resistance protein 1 (MRP1) with important roles in mitochondrial function [333] and drug sensitivity [332], respectively [363]. More importantly, miR-7 is a known tumor-suppressive miRNA commonly found with low levels of expression in NSCLC [324, 326, 366]. In fact, efforts to reintroduce miR-7 using commercially available miRNA mimics were found to suppress NSCLC cell proliferation and induce apoptosis *in vitro* [324, 326, 366].

Moreover, miR-7 is also known and proposed to regulate additional genes important in cell metabolism and mitochondrial function [349, 367] including the solute carrier family 25A37 (*SLC25A37*) and mitochondrial import inner membrane translocase subunit **(***TIM50*) [347]. In addition, previous works have further demonstrated that by modulating mitochondrial function one may alter cancer cell drug-sensitivity [368-372] which may complement the regulation of efflux transporter MRP1 by miR-7 in combination with current pharmacotherapies. Therefore, in the present study, we aim to delineate the biochemical and pharmacological actions of BioRNA/miR-7 to modulate NSCLC cell metabolism and improve drug sensitivity to relevant small-molecule therapeutics (e.g., pemetrexed; PEM) *in vitro* and *in vivo*.

Our *in vitro* data demonstrated the effectiveness of BioRNA/miR-7 to alter EGFR localization and mitochondrial morphology, regulate a few known and putative miR-7 mitochondrial targets, and modulate both mitochondrial respiration and glycolysis in human NSCLC cells. Moreover, we validated a novel and direct miR-7 target, acylglycerol kinase (*AGK*) and revealed synergism between BioRNA/miR-7 and PEM in the inhibition of NSCLC cell growth, in which the latter was associated with a sharp elevation of intracellular PEM accumulation by BioRNA/miR-7. Additionally, through an *in vivo* therapy study using a NSCLC patient-derived xenograft (PDX) mouse model we demonstrated the efficacy of BioRNA/miR-7 to control NSCLC tumor progression in combination with PEM as well as establish the safety profiles for BioRNA/miR-7 mono- and combination therapy. Overall, our findings support the pharmacological actions of BioRNA/miR-7 on NSCLC cell metabolism and synergetic anticancer efficacy with PEM as a novel candidate for NSCLC therapeutic intervention.

Material and Methods

Chemicals and materials

RPMI medium 1640 (Cat# 11875119), 0.05% trypsin-EDTA (Cat# 25300054), phosphate-buffered saline (PBS; Cat# 10010023), fetal bovine serum (Cat# 26140079), opti-MEM (Cat# 31985070), radioimmunoprecipitation assay (RIPA) buffer (Cat# 89901), bicinchoninic acid (BCA) Protein Assay Kit (Cat# 23227), and Lipofectamine 3000 (Cat# L3000001) were purchased from Thermo Fisher Scientific (Waltham, MA). Directzol RNA miniPrep kit (Cat# R2061) was bought from Zymo Research (Irvine, CA). Primers were purchased from Integrated DNA Technologies (IDT; Coralville, IA). Saturated phenol (pH 4.5; Cat# 97064-716) and *in vivo*-jetPEI (Cat# 101000030) were purchased from VWR (Radnor, PA). Pure ethanol (Cat# E7023), complete protease inhibitor cocktail (Cat# P8340), and MK-571 sodium salt hydrate (Cat# M7571) were purchased from Sigma-Aldrich (St. Louis, MO). TGX Stain-Free FastCast Acrylamide Kit (10%; Cat# 1610183), Clarity Western Enhanced Chemiluminescence Substrates (Cat# 1705061), (Cat# 1706404), and polyvinylidene difluoride (PVDF) membranes (Cat# 1620177), and iTaq™ Universal SYBR® Green Supermix (Cat# 1725121) were purchased from Bio-Rad (Hercules, CA). CellTiter-Glo® 2.0 Cell Viability Assay kit (Cat# G9241) was purchased from Promega **(**Madison, WI). Doxorubicin, hydrochloride salt (Cat# D-4000) was purchased from LC Laboratories (Woburn, MA). Pemetrexed disodium heptahydrate (>98%; Cat# SIAL-SML1490) for *in vitro* studies was purchased from Neta Scientific (Hainesport, NJ). Pemetrexed disodium (>98%; Cat# HY-10820A) was purchased from MedChemExpress (Monmouth Junction, NJ) for the *in vivo* therapy study. Pemetrexed-$^{13}C_5$ sodium salt hydrate (Cat# 26677) was purchased from

Cayman Chemicals (Ann Arbor, MI). All remaining chemicals, organic solvents, and materials were purchased from either Thermo Fisher Scientific, VWR, or Sigma-Aldrich. All lab supplies and reagents used in our protocols are DNase and RNase free.

Expression and purification of BioRNA/miR-7-5p and BioRNA Control RNA

The human $tRNA^{Gly}$ fused pre-miR-34a carrier based has-miR-7-5p (BioRNA/miR-7) and control RNA were produced by *in vivo* fermentation production, as detailed very recently [363]. After purified via anion exchange chromatography using an ENrich™ Q 10 × 100 column on an NGC Quest 10 Plus Chromatography fast protein liquid chromatography (FPLC) system (Bio-Rad), quantity of pure RNAs were determined with a Tecan SPARK (Männedorf, Switzerland), purity by high-performance liquid chromatography (HPLC) method using a LC-40 HPLC system (Shimadzu Corporation; Kyoto, Japan) , and endotoxin levels by the Pyrogent-5000 kinetic LAL assay (Lonza; Walkersville, MD) [363]. BioRNA/miR-7-5p and control RNA used for this study had high homogeneity (>98% by HPLC) and low endotoxin level (<5 EU/μg RNA).

Cell culture

Human lung carcinoma A549 (CRM-CCL-185) and H1975 (CRL-5908), and human embryonic kidney HEK293 (CRL-1573) cell lines were purchased from American Type Culture Collection (Manassas, VA). A549 and H1975 cells were maintained in RPMI 1640 medium. HEK293 cells were maintained in DMEM media. All cell growth media was supplemented with 10% fetal bovine

serum and maintained at 37°C in a humidified atmosphere with 5% CO_2. All cell counting was performed using the Countless II FL system (Life Technologies; Carlsbad, CA).

Confocal microscopy

A549 (8.0×10^3 cells/well) and H1975 (1.0×10^4 cells/well) cells were plated in 8-well chamber slides, incubated overnight, and treated with 30 nM of BioRNA/miR-7, control RNA, or Lipofectamine 3000 (Vehicle) only in triplicates (N = 3/group). At 72-h post-transfection, cells were treated with media containing MitoTracker® Red CMXRos (200 nM; Cell Signaling Technology Cat # 9082; Danvers, MA) and incubated for 15 min at 37°C. Cells were then prepared and stained as previously described [261]. In particular, cells were fixed with 4% paraformaldehyde, permeabilized with 0.25% Triton X-100, blocked with 3% BSA in PBS, stained with primary antibodies against target protein EGFR (1:200; Cell Signaling Technology Cat# 4267S) in blocking buffer overnight at 4°C, and incubated with Alexa Fluor® 488-conjugated secondary antibody anti-rabbit (1:2000; Cell Signaling Technology Cat# 4414S). Prior to imaging, cells were stained for F-actin with Alexa Fluor® 680 Phalloidin (1x; Thermo Fisher Scientific Cat# A22286) and with 4′,6-diamidino-2-phenylindole (DAPI; 1 μg/mL; Cell signaling Technology Cat# 4083S) nuclear stain prior to mounting with VECTASHIELD Antifade (20 uL/chamber slide well; Fisher Scientific Cat# NC9524612). Images were acquired by using a Leica Stellaris 5 Confocal Microscope platform coupled to a Leica Dmi8 Inverted Microscope and Leica Application Suite software (v4.4.0.24861; Leica Microsystems; Buffalo Grove, IL) with 10× and 63× objectives. This experiment was repeated three times and similar results were obtained.

Protein isolation and Western blot analysis

Protein isolation and Western blot analysis were performed as described [363]. In brief, A549 and H1975 cells were seeded into 6-well plates (500,000 cell/well) and treated with 30 nM of RNA or Vehicle alone in triplicates (N = 3/group). After 72 h post-transfection, cells were harvested, lysed, and the centrifuged supernatant was used to determine protein concentrations using a BCA Protein Assay Kit. Whole cell proteins (20 μg/lane) were separated via gel electrophoresis on a 10% TGX StainFree SDS-PAGE gel and electrophoretically transferred onto polyvinylidene fluoride (PVDF) membranes using the Trans-Blot Turbo Transfer System (BioRad). Membranes were imaged for total protein using a ChemiDoc MP Imaging System, blocked with 5% blotting-grade blocker, and incubated overnight at 4°C with primary antibodies against target proteins SLC25A37 (1:500; Thermo Fisher Scientific Cat# PA5119913), TIM50 (1:500; Abcam Cat# ab109436, Boston, MA), SLC25A15 (1:500; Abcam Cat# ab228604), AGK (1:100; Santa Cruz Biotechnology Cat# sc-398943). Membranes were incubated with anti-rabbit (1:10,000; Jackson ImmunoResearch Inc.; West Grove, PA) or anti-mouse IgG HRP-linked (1:3,000; Cell Signaling Technology Cat# 7076S) secondary antibody for 2h at room temperature and Clarity Western Enhanced Chemiluminescence Substrates (1:1) were applied to develop and image the membrane using a ChemiDoc MP Imaging System. The intensity values of protein bands were determined by the Image Lab software (BioRad) and normalized to corresponding total protein for comparison. This experiment was repeated at least twice, and similar results were obtained.

Luciferase reporter assay

The AGK 3′-untranslated region (3'UTR) segment (0–1000 nucleotides from stop codon), consisting of one putative miRNA response elements (MREs) for hsa-miR-7-5p identified by using TargetScan (http://www.targetscan.org/), was cloned into the dual-luciferase pEZX-MT06 vector (GeneCopoeia; Rockville, MD) downstream of the firefly luciferase gene as previously described [261]. A mutated MRE was included to validate the interactions between hsa-miR-7-5p and MREs. Both plasmids were constructed by GeneCopoeia and independently validated by DNA sequencing (Azenta US, Inc.; South Plainfield, NJ). Dual luciferase reporter assays were conducted as previously described [262, 265]. In short, HEK293 cells were seeded in flatbottom 96-well plates at 30,000 cells/well, incubated overnight, and co-transfected with 50 ng AGK 3′UTR-luciferase reporter plasmid of either wildtype or mutated MRE alongside 15 nM of BioRNA/miR-7, control RNA, or Vehicle alone with 4 biological replicates (N = 4/group) . After 48 h post-treatment, dual luciferase activity was determined by using the dual-luciferase reporter assay system (Promega) on a SpectraMax® iD5 microplate reader (Molecular Devices). The firefly luciferase activity was normalized to corresponding *Renilla* luciferase activity and then normalized to vehicle control group for comparison. This experiment was repeated at least twice, and similar results were obtained.

Reverse transcription (RT), quantitative real-time PCR (qPCR) analysis of miR-7-5p

HEK293 cells were seeded in 6-well plates (500,000 cells/well) and transfected with 15 nM of BioRNA/miR-7, control RNA, or Vehicle alone in triplicates (N = 3/group). After 48 h, total RNA was isolated and RT-qPCR was performed as described [363]. Briefly, qPCR analyses were carried out on a CFX96 Touch real-time PCR system (BioRad) using gene specific primers (**Table S1**)

and iTaq ™ Universal SYBR® Green Supermix (BioRad) according to the manufacturer's protocols. Each biological sample was assessed with 3 technical replicates. Levels of mature miR-7-5p were normalized to U6 snRNA in corresponding samples and determined using the formula $2^{-\Delta\Delta CT}$. This experiment was repeated at least twice, and similar results were obtained.

Real-time live cell analyses of mitochondrial respiration and glycolysis

A549 and H1975 cells were seeded into 6-well plates (500,000 cell/well) and treated with 30 nM of BioRNA/miR-7-5p, control RNA, or Vehicle alone in triplicates (N = 3/group). After 48 h, A549 and H1975 cells were seeded (40,000 and 30,000 cell/well, respectively) in the XFe24 microplates (Agilent part No. 100777-004; Santa Clara, CA). After another 24 h, cell glycolytic profile and mitochondrial fitness were evaluated using an Agilent Seahorse XF Glycolytic Rate Assay Kit (Agilent Cat# 103344-100) and Agilent Seahorse XF Cell Mito Stress Test Kit (Agilent Cat# 103015-100) on a Seahorse XFe24 Flux Analyzer (Agilent) as previously described [265, 373]. In short, glycolytic profile and mitochondrial fitness were evaluated by measuring the real-time oxygen consumption rate (OCR) and extracellular acidification rate (ECAR) or conversion to real-time proton efflux rate (PER). Each treatment was normalized to corresponding protein concentrations quantified by BCA. Each experiment was repeated at least three times, and similar results were obtained.

Cell growth and viability assays and determination of combination synergism

A549 and H1975 cells were seeded in flatbottom 96-well plates at 5,000 and 8,000 cells/well, respectively. Cells were treated either with 5 or 10 nM of BioRNA/miR-7, control RNA, doxorubicin, pemetrexed, or Vehicle alone or a combination of RNA with DOX or PEM at a concertation of 5 or 10 nM with 3 biological replicates (N = 3/group). Cells were incubated in an IncuCyte® S3 Live-Cell Imaging System (Sartorius, Essen BioScience, Ann Harbor, MI) and well confluency was recorded every 4 h for 72 h with a 4× objective as a proxy for cell viability. Confluence was normalized to vehicle control at 72 h post-transfection (100%). The data were fit to a logistic growth model to estimate rate constant (k) and maximum growth (YM) (Prism (v10.0.2); GraphPad, San Diego, CA), and the equation is $Y = YM * Y0/((YM - Y0) * exp(-k * x) + Y0)$ with starting confluence per well (Y0) was constrained to 10% or 15% for A549 and H1975 respectively, based on the starting confluency of vehicle control wells.

Combination Index (CI) values were calculated by using CompuSyn software (v1.0; ComboSyn, Inc.; Paramus, NJ) as previously described [374] with cell viability data determined in proxy using the CellTiter-Glo® 2.0 Cell Viability Assay kit (Promega), in which the vehicle group was defined as 100%. Chou-Talalay plots were generated by plotting log(CI) against fraction affected (Fa), where log(CI) < 0 indicates synergism, log(CI) = 0 indicates addition, and log(CI) > 0 indicates antagonism. Each experiment was repeated at least twice, and similar results were obtained.

Liquid Chromatography Tandem Mass Spectrometry (LC-MS/MS) analyses of pemetrexed and cAMP

PEM and cAMP intracellular accumulation studies were performed as previously described [374], with some modifications. To assess PEM accumulation, A549 and H1975 cells were seeded in 12-well plates at a density of 100,000 cells/well and transfected with 30 nM of BioRNA/miR-7 or control RNA with 3 biological replicates (N = 3/group) as well as vehicle alone N = 6). After 72 h, cells were washed three times with fresh media and incubated with 10 µM of PEM in RPMI 1640 medium supplemented with 10% FBS for 0.5, 1, 2, or 4 h. Vehicle treatment replicates were pre-treated with or without (N = 3/group) a MRP inhibitor, MK-571 [50 µM], for 30 min before incubation with PEM as previously reported [375]. To assess cAMP accumulation, cells were seeded in 6-well plates at a density of 500,000 cells/well and transfected with 30 nM of BioRNA/miR-7, control RNA, or vehicle alone with 3 biological replicates (N = 3/group).

Cells were then washed three times with ice-cold PBS to terminate the incubation, harvested, pelleted by centrifugation at 1,000 *g* for 10 min at 4°C, and lysed by three sequential freeze-thaw cycles (liquid nitrogen for 20 s or until frozen followed by sonication at room temperature for 2 min in 100 µL of HPLC grade water. An aliquot of cell lysate was subjected to BCA assay for the quantification of protein concentration. Proteins were precipitated with ice-cold acetonitrile (240 µL) containing a final concentration of either 10 nM of pemetrexed-$^{13}C_5$ (IS_1) or 200 nM of chloro-phenylalanine (IS_2) as an internal standard for PEM and cAMP, respectively, from an 80 µL aliquot of cell lysate (1:3 ratio) and removed by centrifugation at 10,000 *g* for 10 min at 4°C. Then supernatant (280 uL) was dried over air, reconstituted in 40 µL of HPLC grade water with 0.1% formic acid, and processed for LC-MS/MS analyses.

PEM, cAMP, and their IS were analyzed using an AQUASIL C18 column (4.6 × 50 mm, 3 µm; Fisher Scientific) on an AB Sciex 4000 QTRAP tandem MS system (AB Sciex; Framingham, MA) coupled with a Shimadzu Prominence Ultra-Fast LC system (Shimadzu Corporation; Kyoto, Japan). PEM and IS_1 were separated from the sample with a gradient elution with mobile phase A (water with 0.1% formic acid) and mobile phase B (acetonitrile): 5%-90% buffer B (0-2 min), 90% buffer B (2-4 min), 90%-5% buffer B (4-4.5 min), and 5% (4.5-5.5 min) at a. cAMP and IS_2 were separated with the same mobile phases under different gradient: 10% buffer B (0-1 min), 10%–20% buffer B (1-5 min), 20%–100% B (5-5.5 min), 100% buffer B (5.5-6 min), 100%–10% buffer B (6-6.5 min), and 10% buffer B (6.5-7.5 min), at a flowrate of 0.8 mL/min with. Samples were analyzed in either positive (PEM and pemetrexed-$^{13}C_5$) or negative (cAMP and chloro-phenylalanine) electrospray ionization mode. Multiple reaction monitoring was conducted for pemetrexed at m/z 428.3→281.1, IS_1 433.1→281.0, cAMP 328.0→133.9, and IS_2 198.1→136.9. Linear calibration range ranging from 1 to 300 nM was established for PEM and 0.3 to 100 nM for cAMP. Accuracies was within ±15% and precisions within 10%. Each experiment was repeated at least twice, and similar results were obtained.

Therapy Study

All animal procedures were approved by the Institute Animal Care and Use Committee at UC Davis. Mice were maintained in sterile cages at constant temperature and humidity, with free access to food and water. Mice housed for one week prior to experimentation. NSCLC patient-derived xenograft (PDX) mouse model was established, as previously described with minor modifications [256, 260, 322]. In brief, de-identified NSCLC adenocarcinoma PDX tissues

(TM00192; LG0567F; generated with specimen from a treatment naïve, 57-year-old Asian or Pacific Islander, male, smoker) were obtained from the Mouse Biology Shared Resources at UC Davis Cancer Center as a joint program with The Jackson Laboratory (Bar Harbor, ME). Tissues sections (2–3 mm^3) were thawed in RPMI containing antibiotics and subcutaneously implanted into the flank of 36 six-week-old, male, NOD/SCID mice (The Jackson Laboratory; Bar Harbor, ME; F6). Tumor volumes were measured with calipers and calculated according to the formula: $tumor\ volume\ (mm^3) = 0.5 \times [length\ (mm) \times width^2\ (mm^2)]$.

Treatment began once tumor sizes reached a diameter of 60-150 mm^3 and were randomized into 4 treatment groups (N=6 mice/group), BioRNA/miR-7, PEM, BioRNA/miR-7 plus PEM co-treatment, or Buffer control (5% glucose). More specifically, treatments were administered with 30 μg of *in vivo*-jetPEI-formulated RNAs via intravenous (*i.v.*) injection, PEM [100 mg/kg] via intraperitoneal (*i.p.*) injection, or BioRNA/miR-7-5p plus PEM through the tail vein *i.v.* or *i.p.* injection. Mice were treated with the following dosing regimen (**Fig. 7A**): BioRNA/miR-7 or Buffer control treatments administered thrice a week for 4 weeks (28 days; 12 doses in total), and PEM administered, concurrently, twice a week for four weeks (8 doses in total). Tumor volume and mouse body weight was monitored 2 times a week. Mice were sacrificed 48 h after the last dose. Whole blood and PDX tumors were collected for blood chemistry profiling (Chem-8 blood panel) and for histopathological studies, respectively, performed by the Comparative Pathology Laboratory at UC Davis (Davis, CA) as previously described [256, 260, 322]. In brief, PDX tumors were fixed with 10% formalin, processed, and stained with hematoxylin and eosin (H&E) or subjected to immunohistochemistry with anti-cleaved-caspase-3, anti-Ki-67, or anti-EGFR

antibody (Cell Signaling Technology Cat# 4267), and then photographed by using an Olympus camera (DP25) and CellSens software (Olympus, Center Valley, PA).

Statistics

Values are mean ± standard deviation (SD) and all data were analyzed with either a One-way or Two-way ANOVA with Bonferroni post-tests (Prism, GraphPad Software; San Diego, CA). Difference between analyzed groups was considered as statistically significant when the probability value (P value) was less than an alpha level of 0.05 ($P < 0.05$).

Results

BioRNA/miR-7 reduces mitochondrial EGFR expression, alters mitochondrial morphology, and represses known mitochondrial miR-7 targets in human NSCLC cells.

To being our investigation we used confocal immunofluorescent imaging on NSCLC cells to observe changes to subcellular EGFR expression upon treatment with 30 nM of BioRNA/miR-7 for 72 h. Here, our imaging data showed that BioRNA/miR-7 sharply reduced EGFR protein levels that is mainly localized to the cell membrane and mitochondria (**Fig. 1A**). Interestingly, compared with vehicle and control RNA treatments, BioRNA/miR-7 elicited an abnormal, condensed mitochondria morphology as manifested by the MitoTracker and co-localized EGFR. These observations confirm the regulation of EGFR by miR-7 and more importantly, suggest a potential role for miR-7 in NSCLC mitochondrial function. We then elected to validate the effects of

BioRNA/miR-7 treatment on the protein outcomes of two other known miR-7 targeted mitochondrial genes, *SLC25A37* and *TIM50*, by conducting Western blot analyses. Our data showed that, after 72 h treatment with 30 nM of BioRNA/miR-7, both SLC25A37 and TIM50 protein levels were significantly reduced in human NSCLC A549 cells by about 40-60% as compared to control RNA treatment (**Fig. 1B**). Together these data further demonstrate BioRNA/miR-7 as a functional miR-7 agent and suggest a role for miR-7 in the regulation of mitochondrial function.

Mitochondrial acylglycerol kinase is validated as a new direct target for miR-7.

Through cross-referencing putative miR-7 target genes from TargetScan [376] with the NIH *Mammalian Metabolic Enzyme Database* [377], we further identified two candidates important to mitochondrial function, namely *AGK* and *SLC25A15*. To evaluate the effects of miR-7 on the two putative targets, we first performed Western blot analyses in cells in response to different treatments for 72 h. Our results showed that AGK protein levels was effectively suppressed by miR-7 in both A549 and H1975 NSCLC cells as demonstrated by reduction in protein band intensity by approximately 80-90%, as compared to control RNA or vehicle treatments (**Fig. 2A**). Conversely, identical miR-7 treatment surprisingly had no or minimal impact on SLC25A15 protein levels in A549 and H1975 cells when compared with control RNA treatments (**Fig. 2A**). As such, only AGK was selected for further validation using a dual luciferase reporter assay. *AGK* 3′UTR-luciferase reporter plasmids with either wild-type or mutated MRE seed sequences (**Fig. 2B**) were thus created, and HEK293 cells were chosen for this study due to their high transfection efficiency and low endogenous expression levels of miR-7 [378]. Stem-loop RT qPCR analysis

confirmed a high level of mature miR-7-5p released from BioRNA/miR-7 in HEK293 cells (**Fig. 2C**), which reduced the wild-type *AGK* 3′UTR-luciferase activities by about 40% when compared to control RNA or vehicle treatments, whereas had no influence on the mutant *AGK* 3′UTR-luciferase activities (**Fig. 2D**). Together, these results indicate that miR-7 directly acts on the *AGK* 3′UTR to suppress the protein levels of AGK in human NSCLC cells that putatively contributes to the modulation of mitochondrial function.

MiR-7 controls mitochondrial respiration and glycolytic capacity of NSCLC cells.

To delineate the impact of miR-7 treatment on overall NSCLC cell mitochondrial respiration and glycolytic capacity, we performed mitochondrial stress test and glycolytic rate assays using a Seahorse XFe24 Analyzer. Our real-time OCR data obtained from the mitochondrial stress test revealed a significant reduction of mitochondrial respiration by miR-7 in both A549 and H1975 (**Fig. 3**) cells. In particular, NSCLC cells treated with miR-7 exhibited lower levels of basal and maximal respiration (30-70%) as well as ATP production (50-70%), compared with control RNA treatment (**Fig. 3C,D**). Additionally, PER levels were calculated from separate real-time OCR and ECAR measurements in the glycolytic rate assay, and the results demonstrated that miR-7 treatment largely repressed the overall glycolytic rates in A549 (**Fig. 4A**) and H1975 (**Fig. 4B**) cells. More specifically, miR-7 decreased the basal and compensatory glycolytic capacity by about 40-80% (**Fig. 4C,D**). Taken together, these results support an important role for miR-7 in modulating NSCLC cell metabolism.

Synergism between BioRNA/miR-7 and small-molecule drugs in the inhibition of human NSCLC cell viability.

To define to what degree BioRNA/miR-7 may improve current treatment to inhibit NSCLC cell viability, we selected two small-molecule drugs, namely DOX and PEM. Here, we treated NSCLC cells with various concentrations of either small-molecule drug, BioRNA/miR-7, or combination, analyzed cell growth over time (**Fig. 5A; Table S2**). Our results demonstrated a significant decrease in the growth of both A549 and H1975 cells by combination treatments as compared with monotherapy or vehicle controls. For instance, both PEM and DOX [10 nM] plus BioRNA/miR-7 [10 nM] treatments resulted in roughly a 60-70% reduction in NSCLC cell growth overtime compared to either drug alone. These results demonstrate a greater inhibition of NSCLC cell growth by either PEM or DOX when treated in combination with BioRNA/miR-7.

To critically define possible synergism we applied the Chou-Talalay method [379] to calculate combination index (CI) values and plotted them against the fraction affected (Fa) values (**Fig. 5B**). Our data showed that co-administration of PEM with BioRNA/miR-7 elicited a consistent synergistic effect on inhibiting both A549 and H1975 cell viability, as manifested by the mean log(CI) values of -0.16 ± 0.13 (95% confidence interval −0.24 to −0.07) and -0.40 ± 0.23 (95% confidence interval −0.55 to −0.25), respectively (**Fig. 5B**). By contrast, synergism was observed for DOX plus BioRNA/miR-7 combination at certain combinations and lower degrees (greater CI values) when compared with PEM and BioRNA/miR-7 combination treatment. Overall, these data suggest that co-administration of BioRNA/miR-7 with PEM offers a synergistic inhibition of

human NSCLC cell growth. Thus, together with the current clinical utility of PEM against NSCLC we selected PEM for further mechanistic and *in vivo* therapeutic studies.

Intracellular accumulation of anticancer drug pemetrexed is strikingly elevated in NSCLC cells following BioRNA/miR-7 treatment.

Given previous discovery on the role of MRP transporters in PEM disposition [380-382] and our own finding on the effectiveness of BioRNA/miR-7 to suppress MRP1 in NSCLC cells [363], we examined the effects of BioRNA/miR-7 on intracellular accumulation of exogenous PEM by using an accurate LC-MS/MS method. Our data showed that BioRNA/miR-7 pre-treatment significantly elevated intracellular concentrations of PEM in A549 and H1975 cells by roughly 10- and 15-fold, respectively, compared with control RNA treatment (**Fig. 6A,B**). Additionally, we assessed changes to a known MRP endogenous substrate, cAMP [383, 384], and our data revealed a significant increase in endogenous cAMP concentrations in A549 and H1975 cells by roughly 3- and 2.5-fold, respectively, compared with control RNA treatment (**Supplementary Fig. S1**). Taken together, these results illustrate an enhancement of PEM accumulation in NSCLC cells by co-administered BioRNA/miR-7, suggesting a pharmacokinetic interaction between BioRNA/miR-7 and PEM besides their independent pharmacological actions.

Antitumor efficacy and safety of BioRNA/miR-7 mono- and combination therapy with pemetrexed in NSCLC PDX mouse models.

We then employed a NSCLC PDX mouse model to determine the efficacy of BioRNA/miR-7 plus PEM combination therapy *in vi*vo. Once the implanted PDX tumors reached 60-150 mm^3, the mice were randomized into four groups receiving either BioRNA/miR-7 and PEM, alone or in combination, or buffer alone over 28 days (**Fig. 7A**). Our data revealed that co-administration of BioRNA/miR-7 with PEM remarkably decreased tumor growth by roughly 5- and 2-fold when compared to 5% glucose buffer treatment or either monotherapy, respectively (**Fig. 7B**). Meanwhile, BioRNA/miR-7 or PEM monotherapy showed roughly equal antitumor activity, resulting in a decrease in tumor growth by roughly 3-fold compared to control buffer treatment. These results were reflected by the measured weights and visual inspection of the harvested PDX tumors (**Fig. 7C, D**).

To investigate the tolerability of combination therapy, we measured mouse body weights throughout the study and determined blood chemistry profiles. No significant changes in body weight of tumor-bearing mice throughout the study and between each treatment groups were noted, while mice in all groups seemed gaining weights slightly over time (less than 9% from the start to the end of the study) (**Supplemental Fig. S2**). Blood chemistry profiling revealed no statistically significant differences between any treatment groups for alanine transaminase (ALT), alkaline phosphatase (ALP), albumin, aspartate transaminase (AST), total bilirubin, blood urea nitrogen (BUN), and creatinine (**Fig. 8**), indicating the lack of liver or kidney toxicities. In addition, all blood biomarkers were within the normal ranges derived from healthy BALB/c mice except ALP and total protein levels as NOD/SCID mice were used in this study. Together, these results demonstrate that BioRNA/miR-7 plus PEM combination therapy is effective to control NSCLC PDX tumor growth and well tolerated in tumor-bearing mice.

Discussion and Conclusions

The advent of RNAi-based therapies has opened novel routes for the study and treatment of NSCLC beyond current pharmacotherapies. Given the increased interest in functional, tumor-suppressive miRNAs in NSCLC [321, 361-363], current strategies employing chemically or enzymatically synthesized miRNA mimics may thwart putative therapeutic benefits with unknown side and long-term effects [15, 26, 273]. However, through the application of our novel, naturally synthesized BioRNA technology, the current study points to an ever-widening regulatory and therapeutic role for miR-7 in NSCLC. Specifically, we provide evidence for BioRNA/miR-7 treatment to disrupt NSCLC cell metabolism and MRP1-mediated drug efflux to increase sensitivity to pharmacotherapeutic PEM *in vitro* and *in vivo*.

Through confocal immunofluorescent microscopy, we visually confirmed the regulation of EGFR immunofluorescence by BioRNA/miR-7 treatment in NSCLC cells thus supporting the use of functional BioRNA/miR-7, as reflected in our previous findings [363]. Further, we confirmed the co-localization of EGFR to the cell membrane and the mitochondria in NSCLC control treatments in support of similar previous findings [385, 386]. Interestingly, co-localization of EGFR to the mitochondria is shown to increase cell progression and ATP production in highly invasive NSCLC cells [385]. Our results support these finds by showing BioRNA/miR-7 treatment to reduce EGFR co-localization with NSCLC mitochondria via confocal microscopy and to decrease ATP production via our analyses of mitochondrial respiration. Importantly, we also observed mitochondria under BioRNA/miR-7 treatment to exhibit an abnormal morphology indicative of

mitochondrial stress-induced fusion, as described in previous studies [387, 388]. We further support these findings through the reduction in basal and maximal mitochondrial respiration upon reintroduction of miR-7. Together these results suggest that miR-7 treated NSCLC cells may enter into a state of metabolic or mitochondrial stress and employed mitochondrial fusion as a compensatory mechanism to exchange contents between healthy and damaged mitochondria and maintain viability [387, 388].

Moreover, to the best of our knowledge these results demonstrate the first evidence of hsa-miR-7-5p to regulate two additional known mitochondrial target genes in NSCLC, namely *SLC25A37* and *TIM50*. Together with known targets, namely *EGFR* and *VDAC1*, regulation of *SLC25A37* and *TIM50* provide an additional molecular role for miR-7 to regulate mitochondrial function and further opens new routes to explore the impact of miR-7 on iron homeostasis and intramitochondrial protein transport in NSCLC. Further, we provide evidence of miR-7 to moderately regulate a putative target mitochondrial gene, *SLC25A15*, and fully validate the regulation of *AGK* via Western blot and luciferase reporter assays. Although a nuclear gene-encoded protein, AGK is primarily located in the mitochondria and functions as a lipid kinase [389], a subcomponent of the mitochondrial protein transport as part of the mitochondrial translocase of the inner membrane 22 complex [390], and an oncogene in several cancer types [391]. In fact, previous works exploring mitochondrial-specific protein regulation by miR-7 report a 0.63-fold decrease in AGK expression in human neuroblastoma cells [392]. This previous finding supports of our validation of *AGK* as a direct target of miR-7. Together, these results contribute to the growing role for miR-7 in the regulation of NSCLC mitochondrial function and supports a route for novel research into the effects of miR-7 on AGK in cancer progression.

In addition to the regulation of mitochondrial respiration, our study also demonstrates miR-7 to regulate glycolysis in NSCLC, an integral metabolic pathway commonly elevated in cancer cells [367]. While mitochondrial respiration may be influenced by the interactions between miR-7 and the targets explored in this study, our observed reduction in basal and compensatory glycolytic capacity may putatively be influenced by the interactions of miR-7 with several established target genes known to contribute to glycolysis (e.g., *EGFR* and *VDAC1*) [393, 394]. However, it should be noted that there may be additional and/or more influential functions of miR-7 that more directly or indirectly regulate NSCLC metabolism in these ways that have not yet been elucidated. Nevertheless, our results suggest that treatment with miR-7 contributes towards a putative cytostatic effect on NSCLC metabolism in corroboration with previous miR-7 findings [347, 365].

Further, metabolic reprogramming in NSCLC has been linked to enhanced drug-resistance [368-370] and may offer a synergistic effect in combination clinically relevant drugs (i.e., PEM) used against NSCLC. Moreover, our previous works revealed miR-7 to regulate the expression of MRP1 in NSCLC [363]. This is important as MRP1 is a transmembrane efflux transporter known for its role in clinical drug resistance in several cancer types including small-cell lung cancer [332]. In fact, our present study shows the combination of BioRNA/miR-7 with PEM exhibit a synergetic effect in the reduction of NSCLC viability. PEM is a clinically relevant antifolate that plays an important role in folate metabolism, and pyrimidine and purine biosynthesis by inhibiting key enzymes, namely thymidylate synthase, dihydrofolate reductase, and glycinamide ribonucleotide formyltransferase [371, 395-398]. Thus, a possible means of observed synergism is through separate and simultaneous pharmacodynamic means to reduce cell viability. In this case, the

independent cytostatic effects of BioRNA/miR-7 on NSCLC metabolism complement the independent inhibition of folate metabolism and downstream DNA synthesis by PEM to reduce NSCLC viability. An alternative explanation of synergism is through a putative connection between *AGK* regulation via miR-7 reintroduction and a possible decrease in AGK-dependent inhibition of phosphatase and tensin homolog (PTEN) [391]. This is because increased PTEN expression is shown to increased PEM efficacy in NSCLC through inhibiting the PI3K/AKT/mTOR pathway [399]. While not directly explored in this study, downregulating AGK expression by BioRNA/miR-7 may offer a possible route for a synergistic increase the effectivity of PEM in NSCLC. While promising, these connections remain putative and should be interpreted with caution until more comprehensive studies on BioRNA/miR-7 plus PEM pharmacodynamics are performed.

Interestingly, our present study also demonstrates that over the course of 4 h, NSCLC cells pre-treated with BioRNA/miR-7 showed a significant accumulation of intracellular PEM levels. While MRP1 is not a confirmed transporter of PEM, MRP1 is part of the MRP family known for its cellular resistance mechanisms in association with antifolate transport [380-382, 400]. Thus, an additional explanation for our observes synergism is through the downregulation of MRP1 by BioRNA/miR-7 resulting in the pharmacokinetic retention of intracellular PEM leading to a decrease in NSCLC viability. However, it should be noted that while miR-7 treatment did exhibit significant changes in exogenous PEM, these results warrant a more comprehensive pharmacokinetic study to compare the effects of miR-7 on MPR1 with known and additional candidate PEM efflux transporters [380-382, 400] which exhibit varied expressions in NSCLC cells [401]. Still, these results suggest that BioRNA/miR-7 treatment plays a putative role in

NSCLC sensitivity to small-molecule pharmacotherapies (i.e., PEM) similar to those previously reported in NSCLC [402], in small cell lung cancer [332], and in other cancer types [342, 403].

Based on our revealed synergism and induced intracellular PEM accumulation upon BioRNA/miR-7 treatment *in vitro*, over our 4-week therapy study we found the combination of BioRNA/miR-7 plus PEM to effectively control tumor growth *in vivo*. These results are supported by the greater degree of suppressed NSCLC PDX tumor growth by BioRNA/miR-7 plus PEM combination treatment. Further, our findings illustrate a novel therapeutic strategy to increase the efficacy of PEM treatment in different and/or more resistant subdivisions of NSCLC through co-administered BioRNA/miR-7 [404, 405]. Importantly, all mice enrolled maintained their body weight throughout the therapy study and blood chemistry profiles remained consistent between all treatment groups and within normal ranges for most metabolites and analytes measured . These reflect similar results found in our previous studies [251, 256, 260, 261, 322, 406, 407]. However, it is of note that the normal range values provided are derived from BALC/c mice while our study used a NOD/SCID mice strain. Nevertheless, caution should be used when interpreting these results until more comprehensive studies are performed in higher animal models. As a note for further investigation, it is our intent to perform H&E and IHC analyses on harvested tumors.

Our findings on BioRNA/miR-7 monotherapy demonstrate a similar or greater control of NSCLC tumor growth compared to those in previous therapy studies using artificial miR-7 mimics [364, 366, 408], with similar findings between our PEM monotherapy and those in previous studies [409-411]. However, interpreting the effectiveness of BioRNA/miR-7 against PEM should be met with caution. This is because our study administered PEM via *i.p.* compared to *i.v.* administration

used clinically [395, 396, 404, 412] and, therefore, may be a less effective route of administration. It is also of note that the PD tumors used in this study are treatment naïve and, thus, may be more sensitive to either mono- or combination therapies than tumors with previous interventions. An additional note should be made regarding the variability of starting tumor volumes and the degree of tumor growth control as tumors with smaller starting volumes may present with greater control in either mono- or combination therapies thus demonstrating the clinical importance of early detection and early intervention in the clinic.

In conclusion, the present study demonstrates the efficacy of BioRNA/miR-7 to modulate NSCLC cell metabolism and improve antitumor activity of small-molecule drug PEM. More specifically, our results show the mechanistic actions of BioRNA/miR-7 to control mitochondrial morphology, respiration and glycolytic capacity through regulating target mitochondrial genes including *AGK* that is newly validated in this study. Moreover, our study supports the utility of BioRNA/miR-7 to induce synergistic antiproliferation activity with PEM by increasing intracellular PEM accumulation. Finally, through an *in vivo* therapy study we demonstrate the efficacy and tolerability for BioRNA/miR-7 mono- and combination therapy with PEM to control tumor progression in NSCLC PDX mouse models. Our collective work in this study demonstrates the widening role for miR-7 in NSCLC biology as well as the therapeutic potential of BioRNA/miR-7 to improve NSCLC therapy.

Table S1. Primer used for real-time qPCR analyses. F, forward primer; R, reverse primer.

Primer		**Primer Sequence (5' to 3')**
hsa-miR-7-5p		
stem-loop reverse transcriptase		GTCGTATCCAGTGCAGGGTCCGAGGTATTCGCACTGGATACGACCAACAA
qPCR	F	CGCGCTGGAAGACTAGTGATT
	R	GTGCAGGGTCCGAGGT
U6 qPCR	F	CTCGCTTCGGCAGCACA
	R	AACGCTTCACGAATTTGCGT

Table S2. Logistic growth parameters of doxorubicin or pemetrexed and BioRNA treated NSCLC cells from growth curves fit to a logistic growth model. The table shows the rate constant, maximum growth (Ymax), and R^2 values for each treatment using the following equation: $Y = YM * Y0/((YM - Y0) * exp(-k * x) + Y0)$ with starting confluence (Y0) constrained to 10%.

Drug	Cell Line		RNA [nM]	Drug [nM]	Rate Constant	± SD	Ymax (% confluence)	± SD	R^2
Doxorubicin	A549	Vehicle Control	0	0	0.049	± 0.001	142.3	± 15.70	0.999
			0	5	0.047	± 0.001	137.4	± 10.74	0.999
			0	10	0.043	± 0.003	116.9	± 15.35	0.999
		BioRNA Control	5	0	0.039	± 0.003	152.7	± 40.63	0.995
			10	0	0.038	± 0.003	139.2	± 36.53	0.987
			5	5	0.033	± 0.003	159.2	± 70.22	0.997
			10	5	0.034	± 0.000	201.7	± 72.49	0.995
			5	10	0.036	± 0.003	213.7	± 32.19	0.997
			10	10	0.037	± 0.002	149.9	± 28.40	0.996
		BioRNA/miR-7-5p	5	0	0.033	± 0.003	148.7	± 35.60	0.988
			10	0	0.041	± 0.013	56.35	± 14.89	0.875
			5	5	0.037	± 0.003	60.77	± 3.600	0.977
			10	5	0.042	± 0.008	30.37	± 5.160	0.949
			5	10	0.031	± 0.007	108.6	± 53.90	0.988
			10	10	0.046	± 0.011	28.83	± 3.210	0.928
	H1975	Vehicle Control	0	0	0.052	± 0.002	129.90	± 0.987	0.986
			0	5	0.052	± 0.002	106.20	± 5.145	0.990
			0	10	0.051	± 0.001	112.30	± 2.551	0.988
		BioRNA Control	5	0	0.043	± 0.001	92.83	± 7.281	0.967
			10	0	0.044	± 0.002	85.29	± 5.097	0.962
			5	5	0.045	± 0.004	83.56	± 6.262	0.946
			10	5	0.043	± 0.003	87.35	± 3.127	0.958
			5	10	0.043	± 0.002	91.89	± 10.070	0.958
			10	10	0.044	± 0.004	76.26	± 11.360	0.939
		BioRNA/miR-7-5p	5	0	0.051	± 0.001	70.65	± 4.297	0.937
			10	0	0.058	± 0.002	48.77	± 4.585	0.884
			5	5	0.059	± 0.007	59.27	± 21.270	0.896

			10	5	0.060	± 0.017	47.76	± 18.030	0.917
			5	10	0.063	± 0.032	55.86	± 21.730	0.916
			10	10	0.055	± 0.015	37.58	± 1.252	0.868
Pemetrexed	**A549**	**Vehicle Control**	0	0	0.047	± 0.001	151.1	± 10.80	0.998
			0	5	0.046	± 0.002	129.4	± 8.660	0.998
			0	10	0.040	± 0.001	129.5	± 2.080	0.998
		BioRNA Control	5	0	0.032	± 0.002	191.4	± 29.27	0.992
			10	0	0.034	± 0.005	165.3	± 80.15	0.988
			5	5	0.036	± 0.002	148.7	± 13.16	0.989
			10	5	0.034	± 0.003	139.0	± 30.94	0.993
			5	10	0.033	± 0.000	168.5	± 12.83	0.995
			10	10	0.030	± 0.003	226.4	± 72.73	0.995
		BioRNA/miR-7-5p	5	0	0.032	± 0.003	132.8	± 36.25	0.983
			10	0	0.032	± 0.001	76.80	± 12.56	0.959
			5	5	0.029	± 0.006	136.6	± 75.93	0.983
			10	5	0.031	± 0.003	54.00	± 6.190	0.971
			5	10	0.028	± 0.005	136.7	± 51.89	0.986
			10	10	0.032	± 0.005	43.1	± 5.61	0.938
	H1975	**Vehicle Control**	0	0	0.057	± 0.002	114.8	± 7.114	0.987
			0	5	0.060	± 0.004	109.4	± 9.506	0.983
			0	10	0.055	± 0.002	99.29	± 3.047	0.989
		BioRNA Control	5	0	0.054	± 0.001	94.18	± 8.622	0.969
			10	0	0.044	± 0.001	101.4	± 1.710	0.961
			5	5	0.051	± 0.002	88.66	± 2.135	0.973
			10	5	0.042	± 0.003	95.50	± 8.552	0.964
			5	10	0.046	± 0.002	100.4	± 4.626	0.961
			10	10	0.048	± 0.002	83.46	± 7.573	0.941
		BioRNA/miR-7-5p	5	0	0.057	± 0.003	56.00	± 3.127	0.891
			10	0	0.092	± 0.015	37.15	± 3.661	0.617
			5	5	0.056	± 0.003	58.88	± 1.692	0.937
			10	5	0.134	± 0.046	26.47	± 4.892	0.797
			5	10	0.050	± 0.003	48.36	± 2.275	0.931

		10	10	0.207 ± 0.042	24.08 ± 3.217	0.783

Figure legends

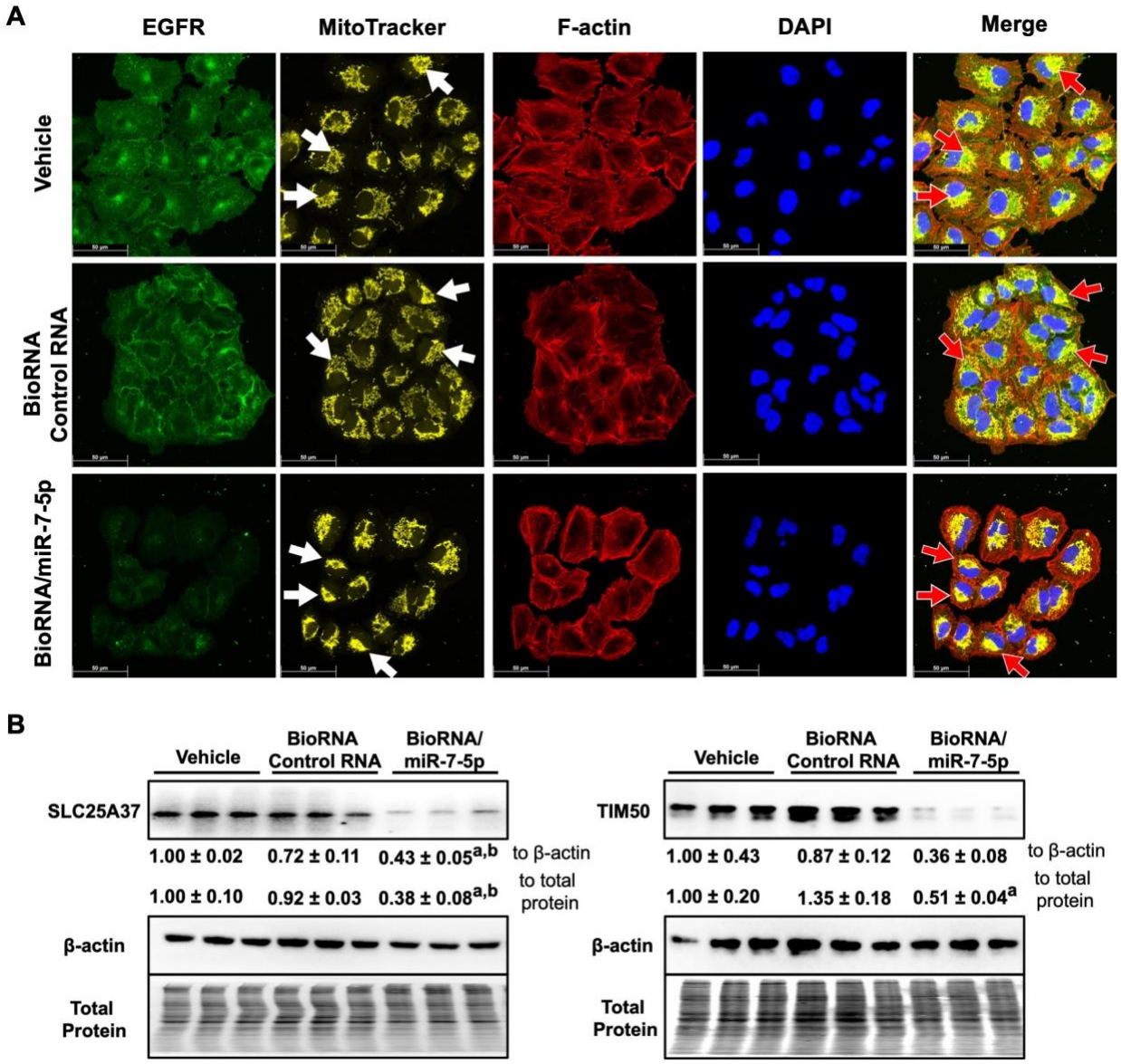

Figure 1. BioRNA/miR-7 affects mitochondrial morphology and mitochondrial protein levels while regulating EGFR expression and localization in human NSCLC A549 cells. (**A**) Confocal imaging studies confirmed EGFR (green) localization to the cell membrane and the mitochondria (MitoTracker; yellow) whose intensities were obviously reduced by BioRNA/miR-7. Interestingly, BioRNA/miR-7-5p led to a condensed mitochondria abnormal morphology indicative of mitochondrial stress-induced fusion, as compared to control RNA or vehicle treatment groups exhibiting relatively more extended mitochondrial distribution and EGFR mitochondrial colocalization (white and red arrows). Cells were treated with 30 nM of BioRNA/miR-7, control RNA, or vehicle alone for 72 h. Scale bar, 50 μm. Imaged with 63x objective. (**B**) Impact of BioRNA/miR-7 on two mitochondrial protein levels, TIM50 and SLC25A37 (known targets of miR-7-5p), in A549 cells after 72 h treatment, as determined by Western blot analyses. Targeted protein levels were normalized to corresponding β-actin or total protein levels, and vehicle control groups were set as 1.0. All values are mean ± SD (N = 3 biological replicates per treatment group). $^{a}P < 0.05$, as compared to control RNA; $^{b}P < 0.05$, compared to vehicle control (One-way ANOVA with Bonferroni *post hoc* tests).

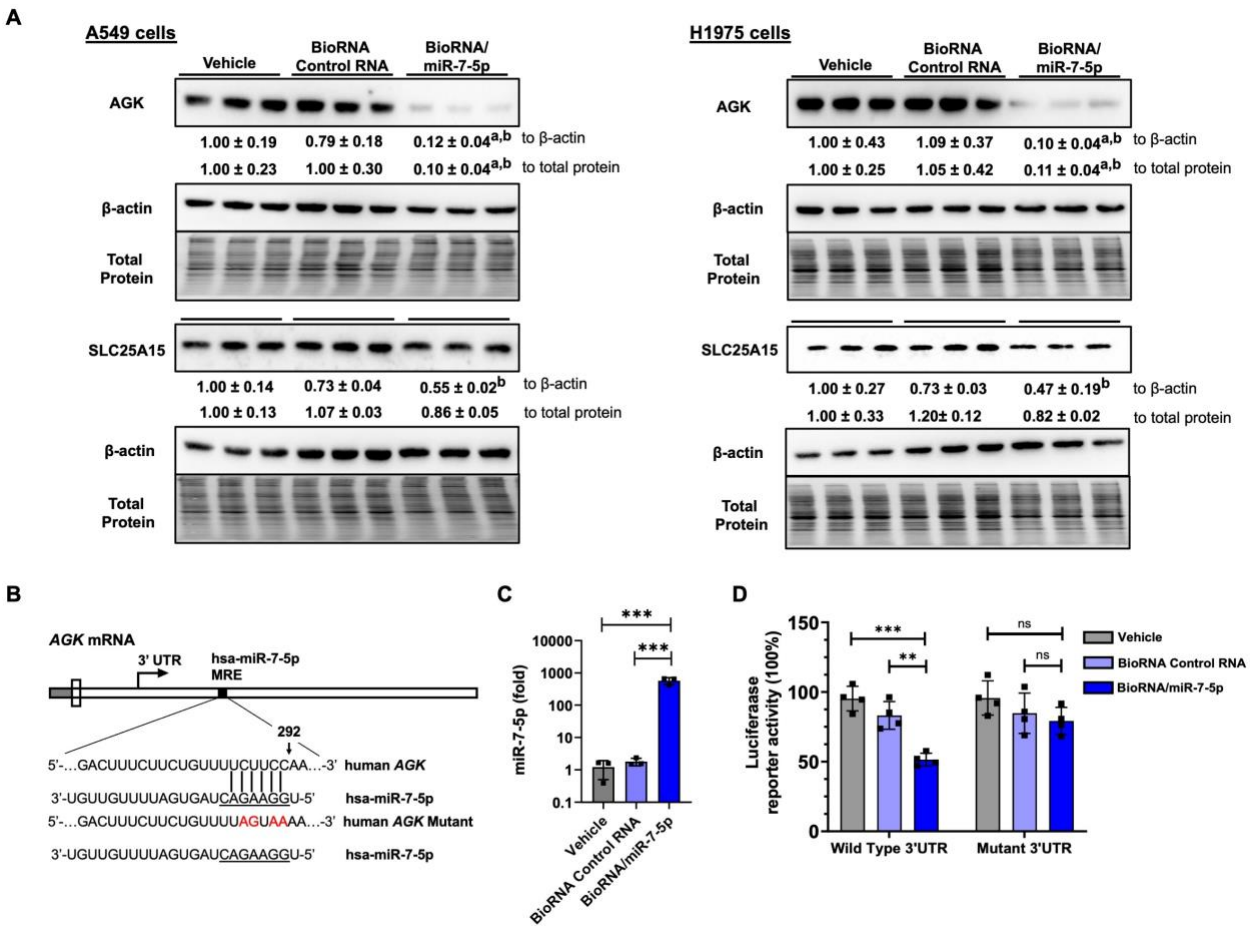

Figure 2. Mitochondrial AGK is revealed as a new target for miR-7. (**A**) Impact of BioRNA/miR-7 versus control RNA and vehicle on predicted miR-7-5p targets, AGK and SLC24A15, was further defined in A549 and H1975 cells. The expression of AGK was reduced sharply by miR-7-5p [30 nM] whereas SLC25A15 was altered by minor degrees. Targeted protein levels were normalized to corresponding β-actin or total protein levels, and vehicle control groups were set as 1.0. All values are mean ± SD (N = 3 biological replicates per treatment group). $^{a}P < 0.05$, compared to control RNA; $^{b}P < 0.05$, compared to vehicle control (One-way ANOVA with Bonferroni *post hoc* tests). (**B**) One MRE site was identified for miR-7-5p within the 3′UTR of *AGK* mRNA, and specific mutant 3'UTR reporter was generated. (**C**) Selective stem-loop RT qPCR assay validated BioRNA/miR-7 [15 nM] is processed to mature miR-7-5p in HEK293 cells. ***P < 0.001 (One-way ANOVA with Bonferroni *post hoc* tests). (**D**) Our luciferase reporter assay demonstrated miR-7-5p [15 nM] to interact with the wild type but not the mutant MRE site in HEK293 cells. All values are mean ± SD (N = 4 biological replicates per treatment group). ***P < 0.001; **P < 0.01; and ns, not significant (Two-way ANOVA with Bonferroni *post hoc* tests). All values are mean ± SD (N = 3 biological replicates per treatment group).

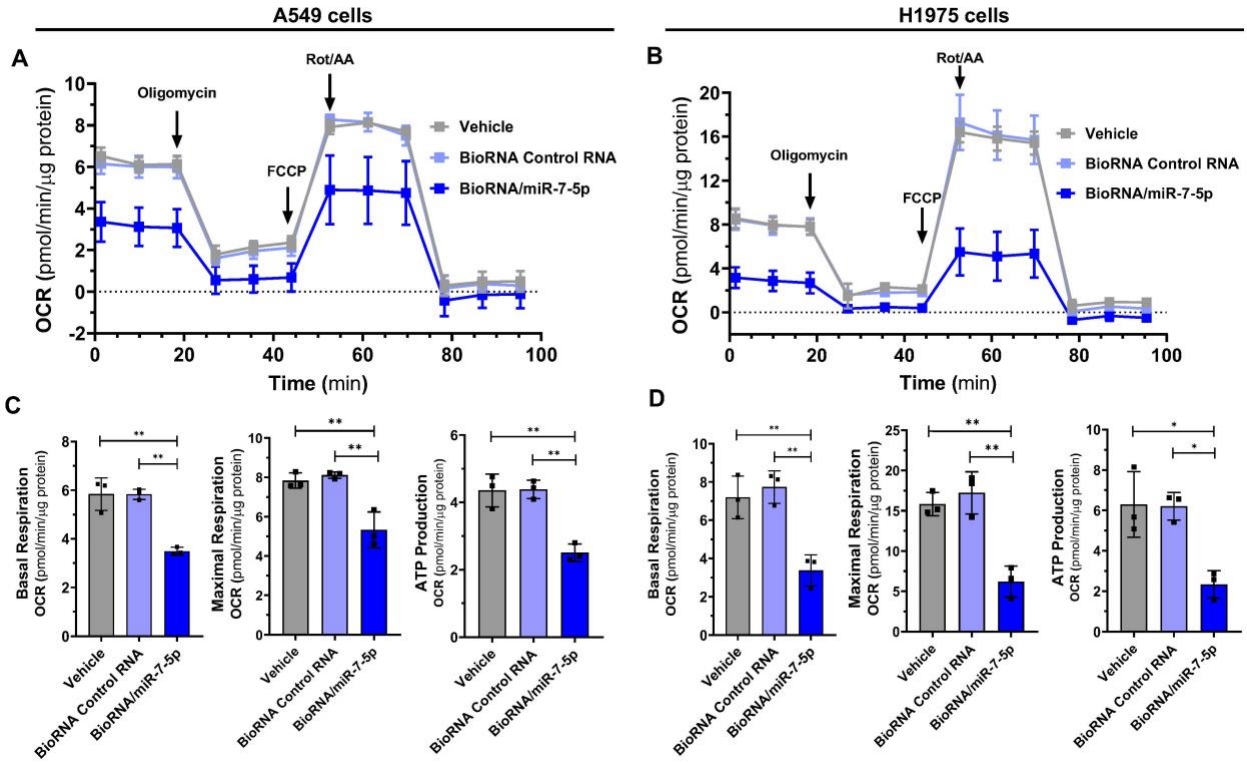

Figure 3. MiR-7 controls mitochondrial respiration in NSCLC cells. Cells were treated with 30 nM of BioRNA/miR-7, control RNA, or vehicle for 72 h. Real-time OCR levels were monitored by the Seahorse XF Cell MitoStress Test Kit. The results revealed that BioRNA/miR-7 reduced overall OCR in A549 (**A**) and H1975 (**B**) cells, which are also indicated by lower levels of basal and maximal respiration, as well as ATP production (**C-D**) as compared with control RNA or vehicle treatments. Values are normalized to protein levels and represent mean ± SD (N = 3/group). *P < 0.05 and **P < 0.01 compared to control RNA or vehicle groups (One-way ANOVA with Bonferroni *post hoc* tests).

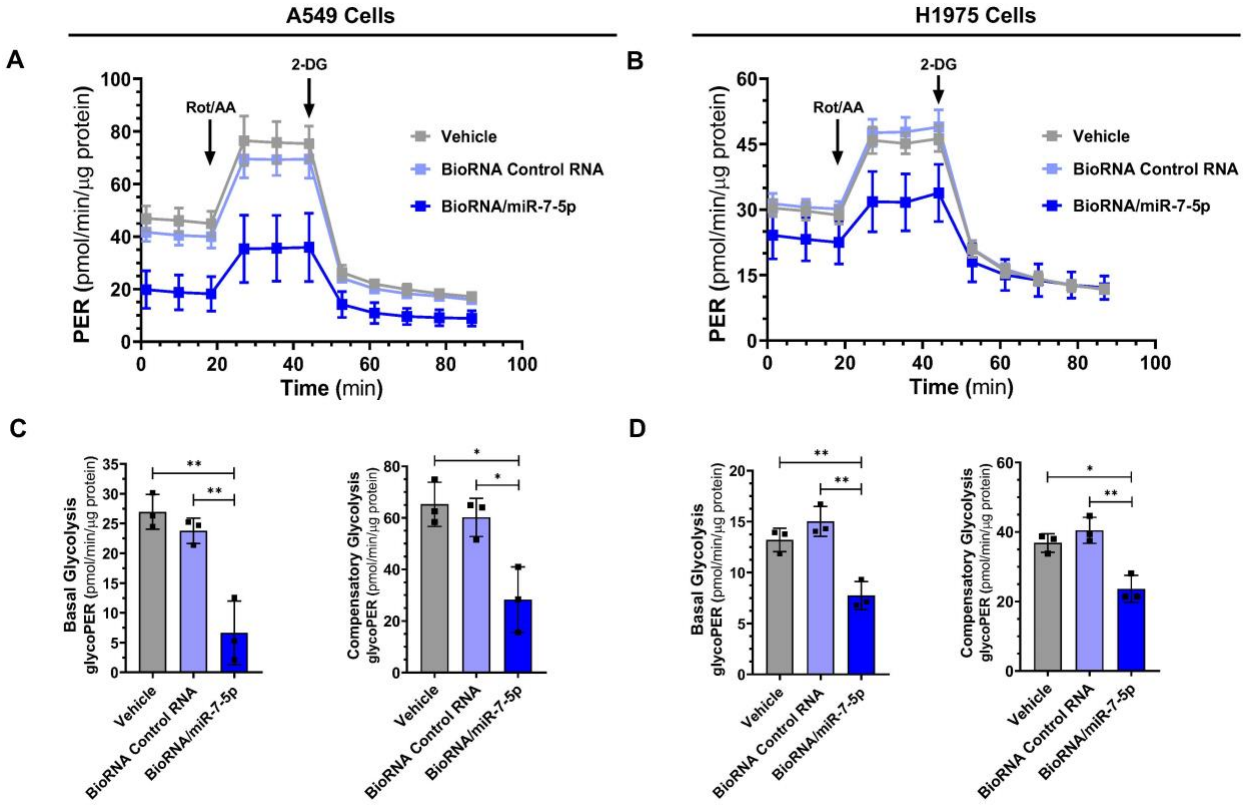

Figure 4. MiR-7 controls glycolytic capacity in NSCLC cells. Cells were treated with 30 nM of BioRNA/miR-7-5p, control RNA, or vehicle for 72 h. Real-time ECAR and OCR were determined by the Seahorse XF Glycolytic Rate Assay Kit and converted to PER which were remarkably reduced by BioRNA/miR-7 in both A549 (**A**) and H1975 (**B**) cells. BioRNA/miR-7 treatment effect on glycolytic capacity is also reflected in the observed decrease in basal and compensatory glycolysis (**C-D**), as compared with control treatments. Values are normalized to protein levels in respective samples and represent mean ± SD (N = 3/group). *P < 0.05 and **P < 0.01 compared to control RNA or vehicle (One-way ANOVA with Bonferroni *post hoc* tests).

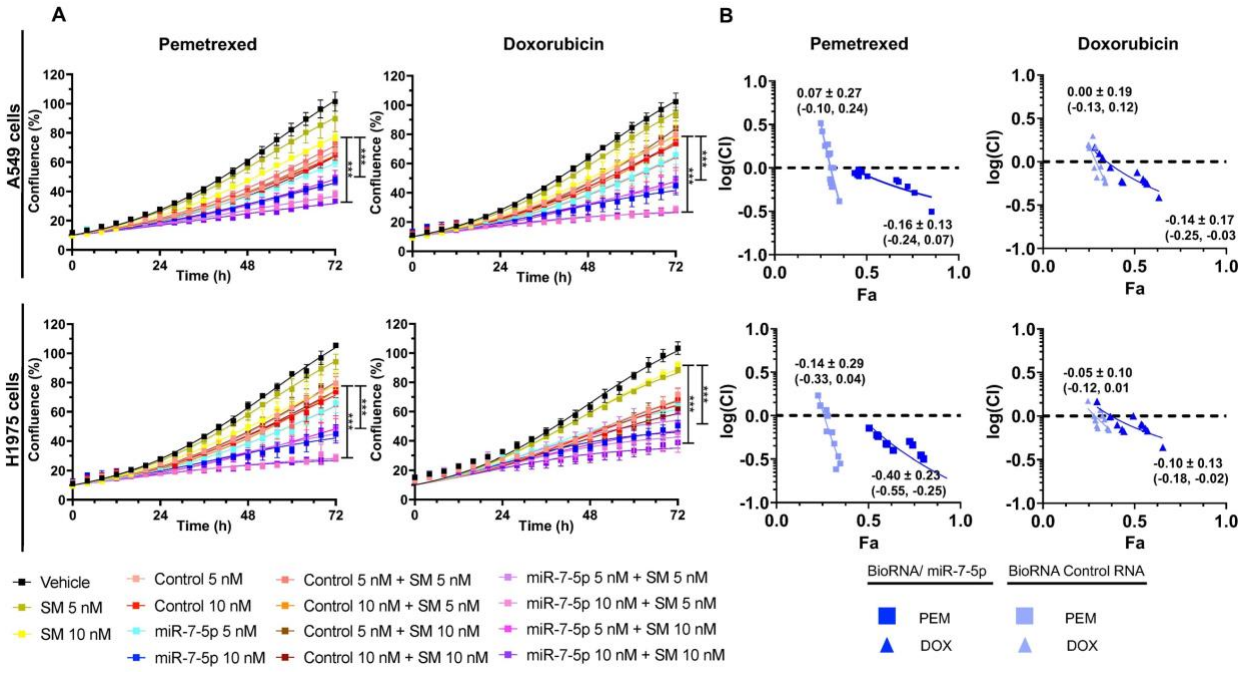

Figure 5. Synergism between BioRNA/miR-7 and chemo-drug in the inhibition of NSCLC cell growth. Cells were treated with 5 or 10 nM of BioRNA/miR-7 (miR-7-5p), control RNA (Control), pemetrexed (PEM), or doxorubicin (DOX) small molecule drug (SM) alone or in combination for 72 h. (**A**) The degrees of cell confluence were monitored at 4 h intervals by using an IncuCyte S3 Live-Cell Analysis System. Data were fit to the logistic growth model, $Y = YM * Y0/((YM - Y0) * exp(-k * x) + Y0)$, and the estimated parameters are presented in Supplementary Table 1. Values are mean ± SD (N = 3 biological replicates per group). ***P < 0.001, SM [10 nM] compared to combination SM [10 nM] plus BioRNA/miR-7 [5 or 10 nM] (Two-way ANOVA with Bonferroni *post hoc* tests). (**B**) The Chou-Talalay plots [log(CI) vs. Fa] revealed a stronger synergism for BioRNA/miR-7 in combination with PEM than DOX. Values represent mean ± SD.

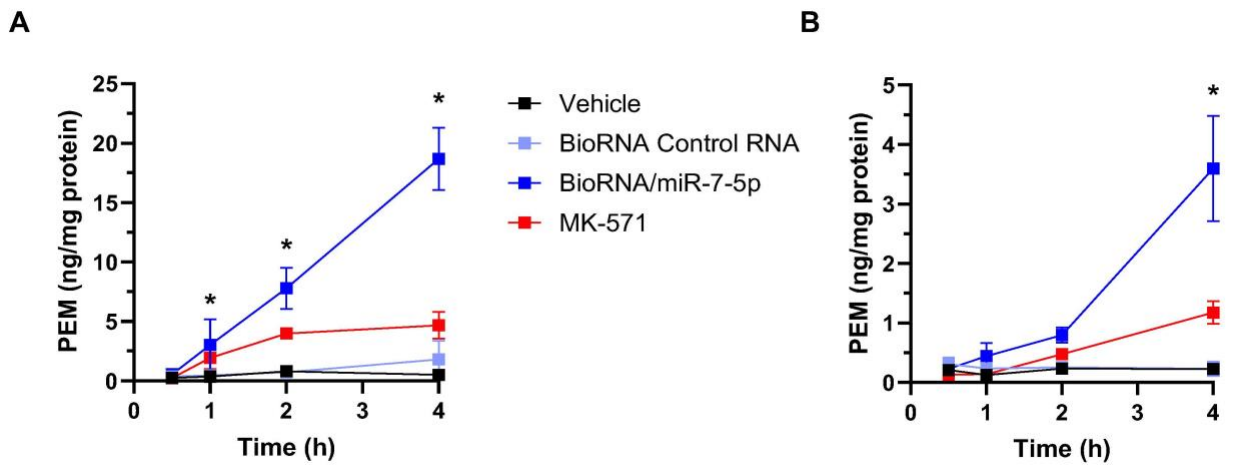

Figure 6. BioRNA/miR-7 increases intracellular accumulation of exogenous pemetrexed (PEM) in both A549 (A) and H1975 (B) cells. Cells were treated with 30 nM of BioRNA/miR-7, control RNA, or vehicle for 72 h followed by media replacement consisting of 10 µM of PEM. Chemical inhibitor MK-571 (50 µM) was used as additional control. PEM levels were quantitated by LC-MS/MS analyses and normalized to protein contents in respective samples. Values are mean ± S.D. (N = 3/group). **P* < 0.05 compared to control RNA group (Two-way ANOVA with Bonferroni's *post hoc* test).

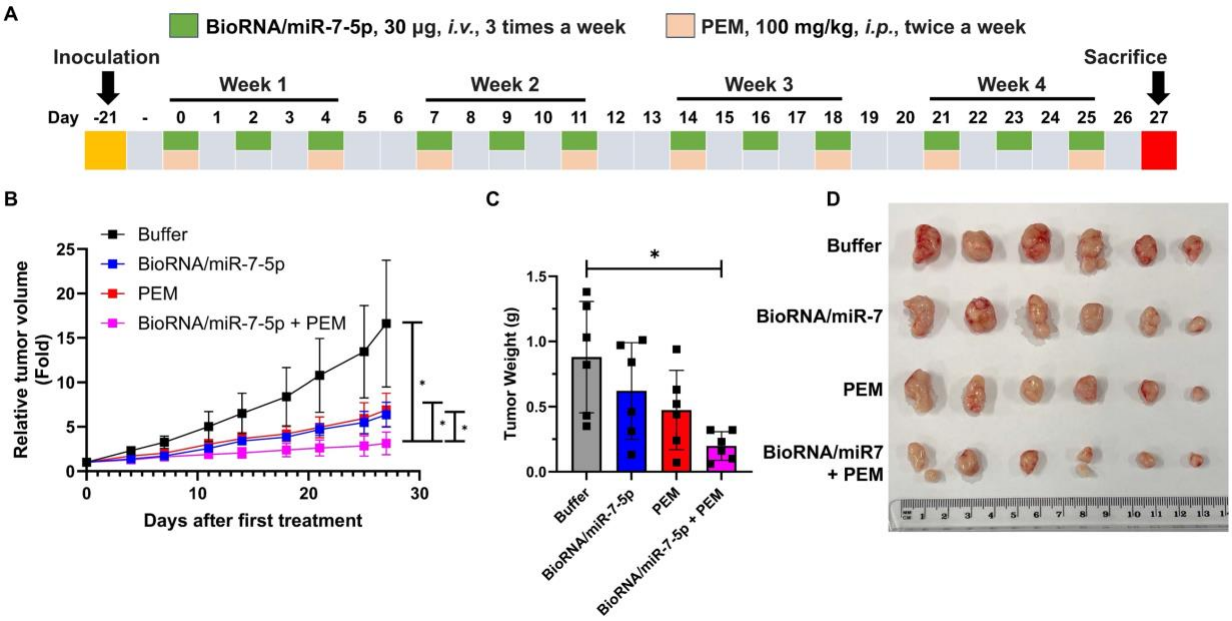

Figure 7. Effectiveness of BioRNA/miR-7 plus pemetrexed (PEM) combination therapy in NSCLC PDX mouse models *in vivo*. (**A**) Schematic illustration of mono- and combination therapy dosing regiments in the NSCLC PDX mouse model. (**B**) Tumor growth curves in mice subjected to different treatments. (**C**) Weights and (**D**) visual comparison of PDX tumors harvested from mice at the end of therapy study. $^{*}P < 0.05$, compared with control RNA (one- or two-way ANOVA with Bonferroni *post hoc* tests).

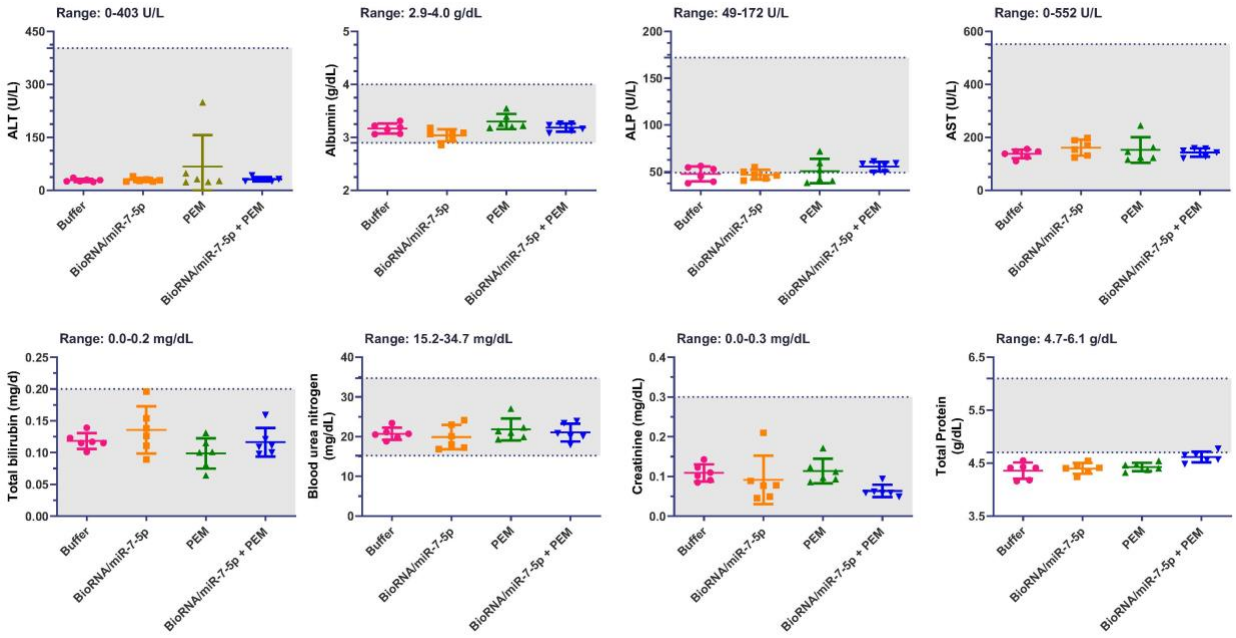

Figure 8. Blood chemistry profiles were not significantly altered by therapeutic doses of BioRNA/miR-7 and pemetrexed in tumor-bearing NOD/SCID mice. No significant differences were found for blood alanine transaminase (ALT), albumin, alkaline phosphatase (ALP), aspartate transaminase (AST), total bilirubin, blood urea nitrogen (BUN), creatinine, or total protein levels between therapy and control groups ($P > 0.05$; one-way ANOVA with Bonferroni *post hoc* tests). Values were within the reference ranges (Grey) of individual markers apart from ALP and total protein (derived from BALB/c mice by the Comparative Pathology Laboratory at UC Davis). Values are mean ± S.D. (N = 6/group).

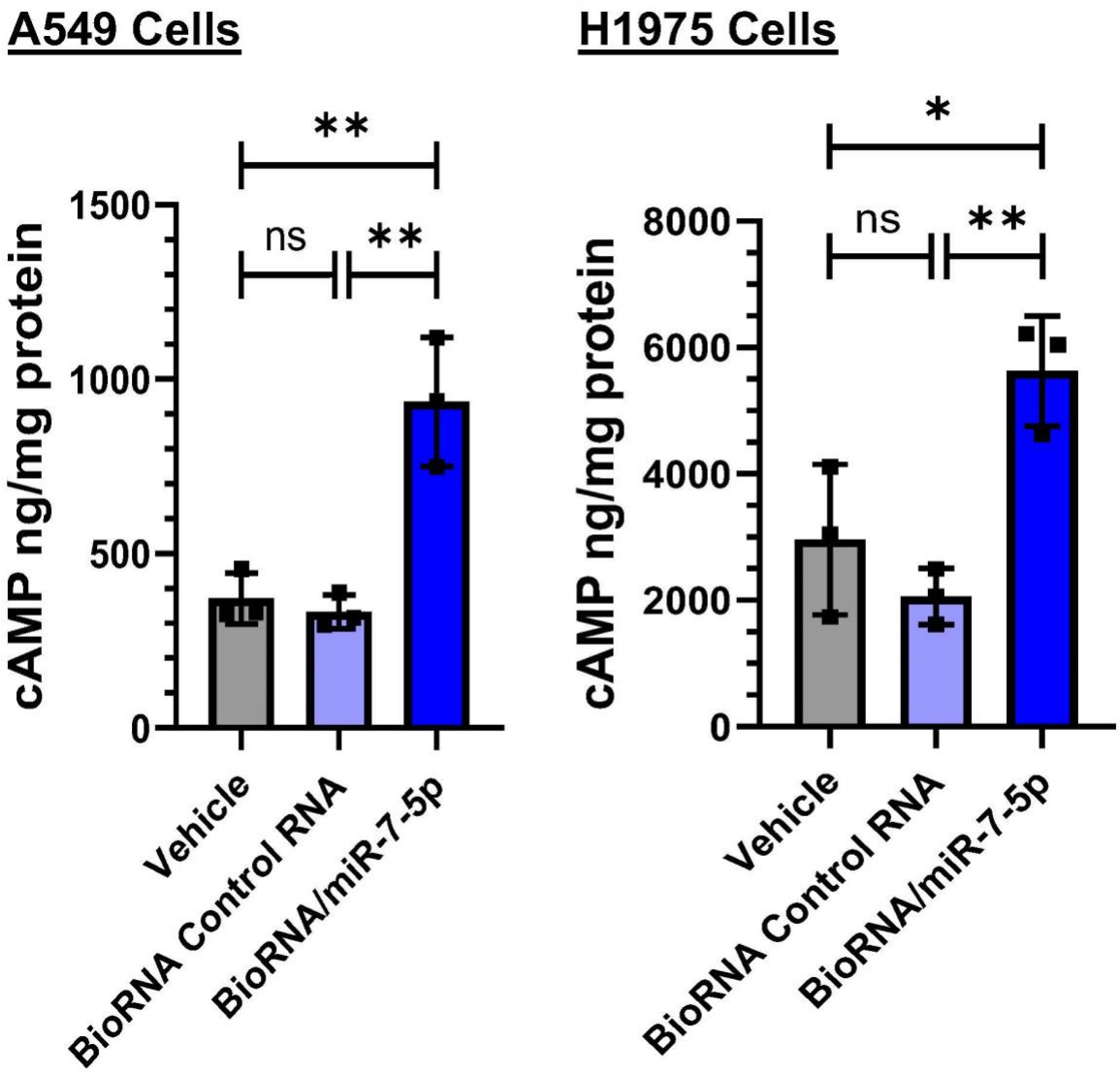

Figure S1. BioRNA/miR-7 improves intracellular cAMP levels in A549 and H1975 NSCLC cells. Values are mean ± S.D. (*N* = 3/group). **P* < 0.05; ***P* < 0.01 (one-way ANOVA with Bonferroni's *post hoc* test).

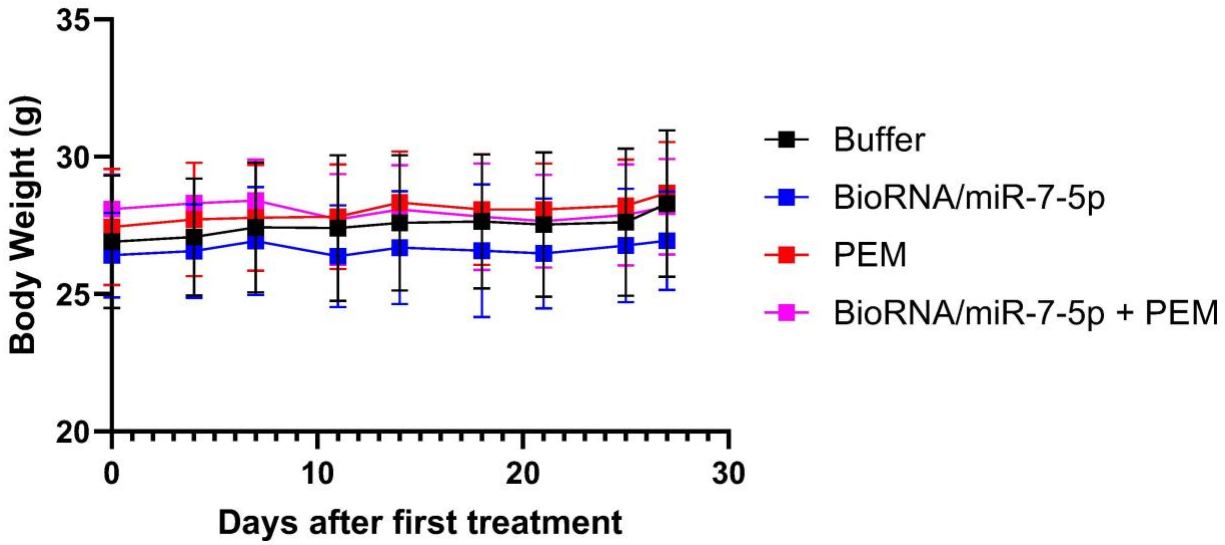

Figure S2. BioRNA/miR-7 plus pemetrexed (PEM) combination therapy is tolerated in PDX NSCLC mouse models. The body weights of mice showed no significant differences between treatment and control buffer treatment ($P > 0.05$; two-way ANOVA with Bonferroni's *post hoc* test). Values are mean ± S.D. (N = 6/group).

References

1. Lee, R.C., R.L. Feinbaum, and V. Ambros, *The C. elegans heterochronic gene lin-4 encodes small RNAs with antisense complementarity to lin-14.* Cell, 1993. **75**(5): p. 843-54.
2. Wightman, B., I. Ha, and G. Ruvkun, *Posttranscriptional regulation of the heterochronic gene lin-14 by lin-4 mediates temporal pattern formation in C. elegans.* Cell, 1993. **75**(5): p. 855-62.
3. Pasquinelli, A.E., et al., *Conservation of the sequence and temporal expression of let-7 heterochronic regulatory RNA.* Nature, 2000. **408**(6808): p. 86-9.
4. Li, S.C., et al., *Identification of homologous microRNAs in 56 animal genomes.* Genomics, 2010. **96**(1): p. 1-9.
5. Friedlander, M.R., et al., *Evidence for the biogenesis of more than 1,000 novel human microRNAs.* Genome Biol, 2014. **15**(4): p. R57.
6. Fire, A., et al., *Potent and specific genetic interference by double-stranded RNA in Caenorhabditis elegans.* Nature, 1998. **391**(6669): p. 806-11.
7. Napoli, C., C. Lemieux, and R. Jorgensen, *Introduction of a Chimeric Chalcone Synthase Gene into Petunia Results in Reversible Co-Suppression of Homologous Genes in trans.* Plant Cell, 1990. **2**(4): p. 279-289.
8. Sen, G.L. and H.M. Blau, *A brief history of RNAi: the silence of the genes.* FASEB J, 2006. **20**(9): p. 1293-9.
9. Setten, R.L., J.J. Rossi, and S.P. Han, *The current state and future directions of RNAi-based therapeutics.* Nat Rev Drug Discov, 2019. **18**(6): p. 421-446.
10. Catalanotto, C., C. Cogoni, and G. Zardo, *MicroRNA in Control of Gene Expression: An Overview of Nuclear Functions.* Int J Mol Sci, 2016. **17**(10).
11. Han, Y.N., et al., *PIWI Proteins and PIWI-Interacting RNA: Emerging Roles in Cancer.* Cell Physiol Biochem, 2017. **44**(1): p. 1-20.
12. Lai, C.F., C.Y. Chen, and L.C. Au, *Comparison between the repression potency of siRNA targeting the coding region and the 3'-untranslated region of mRNA.* Biomed Res Int, 2013. **2013**: p. 637850.
13. Hayes, J., P.P. Peruzzi, and S. Lawler, *MicroRNAs in cancer: biomarkers, functions and therapy.* Trends Mol Med, 2014. **20**(8): p. 460-9.
14. Mollaei, H., R. Safaralizadeh, and Z. Rostami, *MicroRNA replacement therapy in cancer.* J Cell Physiol, 2019. **234**(8): p. 12369-12384.
15. Yu, A.M., Y.H. Choi, and M.J. Tu, *RNA Drugs and RNA Targets for Small Molecules: Principles, Progress, and Challenges.* Pharmacol Rev, 2020. **72**(4): p. 862-898.
16. Smith, E.S., et al., *Clinical Applications of Short Non-Coding RNA-Based Therapies in the Era of Precision Medicine.* Cancers (Basel), 2022. **14**(6).
17. FDA, *Alnylam Pharmaceuticals. Onpattro (Patisiran) [package insert]. U.S. Food and Drug Administration website. https://www.accessdata.fda.gov/drugsatfda_docs/label/2018/210922s000lbl.pdf. 2018. Accessed 27 Jan, 2022.* 2018.
18. FDA, *Alnylam Pharmaceuticals. Givlaari (Givosiran) [package insert]. U.S. Food and Drug Administration website. https://www.accessdata.fda.gov/drugsatfda_docs/label/2019/0212194s000lbl.pdf. 2019. Accessed 27 Jan, 2022.* 2019.

19. FDA, *Alnylam Pharmaceuticals. Oxlumo (Lumasiran) [package insert]. U.S. Food and Drug Administration website. https://www.accessdata.fda.gov/drugsatfda_docs/label/2020/214103lbl.pdf. 2020. Accessed 27 Jan 2022.* 2020.
20. FDA, *Novartis Pharmaceuticals. Leqvio (Inclisiran) [package insert]. U.S. Food and Drug Administration website. https://www.accessdata.fda.gov/drugsatfda_docs/label/2021/214012lbl.pdf. 2021. Accessed 27 Jan 2022.* 2021.
21. Zhang, M.M., et al., *The growth of siRNA-based therapeutics: Updated clinical studies.* Biochem Pharmacol, 2021. **189**: p. 114432.
22. Fan, J. and I.A. de Lannoy, *Pharmacokinetics.* Biochem Pharmacol, 2014. **87**(1): p. 93-120.
23. Johannes, L. and M. Lucchino, *Current Challenges in Delivery and Cytosolic Translocation of Therapeutic RNAs.* Nucleic Acid Ther, 2018. **28**(3): p. 178-193.
24. Seth, P.P., M. Tanowitz, and C.F. Bennett, *Selective tissue targeting of synthetic nucleic acid drugs.* J Clin Invest, 2019. **129**(3): p. 915-925.
25. Maguregui, A. and H. Abe, *Developments in siRNA Modification and Ligand Conjugated Delivery To Enhance RNA Interference Ability.* Chembiochem, 2020. **21**(13): p. 1808-1815.
26. Yu, A.M., et al., *RNA therapy: Are we using the right molecules?* Pharmacol Ther, 2019. **196**: p. 91-104.
27. Morena, F., et al., *Above the Epitranscriptome: RNA Modifications and Stem Cell Identity.* Genes (Basel), 2018. **9**(7).
28. Carthew, R.W. and E.J. Sontheimer, *Origins and Mechanisms of miRNAs and siRNAs.* Cell, 2009. **136**(4): p. 642-55.
29. Huntzinger, E. and E. Izaurralde, *Gene silencing by microRNAs: contributions of translational repression and mRNA decay.* Nat Rev Genet, 2011. **12**(2): p. 99-110.
30. Vasudevan, S., *Posttranscriptional upregulation by microRNAs.* Wiley Interdiscip Rev RNA, 2012. **3**(3): p. 311-30.
31. Piletic, K. and T. Kunej, *MicroRNA epigenetic signatures in human disease.* Archives of Toxicology, 2016. **90**(10): p. 2405-2419.
32. Ha, M. and V.N. Kim, *Regulation of microRNA biogenesis.* Nat Rev Mol Cell Biol, 2014. **15**(8): p. 509-24.
33. Liu, B., et al., *Interplay between miRNAs and host genes and their role in cancer.* Brief Funct Genomics, 2018. **18**(4): p. 255-266.
34. Valinezhad Orang, A., R. Safaralizadeh, and M. Kazemzadeh-Bavili, *Mechanisms of miRNA-Mediated Gene Regulation from Common Downregulation to mRNA-Specific Upregulation.* Int J Genomics, 2014. **2014**: p. 970607.
35. Denli, A.M., et al., *Processing of primary microRNAs by the Microprocessor complex.* Nature, 2004. **432**(7014): p. 231-5.
36. Okada, C., et al., *A high-resolution structure of the pre-microRNA nuclear export machinery.* Science, 2009. **326**(5957): p. 1275-9.
37. Zhang, H., et al., *Single processing center models for human Dicer and bacterial RNase III.* Cell, 2004. **118**(1): p. 57-68.
38. Yoda, M., et al., *ATP-dependent human RISC assembly pathways.* Nat Struct Mol Biol, 2010. **17**(1): p. 17-23.

39. Meijer, H.A., E.M. Smith, and M. Bushell, *Regulation of miRNA strand selection: follow the leader?* Biochem Soc Trans, 2014. **42**(4): p. 1135-40.
40. Khvorova, A., A. Reynolds, and S.D. Jayasena, *Functional siRNAs and miRNAs exhibit strand bias.* Cell, 2003. **115**(2): p. 209-16.
41. Westholm, J.O. and E.C. Lai, *Mirtrons: microRNA biogenesis via splicing.* Biochimie, 2011. **93**(11): p. 1897-904.
42. Berezikov, E., et al., *Mammalian mirtron genes.* Mol Cell, 2007. **28**(2): p. 328-36.
43. Ruby, J.G., C.H. Jan, and D.P. Bartel, *Intronic microRNA precursors that bypass Drosha processing.* Nature, 2007. **448**(7149): p. 83-6.
44. Cheloufi, S., et al., *A dicer-independent miRNA biogenesis pathway that requires Ago catalysis.* Nature, 2010. **465**(7298): p. 584-9.
45. Yang, J.S., et al., *Conserved vertebrate mir-451 provides a platform for Dicer-independent, Ago2-mediated microRNA biogenesis.* Proc Natl Acad Sci U S A, 2010. **107**(34): p. 15163-8.
46. Ender, C., et al., *A human snoRNA with microRNA-like functions.* Mol Cell, 2008. **32**(4): p. 519-28.
47. Hasler, D., et al., *The Lupus Autoantigen La Prevents Mis-channeling of tRNA Fragments into the Human MicroRNA Pathway.* Mol Cell, 2016. **63**(1): p. 110-24.
48. Li, S., Z. Xu, and J. Sheng, *tRNA-Derived Small RNA: A Novel Regulatory Small Non-Coding RNA.* Genes (Basel), 2018. **9**(5).
49. Patterson, D.G., et al., *Human snoRNA-93 is processed into a microRNA-like RNA that promotes breast cancer cell invasion.* NPJ Breast Cancer, 2017. **3**: p. 25.
50. Pan, Y.Z., et al., *Small nucleolar RNA-derived microRNA hsa-miR-1291 modulates cellular drug disposition through direct targeting of ABC transporter ABCC1.* Drug Metab Dispos, 2013. **41**(10): p. 1744-51.
51. Kufel, J. and P. Grzechnik, *Small Nucleolar RNAs Tell a Different Tale.* Trends Genet, 2019. **35**(2): p. 104-117.
52. Kumar, P., et al., *Meta-analysis of tRNA derived RNA fragments reveals that they are evolutionarily conserved and associate with AGO proteins to recognize specific RNA targets.* BMC Biol, 2014. **12**: p. 78.
53. Kuscu, C., et al., *tRNA fragments (tRFs) guide Ago to regulate gene expression post-transcriptionally in a Dicer-independent manner.* RNA, 2018. **24**(8): p. 1093-1105.
54. Hamilton, A.J. and D.C. Baulcombe, *A species of small antisense RNA in posttranscriptional gene silencing in plants.* Science, 1999. **286**(5441): p. 950-2.
55. Gaglione, M. and A. Messere, *Recent progress in chemically modified siRNAs.* Mini Rev Med Chem, 2010. **10**(7): p. 578-95.
56. Amarzguioui, M., J.J. Rossi, and D. Kim, *Approaches for chemically synthesized siRNA and vector-mediated RNAi.* FEBS Lett, 2005. **579**(26): p. 5974-81.
57. Beaucage, S.L., *Solid-phase synthesis of siRNA oligonucleotides.* Curr Opin Drug Discov Devel, 2008. **11**(2): p. 203-16.
58. Francis, A.J. and M.J.E. Resendiz, *Protocol for the Solid-phase Synthesis of Oligomers of RNA Containing a 2'-O-thiophenylmethyl Modification and Characterization via Circular Dichroism.* J Vis Exp, 2017(125).
59. Wilson, C. and A.D. Keefe, *Building oligonucleotide therapeutics using non-natural chemistries.* Curr Opin Chem Biol, 2006. **10**(6): p. 607-14.

60. Foster, D.J., et al., *Advanced siRNA Designs Further Improve In Vivo Performance of GalNAc-siRNA Conjugates.* Mol Ther, 2018. **26**(3): p. 708-717.
61. Beckert, B. and B. Masquida, *Synthesis of RNA by in vitro transcription.* Methods Mol Biol, 2011. **703**: p. 29-41.
62. Yu, A.M., et al., *Novel approaches for efficient in vivo fermentation production of noncoding RNAs.* Appl Microbiol Biotechnol, 2020. **104**(5): p. 1927-1937.
63. Donze, O. and D. Picard, *RNA interference in mammalian cells using siRNAs synthesized with T7 RNA polymerase.* Nucleic Acids Res, 2002. **30**(10): p. e46.
64. Wianny, F. and M. Zernicka-Goetz, *Specific interference with gene function by double-stranded RNA in early mouse development.* Nat Cell Biol, 2000. **2**(2): p. 70-5.
65. Yang, D., et al., *Short RNA duplexes produced by hydrolysis with Escherichia coli RNase III mediate effective RNA interference in mammalian cells.* Proc Natl Acad Sci U S A, 2002. **99**(15): p. 9942-7.
66. Guiley, K.Z., A.J. Pratt, and I.J. MacRae, *Single-pot enzymatic synthesis of Dicer-substrate siRNAs.* Nucleic Acids Res, 2012. **40**(5): p. e40.
67. Myers, J.W., et al., *Recombinant Dicer efficiently converts large dsRNAs into siRNAs suitable for gene silencing.* Nat Biotechnol, 2003. **21**(3): p. 324-8.
68. Bramsen, J.B., et al., *A large-scale chemical modification screen identifies design rules to generate siRNAs with high activity, high stability and low toxicity.* Nucleic Acids Res, 2009. **37**(9): p. 2867-81.
69. Janas, M.M., et al., *Selection of GalNAc-conjugated siRNAs with limited off-target-driven rat hepatotoxicity.* Nat Commun, 2018. **9**(1): p. 723.
70. Robbins, M., et al., *2'-O-methyl-modified RNAs act as TLR7 antagonists.* Mol Ther, 2007. **15**(9): p. 1663-9.
71. Lonn, P., et al., *Enhancing Endosomal Escape for Intracellular Delivery of Macromolecular Biologic Therapeutics.* Sci Rep, 2016. **6**: p. 32301.
72. Shum, K. and J. Rossi, *SiRNA Delivery Methods Methods and Protocols Preface.* Sirna Delivery Methods: Methods and Protocols, 2016. **1364**: p. V-Vi.
73. Chakraborty, C., et al., *Therapeutic miRNA and siRNA: Moving from Bench to Clinic as Next Generation Medicine.* Mol Ther Nucleic Acids, 2017. **8**: p. 132-143.
74. Khvorova, A. and J.K. Watts, *The chemical evolution of oligonucleotide therapies of clinical utility.* Nat Biotechnol, 2017. **35**(3): p. 238-248.
75. Lima, W.F., et al., *Single-stranded siRNAs activate RNAi in animals.* Cell, 2012. **150**(5): p. 883-94.
76. Meade, B.R., et al., *Efficient delivery of RNAi prodrugs containing reversible charge-neutralizing phosphotriester backbone modifications.* Nat Biotechnol, 2014. **32**(12): p. 1256-61.
77. Ipsaro, J.J. and L. Joshua-Tor, *From guide to target: molecular insights into eukaryotic RNA-interference machinery.* Nat Struct Mol Biol, 2015. **22**(1): p. 20-8.
78. Coelho, T., et al., *Safety and efficacy of RNAi therapy for transthyretin amyloidosis.* N Engl J Med, 2013. **369**(9): p. 819-29.
79. Khvorova, A., *Oligonucleotide Therapeutics - A New Class of Cholesterol-Lowering Drugs.* N Engl J Med, 2017. **376**(1): p. 4-7.
80. Liebow, A., et al., *An Investigational RNAi Therapeutic Targeting Glycolate Oxidase Reduces Oxalate Production in Models of Primary Hyperoxaluria.* J Am Soc Nephrol, 2017. **28**(2): p. 494-503.

81. Goldman, L. and A.I. Schafer, *Amyloidosis. In: Goldman-Cecil medicine*. 25th edition. ed. 2016, Philadelphia, PA: Elsevier/Saunders. 2 volumes (xl, 2722, I108 pages).
82. Kristen, A.V., et al., *Patisiran, an RNAi therapeutic for the treatment of hereditary transthyretin-mediated amyloidosis.* Neurodegener Dis Manag, 2019. **9**(1): p. 5-23.
83. Ando, T., et al., *Characterization of extracellular RNAs produced by the marine photosynthetic bacterium Rhodovulum sulfidophilum.* J Biochem, 2006. **139**(4): p. 805-11.
84. Dungu, J.N., et al., *Cardiac transthyretin amyloidosis.* Heart, 2012. **98**(21): p. 1546-54.
85. Shin, S.C. and J. Robinson-Papp, *Amyloid neuropathies.* Mt Sinai J Med, 2012. **79**(6): p. 733-48.
86. Leung, A.K., et al., *Lipid Nanoparticles Containing siRNA Synthesized by Microfluidic Mixing Exhibit an Electron-Dense Nanostructured Core.* J Phys Chem C Nanomater Interfaces, 2012. **116**(34): p. 18440-18450.
87. Paunovska, K., D. Loughrey, and J.E. Dahlman, *Drug delivery systems for RNA therapeutics.* Nature Reviews Genetics, 2022.
88. Zhang, X., V. Goel, and G.J. Robbie, *Pharmacokinetics of Patisiran, the First Approved RNA Interference Therapy in Patients With Hereditary Transthyretin-Mediated Amyloidosis.* J Clin Pharmacol, 2019.
89. Suhr, O.B., et al., *Efficacy and safety of patisiran for familial amyloidotic polyneuropathy: a phase II multi-dose study.* Orphanet J Rare Dis, 2015. **10**: p. 109.
90. Taylor, L., et al., *A Phase I, Randomized, Double-Blind, Placebo-Controlled, Single Ascending Dose, Multiple Dose, and Food Effect Trial of the Safety, Tolerability and Pharmacokinetics of Highly Purified Cannabidiol in Healthy Subjects.* CNS Drugs, 2018. **32**(11): p. 1053-1067.
91. Gonzalez-Duarte, A., et al., *Analysis of autonomic outcomes in APOLLO, a phase III trial of the RNAi therapeutic patisiran in patients with hereditary transthyretin-mediated amyloidosis.* J Neurol, 2020. **267**(3): p. 703-712.
92. Obici, L., et al., *Quality of life outcomes in APOLLO, the phase 3 trial of the RNAi therapeutic patisiran in patients with hereditary transthyretin-mediated amyloidosis.* Amyloid, 2020. **27**(3): p. 153-162.
93. Adams, D., et al., *Patisiran, an RNAi Therapeutic, for Hereditary Transthyretin Amyloidosis.* N Engl J Med, 2018. **379**(1): p. 11-21.
94. Solomon, S.D., et al., *Effects of Patisiran, an RNA Interference Therapeutic, on Cardiac Parameters in Patients With Hereditary Transthyretin-Mediated Amyloidosis.* Circulation, 2019. **139**(4): p. 431-443.
95. Adams, D., et al., *Long-term safety and efficacy of patisiran for hereditary transthyretin-mediated amyloidosis with polyneuropathy: 12-month results of an open-label extension study.* Lancet Neurol, 2021. **20**(1): p. 49-59.
96. Anderson, K.E., *Acute hepatic porphyrias: Current diagnosis & management.* Mol Genet Metab, 2019. **128**(3): p. 219-227.
97. Kothadia, J.P., K. LaFreniere, and J.M. Shah, *Acute Hepatic Porphyria*, in *StatPearls*. 2022: Treasure Island (FL).
98. Scott, L.J., *Givosiran: First Approval.* Drugs, 2020. **80**(3): p. 335-339.
99. Bissell, D.M., K.E. Anderson, and H.L. Bonkovsky, *Porphyria.* N Engl J Med, 2017. **377**(9): p. 862-872.

100. Sardh, E. and P. Harper, *RNAi therapy with givosiran significantly reduces attack rates in acute intermittent porphyria.* J Intern Med, 2022. **291**(5): p. 593-610.
101. Besur, S., et al., *Clinically important features of porphyrin and heme metabolism and the porphyrias.* Metabolites, 2014. **4**(4): p. 977-1006.
102. Pallet, N., et al., *Porphyria and kidney diseases.* Clin Kidney J, 2018. **11**(2): p. 191-197.
103. Debacker, A.J., et al., *Delivery of Oligonucleotides to the Liver with GalNAc: From Research to Registered Therapeutic Drug.* Mol Ther, 2020. **28**(8): p. 1759-1771.
104. Agarwal, S., et al., *Pharmacokinetics and Pharmacodynamics of the Small Interfering Ribonucleic Acid, Givosiran, in Patients With Acute Hepatic Porphyria.* Clin Pharmacol Ther, 2020. **108**(1): p. 63-72.
105. Sardh, E., et al., *Phase 1 Trial of an RNA Interference Therapy for Acute Intermittent Porphyria.* N Engl J Med, 2019. **380**(6): p. 549-558.
106. Bissell, M., et al., *A phase 1/2 open-label extension study of givosiran, an investigational RNAi therapeutic, in patients with acute intermittent porphyria.* European Journal of Neurology, 2019. **26**: p. 52-52.
107. Balwani, M., et al., *Phase 3 Trial of RNAi Therapeutic Givosiran for Acute Intermittent Porphyria.* N Engl J Med, 2020. **382**(24): p. 2289-2301.
108. Ventura, P., et al., *Efficacy and safety of givosiran for acute hepatic porphyria: 24-month interim analysis of the randomized phase 3 ENVISION study.* Liver Int, 2022. **42**(1): p. 161-172.
109. Cochat, P. and G. Rumsby, *Primary hyperoxaluria.* N Engl J Med, 2013. **369**(7): p. 649-58.
110. Garrelfs, S.F., et al., *Lumasiran, an RNAi Therapeutic for Primary Hyperoxaluria Type 1.* N Engl J Med, 2021. **384**(13): p. 1216-1226.
111. Frishberg, Y., et al., *Phase 1/2 Study of Lumasiran for Treatment of Primary Hyperoxaluria Type 1: A Placebo-Controlled Randomized Clinical Trial.* Clin J Am Soc Nephrol, 2021. **16**(7): p. 1025-1036.
112. Sas, D.J., et al., *Phase 3 trial of lumasiran for primary hyperoxaluria type 1: A new RNAi therapeutic in infants and young children.* Genet Med, 2021.
113. Scott, L.J. and S.J. Keam, *Lumasiran: First Approval.* Drugs, 2021. **81**(2): p. 277-282.
114. Bardolia, C., N.S. Amin, and J. Turgeon, *Emerging Non-statin Treatment Options for Lowering Low-Density Lipoprotein Cholesterol.* Front Cardiovasc Med, 2021. **8**: p. 789931.
115. McGowan, M.P., et al., *Diagnosis and Treatment of Heterozygous Familial Hypercholesterolemia.* J Am Heart Assoc, 2019. **8**(24): p. e013225.
116. Abifadel, M., et al., *Mutations in PCSK9 cause autosomal dominant hypercholesterolemia.* Nat Genet, 2003. **34**(2): p. 154-6.
117. Santulli, G., S.S. Jankauskas, and J. Gambardella, *Inclisiran: a new milestone on the PCSK9 road to tackle cardiovascular risk.* Eur Heart J Cardiovasc Pharmacother, 2021. **7**(3): p. e11-e12.
118. van Bruggen, F.H., et al., *Serious adverse events and deaths in PCSK9 inhibitor trials reported on ClinicalTrials.gov: a systematic review.* Expert Rev Clin Pharmacol, 2020. **13**(7): p. 787-796.
119. Lamb, Y.N., *Inclisiran: First Approval.* Drugs, 2021. **81**(3): p. 389-395.

120. Nair, J.K., et al., *Multivalent N-acetylgalactosamine-conjugated siRNA localizes in hepatocytes and elicits robust RNAi-mediated gene silencing.* J Am Chem Soc, 2014. **136**(49): p. 16958-61.
121. Fitzgerald, K., et al., *A Highly Durable RNAi Therapeutic Inhibitor of PCSK9.* N Engl J Med, 2017. **376**(1): p. 41-51.
122. Ray, K.K., et al., *Inclisiran in Patients at High Cardiovascular Risk with Elevated LDL Cholesterol.* N Engl J Med, 2017. **376**(15): p. 1430-1440.
123. Raal, F.J., et al., *Inclisiran for the Treatment of Heterozygous Familial Hypercholesterolemia.* N Engl J Med, 2020. **382**(16): p. 1520-1530.
124. Ray, K.K., et al., *Two Phase 3 Trials of Inclisiran in Patients with Elevated LDL Cholesterol.* N Engl J Med, 2020. **382**(16): p. 1507-1519.
125. Brandts, J. and K.K. Ray, *Clinical implications and outcomes of the ORION Phase III trials.* Future Cardiol, 2021. **17**(5): p. 769-777.
126. Reijman, M.D., et al., *Rationale and design of two trials assessing the efficacy, safety, and tolerability of inclisiran in adolescents with homozygous and heterozygous familial hypercholesterolaemia.* Eur J Prev Cardiol, 2022.
127. Kallend, D., et al., *Pharmacokinetics and pharmacodynamics of inclisiran, a small interfering RNA therapy, in patients with hepatic impairment.* J Clin Lipidol, 2022. **16**(2): p. 208-219.
128. Wang, Z., et al., *Inclisiran inhibits oxidized low-density lipoprotein-induced foam cell formation in Raw264.7 macrophages via activating the PPARgamma pathway.* Autoimmunity, 2022: p. 1-10.
129. Christofides, A., et al., *The role of peroxisome proliferator-activated receptors (PPAR) in immune responses.* Metabolism, 2021. **114**: p. 154338.
130. Machin, N. and M.V. Ragni, *An investigational RNAi therapeutic targeting antithrombin for the treatment of hemophilia A and B.* J Blood Med, 2018. **9**: p. 135-140.
131. Kletzmayr, A., M.E. Ivarsson, and J.C. Leroux, *Investigational Therapies for Primary Hyperoxaluria.* Bioconjug Chem, 2020. **31**(7): p. 1696-1707.
132. Gallagher, K.M., et al., *Recent early clinical drug development for acute kidney injury.* Expert Opin Investig Drugs, 2017. **26**(2): p. 141-154.
133. Moreno-Montanes, J., A.M. Bleau, and A.I. Jimenez, *Tivanisiran, a novel siRNA for the treatment of dry eye disease.* Expert Opin Investig Drugs, 2018. **27**(4): p. 421-426.
134. Habtemariam, B.A., et al., *Single-Dose Pharmacokinetics and Pharmacodynamics of Transthyretin Targeting N-acetylgalactosamine-Small Interfering Ribonucleic Acid Conjugate, Vutrisiran, in Healthy Subjects.* Clin Pharmacol Ther, 2021. **109**(2): p. 372-382.
135. Castaman, G. and D. Matino, *Hemophilia A and B: molecular and clinical similarities and differences.* Haematologica, 2019. **104**(9): p. 1702-1709.
136. Berk, C., et al., *Pharmacodynamic and Pharmacokinetic Properties of Full Phosphorothioate Small Interfering RNAs for Gene Silencing In Vivo.* Nucleic Acid Ther, 2021. **31**(3): p. 237-244.
137. Sehgal, A., et al., *An RNAi therapeutic targeting antithrombin to rebalance the coagulation system and promote hemostasis in hemophilia.* Nat Med, 2015. **21**(5): p. 492-7.

138. Lai, C., et al., *Specific Inhibition of Hepatic Lactate Dehydrogenase Reduces Oxalate Production in Mouse Models of Primary Hyperoxaluria.* Mol Ther, 2018. **26**(8): p. 1983-1995.
139. Davidson, B.L. and P.B. McCray, Jr., *Current prospects for RNA interference-based therapies.* Nat Rev Genet, 2011. **12**(5): p. 329-40.
140. Makris, K. and L. Spanou, *Acute Kidney Injury: Definition, Pathophysiology and Clinical Phenotypes.* Clin Biochem Rev, 2016. **37**(2): p. 85-98.
141. Molitoris, B.A., et al., *siRNA targeted to p53 attenuates ischemic and cisplatin-induced acute kidney injury.* J Am Soc Nephrol, 2009. **20**(8): p. 1754-64.
142. Thompson, J.D., et al., *Toxicological and pharmacokinetic properties of chemically modified siRNAs targeting p53 RNA following intravenous administration.* Nucleic Acid Ther, 2012. **22**(4): p. 255-64.
143. Shimazaki, J., *Definition and Diagnostic Criteria of Dry Eye Disease: Historical Overview and Future Directions.* Invest Ophthalmol Vis Sci, 2018. **59**(14): p. DES7-DES12.
144. Weng, Y., et al., *RNAi therapeutic and its innovative biotechnological evolution.* Biotechnol Adv, 2019. **37**(5): p. 801-825.
145. Bonneau, E., et al., *How close are miRNAs from clinical practice? A perspective on the diagnostic and therapeutic market.* EJIFCC, 2019. **30**(2): p. 114-127.
146. Hanna, J., G.S. Hossain, and J. Kocerha, *The Potential for microRNA Therapeutics and Clinical Research.* Front Genet, 2019. **10**: p. 478.
147. Bader, A.G., D. Brown, and M. Winkler, *The promise of microRNA replacement therapy.* Cancer Res, 2010. **70**(18): p. 7027-30.
148. Yu, A.M. and M.J. Tu, *Deliver the promise: RNAs as a new class of molecular entities for therapy and vaccination.* Pharmacol Ther, 2022. **230**: p. 107967.
149. Lima, J.F., et al., *Anti-miRNA oligonucleotides: A comprehensive guide for design.* RNA Biol, 2018. **15**(3): p. 338-352.
150. Lennox, K.A. and M.A. Behlke, *Chemical modification and design of anti-miRNA oligonucleotides.* Gene Ther, 2011. **18**(12): p. 1111-20.
151. Lennox, K.A., et al., *Improved Performance of Anti-miRNA Oligonucleotides Using a Novel Non-Nucleotide Modifier.* Mol Ther Nucleic Acids, 2013. **2**: p. e117.
152. Mie, Y., et al., *Function Control of Anti-microRNA Oligonucleotides Using Interstrand Cross-Linked Duplexes.* Mol Ther Nucleic Acids, 2018. **10**: p. 64-74.
153. Costales, M.G., et al., *Small Molecule Inhibition of microRNA-210 Reprograms an Oncogenic Hypoxic Circuit.* J Am Chem Soc, 2017. **139**(9): p. 3446-3455.
154. Meyer, S.M., et al., *Small molecule recognition of disease-relevant RNA structures.* Chem Soc Rev, 2020. **49**(19): p. 7167-7199.
155. Velagapudi, S.P., S.M. Gallo, and M.D. Disney, *Sequence-based design of bioactive small molecules that target precursor microRNAs.* Nat Chem Biol, 2014. **10**(4): p. 291-7.
156. Stenvang, J., et al., *Inhibition of microRNA function by antimiR oligonucleotides.* Silence, 2012. **3**(1): p. 1.
157. Yu, A.M., et al., *MicroRNA Pharmacoepigenetics: Posttranscriptional Regulation Mechanisms behind Variable Drug Disposition and Strategy to Develop More Effective Therapy.* Drug Metab Dispos, 2016. **44**(3): p. 308-19.
158. Montgomery, R.L., et al., *MicroRNA mimicry blocks pulmonary fibrosis.* EMBO Mol Med, 2014. **6**(10): p. 1347-56.

159. He, Y., et al., *MicroRNA-29 family, a crucial therapeutic target for fibrosis diseases.* Biochimie, 2013. **95**(7): p. 1355-9.
160. To, K.K.W., et al., *Advances in the discovery of microRNA-based anticancer therapeutics: latest tools and developments.* Expert Opin Drug Discov, 2020. **15**(1): p. 63-83.
161. Casarotto, M., et al., *Beyond MicroRNAs: Emerging Role of Other Non-Coding RNAs in HPV-Driven Cancers.* Cancers (Basel), 2020. **12**(5).
162. To, K.K., et al., *MicroRNAs in the prognosis and therapy of colorectal cancer: From bench to bedside.* World J Gastroenterol, 2018. **24**(27): p. 2949-2973.
163. Xue, J., et al., *MicroRNA-targeted therapeutics for lung cancer treatment.* Expert Opin Drug Discov, 2017. **12**(2): p. 141-157.
164. Lovat, F., et al., *Combined loss of function of two different loci of miR-15/16 drives the pathogenesis of acute myeloid leukemia.* Proc Natl Acad Sci U S A, 2020. **117**(22): p. 12332-12340.
165. Nguyen, D.D. and S. Chang, *Development of Novel Therapeutic Agents by Inhibition of Oncogenic MicroRNAs.* Int J Mol Sci, 2017. **19**(1).
166. Wang, Z., *The principles of MiRNA-masking antisense oligonucleotides technology.* Methods Mol Biol, 2011. **676**: p. 43-9.
167. Ebert, M.S., J.R. Neilson, and P.A. Sharp, *MicroRNA sponges: competitive inhibitors of small RNAs in mammalian cells.* Nat Methods, 2007. **4**(9): p. 721-6.
168. Meng, Z. and M. Lu, *RNA Interference-Induced Innate Immunity, Off-Target Effect, or Immune Adjuvant?* Front Immunol, 2017. **8**: p. 331.
169. To, K.K., *MicroRNA: a prognostic biomarker and a possible druggable target for circumventing multidrug resistance in cancer chemotherapy.* J Biomed Sci, 2013. **20**: p. 99.
170. Zhang, Y. and J. Wang, *MicroRNAs are important regulators of drug resistance in colorectal cancer.* Biol Chem, 2017. **398**(8): p. 929-938.
171. Cortez, M.A., et al., *Role of miRNAs in immune responses and immunotherapy in cancer.* Genes Chromosomes Cancer, 2019. **58**(4): p. 244-253.
172. Hand, T.W., et al., *Differential effects of STAT5 and PI3K/AKT signaling on effector and memory CD8 T-cell survival.* Proc Natl Acad Sci U S A, 2010. **107**(38): p. 16601-6.
173. Ji, Y., J.D. Hocker, and L. Gattinoni, *Enhancing adoptive T cell immunotherapy with microRNA therapeutics.* Semin Immunol, 2016. **28**(1): p. 45-53.
174. Babar, I.A., et al., *Inhibition of hypoxia-induced miR-155 radiosensitizes hypoxic lung cancer cells.* Cancer Biol Ther, 2011. **12**(10): p. 908-14.
175. El Bezawy, R., et al., *miR-205 enhances radiation sensitivity of prostate cancer cells by impairing DNA damage repair through PKCepsilon and ZEB1 inhibition.* J Exp Clin Cancer Res, 2019. **38**(1): p. 51.
176. Moertl, S., et al., *MicroRNAs as novel elements in personalized radiotherapy.* Translational Cancer Research, 2016: p. S1262-S1269.
177. Overgaard, J., *Hypoxic radiosensitization: adored and ignored.* J Clin Oncol, 2007. **25**(26): p. 4066-74.
178. Kessel, D. and N.L. Oleinick, *Cell Death Pathways Associated with Photodynamic Therapy: An Update.* Photochem Photobiol, 2018. **94**(2): p. 213-218.
179. El-Daly, S.M., M.L. Abba, and A.M. Gamal-Eldeen, *The role of microRNAs in photodynamic therapy of cancer.* Eur J Med Chem, 2017. **142**: p. 550-555.

180. Jung, J., et al., *Simultaneous inhibition of multiple oncogenic miRNAs by a multi-potent microRNA sponge.* Oncotarget, 2015. **6**(24): p. 20370-87.
181. Orellana, E.A., et al., *Identification and validation of microRNAs that synergize with miR-34a - a basis for combinatorial microRNA therapeutics.* Cell Cycle, 2019. **18**(15): p. 1798-1811.
182. Xue, J., et al., *MiRNA-621 sensitizes breast cancer to chemotherapy by suppressing FBXO11 and enhancing p53 activity.* Oncogene, 2016. **35**(4): p. 448-58.
183. Hermeking, H., *The miR-34 family in cancer and apoptosis.* Cell Death Differ, 2010. **17**(2): p. 193-9.
184. Misso, G., et al., *Mir-34: a new weapon against cancer?* Mol Ther Nucleic Acids, 2014. **3**: p. e194.
185. Dimopoulos, K., P. Gimsing, and K. Gronbaek, *Aberrant microRNA expression in multiple myeloma.* Eur J Haematol, 2013. **91**(2): p. 95-105.
186. Lodygin, D., et al., *Inactivation of miR-34a by aberrant CpG methylation in multiple types of cancer.* Cell Cycle, 2008. **7**(16): p. 2591-600.
187. Beg, M.S., et al., *Phase I study of MRX34, a liposomal miR-34a mimic, administered twice weekly in patients with advanced solid tumors.* Invest New Drugs, 2017. **35**(2): p. 180-188.
188. Hong, D.S., et al., *Phase 1 study of MRX34, a liposomal miR-34a mimic, in patients with advanced solid tumours.* Br J Cancer, 2020. **122**(11): p. 1630-1637.
189. Kansakar, U., et al., *Functional Role of microRNAs in Regulating Cardiomyocyte Death.* Cells, 2022. **11**(6).
190. Varzideh, F., et al., *Cardiac Remodeling After Myocardial Infarction: Functional Contribution of microRNAs to Inflammation and Fibrosis.* Front Cardiovasc Med, 2022. **9**: p. 863238.
191. Hu, J., et al., *MiR-122 in hepatic function and liver diseases.* Protein Cell, 2012. **3**(5): p. 364-71.
192. Gebert, L.F., et al., *Miravirsen (SPC3649) can inhibit the biogenesis of miR-122.* Nucleic Acids Res, 2014. **42**(1): p. 609-21.
193. Janssen, H.L., et al., *Treatment of HCV infection by targeting microRNA.* N Engl J Med, 2013. **368**(18): p. 1685-94.
194. Lindow, M. and S. Kauppinen, *Discovering the first microRNA-targeted drug.* J Cell Biol, 2012. **199**(3): p. 407-12.
195. Segal, M. and F.J. Slack, *Challenges identifying efficacious miRNA therapeutics for cancer.* Expert Opin Drug Discov, 2020. **15**(9): p. 987-992.
196. Zhang, S., et al., *The Risks of miRNA Therapeutics: In a Drug Target Perspective.* Drug Des Devel Ther, 2021. **15**: p. 721-733.
197. Weaver, D.T., et al., *Network potential identifies therapeutic miRNA cocktails in Ewing sarcoma.* PLoS Comput Biol, 2021. **17**(10): p. e1008755.
198. Dowdy, S.F., *Overcoming cellular barriers for RNA therapeutics.* Nat Biotechnol, 2017. **35**(3): p. 222-229.
199. Micklefield, J., *Backbone modification of nucleic acids: synthesis, structure and therapeutic applications.* Curr Med Chem, 2001. **8**(10): p. 1157-79.
200. Cheng, Z., et al., *Multifunctional nanoparticles: cost versus benefit of adding targeting and imaging capabilities.* Science, 2012. **338**(6109): p. 903-10.

201. Boca, S., et al., *Nanoscale delivery systems for microRNAs in cancer therapy.* Cell Mol Life Sci, 2020. **77**(6): p. 1059-1086.
202. Forterre, A., et al., *A Comprehensive Review of Cancer MicroRNA Therapeutic Delivery Strategies.* Cancers (Basel), 2020. **12**(7).
203. Karra, N. and S. Benita, *The ligand nanoparticle conjugation approach for targeted cancer therapy.* Curr Drug Metab, 2012. **13**(1): p. 22-41.
204. Leung, A.K., Y.Y. Tam, and P.R. Cullis, *Lipid nanoparticles for short interfering RNA delivery.* Adv Genet, 2014. **88**: p. 71-110.
205. Pitulle, C., K.O. Hedenstierna, and G.E. Fox, *A novel approach for monitoring genetically engineered microorganisms by using artificial, stable RNAs.* Appl Environ Microbiol, 1995. **61**(10): p. 3661-6.
206. Gao, Y., et al., *RNA interference-based osteoanabolic therapy for osteoporosis by a bone-formation surface targeting delivery system.* Biochem Biophys Res Commun, 2022. **601**: p. 86-92.
207. Dasgupta, I. and A. Chatterjee, *Recent Advances in miRNA Delivery Systems.* Methods Protoc, 2021. **4**(1).
208. Mitchell, M.J., et al., *Engineering precision nanoparticles for drug delivery.* Nat Rev Drug Discov, 2021. **20**(2): p. 101-124.
209. Lu, M., et al., *Exosome-based small RNA delivery: Progress and prospects.* Asian J Pharm Sci, 2018. **13**(1): p. 1-11.
210. Xu, C., et al., *Favorable biodistribution, specific targeting and conditional endosomal escape of RNA nanoparticles in cancer therapy.* Cancer Lett, 2018. **414**: p. 57-70.
211. Kumar, L., et al., *Exosomes: Natural Carriers for siRNA Delivery.* Curr Pharm Des, 2015. **21**(31): p. 4556-65.
212. Barile, L. and G. Vassalli, *Exosomes: Therapy delivery tools and biomarkers of diseases.* Pharmacol Ther, 2017. **174**: p. 63-78.
213. Ha, D., N. Yang, and V. Nadithe, *Exosomes as therapeutic drug carriers and delivery vehicles across biological membranes: current perspectives and future challenges.* Acta Pharm Sin B, 2016. **6**(4): p. 287-96.
214. van den Boorn, J.G., et al., *SiRNA delivery with exosome nanoparticles.* Nat Biotechnol, 2011. **29**(4): p. 325-6.
215. Alvarez-Erviti, L., et al., *Delivery of siRNA to the mouse brain by systemic injection of targeted exosomes.* Nat Biotechnol, 2011. **29**(4): p. 341-5.
216. Shtam, T.A., et al., *Exosomes are natural carriers of exogenous siRNA to human cells in vitro.* Cell Commun Signal, 2013. **11**: p. 88.
217. Haney, M.J., et al., *Exosomes as drug delivery vehicles for Parkinson's disease therapy.* J Control Release, 2015. **207**: p. 18-30.
218. Ohno, S., et al., *Systemically injected exosomes targeted to EGFR deliver antitumor microRNA to breast cancer cells.* Mol Ther, 2013. **21**(1): p. 185-91.
219. Akuma, P., O.D. Okagu, and C.C. Udenigwe, *Naturally Occurring Exosome Vesicles as Potential Delivery Vehicle for Bioactive Compounds.* Frontiers in Sustainable Food Systems, 2019. **3**.
220. Fu, Y., J. Chen, and Z. Huang, *Recent progress in microRNA-based delivery systems for the treatment of human disease.* ExRNA, 2019. **1**(1): p. 24.
221. Vannucci, L., et al., *Viral vectors: a look back and ahead on gene transfer technology.* New Microbiol, 2013. **36**(1): p. 1-22.

222. Chen, Y., Y. Xianyu, and X. Jiang, *Surface Modification of Gold Nanoparticles with Small Molecules for Biochemical Analysis.* Acc Chem Res, 2017. **50**(2): p. 310-319.
223. Cai, W., et al., *Bio responsive self-assembly of Au-miRNAs for targeted cancer theranostics.* EBioMedicine, 2020. **54**: p. 102740.
224. Mamaeva, V., C. Sahlgren, and M. Linden, *Mesoporous silica nanoparticles in medicine--recent advances.* Adv Drug Deliv Rev, 2013. **65**(5): p. 689-702.
225. Loh, K.P., et al., *Graphene oxide as a chemically tunable platform for optical applications.* Nat Chem, 2010. **2**(12): p. 1015-24.
226. Sun, S., et al., *Targeting and Regulating of an Oncogene via Nanovector Delivery of MicroRNA using Patient-Derived Xenografts.* Theranostics, 2017. **7**(3): p. 677-693.
227. Pereira, P., et al., *New insights for therapeutic recombinant human miRNAs heterologous production: Rhodovolum sulfidophilum vs Escherichia coli.* Bioengineered, 2017. **8**(5): p. 670-677.
228. Hashiro, S., M. Mitsuhashi, and H. Yasueda, *Overexpression system for recombinant RNA in Corynebacterium glutamicum using a strong promoter derived from corynephage BFK20.* J Biosci Bioeng, 2019. **128**(3): p. 255-263.
229. Kikuchi, Y. and S. Umekage, *Extracellular nucleic acids of the marine bacterium Rhodovulum sulfidophilum and recombinant RNA production technology using bacteria.* FEMS Microbiol Lett, 2018. **365**(3).
230. Nagao, N., et al., *Complete Genome Sequence of Rhodovulum sulfidophilum DSM 2351, an Extracellular Nucleic Acid-Producing Bacterium.* Genome Announc, 2015. **3**(2).
231. Nagao, N., et al., *Short hairpin RNAs of designed sequences can be extracellularly produced by the marine bacterium Rhodovulum sulfidophilum.* J Gen Appl Microbiol, 2014. **60**(6): p. 222-6.
232. Suzuki, H., et al., *Extracellular production of an RNA aptamer by ribonuclease-free marine bacteria harboring engineered plasmids: a proposal for industrial RNA drug production.* Appl Environ Microbiol, 2010. **76**(3): p. 786-93.
233. Pereira, P., et al., *Advances in time course extracellular production of human pre-miR-29b from Rhodovulum sulfidophilum.* Appl Microbiol Biotechnol, 2016. **100**(8): p. 3723-34.
234. Hashiro, S., et al., *Construction of Corynebacterium glutamicum cells as containers encapsulating dsRNA overexpressed for agricultural pest control.* Appl Microbiol Biotechnol, 2019. **103**(20): p. 8485-8496.
235. Qiu, W., J.W. Park, and H.B. Scholthof, *Tombusvirus P19-mediated suppression of virus-induced gene silencing is controlled by genetic and dosage features that influence pathogenicity.* Mol Plant Microbe Interact, 2002. **15**(3): p. 269-80.
236. Silhavy, D., et al., *A viral protein suppresses RNA silencing and binds silencing-generated, 21- to 25-nucleotide double-stranded RNAs.* EMBO J, 2002. **21**(12): p. 3070-80.
237. Huang, L., et al., *Efficient and specific gene knockdown by small interfering RNAs produced in bacteria.* Nat Biotechnol, 2013. **31**(4): p. 350-6.
238. Daros, J.A., V. Aragones, and T. Cordero, *A viroid-derived system to produce large amounts of recombinant RNA in Escherichia coli.* Sci Rep, 2018. **8**(1): p. 1904.
239. Branch, A.D., B.J. Benenfeld, and H.D. Robertson, *Evidence for a single rolling circle in the replication of potato spindle tuber viroid.* Proc Natl Acad Sci U S A, 1988. **85**(23): p. 9128-32.

240. Branch, A.D. and H.D. Robertson, *A replication cycle for viroids and other small infectious RNA's.* Science, 1984. **223**(4635): p. 450-5.
241. Zhang, X., et al., *Engineered 5S ribosomal RNAs displaying aptamers recognizing vascular endothelial growth factor and malachite green.* J Mol Recognit, 2009. **22**(2): p. 154-61.
242. D'Souza, L.M., et al., *Small RNA sequences are readily stabilized by inclusion in a carrier rRNA.* Biotechnol Prog, 2003. **19**(3): p. 734-8.
243. Liu, Y., et al., *DNAzyme-mediated recovery of small recombinant RNAs from a 5S rRNA-derived chimera expressed in Escherichia coli.* BMC Biotechnol, 2010. **10**: p. 85.
244. Nelissen, F.H., et al., *Fast production of homogeneous recombinant RNA--towards large-scale production of RNA.* Nucleic Acids Res, 2012. **40**(13): p. e102.
245. Ponchon, L., et al., *A generic protocol for the expression and purification of recombinant RNA in Escherichia coli using a tRNA scaffold.* Nat Protoc, 2009. **4**(6): p. 947-59.
246. Ponchon, L. and F. Dardel, *Recombinant RNA technology: the tRNA scaffold.* Nat Methods, 2007. **4**(7): p. 571-6.
247. Gaudin, C., et al., *The tRNA-like domains of E coli and A.aeolicus transfer-messenger RNA: structural and functional studies.* J Mol Biol, 2003. **331**(2): p. 457-71.
248. Meinnel, T., Y. Mechulam, and G. Fayat, *Fast purification of a functional elongator tRNAmet expressed from a synthetic gene in vivo.* Nucleic Acids Res, 1988. **16**(16): p. 8095-6.
249. Li, M.M., et al., *Chimeric MicroRNA-1291 Biosynthesized Efficiently in Escherichia coli Is Effective to Reduce Target Gene Expression in Human Carcinoma Cells and Improve Chemosensitivity.* Drug Metab Dispos, 2015. **43**(7): p. 1129-36.
250. Li, M.M., et al., *Rapid production of novel pre-microRNA agent hsa-mir-27b in Escherichia coli using recombinant RNA technology for functional studies in mammalian cells.* Drug Metab Dispos, 2014. **42**(11): p. 1791-5.
251. Wang, W.P., et al., *Bioengineering Novel Chimeric microRNA-34a for Prodrug Cancer Therapy: High-Yield Expression and Purification, and Structural and Functional Characterization.* J Pharmacol Exp Ther, 2015. **354**(2): p. 131-41.
252. Peng, Y., et al., *Co-expression and co-purification of archaeal and eukaryal box C/D RNPs.* PLoS One, 2014. **9**(7): p. e103096.
253. Li, P.C., et al., *In vivo fermentation production of humanized noncoding RNAs carrying payload miRNAs for targeted anticancer therapy.* Theranostics, 2021. **11**(10): p. 4858-4871.
254. Chen, Q.X., et al., *A general approach to high-yield biosynthesis of chimeric RNAs bearing various types of functional small RNAs for broad applications.* Nucleic Acids Res, 2015. **43**(7): p. 3857-69.
255. Ho, P.Y., et al., *Bioengineered Noncoding RNAs Selectively Change Cellular miRNome Profiles for Cancer Therapy.* J Pharmacol Exp Ther, 2018. **365**(3): p. 494-506.
256. Petrek, H., et al., *Single bioengineered ncRNA molecule for dual-targeting toward the control of non-small cell lung cancer patient-derived xenograft tumor growth.* Biochem Pharmacol, 2021. **189**: p. 114392.
257. Ho, P.Y. and A.M. Yu, *Bioengineering of noncoding RNAs for research agents and therapeutics.* Wiley Interdiscip Rev RNA, 2016. **7**(2): p. 186-97.
258. Dominska, M. and D.M. Dykxhoorn, *Breaking down the barriers: siRNA delivery and endosome escape.* J Cell Sci, 2010. **123**(Pt 8): p. 1183-9.

259. Jilek, J.L., et al., *Bioengineered Let-7c Inhibits Orthotopic Hepatocellular Carcinoma and Improves Overall Survival with Minimal Immunogenicity.* Mol Ther Nucleic Acids, 2019. **14**: p. 498-508.
260. Tu, M.J., et al., *Bioengineered miRNA-1291 prodrug therapy in pancreatic cancer cells and patient-derived xenograft mouse models.* Cancer Lett, 2019. **442**: p. 82-90.
261. Deng, L., et al., *Bioengineered miR-124-3p prodrug selectively alters the proteome of human carcinoma cells to control multiple cellular components and lung metastasis in vivo.* Acta Pharm Sin B, 2021. **11**(12): p. 3950-3965.
262. Yi, W., et al., *Bioengineered miR-328-3p modulates GLUT1-mediated glucose uptake and metabolism to exert synergistic antiproliferative effects with chemotherapeutics.* Acta Pharm Sin B, 2020. **10**(1): p. 159-170.
263. Li, X., et al., *Bioengineered miR-27b-3p and miR-328-3p modulate drug metabolism and disposition via the regulation of target ADME gene expression.* Acta Pharm Sin B, 2019. **9**(3): p. 639-647.
264. Alegre, F., et al., *A genetically engineered microRNA-34a prodrug demonstrates anti-tumor activity in a canine model of osteosarcoma.* PLoS One, 2018. **13**(12): p. e0209941.
265. Tu, M.J., et al., *MicroRNA-1291-5p Sensitizes Pancreatic Carcinoma Cells to Arginine Deprivation and Chemotherapy through the Regulation of Arginolysis and Glycolysis.* Mol Pharmacol, 2020. **98**(6): p. 686-694.
266. Jian, C., et al., *Co-targeting of DNA, RNA, and protein molecules provides optimal outcomes for treating osteosarcoma and pulmonary metastasis in spontaneous and experimental metastasis mouse models.* Oncotarget, 2017. **8**(19): p. 30742-30755.
267. Jilek, J.L., Y. Tian, and A.M. Yu, *Effects of MicroRNA-34a on the Pharmacokinetics of Cytochrome P450 Probe Drugs in Mice.* Drug Metab Dispos, 2017. **45**(5): p. 512-522.
268. Umeh-Garcia, M., et al., *A Novel Bioengineered miR-127 Prodrug Suppresses the Growth and Metastatic Potential of Triple-Negative Breast Cancer Cells.* Cancer Res, 2020. **80**(3): p. 418-429.
269. Xu, J., et al., *Creatine based polymer for codelivery of bioengineered MicroRNA and chemodrugs against breast cancer lung metastasis.* Biomaterials, 2019. **210**: p. 25-40.
270. Zhang, Q.Y., et al., *Lipidation of polyethylenimine-based polyplex increases serum stability of bioengineered RNAi agents and offers more consistent tumoral gene knockdown in vivo.* Int J Pharm, 2018. **547**(1-2): p. 537-544.
271. Feng, R., et al., *RNA Therapeutics - Research and Clinical Advancements.* Front Mol Biosci, 2021. **8**: p. 710738.
272. Gogate, A., et al., *Targeting the Liver with Nucleic Acid Therapeutics for the Treatment of Systemic Diseases of Liver Origin.* Pharmacol Rev, 2023.
273. Traber, G.M. and A.-M. Yu, *RNAi-Based Therapeutics and Novel RNA Bioengineering Technologies.* Journal of Pharmacology and Experimental Therapeutics, 2023. **384**(1): p. 133-154.
274. Sheng, P., K.A. Flood, and M. Xie, *Short Hairpin RNAs for Strand-Specific Small Interfering RNA Production.* Front Bioeng Biotechnol, 2020. **8**: p. 940.
275. Ning, B. and A.M. Yu, *RNA therapeutics: From biochemical pharmacology to technology development and clinical applications.* Biochem Pharmacol, 2021. **189**: p. 114567.
276. Shang, R., et al., *microRNAs in action: biogenesis, function and regulation.* Nat Rev Genet, 2023. **24**(12): p. 816-833.

277. Gebert, L.F.R. and I.J. MacRae, *Regulation of microRNA function in animals.* Nat Rev Mol Cell Biol, 2019. **20**(1): p. 21-37.
278. Bazzini, A.A., M.T. Lee, and A.J. Giraldez, *Ribosome profiling shows that miR-430 reduces translation before causing mRNA decay in zebrafish.* Science, 2012. **336**(6078): p. 233-7.
279. Djuranovic, S., A. Nahvi, and R. Green, *miRNA-mediated gene silencing by translational repression followed by mRNA deadenylation and decay.* Science, 2012. **336**(6078): p. 237-40.
280. Yekta, S., I.H. Shih, and D.P. Bartel, *MicroRNA-directed cleavage of HOXB8 mRNA.* Science, 2004. **304**(5670): p. 594-6.
281. Hu, B., et al., *Therapeutic siRNA: state of the art.* Signal Transduct Target Ther, 2020. **5**(1): p. 101.
282. Hauptmann, J., et al., *Engineering miRNA features into siRNAs: Guide-strand bulges are compatible with gene repression.* Mol Ther Nucleic Acids, 2022. **27**: p. 1116-1126.
283. Birmingham, A., et al., *A protocol for designing siRNAs with high functionality and specificity.* Nat Protoc, 2007. **2**(9): p. 2068-78.
284. Friedrich, M. and A. Aigner, *Therapeutic siRNA: State-of-the-Art and Future Perspectives.* BioDrugs, 2022. **36**(5): p. 549-571.
285. Jagla, B., et al., *Sequence characteristics of functional siRNAs.* RNA, 2005. **11**(6): p. 864-72.
286. Miller, V.M., et al., *Allele-specific silencing of dominant disease genes.* Proc Natl Acad Sci U S A, 2003. **100**(12): p. 7195-200.
287. Naito, Y. and K. Ui-Tei, *Designing functional siRNA with reduced off-target effects.* Methods Mol Biol, 2013. **942**: p. 57-68.
288. Ui-Tei, K., et al., *Guidelines for the selection of highly effective siRNA sequences for mammalian and chick RNA interference.* Nucleic Acids Res, 2004. **32**(3): p. 936-48.
289. Jung, E., et al., *Global analysis of AGO2-bound RNAs reveals that miRNAs induce cleavage of target RNAs with limited complementarity.* Biochim Biophys Acta Gene Regul Mech, 2017. **1860**(11): p. 1148-1158.
290. Moore, C.B., et al., *Short hairpin RNA (shRNA): design, delivery, and assessment of gene knockdown.* Methods Mol Biol, 2010. **629**: p. 141-58.
291. Brummelkamp, T.R., R. Bernards, and R. Agami, *A system for stable expression of short interfering RNAs in mammalian cells.* Science, 2002. **296**(5567): p. 550-3.
292. Siolas, D., et al., *Synthetic shRNAs as potent RNAi triggers.* Nat Biotechnol, 2005. **23**(2): p. 227-31.
293. Ketting, R.F., et al., *Dicer functions in RNA interference and in synthesis of small RNA involved in developmental timing in C. elegans.* Genes Dev, 2001. **15**(20): p. 2654-9.
294. Grimson, A., et al., *MicroRNA targeting specificity in mammals: determinants beyond seed pairing.* Mol Cell, 2007. **27**(1): p. 91-105.
295. Fakhr, E., F. Zare, and L. Teimoori-Toolabi, *Precise and efficient siRNA design: a key point in competent gene silencing.* Cancer Gene Ther, 2016. **23**(4): p. 73-82.
296. Diener, C., A. Keller, and E. Meese, *Emerging concepts of miRNA therapeutics: from cells to clinic.* Trends Genet, 2022. **38**(6): p. 613-626.
297. FDA, *Novo Nordisk Inc. Rivfloza (Nedosiran) [package insert]. U.S. Food and Drug Administration website.*

https://www.accessdata.fda.gov/drugsatfda_docs/label/2023/215842s000lbl.pdf. *2023. Accessed 3 Oct, 2023.* 2023.
298. Adams, D., et al., *Efficacy and safety of vutrisiran for patients with hereditary transthyretin-mediated amyloidosis with polyneuropathy: a randomized clinical trial.* Amyloid, 2023. **30**(1): p. 1-9.
299. FDA, *Alnylam Pharmaceuticals. Amvuttra (Vutrisiran) [package insert]. U.S. Food and Drug Administration website.* https://www.accessdata.fda.gov/drugsatfda_docs/label/2022/215515s000lbl.pdf. *2022. Accessed 15 June, 2022.* 2022.
300. O'Leary, N.A., et al., *Reference sequence (RefSeq) database at NCBI: current status, taxonomic expansion, and functional annotation.* Nucleic Acids Res, 2016. **44**(D1): p. D733-45.
301. Siramshetty, V.B., et al., *NCATS Inxight Drugs: a comprehensive and curated portal for translational research.* Nucleic Acids Res, 2022. **50**(D1): p. D1307-D1316.
302. Martin, S.E. and N.J. Caplen, *Mismatched siRNAs downregulate mRNAs as a function of target site location.* FEBS Lett, 2006. **580**(15): p. 3694-8.
303. Saxena, S., Z.O. Jonsson, and A. Dutta, *Small RNAs with imperfect match to endogenous mRNA repress translation. Implications for off-target activity of small inhibitory RNA in mammalian cells.* J Biol Chem, 2003. **278**(45): p. 44312-9.
304. Ahn, I., C.S. Kang, and J. Han, *Where should siRNAs go: applicable organs for siRNA drugs.* Exp Mol Med, 2023. **55**(7): p. 1283-1292.
305. Zhang, X., et al., *Patisiran Pharmacokinetics, Pharmacodynamics, and Exposure-Response Analyses in the Phase 3 APOLLO Trial in Patients With Hereditary Transthyretin-Mediated (hATTR) Amyloidosis.* J Clin Pharmacol, 2020. **60**(1): p. 37-49.
306. Yang, A.C., et al., *Physiological blood-brain transport is impaired with age by a shift in transcytosis.* Nature, 2020. **583**(7816): p. 425-430.
307. Baum, M.A., et al., *PHYOX2: a pivotal randomized study of nedosiran in primary hyperoxaluria type 1 or 2.* Kidney Int, 2023. **103**(1): p. 207-217.
308. Li, J., et al., *Nonclinical Pharmacokinetics and Absorption, Distribution, Metabolism, and Excretion of Givosiran, the First Approved N-Acetylgalactosamine-Conjugated RNA Interference Therapeutic.* Drug Metab Dispos, 2021. **49**(7): p. 572-580.
309. Tian, B. and J.L. Manley, *Alternative polyadenylation of mRNA precursors.* Nat Rev Mol Cell Biol, 2017. **18**(1): p. 18-30.
310. Iacomino, G., *miRNAs: The Road from Bench to Bedside.* Genes (Basel), 2023. **14**(2).
311. Seyhan, A.A., *Trials and Tribulations of MicroRNA Therapeutics.* Int J Mol Sci, 2024. **25**(3).
312. Jackson, A.L., et al., *Widespread siRNA "off-target" transcript silencing mediated by seed region sequence complementarity.* RNA, 2006. **12**(7): p. 1179-87.
313. Lin, X., et al., *siRNA-mediated off-target gene silencing triggered by a 7 nt complementation.* Nucleic Acids Res, 2005. **33**(14): p. 4527-35.
314. Vickers, T.A., et al., *Off-target and a portion of target-specific siRNA mediated mRNA degradation is Ago2 'Slicer' independent and can be mediated by Ago1.* Nucleic Acids Res, 2009. **37**(20): p. 6927-41.
315. Bumcrot, D., et al., *RNAi therapeutics: a potential new class of pharmaceutical drugs.* Nat Chem Biol, 2006. **2**(12): p. 711-9.

316. Ambros, V., *MicroRNA pathways in flies and worms: growth, death, fat, stress, and timing.* Cell, 2003. **113**(6): p. 673-6.
317. Ambros, V., *The functions of animal microRNAs.* Nature, 2004. **431**(7006): p. 350-5.
318. Thai, A.A., et al., *Lung cancer.* Lancet, 2021. **398**(10299): p. 535-554.
319. Siegel, R.L., et al., *Cancer statistics, 2023.* CA Cancer J Clin, 2023. **73**(1): p. 17-48.
320. Grodzka, A., et al., *Molecular alterations of driver genes in non-small cell lung cancer: from diagnostics to targeted therapy.* EXCLI J, 2023. **22**: p. 415-432.
321. Petrek, H. and A.M. Yu, *MicroRNAs in non-small cell lung cancer: Gene regulation, impact on cancer cellular processes, and therapeutic potential.* Pharmacol Res Perspect, 2019. **7**(6): p. e00528.
322. Chen, Y., et al., *Use of recombinant microRNAs as antimetabolites to inhibit human non-small cell lung cancer.* Acta Pharm Sin B, 2023. **13**(10): p. 4273-4290.
323. Yi, W.R., et al., *Bioengineered miR-328-3p modulates GLUT1-mediated glucose uptake and metabolism to exert synergistic antiproliferative effects with chemotherapeutics.* Acta Pharmaceutica Sinica B 2020. **10**(1): p. 159-170.
324. Xiong, S., et al., *MicroRNA-7 inhibits the growth of human non-small cell lung cancer A549 cells through targeting BCL-2.* Int J Biol Sci, 2011. **7**(6): p. 805-14.
325. Guo, G., et al., *miR7/SP1/TP53BP1 axis may play a pivotal role in NSCLC radiosensitivity.* Oncol Rep, 2020. **44**(6): p. 2678-2690.
326. Li, Q., et al., *MicroRNA-7-5p induces cell growth inhibition, cell cycle arrest and apoptosis by targeting PAK2 in non-small cell lung cancer.* FEBS Open Bio, 2019. **9**(11): p. 1983-1993.
327. Porat, J., U. Kothe, and M.A. Bayfield, *Revisiting tRNA chaperones: New players in an ancient game.* RNA, 2021. **27**(5): p. 543-59.
328. Foster, K.A., et al., *Characterization of the A549 cell line as a type II pulmonary epithelial cell model for drug metabolism.* Exp Cell Res, 1998. **243**(2): p. 359-66.
329. Neuperger, P., et al., *Analysis of the Single-Cell Heterogeneity of Adenocarcinoma Cell Lines and the Investigation of Intratumor Heterogeneity Reveals the Expression of Transmembrane Protein 45A (TMEM45A) in Lung Adenocarcinoma Cancer Patients.* Cancers (Basel), 2021. **14**(1).
330. Pao, W., et al., *Acquired resistance of lung adenocarcinomas to gefitinib or erlotinib is associated with a second mutation in the EGFR kinase domain.* PLoS Med, 2005. **2**(3): p. e73.
331. Kefas, B., et al., *microRNA-7 inhibits the epidermal growth factor receptor and the Akt pathway and is down-regulated in glioblastoma.* Cancer Res, 2008. **68**(10): p. 3566-72.
332. Liu, H., et al., *miR-7 modulates chemoresistance of small cell lung cancer by repressing MRP1/ABCC1.* Int J Exp Pathol, 2015. **96**(4): p. 240-7.
333. Chaudhuri, A.D., et al., *MicroRNA-7 Regulates the Function of Mitochondrial Permeability Transition Pore by Targeting VDAC1 Expression.* J Biol Chem, 2016. **291**(12): p. 6483-93.
334. Kaur, H., V. Scaria, and S. Maiti, *"Locked onto the target": increasing the efficiency of antagomirzymes using locked nucleic acid modifications.* Biochemistry, 2010. **49**(44): p. 9449-56.
335. Lundin, K.E., et al., *Biological activity and biotechnological aspects of locked nucleic acids.* Adv Genet, 2013. **82**: p. 47-107.

336. Bergeron, L., Jr., J.P. Perreault, and S. Abou Elela, *Short RNA duplexes guide sequence-dependent cleavage by human Dicer.* RNA, 2010. **16**(12): p. 2464-73.
337. Bonilla, S.L. and J.S. Kieft, *The promise of cryo-EM to explore RNA structural dynamics.* J Mol Biol, 2022. **434**(18): p. 167802.
338. Liu, D., et al., *Sub-3-A cryo-EM structure of RNA enabled by engineered homomeric self-assembly.* Nat Methods, 2022. **19**(5): p. 576-585.
339. Ma, H., et al., *Cryo-EM advances in RNA structure determination.* Signal Transduct Target Ther, 2022. **7**(1): p. 58.
340. Webster, R.J., et al., *Regulation of epidermal growth factor receptor signaling in human cancer cells by microRNA-7.* J Biol Chem, 2009. **284**(9): p. 5731-41.
341. Pogribny, I.P., et al., *Alterations of microRNAs and their targets are associated with acquired resistance of MCF-7 breast cancer cells to cisplatin.* Int J Cancer, 2010. **127**(8): p. 1785-94.
342. Hong, T., J. Ding, and W. Li, *miR-7 Reverses Breast Cancer Resistance To Chemotherapy By Targeting MRP1 And BCL2.* Onco Targets Ther, 2019. **12**: p. 11097-11105.
343. Hu, H., et al., *Long non-coding RNA KCNQ1OT1 modulates oxaliplatin resistance in hepatocellular carcinoma through miR-7-5p/ ABCC1 axis.* Biochem Biophys Res Commun, 2018. **503**(4): p. 2400-2406.
344. Liu, H., et al., *Upregulation of the inwardly rectifying potassium channel Kir2.1 (KCNJ2) modulates multidrug resistance of small-cell lung cancer under the regulation of miR-7 and the Ras/MAPK pathway.* Mol Cancer, 2015. **14**: p. 59.
345. Zhang, X., et al., *Long noncoding RNA SOX21-AS1 promotes cervical cancer progression by competitively sponging miR-7/VDAC1.* J Cell Physiol, 2019. **234**(10): p. 17494-17504.
346. Wang, F., et al., *MicroRNA-7 downregulates the oncogene VDAC1 to influence hepatocellular carcinoma proliferation and metastasis.* Tumour Biol, 2016. **37**(8): p. 10235-46.
347. Yang, L., et al., *MiR-7 mediates mitochondrial impairment to trigger apoptosis and necroptosis in Rhabdomyosarcoma.* Biochim Biophys Acta Mol Cell Res, 2020. **1867**(12): p. 118826.
348. Chan, P.P. and T.M. Lowe, *GtRNAdb 2.0: an expanded database of transfer RNA genes identified in complete and draft genomes.* Nucleic Acids Res, 2016. **44**(D1): p. D184-9.
349. Kozomara, A., M. Birgaoanu, and S. Griffiths-Jones, *miRBase: from microRNA sequences to function.* Nucleic Acids Res, 2019. **47**(D1): p. D155-D162.
350. Griffiths-Jones, S., et al., *miRBase: tools for microRNA genomics.* Nucleic Acids Res, 2008. **36**(Database issue): p. D154-8.
351. Popenda, M., et al., *Automated 3D structure composition for large RNAs.* Nucleic Acids Res, 2012. **40**(14): p. e112.
352. Antczak, M., et al., *New functionality of RNAComposer: an application to shape the axis of miR160 precursor structure.* Acta Biochim Pol, 2016. **63**(4): p. 737-744.
353. Leiter, A., R.R. Veluswamy, and J.P. Wisnivesky, *The global burden of lung cancer: current status and future trends.* Nat Rev Clin Oncol, 2023. **20**(9): p. 624-639.
354. Alduais, Y., et al., *Non-small cell lung cancer (NSCLC): A review of risk factors, diagnosis, and treatment.* Medicine (Baltimore), 2023. **102**(8): p. e32899.
355. Kratzer, T.B., et al., *Lung cancer statistics, 2023.* Cancer, 2024. **130**(8): p. 1330-1348.

356. Siegel, R.L., A.N. Giaquinto, and A. Jemal, *Cancer statistics, 2024.* CA Cancer J Clin, 2024. **74**(1): p. 12-49.
357. Duma, N., R. Santana-Davila, and J.R. Molina, *Non-Small Cell Lung Cancer: Epidemiology, Screening, Diagnosis, and Treatment.* Mayo Clin Proc, 2019. **94**(8): p. 1623-1640.
358. Ettinger, D.S., et al., *Non-Small Cell Lung Cancer, Version 3.2022, NCCN Clinical Practice Guidelines in Oncology.* J Natl Compr Canc Netw, 2022. **20**(5): p. 497-530.
359. Wu, F., et al., *Single-cell profiling of tumor heterogeneity and the microenvironment in advanced non-small cell lung cancer.* Nat Commun, 2021. **12**(1): p. 2540.
360. Leong, T.L., et al., *Heterogeneity of tumour mutational burden in metastatic NSCLC demonstrated by endobronchial ultrasound sampling.* Front Oncol, 2023. **13**: p. 1150349.
361. Frydrychowicz, M., et al., *MicroRNA in lung cancer—a novel potential way for early diagnosis and therapy.* Journal of Applied Genetics, 2023.
362. Liang, X., et al., *MicroRNAs as early diagnostic biomarkers for non-small cell lung cancer (Review).* Oncol Rep, 2023. **49**(1).
363. Traber, G.M., et al., *Novel RNA molecular bioengineering technology efficiently produces functional miRNA agents.* RNA, 2024.
364. Liu, S., et al., *Exosome-mediated miR-7-5p delivery enhances the anticancer effect of Everolimus via blocking MNK/eIF4E axis in non-small cell lung cancer.* Cell Death Dis, 2022. **13**(2): p. 129.
365. Woo, S.Y., et al., *MicroRNA-7-5p's role in the O-GlcNAcylation and cancer metabolism.* Noncoding RNA Res, 2020. **5**(4): p. 201-207.
366. Xiao, H., *MiR-7-5p suppresses tumor metastasis of non-small cell lung cancer by targeting NOVA2.* Cell Mol Biol Lett, 2019. **24**: p. 60.
367. Stine, Z.E., et al., *Targeting cancer metabolism in the era of precision oncology.* Nat Rev Drug Discov, 2022. **21**(2): p. 141-162.
368. Jin, P., et al., *Mitochondrial adaptation in cancer drug resistance: prevalence, mechanisms, and management.* J Hematol Oncol, 2022. **15**(1): p. 97.
369. Peng, J., et al., *Altered glycolysis results in drug-resistant in clinical tumor therapy.* Oncol Lett, 2021. **21**(5): p. 369.
370. Wu, Y., W. Gao, and H. Liu, *Role of metabolic reprogramming in drug resistance to epidermal growth factor tyrosine kinase inhibitors in non-small cell lung cancer.* Zhong Nan Da Xue Xue Bao Yi Xue Ban, 2021. **46**(5): p. 545-551.
371. Mo, J., et al., *Targeting mitochondrial one-carbon enzyme MTHFD2 together with pemetrexed confers therapeutic advantages in lung adenocarcinoma.* Cell Death Discov, 2022. **8**(1): p. 307.
372. Sainero-Alcolado, L., et al., *Targeting mitochondrial metabolism for precision medicine in cancer.* Cell Death Differ, 2022. **29**(7): p. 1304-1317.
373. Yi, W.R., et al., *Bioengineered miR-34a modulates mitochondrial inner membrane protein 17 like 2 (MPV17L2) expression toward the control of cancer cell mitochondrial functions.* Bioengineered, 2022. **13**(5): p. 12489-12503.
374. Jilek, J.L., et al., *Pharmacokinetic and Pharmacodynamic Factors Contribute to Synergism between Let-7c-5p and 5-Fluorouracil in Inhibiting Hepatocellular Carcinoma Cell Viability.* Drug Metab Dispos, 2020. **48**(12): p. 1257-1263.

375. Sampson, A., et al., *Doxorubicin as a fluorescent reporter identifies novel MRP1 (ABCC1) inhibitors missed by calcein-based high content screening of anticancer agents.* Biomed Pharmacother, 2019. **118**: p. 109289.
376. Kozomara, A. and S. Griffiths-Jones, *miRBase: annotating high confidence microRNAs using deep sequencing data.* Nucleic Acids Res, 2014. **42**(Database issue): p. D68-73.
377. Corcoran, C.C., et al., *From 20th century metabolic wall charts to 21st century systems biology: database of mammalian metabolic enzymes.* Am J Physiol Renal Physiol, 2017. **312**(3): p. F533-F542.
378. Doxakis, E., *Post-transcriptional regulation of alpha-synuclein expression by mir-7 and mir-153.* J Biol Chem, 2010. **285**(17): p. 12726-34.
379. Chou, T.C., *Drug combination studies and their synergy quantification using the Chou-Talalay method.* Cancer Res, 2010. **70**(2): p. 440-6.
380. Chen, J., et al., *Human drug efflux transporter ABCC5 confers acquired resistance to pemetrexed in breast cancer.* Cancer Cell Int, 2021. **21**(1): p. 136.
381. O'Connor, C., et al., *Folate transporter dynamics and therapy with classic and tumor-targeted antifolates.* Sci Rep, 2021. **11**(1): p. 6389.
382. Uemura, T., et al., *ABCC11/MRP8 confers pemetrexed resistance in lung cancer.* Cancer Sci, 2010. **101**(11): p. 2404-10.
383. Xie, M., et al., *Inactivation of multidrug resistance proteins disrupts both cellular extrusion and intracellular degradation of cAMP.* Mol Pharmacol, 2011. **80**(2): p. 281-93.
384. Wielinga, P.R., et al., *Characterization of the MRP4- and MRP5-mediated transport of cyclic nucleotides from intact cells.* J Biol Chem, 2003. **278**(20): p. 17664-71.
385. Che, T.F., et al., *Mitochondrial translocation of EGFR regulates mitochondria dynamics and promotes metastasis in NSCLC.* Oncotarget, 2015. **6**(35): p. 37349-66.
386. Demory, M.L., et al., *Epidermal growth factor receptor translocation to the mitochondria: regulation and effect.* J Biol Chem, 2009. **284**(52): p. 36592-36604.
387. Youle, R.J. and A.M. van der Bliek, *Mitochondrial fission, fusion, and stress.* Science, 2012. **337**(6098): p. 1062-5.
388. Valera-Alberni, M. and C. Canto, *Mitochondrial stress management: a dynamic journey.* Cell Stress, 2018. **2**(10): p. 253-274.
389. Bektas, M., et al., *A novel acylglycerol kinase that produces lysophosphatidic acid modulates cross talk with EGFR in prostate cancer cells.* J Cell Biol, 2005. **169**(5): p. 801-11.
390. Vukotic, M., et al., *Acylglycerol Kinase Mutated in Sengers Syndrome Is a Subunit of the TIM22 Protein Translocase in Mitochondria.* Mol Cell, 2017. **67**(3): p. 471-483 e7.
391. Chu, B., Z. Hong, and X. Zheng, *Acylglycerol Kinase-Targeted Therapies in Oncology.* Front Cell Dev Biol, 2021. **9**: p. 659158.
392. Shoshan-Barmatz, V., E.N. Maldonado, and Y. Krelin, *VDAC1 at the crossroads of cell metabolism, apoptosis and cell stress.* Cell Stress, 2017. **1**(1): p. 11-36.
393. Uribe, M.L., I. Marrocco, and Y. Yarden, *EGFR in Cancer: Signaling Mechanisms, Drugs, and Acquired Resistance.* Cancers (Basel), 2021. **13**(11).
394. Haloi, N., et al., *Structural basis of complex formation between mitochondrial anion channel VDAC1 and Hexokinase-II.* Commun Biol, 2021. **4**(1): p. 667.

395. Zhao, W., et al., *Pemetrexed long-term maintenance therapy for advanced severe lung cancer with long-term progression-free survival: a case report.* Anticancer Drugs, 2023. **34**(5): p. 686-689.
396. Li, J., et al., *Efficacy and safety of pemetrexed maintenance chemotherapy for advanced non-small cell lung cancer in a real-world setting.* J Thorac Dis, 2021. **13**(3): p. 1813-1821.
397. Li, K.M., L.P. Rivory, and S.J. Clarke, *Pemetrexed pharmacokinetics and pharmacodynamics in a phase I/II study of doublet chemotherapy with vinorelbine: implications for further optimisation of pemetrexed schedules.* Br J Cancer, 2007. **97**(8): p. 1071-6.
398. Adjei, A.A., *Pharmacology and mechanism of action of pemetrexed.* Clin Lung Cancer, 2004. **5 Suppl 2**: p. S51-5.
399. Li, B., et al., *Overexpression of PTEN may increase the effect of pemetrexed on A549 cells via inhibition of the PI3K/AKT/mTOR pathway and carbohydrate metabolism.* Mol Med Rep, 2019. **20**(4): p. 3793-3801.
400. Ifergan, I. and Y.G. Assaraf, *Molecular mechanisms of adaptation to folate deficiency.* Vitam Horm, 2008. **79**: p. 99-143.
401. Uhlen, M., et al., *A pathology atlas of the human cancer transcriptome.* Science, 2017. **357**(6352).
402. Liu, R., et al., *MicroRNA-7 sensitizes non-small cell lung cancer cells to paclitaxel.* Oncol Lett, 2014. **8**(5): p. 2193-2200.
403. Xu, N., et al., *miR-7 Increases Cisplatin Sensitivity of Gastric Cancer Cells Through Suppressing mTOR.* Technol Cancer Res Treat, 2017. **16**(6): p. 1022-1030.
404. Choi, M., et al., *Phase II Study of Pemetrexed as a Salvage Chemotherapy for Thymidylate Synthase-Low Squamous Cell Lung Cancer.* Cancer Res Treat, 2021. **53**(1): p. 87-92.
405. Takezawa, K., et al., *Thymidylate synthase as a determinant of pemetrexed sensitivity in non-small cell lung cancer.* Br J Cancer, 2011. **104**(10): p. 1594-601.
406. Zhao, Y., et al., *Genetically engineered pre-microRNA-34a prodrug suppresses orthotopic osteosarcoma xenograft tumor growth via the induction of apoptosis and cell cycle arrest.* Sci Rep, 2016. **6**: p. 26611.
407. Zhao, Y., et al., *Combination therapy with bioengineered miR-34a prodrug and doxorubicin synergistically suppresses osteosarcoma growth.* Biochem Pharmacol, 2015. **98**(4): p. 602-13.
408. Chen, R., et al., *Exosomes-transmitted miR-7 reverses gefitinib resistance by targeting YAP in non-small-cell lung cancer.* Pharmacol Res, 2021. **165**: p. 105442.
409. Cui, J., et al., *Efficacy of combined icotinib and pemetrexed in EGFR mutant lung adenocarcinoma cell line xenografts.* Thorac Cancer, 2018. **9**(9): p. 1156-1165.
410. Hatakeyama, Y., et al., *Synergistic effects of pemetrexed and amrubicin in non-small cell lung cancer cell lines: Potential for combination therapy.* Cancer Lett, 2014. **343**(1): p. 74-9.
411. La Monica, S., et al., *Third generation EGFR inhibitor osimertinib combined with pemetrexed or cisplatin exerts long-lasting anti-tumor effect in EGFR-mutated pre-clinical models of NSCLC.* J Exp Clin Cancer Res, 2019. **38**(1): p. 222.

412. Sha, Z., et al., *Clinical observation of Pemetrexed first-line treatment in advanced non-squamous lung cancer or non-small cell lung cancer without driver-mutations: a phase 2, single-arm trial.* Ann Transl Med, 2020. **8**(20): p. 1315.